Arching in Granular Materials with Particular Reference to Inclined Mine Stopes

Thesis submitted by

Ting ChingHung BEng(Hons)

In September 2011

for the degree of Doctor of Philosophy

In the School of Engineering and Physical Sciences

James Cook University

STATEMENT OF ACCESS

I, the undersigned, the author of this thesis, understand that James Cook University will make it available for use within the University Library and, by microfilm or other means, allow access to users in other approved libraries.

All users consulting this thesis will have to sign the following statement:

> In consulting this thesis, I agree not to copy or closely paraphrase it in whole or in part without the written consent of the author; and to make proper public written acknowledgement for any assistance which I have obtained from it.

Beyond this, I do not wish to place any restriction on access to this thesis.

19/9/2011

…….

Signature Date

STATEMENT OF SOURCES

DECLARATION

I declare that this thesis is my own work and has not been submitted in any form of another degree or diploma at any university or other institution of tertiary education. Information derived from the published or unpublished work of others has been acknowledged in the text and a list of references is given.

19/9/2011

…….. ……

Signature Date

DECLARATION – ELECTRONIC COPY

I, the undersigned, the author of this work, declare that to the best of my knowledge, the electronic copy of this thesis submitted to the library at James Cook University is an accurate copy of the printed thesis submitted.

19/9/2011

…….. ……

Signature Date

ACKNOWLEDGEMENTS

I would like to express my heartfelt thanks and gratitude to all the professors, supervisors, friends and my family for their guidance, encouragement, love and support over the course of my research study. This research study would not have been possible without their valuable support. My deepest gratitude is to my direct supervisor, A/Prof. Nagaratnam Sivakugan, who is extremely helpful and always offered invaluable guidance, assistance and support. I want to thank A/Prof. Sanjay Kumar, Prof Wayne Read and Mr Warren O'Donnell for their guidance and advice during this period. I would also like to thank all my friends and colleagues, especially James Tan, Julie Lovisa, Lu Jun and William Huang for their ongoing support and valuable assistance. I also wish to express my sincere love and gratitude to my beloved family for their understanding and endless love throughout the duration of my studies.

ABSTRACT

Determination of stress distribution, giving due consideration to arching mechanism within minefill stopes, is of great importance because of its influence on the ground stability, ore recovery and cost effectiveness. Most previous studies on stress determination and arching effects have been applied to vertical stopes, whereas research is lacking on inclined stopes. The objective of this study is to investigate the effect of inclination on arching action on stress distributions, with particular interest on the stress distribution at the base and on the side walls of the stope. Three separate modeling techniques are carried out to achieve the goal of the study, which are numerical, analytical and experimental methods.

The studies develop analytical solutions from Marston's theory for inclined stopes with parallel and non-parallel walls, incorporating arching effects within the backfill, and propose a new analytical method developed from Pascal's triangle and binomial series for vertical stress determination in vertical and inclined minefill stope. Good agreement is seen between the two analytical methods for vertical and inclined stopes. The results show that with the same overburden pressure γz and base width B, the stress magnitude experienced by fill material can vary significantly with wall inclination. It is shown that lateral earth pressure coefficient, K and interfacial friction angle, δ has significant influence on vertical stress profile. K and δ should be taken as either $K = K_0$ and $\delta = 2/3\ \phi$ or $K = K_a$ and $\delta = \phi$ to better describe the state of stress within the minefills in underground stopes.

A laboratory model is designed to simulate mine backfilling in an inclined stope and determine the average vertical stress at any depth within the fill. Stope inclination, wall roughness, relative density and aspect ratio are varied independently to study their influence on the stress distribution and arching effects. The highest vertical stress is observed at inclination about 80° to the horizontal and shear stress experienced by the footwall increases with increasing stope inclination and wall roughness. The average interfacial friction angle can be used in analytical expression to predict the vertical stress within a stope with dissimilar wall characteristics.

The study undertaken has also developed approximate solutions for the stress distribution within inclined stopes based on FLAC simulation. Three separate models are conducted in the simulation. They are laboratory model stope, a prototype minefill stope, and laboratory stope incorporated into rock mass to simulate minefill environments. There is good agreement among the analytical, numerical and the laboratory model results. Lateral earth pressure coefficient, K is better described by K_a for inclined minefill stopes.

The findings from this dissertation have been disseminated through the following three journal papers.

1. Ting, C. H., Shukla, S. K., and Sivakugan, N. (2011). "Arching in Soils Applied to Inclined Mine Stopes." *International Journal of Geomechanics, ASCE 11(1), 29-35.*

2. Ting, C.H., Sivakugan, N., Read, W., and Shukla, S.K.(2010). "An Analytical Method to Determine Vertical Stresses within a Granular Material Contained in Right Vertical Prisms." *International Journal of Geomechanics, ASCE (In print).*

3. Ting, C.H., Sivakugan, N., and Shukla, S.K. (2011). "Laboratory Simulation of the Stresses within Inclined Stopes." *Geotechnical Testing Journal, ASTM (In print).*

Table of Contents

List of Figures

List of Tables

List of Symbols

α	=	Wall inclination at hangingwall to the horizontal
β	=	Wall inclination to the horizontal (for parallel wall) or Wall inclination at footwall (for non-parallel wall)
δ	=	Interfacial friction angle
δ_M	=	Interfacial friction angle for medium wall roughness
δ_R	=	Interfacial friction angle for high wall roughness
δ_S	=	Interfacial friction angle for low wall roughness
ϕ	=	Friction angle
ϕ_{cv}	=	Residual friction angle
ϕ_{ds}	=	Friction angle measured from direct shear test
ϕ_{peak}	=	Peak friction angle
ϕ_{ps}	=	Friction angle for plane strain condition
γ	=	Unit weight
φ	=	Dilation angle
ν	=	Poisson's ratio
ρ	=	Fill density
ρ_d	=	Dry density
$\rho_{d,\,max}$	=	Maximum dry density
$\rho_{d,min}$	=	Minimum dry density
θ	=	Angle of minor stress plane to the horizontal at the wall
ξ	=	Modified cohesion of the fill for an inclined stope
ζ_1 , ζ_2	=	Modified fill cohesion for hangingwall and footwall respectively
τ	=	Shear stress along the wall
τ_{xz}	=	Shear stress along the wall in x-z direction
τ_1 , τ_2	=	Shear stress acting at hangingwall and footwall respectively
τ_m	=	Shear stress at the wall of layer-m
σ_1	=	Major principle stress
σ_3	=	Minor principle stress
σ_h	=	Lateral stress
σ_n	=	Normal stress at the wall at depth z
σ_{n1} , σ_{n2}	=	Normal stress on hangingwall and footwall respectively
σ_v	=	Vertical stress
σ_x	=	Lateral stress at depth z

σ_z	=	Vertical stress at depth z
ψ	=	Factor with respect to different cross-sectional shape (see Table 4.2) or Factor with respect to plane strain cross-sectional shape
ψ_c, ψ_R, ψ_S	=	Factor with respect to circular, rectangular and square cross-section respectively
Δz_{min}	=	The smallest width of an adjoining zone in the normal direction (FLAC)
b	=	Distance between rock boundaries and stope walls
c	=	Cohesion of the fill
d	=	Depth of rock below the base of stope and the depth of rock above the stope
h	=	Thickness of layer (Chapter 4) or Height of the fill measured from the base of stope (Chapter 5)
h_v	=	Gap between the rock roof and fill material (in FLAC modeling)
k_n	=	Normal stiffness of interface element used in FLAC modeling
k_s	=	Shear stiffness of interface element used in FLAC modeling
q	=	Surcharge on top of fill material
w	=	Moisture content
x	=	Fraction of force transferred to the wall
x_1, x_2, x_3, x_4	=	Horizontal distance between toe of the stope to edge of differential element at hangingwall and footwall
z	=	Fill depth measured from top of the backfill
A_{strip}	=	Area of the differential element
B	=	Stope width at the base of backfill
B_T	=	Stope width at the top of backfill
D	=	Oedometer modulus
Dr	=	Relative fill density
E	=	Young's modulus
F_{FW}	=	Load acting at footwall
F_{HW}	=	Load acting at hangingwall
F_m	=	Shear force acting along the wall of layer-m
F_n	=	Normal compressive force on the wall
FW	=	Footwall
G	=	Shear modulus
G_s	=	Specific gravity
H	=	Total height of backfill or stope
HW	=	Hangingwall
K	=	Lateral stress ratio or earth pressure coefficient
K_o	=	At rest lateral stress ratio or at rest earth pressure coefficient
K_a	=	Active lateral stress ratio or active earth pressure coefficient

K_b	=	Bulk modulus
K_p	=	Passive lateral stress ratio or passive earth pressure coefficient
K'	=	Modified lateral stress ratio for inclined stope
K_1,K_2	=	Modified lateral stress ratio for hangingwall and footwall respectively
K_{wall}	=	Lateral stress ratio at the wall
L	=	Length of the stope in plan
L_1, L_2	=	Stope width of differential element
M	=	Total number of layers
Q	=	Surcharge load at the top of the fill
R	=	Radius of circular stope
S	=	Shearing force along the wall
S_1, S_2	=	Shear force acting along hangingwall and footwall respectively
N_1, N_2	=	Normal force acting on hangingwall and footwall respectively
V	=	Internal vertical force
V_o	=	Self weight of layer
V_m	=	Vertical force at the base of layer-m
W	=	Self-weight of the backfill
W_b	=	Fill weight acting at the base of stope
W_w	=	Fill weight transferred to the wall of stope

Chapter 1 Introduction

1.1 General

Mining is a multibillion dollar industry in Australia, Brazil, Canada, Chile, China, South Africa and the United States of America (Rankine et al. 2007). While open cut mining methods are used for recovering minerals from shallow ore bodies, underground mining is the only way to recover minerals from large depths. In the process of underground mining, ore is removed from deep rectangular underground voids in the form of right prisms, known as *stopes*. Ore is removed through horizontal access tunnel located at various levels. Once the minerals are extracted, the crushed waste rocks, in the form of tailings, are returned to the ground to backfill these voids. Backfilling of the stopes improves the regional stability within the mine, so that ore can be removed from the adjacent stopes. It is also an effective means of tailing disposal.

The voids that are created and need to be backfilled can be seen as approximately vertical or inclined rectangular prisms, with the base dimensions in the order of 30-70 m, and heights as much as 200 m. To ensure safety within the access tunnels and other regions of the mines, appropriate barricades are used to block the horizontal access drives while filling the empty stopes with minefills (Rankine et al. 2006). The barricade is designed to resist the horizontal stress exerted on it by the backfill and allow the drainage of the free water from the fill. The failure of barricade may result in fatalities and damage to equipment and machineries. Due to the failure of barricades, accidents take place in the mining environment worldwide every year (Christopher et al. 2007). Therefore, it is necessary to understand the stress developments in the stope, particularly within the access drives.

Before understanding the loadings on the barricades for their safe and economical design, it is necessary to understand the stress developments within the mine stopes adequately. It has been established that a substantial stress reduction takes place due to arching, and it is therefore necessary to determine the vertical stresses within the minefills more realistically with due consideration to arching.

1.2 Arching within minefills

Arching is a universal phenomenon observed in granular materials including soil masses. It involves a stress redistribution process in which differential straining mobilizes shear

strength and transfers part of the pressure of yielding mass to relatively stable neighboring zones. Arching has been observed in many geotechnical applications as well as storage of bulk solids through experimental studies, mathematical analyses, and in-situ measurements, which include:

- Earth pressure on retaining structures (Dalvi and Pise 2008; Goel and Patra 2008; Handy 1985; Harrop-williams 1989; Ono and Yamada 1993; Paik and Salgado 2003; Take and Valsangkar 2001);
- Pressure from the soil mass lying over buried structures or conduits (Handy 1985; Marston 1930; Marston and Anderson 1913; Spangler and Handy 1982; Terzaghi 1943)
- Pressure acting on piles or piled embankments (Bosscher and Gray 1985; Sabiti et al. 2007; Shelke and Patra 2008);
- Earth pressure on underground openings or tunnels (Ladanyi and Hoyaux 1969; Ono and Yamada 1993; Potts and Zdravkovic 2008; Terzaghi 1943);
- Stress distribution within mine backfilling (Aubertin et al. 2003; Caceres Doerner 2005; DeSouza and Dirige 2002; Knutsson 1981; Li and Aubertin 2008, 2009; Li et al. 2005, 2007; Pirapakaran and Sivakugan 2006, 2007a, 2007b); and
- Stress distribution in a storage vessel of bulk solids such as grain, cement and coals (Barrette and Sayed 2007; Drescher 1991; Janssen 1895; Walters 1973).

A comprehensive review on arching study can be found in Tien (1996).

In a backfilled stope, arching occurs when the fill tends to move down relative to the surrounding stiffer rock walls, while the shear resistance along the rock-fill interface tends to keep the fill in its original position. This phenomenon, in effect, transfers part of the overburden weight of fill material by shearing stresses to the adjacent rock walls as shown in Fig. 1.1. In contrast, if the fill is surrounded by a softer material that can settle relative to the fill, reverse arching may occur where the load is transferred from the surroundings to the backfill and stresses within the backfill will increase. Udd and Annor (1993) concluded from their site monitoring on backfill behavior that "*There is a definite tendency for backfill to be self-supporting and to arch within the stope. Most of the earth-pressure cells indicated pressures that were significantly less than the overburden pressures expected from backfill*".

Therefore, it is important to investigate the actual stress distribution in a stope for more effective backfill design.

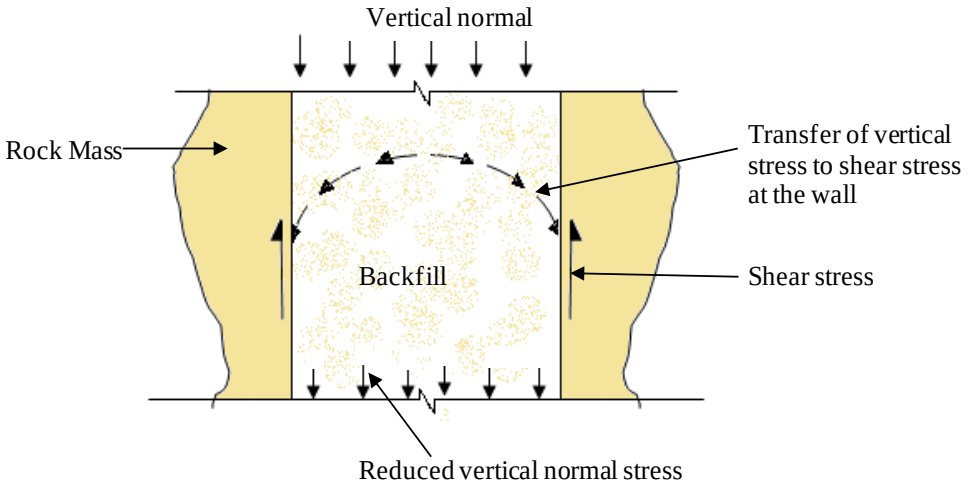

Figure 1.1. Schematic diagram of arching within mine stopes (Reproduced from Pirapakaran (2008))

Figures. 1.2 and 1.3 show the stress profiles obtained by Pirapakaran and Sivakugan (2007a) in a 2-D vertical stope. It is clearly shown in the figures that the stress magnitude along the walls is smaller than the central part of stope at any elevation, which indicates the occurrence of arching. The results obtained from these studies also show that vertical stress can be 40-60% less than overburden pressure, that is defined as the product of unit weight of the fill and depth. If the wall is smooth, there will be no arching and hence the vertical stress at any depth will be the same as the overburden pressure.

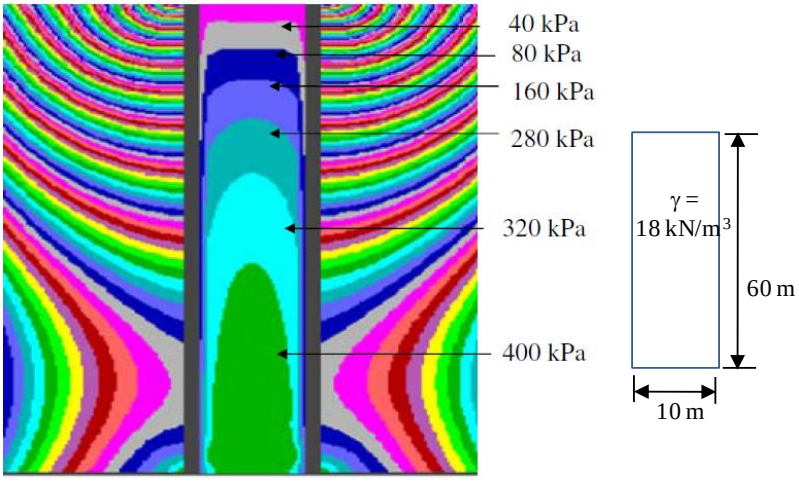

Figure 1.2. Vertical stress distribution contours within backfill and rock surroundings as obtained from FLAC (Pirapakaran and Sivakugan 2007a)

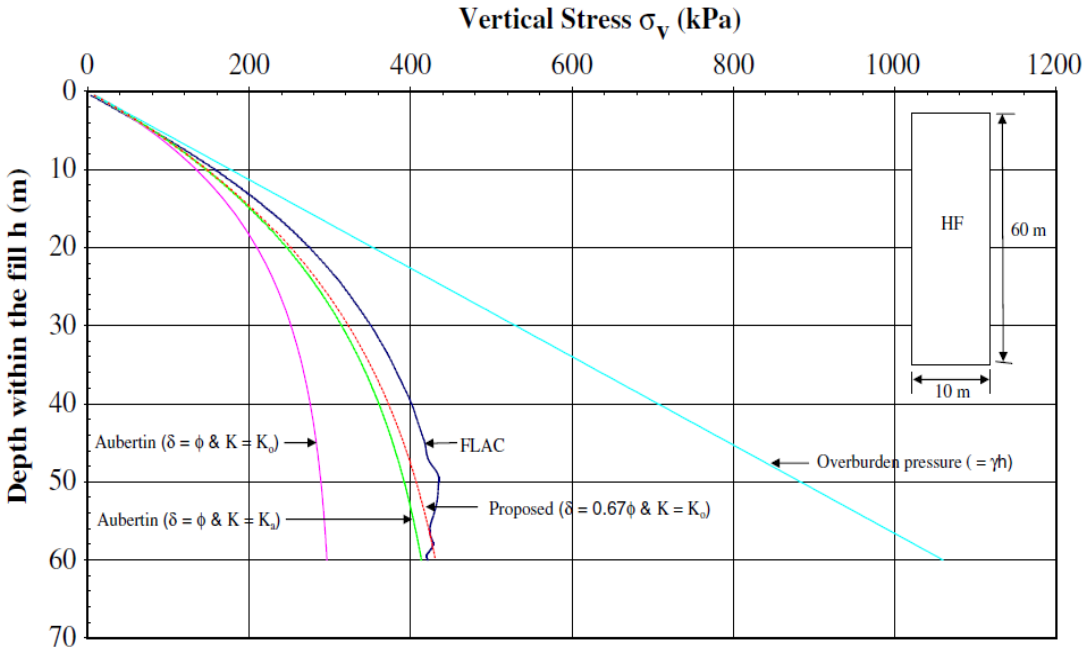

Figure 1.3. Comparison of vertical normal stress from analytical, numerical and overburden stress along the vertical centre line (Pirapakaran and Sivakugan 2007a)

1.3 Current State-of-the-Art

Various studies were carried out by researchers to understand stress distribution and arching mechanisms within a *vertical* stope (Aubertin et al. 2003; Li and Aubertin 2008; Li et al. 2003, 2005; Mitchell et al. 1982; Pirapakaran and Sivakugan 2006, 2007a, 2007b). However, in reality, not all the mine stopes are vertical. Some of the mine stopes are inclined, where the backfill is bounded between the footwall (FW) and hangingwall (HW) as shown in Fig. 1.4. In mining, hangingwall (HW) is referred to the rock lying above the ore body, and footwall (FW) is referred to the rock lying below the ore body. Due to the geometry of the stope, the convergence of HW may induce additional stresses within the backfill, and part of the pressure of backfill may transfer to FW due to gravity, which subsequently may alter the stress profiles from vertical to inclined stope. The observation of Caceres Doerner (2005), Hassani et al. (2008) and Li and Aubertin (2009), from numerical modeling, have shown that the load distribution and arching formation are different between the vertical and inclined stopes.

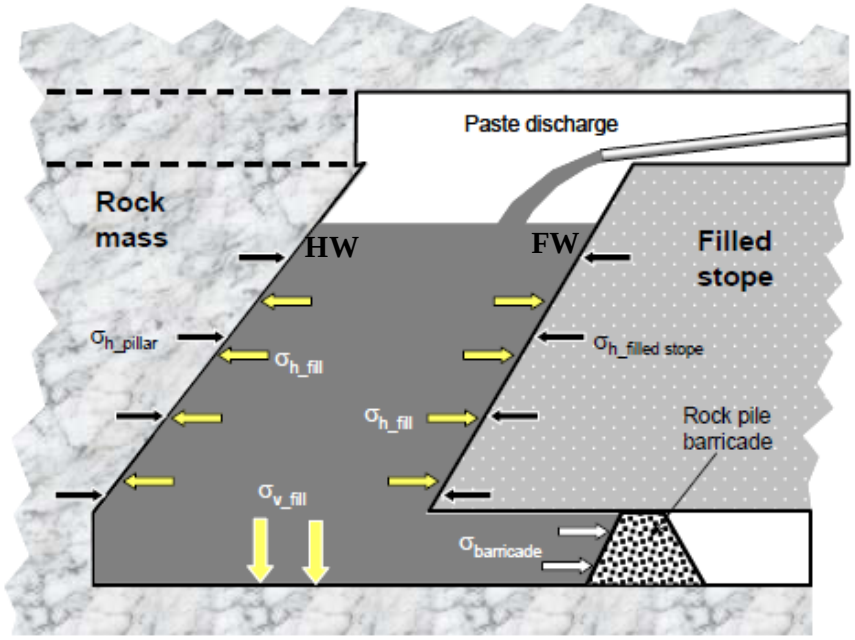

Figure 1.4. Schematic showing the components of an inclined backfilled stope and the stress field distribution (Belem and Benzaazoua 2004)

The current design approach for an inclined stope is based on the results obtained from a vertical stope by incorporating some minor modifications. In 1960, Jahns and Brauner (vide Robertson et al. 1986) suggested that, when the inclination is less than 30^{o} to vertical, the error in vertical stress due to stope inclination is less than 10%. Shukla et al. (2009b) suggested that analytical expressions developed for vertical walls can be used to estimate the active stress coefficient for wall inclination less than 15^{0} without compromising the accuracy of the results. Li and Aubertin (2009) suggested that the analytical solution developed for vertical stopes in Aubertin et al. (2003) can be used to estimate the vertical and horizontal stresses of an inclined stope with inclination less than 10^{o} to vertical, however, a stope inclination of more than 10^{0} will induce a significant difference when compared to the vertical stope situation. Their observation from the numerical modeling has also shown that the load distribution profile is different between the vertical and inclined stopes, and the arching is less well developed for the inclined stopes.

It can be concluded from the above findings that the analytical solutions developed for vertical stopes are applicable only for an inclined stope with inclination less than 10^{o} to vertical; beyond that, the solutions provided are unreliable. Therefore, to ensure the viability of mines and workforce safety, it is important for miners to have a good understanding of stress distribution and development for inclined stopes and to develop a rational methodology to account for stope inclination in the stress analysis within mine fills.

1.4 Objectives and scope of research

The primary goal of this dissertation is to investigate the effect of inclination on arching action on stress distributions, with particular interest on the normal stress distribution at the base of stope and the shear stress on the side walls of stope. The scope of study includes the following:

- To identify the mechanism of arching action in inclined stopes containing granular backfills through laboratory, numerical and analytical approaches.
- To develop analytical solutions that can be used to evaluate the stress distributions within a stope having parallel and non-parallel walls.
- To develop a laboratory model for inclined stope and investigate the effect of arching mechanism and stress distribution within a granular backfill.
- To develop 2-dimensional plane strain numerical models using FLAC that can accurately predict the stress distributions by incorporating arching mechanism in inclined stopes containing granular backfills.

There are three independent techniques that will be undertaken in this study. They are:

1. Analytical Method
2. Experimental Method
3. Numerical Method

All three techniques are performed concurrently and the outcomes of each technique are compared to verify that the results are in close agreement in order to fully understand the theory behind the arching mechanism on stress development within an inclined model. The research will result in

- Better understanding of the arching mechanism that will improve the current state-of-the-art.
- A rational methodology to account for stope inclination in the stress analysis within granular backfills contained within inclined stopes.
- Simple design procedures and design charts derived from sound fundamentals, supported by numerical models and experimental data.

1.5 Relevance of the research

From the observations of the numerical modeling for an inclined stope by Caceres Doerner (2005), Hassani et al. (2008), Li and Aubertin (2009) and Li et al. (2007), the stress profiles and arching formation for an inclined stope are different from that of a vertical stope. They have shown that the vertical stress decreases as the inclination of the stope increases. The maximum vertical stress tends to be located near the stope's footwall and the horizontal stress along the hangingwall is higher than along the footwall. These results illustrate that the existing analytical expression and design approach for horizontal and vertical stress evaluation may not be appropriate when wall inclination is involved. As numerical analysis is not routinely used in practice and simple analytical expressions remain the principal tool among practicing engineers, analytical solutions by considering different wall inclinations for an inclined stope are developed in this study. In addition, most of the analytical expressions available in the literature are developed based on shear plane method or equilibrium considerations. A new analytical method for determining the vertical stresses in a long container or mine stopes, assuming plane strain condition is introduced.

The numerical results of Caceres Doerner (2005), Li and Aubertin (2009) and Li et al. (2007) as mentioned above also reveal that stope inclination may affect the load distribution between hangingwall and footwall. The load transferred to the walls due to arching for vertical stope can be assumed to be equally distributed, assuming wall characteristics are identical. However stope inclination may results in unequal load distribution to the walls. Therefore, this study will examine the influence of stope inclination on load distribution between hangingwall and footwall.

In soil mechanics, earth pressure coefficient or lateral stress ratio, K is defined as the ratio of horizontal to vertical normal stress when they are both principal stresses. The theoretical value of K may vary from passive state to active state depending on wall displacement. For vertical stope, as very little lateral deformation of stope wall may occur, at-rest condition may be appropriate to consider in stress analysis. However, for an inclined stope, dipping hangingwall and footwall may induce additional stresses on backfills or on footwalls under gravity or wall convergence, which may change the state of stress within the backfill. Therefore, it is important to investigate the effect of inclination on stress state experienced within backfill in order to produce an effective design criterion.

Most of the past studies on inclined stopes are based on numerical modeling, and there is a lack of research effort involving laboratory or in-situ work. A laboratory model is developed in this dissertation to simulate mine backfilling in an inclined stope. The model is expected

to serve as a verification tool for numerical and analytical models and to enable determination of the average vertical stress at any depth within the fill. Therefore, it is not necessary to use minefill in the laboratory model. Instead, river sand is used in the entire laboratory testing program. The geotechnical parameters of the same sand are used in the analytical and numerical model.

1.6 Thesis overview

Chapter 1 introduces the research work presented in this thesis, objectives and the relevance of the research. Chapter 2 provides an overview of previous research that has been conducted in estimating stress distribution within mine stopes, both vertical and inclined, which includes analytical, numerical and laboratory/field works. Chapter 3 extends Marston's theory to the development of analytical expression for estimating stress distribution within an inclined stope with parallel and non-parallel walls. A parametric study is conducted to examine the effects of inclination, aspect ratio and fill properties on the vertical normal stress distribution. In addition, an analysis on vertical stress optimization for an inclined stope is carried out in order to support the findings observed in Chapter 5. Chapter 4 describes the development and application of a new and simple analytical method to determine vertical stresses within a granular material contained in right vertical or inclined containment. Chapter 5 gives the details of the development of a small-scale plane strain laboratory model for inclined stope. A parametric study on stope aspect ratio, inclination and wall roughness is also presented in this chapter. Chapter 6 describes the simulation of numerical models using FLAC for laboratory model (described in Chapter 5) and a prototype underground mine stope. A comparison among the three major techniques (numerical, analytical and experimental) is discussed in this chapter. Chapter 7 provides a summary and conclusions of the research and some recommendations for future research.

Chapter 2 Literature review

There are two major types of mines: open cut mines and underground mines. Open cut mining is used when the overburden is relatively thin and the mineral of interest is located near the surface. For ore deposits deep below the surface, underground mining techniques are used to extract the mineral to the surface through tunnels and shafts. Both mining methods result in the creation of voids. For open cut mines, the large voids or mine area must undergo rehabilitation or sometimes are converted to landfills for disposal of solid wastes. In underground mining, backfilling the mine void is a standard practice in managing the large void created after mining is completed.

Backfilling helps in limiting the amount of wall convergence using minefill as mass support and reducing the relaxation of rock mass within the walls, which in turn retains the load-carrying capacity of the rock mass and improves regional stability of the mine. Backfilling is also one of the most effective tools for providing ground support for mining operation, reducing mine waste created on the earth surface after ore extraction, and maximizing the ore recovery. This chapter gives a broad overview of current backfill practice used in underground mining with emphasis on the techniques used to investigate the stress distribution within the stope.

2.1 An overview of mine backfill

The backfilled process commences when the full stope area has been mined out. The voids are backfilled with tailings or waste rocks. Backfills are the rock mass that remains after ore extraction. They are crushed and graded into aggregate of different sizes before they are used to backfill the stope, which includes waste rock, deslimed and whole mill tailings, quarried and crushed aggregate, and alluvial or aeolian sand (Grice 1998). The most common backfilling method is to place mill tailings in the form of slurry by adding a substantial amount of water to the fills and deliver through boreholes and pipelines to the stope under gravitational effects (Grice 1998). The filling rate of the slurry depends on drainage conditions, fill and barricade permeability. Slow and progressive filling is preferred for a large open stope. For example, the filling of a typical 40 m x 200 m stope takes more than fifty pours over a six-month period (Barrett et al. 1978). The current state of backfill usage, operational practices and costs associated in Canadian mines has been reported through two comprehensive surveys by DeSouza and Dirige (2003).

Depending on the addition of cement (binding agent), two basic ways of backfilling strategies are used; cemented backfilling and uncemented backfilling (Sivakugan et.al. 2006). Uncemented backfill can be used as a void filler where only sufficient strength is required to prevent it from remobilisation whereas cemented backfill can be used as an engineering material where sufficient strength is required to enable it to be exposed by ore pillar mining or undercuts (Grice 1998). Therefore, it is important to know the material properties and their constituents to produce reliable, consistent quality and cost optimized fill materials. Researches into various types of backfills have been discussed in detail elsewhere (Belem and Benzaazoua 2004; Grice 1998; Potvin et al. 2005; Rankine et al. 2007; Udd 1989; Udd and Annor 1993). Only a brief summary of the different types of minefills will be presented here.

Backfills are non-uniform with a wide range of size distribution. They can vary from very coarse aggregates to very fine-grained tailings and their properties vary with the fill type. A small amount of binding agent (e.g. Portland cement or any pozzolanic material), of between 3% and 6% by weight, can be added to the filling materials to improve the strength of fill and also to eliminate the risk of liquefaction.

Depending on the function of backfill, whether it is used as void filler or as an engineering material, it can be divided into two broad categories (Grice 1998). The first category is bulk backfill, where the fill materials are disposed into stopes to provide confinement to surrounding rock walls. The second category is exposable backfill, which serves as an engineered material and enables the fill to be exposed on one or more sides or to withstand the blasting of adjacent pillar ore. In this case, a small amount of binder is added to provide sufficient strength to the fill. The most common backfills used in mine industry today are hydraulic fill, paste fill and rock fill which will be discussed below.

Hydraulic fill

Hydraulic fill is the product resulting from the partial dewatering and desliming of tailings and has less than 9% by weight of size fraction less than 10 μm, to ensure acceptable permeability of the fills. The pulp density is maintained at 50-70% solids by weight (Potvin et al. 2005). In other words, hydraulic fills have no clay fraction and can be seen as silty sand or sandy silts that are classified as SM or ML respectively (Qiu and Sego 2001; Rankine 2005). When served as an exposable backfill, binders such as cement, flyash, or crushed slag are added to produce cemented hydraulic fill. The production of hydraulic backfill is relatively simple and very low in cost. The main disadvantages of hydraulic

backfill are the management of water in the fill and at the retaining barricades. The barricades are supposed to be free draining and are made of special porous concrete. Draining pipes are placed through the barricades which are shotcreted. The fill placement rate and the control of slurry density have to be monitored to ensure that no excessive water ponding occurs in the stope to avoid the development of erosion piping and barricade failures.

Paste fill

Paste fill is a high density, non-segregating and low plastic mixture of mine tailings with negligible excess water when placed. It contains at least 15% by weight of size fraction less than 20 μm. The solids content of paste fill may vary from 75% to 85% by weight, with enough fines to inhibit particle settlement and segregation during pipeline transport. It contains significant clay fraction. In rheological terms, this slurry behaves as a non-Newtonian fluid. The rate of binder addition depends on the type of binder and use of the fill to act as bulk or exposable material. Compared to hydraulic fill, the main advantage of paste fill is the early removal of water from the tailings stream, which will eliminate the need for engineered barricades and the problem of drainage water. However, the operating cost of paste fill is higher due to the expensive filter dewatering systems and paste fill operations require supervision to ensure no line plugging occurs. In addition, a minimum of 1.5% by weight of binder content is required to eliminate the risk of liquefaction, which adds a significant operating cost to the paste.

Rock fill

Rock fill is a loosely dumped, granular fill with fiction angle of between 35^{o} and 55^{o}depending on the relative density of the fill. The fills can be waste rock, quarried rock, or aggregate. Rock fill can be placed into the stope as it is to serve as bulk backfilling material. The performance of rock fill can be improved by adding a hydraulic component (cement slurry or cemented tailings) to produce cemented rock fill, which may increase the strength and enable the fill to be exposed. The amount of binder can be optimized by selecting appropriate grading of rock fill, which can be produced with graded rock fill and deslimed tailings fill. Care should be taken during the fill placement due to the material's high tendency toward segregation.

2.2 Techniques used to investigate the arching mechanism on stress distribution

There are generally three major techniques that have been undertaken in the past to investigate the arching mechanism on stress distribution for backfill within vertical and inclined stopes; numerical modeling, analytical assessments and experimental/field measurement. A brief overview will be discussed in the following section.

2.2.1 Numerical modeling

As the mechanism of behaviour relating to mine geotechnical systems is complex, numerical computation appears to be a useful and reliable tool in predicting the stress-strain behaviour of backfill within a stope and the interaction between the fill and stope walls. Various influencing factors such as natural stress conditions, interface, excavation and backfilling sequence have been considered in the models (Aubertin et al. 2003; Barrett et al. 1978; Bloss et al. 1993; Caceres Doerner 2005; Li and Aubertin 2009; Li et al. 2003, 2007; Pakalnis et al. 1991; Pirapakaran and Sivakugan 2006, 2007a). Table 2.1 summarizes some of the numerical modeling programs that have been used in studying the stress developments and stability of mine stopes.

The results obtained from these studies reveal that stope geometry, fill properties (shear strength parameters, density, particle size distribution), and stope inclination are critical factors in predicting the stress distribution in mine stope (Caceres Doerner 2005; Li et al. 2007; Pirapakaran and Sivakugan 2006, 2007a). Observation of Fahey et al. (2009), Li and Aubertin (2009) and Li et al. (2007) also shows that Poisson's ratio and dilatancy angle may have significant effects on the stress distribution. They show that the dilatancy angle may directly affect the value of earth pressure coefficient, K which is the ratio of horizontal stress to vertical stress. On the other hand, the degree of arching is a function of stope geometry, wall roughness, fill properties, fill placement method and wall closure (the relative inward movement of stope walls) (DeSouza and Dirige 2002; Take and Valsangkar 2001).

Table 2.1. Numerical modeling programs used in the investigation of stress distribution and stability of mine stope

Program	Descriptions	References
TNJTEP and NONSAP	Two and three dimensional finite-element program; used to analyse the stress developments and stability of exposed vertical walls for cemented fill.	Barrett et al. 1978
TVIS	Three dimensional finite element program; used to assess the fill stability at Mount Isa mines.	Bloss et al. 1993
UTAH2	Two dimensional finite element program; used to investigate the interface between backfill and rock pillars.	Boldt et al. 1993
Phase^2	A finite element code from RocScience; used to simulate the stress developments for vertical stopes with converging walls; and the load transferred along the interface between rock mass and mine fill.	Aubertin et al. 2003
CeMinTaCo and Minefill-2D	One and two dimensional finite element program; used to study the barricade stresses and the development of effective stresses during fill curing	Fourie et al. 2007; Helinski 2007
PLAXIS	A finite element program; used to study the mechanisms of arching within backfilled stopes dealing with dry and saturated backfill.	Fahey et al. 2009
FLAC and FLAC^{3D}	Two and three dimensional finite difference program; used to analyse stresses generated when an open stope is filled and the stability when the fill is exposed.	Coulthard 1999; Pierce 2001; Sainsbury and Urie 2007
FLAC^{3D}	Used to investigate the arching mechanism in pastefill during a complete mining sequence.	Rankine 2004
FLAC and FLAC^{3D}	Used to investigate the arching effects within mine fill stopes by incorporating interface elements between rock and backfill.	Pierce 2001; Pirapakaran 2008; Pirapakaran and Sivakugan 2006
FLAC	Used to assess the stress stated in vertical and inclined backfilled stopes for a variety of conditions and parametric analyses.	Caceres Doerner 2005; Li and Aubertin 2009; Li et al. 2003, 2007
FLAC	Used to investigate the mechanism and behaviour related to backfill – rock mass interaction for an inclined stope.	Hassani et al. 2008

In his simulation of vertical stress distribution on inclined sillmat design, Caceres Doerner (2005) reports that the vertical stress decreases as the stope dip decreases (i.e., increases inclination from vertical), and the maximum stress tends to be located near the stope's footwall as shown in Figure 2.1.

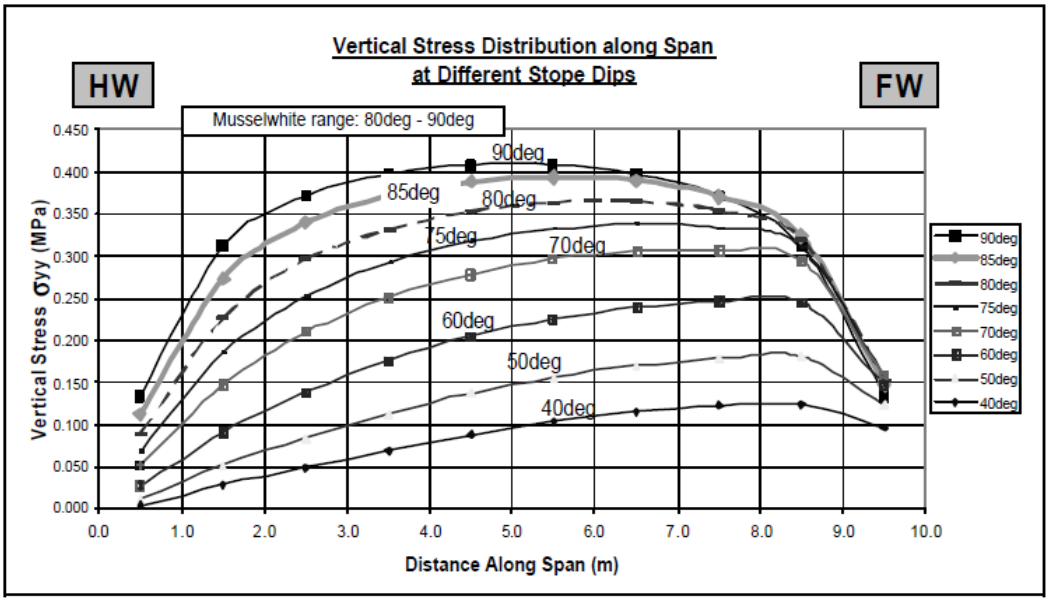

Figure 2.1. Vertical stress distribution along span at different stope dips (Caceres Doerner 2005)

Similar observation is reported by Li and Aubertin (2009) and Li et al. (2007) where they state that the stress distribution in an inclined stope is asymmetric (Fig. 2.2). Vertical normal stress along the hangingwall (HW) in the lower part of the stope is smaller than that along the footwall (FW), and the horizontal stress along the HW is higher than that on the FW. These results illustrate that the stress distribution across the span of an inclined stope is neither uniform nor symmetrical, and differs from the stress profiles of a vertical stope (see Fig. 1.2) where the stress profile is symmetrical about the vertical centreline.

Hassani et al. (2008) conducted a numerical modeling study of deep mining inclined stope to investigate the interaction between backfill and rock mass, considering a nonlinear behavior for both backfill and rock mass. They showed that stress distribution for an inclined stope (see Fig. 2.3) was very complex and the arching formation had a different scenario from that of vertical stope (see Fig.1.2). They observed that, in inclined stopes, arching occurred at about mid height of the stope and the stresses (both vertical and horizontal) dropped below the arch level as shown in Figure 2.4, whereas arching occurred at the top portion for a vertical stope and no subsequent changes in stress occurred.

Comparing Figs.2.2 and 2.3, the results obtained were very different. Li et al. (2007) assumed a linear elastic rock mass and the backfill was assumed to follow Mohr Coulomb failure criterion. On the other hand, Hassani et al. (2008) considered post-peak strain softening behavior for rock mass and post-peak strain hardening behavior for backfill with interface elements in between the host rock and backfill. Therefore, a more in-depth research of the constitutive model is required in this field.

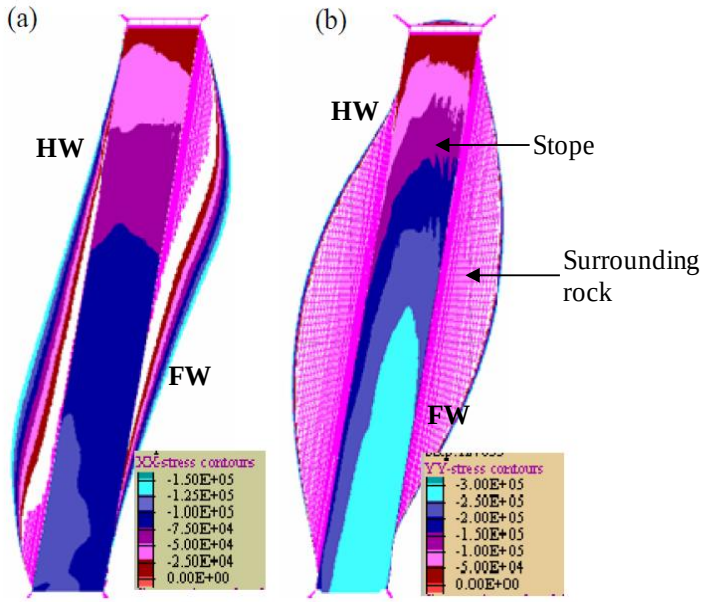

Figure 2.2. Numerical modeling results for (a) horizontal and (b) vertical stress distribution for inclined stope surrounded by rock mass (Li et al. 2007)

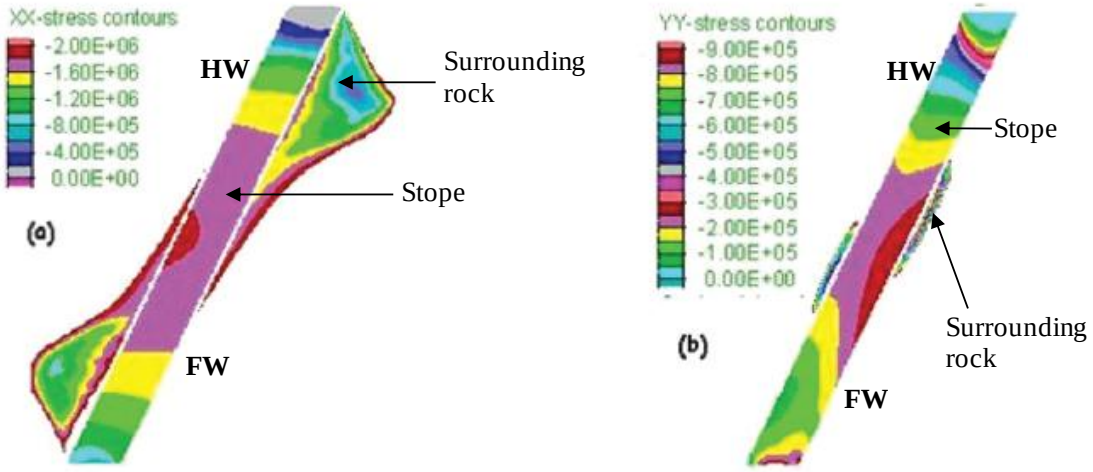

Figure 2.3. Contours of (a) horizontal stress, and (b) vertical stress distribution within the backfill in an inclined stope (Hassani et al. 2008)

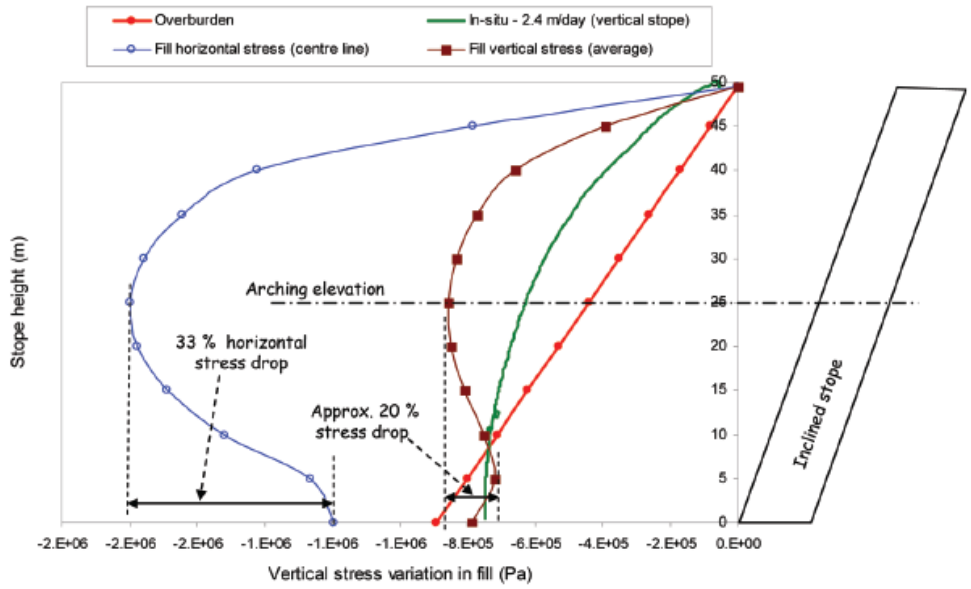

Figure 2.4. Vertical stress distribution within backfill showing the formation of arch (Hassani et al. 2008)

The observations of numerical modeling conducted by Caceres Doerner (2005), Hassani et al. (2008) and Li et al. (2007) for an inclined stope reveal that the stress profiles and arching formation within an inclined stope are different to that of a vertical stope. These results illustrate that the existing analytical expression and design approach for vertical stope may not be appropriate for an inclined stope, especially when there is significant tilt from vertical.

2.2.2 Analytical Derivations

Numerical analysis is not routinely used in practice, and simple analytical expressions remain the principal tool among practicing engineers. Depending on the confinement of surrounding boundaries and resulting arching action, theoretical derivations have been established for estimating vertical (σ_v) and horizontal (σ_h) stresses at any depth of a bin/silo structure or backfilled stope. In most cases, the expressions are developed based on shear plane method which involves the equilibrium of forces acting on a differential layer across the stope width. In these methods, the coefficient of lateral earth pressure, K is introduced as a critical input variable to relate the horizontal normal stress to vertical normal stress as:

$$\sigma_h = K\sigma_v \qquad (2.1)$$

There are limited analytical expressions available in the literature to determine the vertical stresses considering arching effect within vertical stopes (Aubertin et al. 2003; Caceres Doerner 2005; Li and Aubertin 2008; Li et al. 2005; Marston 1930; Pirapakaran and Sivakugan 2007a; Terzaghi 1943). Among these solutions, the expression of Marston (1930) appears to be the oldest and the simplest for determining the average stress variation with depth by considering arching effect. He developed an expression for vertical normal stress (σ_z) within a narrow trench backfilled with granular soil, based on 2-dimensional plane strain analysis. The derivation is fairly straightforward, where he considered the equilibrium of an infinitesimally thin horizontal slice shown in Figs. 2.5(a) and 2.5(b), and integrated across the fill depth. Terzaghi (1943) extended this expression to incorporate cohesion as:

$$\sigma_z = \frac{\gamma B - 2c}{2K\tan\delta}\left[1 - exp\left\{-\frac{2Kz\tan\delta}{B}\right\}\right] \tag{2.2}$$

where B = breadth of the trench, z = height of the fill, γ = unit weight of the fill, c = cohesion of the fill, δ = friction angle between the fill and the wall, K = lateral earth pressure coefficient, σ_x/σ_z at the wall, and σ_x = horizontal stress. The shear stress on the wall at depth z is $K\sigma_z \tan\delta$, as shown in Fig. 2.5.

Pirapakaran and Sivakugan (2007a) further extended the expression to a 3-dimensional cross section. For a stope with rectangular cross section in plan (Fig. 2.5(c)), Eq. 2.2 becomes:

$$\sigma_z = \frac{\gamma B - 2c}{2K\tan\delta}\left(\frac{L}{L+B}\right)\left[1 - exp\left\{-\frac{2Kz\tan\delta}{B}\left(\frac{L+B}{LB}\right)\right\}\right] \tag{2.3}$$

where L = length of the stope in plan. For $L>>B$, Eq. 2.3 becomes the same as Eq. 2.2. For square stope, Eq. 2.3 becomes:

$$\sigma_z = \frac{\gamma B - 2c}{4K\tan\delta}\left[1 - exp\left\{-\frac{4Kz\tan\delta}{B}\right\}\right] \tag{2.4}$$

By following the Marston's procedure, it can be shown that the expression for the circular stope or silo of diameter B (Fig. 2.5(d)) is the same as that of a square one.

A summary of analytical solutions developed to evaluate the vertical and horizontal stresses within minefill stope for vertical and inclined stopes are listed in Tables 2.2, 2.3 and 2.4. The common notation used in the tables to compute vertical stress σ_z and horizontal stress σ_x at depth z are: γ = unit weight of the fill, c = cohesion of the fill, ϕ = friction angle of the fill, δ = friction angle between the fill and wall, K = lateral stress ratio, B = breath of the stope,

H = height of the stope , L= length of the stope in plan and β = stope inclination to the horizontal.

As can be seen from the equations listed in the Tables 2.2, 2.3 and 2.4, most of the analytical expressions are developed based on uniformly distributed vertical stress across the span that varies with the depth of the stope. These equations differ mainly in the way K and δ are assumed whereas the fundamental equation is the same. Lateral stress ratio, K is developed as a function of friction angle of the fill, which subsequently gives a constant value of K throughout the fill body of the stope. The results of these settings provide a constant vertical and horizontal stresses across the span, which differ from the observations in numerical modeling. In numerical simulations, it is clearly shown that the stress profiles are not uniform across the span. This outcome suggests that analytical solution with non-uniformly distributed vertical stress across the span is more realistic and should be considered in the design. Li and Aubertin (2008) modified Eq. 2.7 by adding some coefficients of curvature to allow for a non-uniform vertical stress distribution across the span (Eq. 2.8). An improvement is obtained with this modified solution, where the vertical stresses along the wall and across the span compare well with the results from numerical modeling using FLAC (Li and Aubertin 2008).

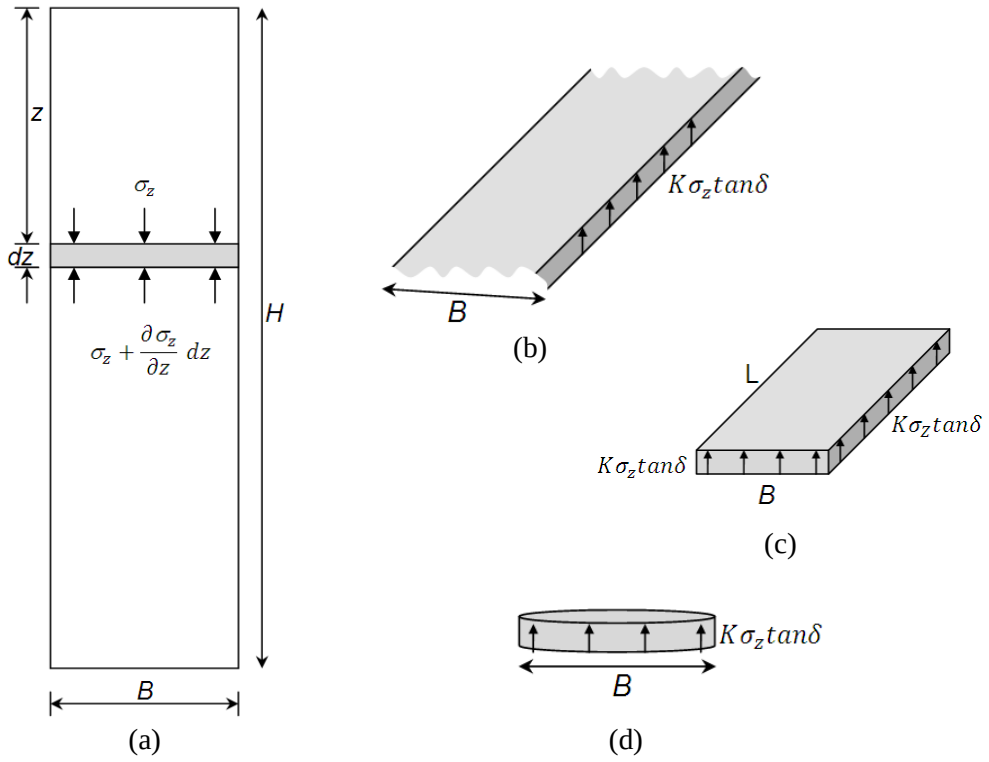

Figure 2.5. Equilibrium consideration of a thin horizontal layer within the granular material: (a) sectional elevation; (b) plane strain with $L = \infty$; (c) rectangular; (d) circular

Table 2.2. Analytical solutions developed to evaluate the vertical and horizontal stresses of mine fill for *2-D vertical stope*

Eq.	Analytical Expression
2.5	**Marston (1930):** $\sigma_z = \frac{\gamma B}{2K_a tan\delta}\left[1 - exp\left(-\frac{2K_a z\, tan\delta}{B}\right)\right]$ $\sigma_x = K_a\sigma_z$ $\delta = (0.33\phi \sim 0.67\phi)$ Applicable for cohesionless backfill
2.6	**Terzaghi (1943):** $\sigma_z = \frac{\gamma B - 2c}{2K\, tan\phi}\left[1 - exp\left(-\frac{2Kz\, tan\phi}{B}\right)\right] + q * \exp\left(-\frac{2Kz\, tan\phi}{B}\right)$ $\sigma_x = K\sigma_z$; q = surcharge at the top of the fill
2.7	**Aubertin et al. (2003):** $\sigma_z = \frac{\gamma B}{2K\, tan\phi'}\left[1 - exp\left(-\frac{2Kz\, tan\phi'}{B}\right)\right]$ $\sigma_x = K\sigma_z$ $K = \begin{cases} K_o = 1 - sin\phi' & (at\ rest\ condition) \\ K_p = \frac{1+sin\phi'}{1-sin\phi'} & (passive\ condition) \\ K_a = \frac{1-sin\phi'}{1+sin\phi'} & (active\ condition) \end{cases}$
2.8	**Li and Aubertin (2008):** Vertical stress across the width of the stope at distance *w*: $\sigma_{zw} = \frac{\gamma B}{2K\, tan\delta}\left[1 - exp\left(-\frac{2Kz\, tan\delta}{B\left(1-\frac{a}{2^s(s+1)}\right)}\right)\right]\left(1 - a\left(\frac{w}{B}\right)^s\right)$ where w = distance from the centre line, $w \leq B/2$ Horizontal stress: $\sigma_x = \frac{\gamma B}{2\, tan\delta}\left[1 - exp\left(-\frac{2Kz\, tan\delta}{B\left(1-\frac{a}{2^s(s+1)}\right)}\right)\right]$ $a = 2^{\left(1-\frac{1}{s}\right)} tan^{-2}(\phi_o + \phi);\quad \phi_o = 50^o,\ \lambda = 0.1,\ s = 3$ a, s, λ : control of the stress distribution curvature

Table 2.3. Analytical solutions developed to evaluate the vertical and horizontal stresses of mine fill for *3-D vertical stope*

Eq.	Analytical Expression

2.9 **Belem and Benzaazoua (2004) :**

Longitudinal pressure,

$$\sigma_x = \frac{\gamma H(H-z_o)}{3(B+L)}\left[1 - exp\left(-\frac{2(z-z_o)}{B}\right)\right]$$

Transverse pressure,

$$\sigma_y = \frac{0.185\,\gamma H(H-z_o)}{B+L}\left[1 - exp\left(-\frac{2(z-z_o)}{B}\right)\right]$$

Vertical pressure,

$$\sigma_z = \sigma_y \quad ; \quad z_o \le z \le H$$

z_o = considered elevation point: $z_o = 0$ at the floor or $z_o = H$ at the top of the stope

2.10 **Li et al. (2005) :**

The vertical stress acting across the horizontal plane at depth *z*:

$$\sigma_{vz} = \frac{\gamma - \left(\kappa_{13}B^{-1} + \kappa_{24}L^{-1}\right)}{\lambda_{13}B^{-1} + \lambda_{24}L^{-1}}\{1 - exp[-z(\lambda_{13}B^{-1} + \lambda_{24}L^{-1})]\}$$

The horizontal stress at depth z at wall *i*

$$\sigma_{hzi} = K_i\sigma_{vz} + 2c\,tan\,\alpha_i$$

where $\lambda_{13} = K_1 tan\delta_1 + K_3 tan\delta_3$; $\lambda_{24} = K_2 tan\delta_2 + K_4 tan\delta_4$

$\kappa_{13} = c_1 + c_3 + 2c(tan\alpha_1 tan\delta_1 + tan\alpha_3 tan\delta_3)$

$\kappa_{24} = c_2 + c_4 + 2c(tan\alpha_2 tan\delta_2 + tan\alpha_4 tan\delta_4)$

K_i, δ_i, c_i = lateral stress ratio, friction angle and cohesion at fill-wall interface *i*

$\alpha_i = 0^o$ for at rest state; (ϕ/2-45^o) for active state; (45^o+ϕ/2) for passive state

(*i* = 1 to 4 in which 1 for left wall, 2 for front wall, 3 for right wall and 4 for back wall)

2.11 **Pirapakaran and Sivakugan (2007a):**

$$\sigma_z = \frac{\gamma B - 2c}{2K\,tan\delta}\left(\frac{L}{L+B}\right)\left[1 - exp\left(-2\left(\frac{L+B}{LB}\right)Kz\,tan\delta\right)\right]$$

$\sigma_x = K\sigma_z$

$\delta = 0.67\,\phi$ and $K = K_o$

Table 2.4. Analytical solutions developed to evaluate the vertical stress of mine fill for *2-D Inclined stope*

Eq.	Analytical Expression
2.12	**Caceres Doerner (2005):** $\sigma_z = \left(\frac{\gamma B}{2K\tan\phi}\right) sin^2\beta \left[1 - exp\left(-\frac{2Kz\tan\phi}{Bsin^2\beta}\right)\right]$ $K=1.4\ sin^2\phi - 2\ sin\ \phi\ + 1$ Applicable for cohesionless backfill with ϕ ranging from 0^0 to 40^0
2.13	**Singh (2009) & Singh et al. (2011):** $\sigma_v = \frac{\gamma\delta B\ sin^2\beta\ cosec\ \delta}{2(sin^2\delta + Kcos^2\delta)tan\delta}\left[1 - exp\left(-\frac{8(sin^2\delta + Kcos^2\delta)tan\delta\ sin\delta}{B[2(1+K)\delta - (1-K)sin2\delta\ cos2\beta]sin^3\beta} z\right)\right]$

Most of the present studies on inclined stopes are based on numerical simulation and there are very limited analytical studies on inclined stopes. Caceras Doerner (2005) modified Marston's (1930) equation for inclined stope (Eq. 2.12) with lateral stress ratio, *K* estimated by analyzing the data from numerical simulation. Singh (2009) and Singh et al. (2011) developed an analytical equation (Eq. 2.13) for inclined stope based on Handy's (1985) approach, where a circular arch of principal stresses has been used to estimate the vertical stresses within an inclined stope. A method to estimate vertical stress distribution across the width of stope is also introduced in his PhD dissertation.

Lateral stress ratio or lateral earth pressure coefficient, *K* appears to be an important parameter for analytical solution in evaluating stress distribution. Since the development of Janssen's (1895) theory, several semi-empirical and analytical expressions have been proposed for estimating lateral pressure coefficient (Marston 1930; Terzaghi 1943). Marston (1930) takes *K* as K_a, whereas Li and Aubertin (2008) compare K_o, K_a and K_p in their numerical modeling and conclude that K_a is more appropriate to describe the stress state within backfill, where K_o, K_a and K_p are defined as follows:

$$K_o = 1 - sin\phi \tag{2.14}$$

where K_o is the earth pressure coefficient at rest.

$$K_a = \frac{1-sin\phi}{1+sin\phi} \tag{2.15}$$

where K_a is the Rankine's active earth pressure coefficient.

$$K_p = \frac{1+sin\phi}{1-sin\phi} \quad (2.16)$$

where K_p is the Rankine's passive earth pressure coefficient

Terzaghi (1943) assumed an empirical constant K at every point of the fill. From experimental investigations, he showed that the value of K for sand could be increased from 1 to a maximum of 1.5. Krynine (1945) showed that, with wall roughness, the rotation of principal stresses gives horizontal wall pressure, σ_h instead of σ_3. Therefore, the principle stress ratio, K is no more equal to σ_3/σ_1 when there is wall friction ($\tau \neq 0$) involved. He proposed

$$K = \frac{\sigma_h}{\sigma_v} = \frac{1-sin^2\phi}{1+sin^2\phi} \quad (2.17)$$

Handy (1985) defined a continuous compression arch for σ_3 for a partially supported soil in a state of plastic equilibrium where the slip is allowed to occur along directions defined by the slip lines. From there, Handy derived an expression for K and the stress distribution for backfills contained within two parallel, unyielding, rough vertical walls retaining granular fill, where

$$K = \frac{\sigma_h}{\sigma_v} = \frac{cos^2\theta + K_a sin^2\theta}{sin^2\theta + K_a cos^2\theta} \quad (2.18)$$

and θ is the angle of minor stress plane with respect to the horizontal at the wall.

Handy's approach remains a popular analytical technique in developing analytical solutions for lateral stress ratio and stress distribution when wall roughness and arching action are involved. It has been used by Dalvi and Pise (2008), Goel and Patra (2008) and Paik and Salgado (2003) in deriving the active lateral stress ratio at the wall, K_{wall} for a horizontally translating rigid vertical retaining wall.

For vertical stope, as very little lateral deformation of stope wall may occur, at-rest condition may be appropriate to consider in stress analysis. However, for an inclined stope, dipping hangingwall and footwall may induce additional stresses to backfill or to footwall under gravity or wall convergence, which may change the state of stress within the backfill. Caceres Doerner (2005) derived an empirical equation for K using numerical analysis, where

$$K=1.4\ sin^2\phi - 2\ sin\phi + 1\ ;\ \text{where } 0^o < \phi < 40^o\ . \quad (2.19)$$

However, this equation is developed solely based on friction angle of fill mass, and K is assumed to be constant throughout the fill body without taking into consideration the effects of stope inclination and interfacial friction angle. Therefore, a better understanding of K can be obtained by considering the effect of stope inclination and interface behaviour in order to produce a more effective design criterion.

The interface friction angle δ, is used to describe the shear resistance along the wall-fill interface. The rough wall surface of mine stope enables arching to take place at a few grains away from the wall. Therefore δ should be taken as friction angle, ϕ when dealing with stress distribution within a mine stope. In most cases listed in Tables 2.2, 2.3 and 2.4, δ is taken as ϕ. As the stiffness of the rock is about two orders of magnitude larger than the backfill material, the wall movement is expected to be small. With loose backfill, where $c = 0$, Pirapakaran and Sivakugan (2007a) have shown that a combination of $\delta = 2/3$ of ϕ and $K = K_o$ gives a reasonable estimation of the vertical stress when compared with the results from a numerical model of a mine stope. This result reveals that the combination of different values of K and δ may have a significant effect on stress distribution as well as interface shear behaviour within a mine stope.

2.2.3 Experimental and in-situ fill measurements

Due to the difficulties in conducting in-situ tests within a mine, field records related to stress measurements demonstrating arching effect are very rare. The observation of Zahary et al. (1972) (vide Dhar et al. 1983) on fill measurement reported a 2% average strain in the fill at the end of two year period and an increase of wall convergence with width of the stope. Udd and Annor (1993) confirmed the occurrence of arching action in their monitoring of in-situ backfill behavior. Based on Cayeli mine in-situ pressure monitoring test results, Yumlu (2007) concluded that staged filling will result in lower bulkhead pressure. The rest time stage between enables water pressure dissipation and enhances distribution of ongoing fill weight to the walls due to arching.

Take and Valsangkar (2001) conducted centrifuge modeling of a narrow retaining wall supporting a granular fill bounded by vertical plane with dissimilar frictional characteristics. The results show that the governing factors for arching behavior are the geometry of model, interface friction angle and the coefficient of lateral earth pressure. The results also reveal that a reasonable estimate of lateral earth pressure can be obtained with an average interface friction angle. DeSouza and Dirige (2002) reported, in their centrifuge tests on sillmat behavior during undercut mining, that the degree of arching is a function of stope geometry,

wall roughness, fill cohesion, and wall closure. Udd and Annor (1993) conducted a centrifuge modeling for situations where a free-standing wall of fill was to be exposed. The results reveal that a free-standing inclined-fill wall is three times more stable than vertical-fill wall, showing that significant operating cost can be reduced when dealing with inclined stopes. Similar observations are reported by Mitchell (1989) that the fill confined between sloped walls is much more stable than fill between vertical rock walls.

Laboratory work associated with arching action within a vertical hydraulic fill mine stope had been conducted by Pirapakaran and Sivakugan (2006, 2007b). A simple 1:100 scaled laboratory model as shown in Fig 2.6 was developed at James Cook University to investigate the stress development and to quantify arching effects within the fill in a vertical stope. Significant reduction of vertical stress was observed compared to that of overburden pressure, showing that arching took place in the model. The model successfully simulates the filling process within a vertical mine stope and serves as a useful tool in validating the solutions obtained from analytical and numerical modeling work.

Many experimental studies have been carried out in investigating the influence of aspect ratio of stope geometry on stress distribution and arching mechanism. Terzaghi (1943), in his trap door experimental model, shows that the stress state of fill remains the same when the door is lowered more than 2.5 times of the span width. McNulty (1965) also concludes that the height, H to width, B ratio of model has a significant influence on the load distribution. Observation of Cowing (1977) (vide Li et al. 2003) suggests that when H is greater than (2-3)B, pressure near the stope bottom is almost independent of the fill depth. Similar conclusion is drawn by Pirapakaran (2008) that the increment of vertical stress within a stope is insignificant when H/B is greater than 5. In terms of length, L to width, B ratio, Pirapakaran (2008), in his numerical modeling analysis, also shows that arching effect is reduced with the increase of L/B and remain approximately constant when L/B is greater than 5. Thus, any geometry with $L/B \geq 5$ and $H/B > 5$ is suitable to model the plane strain condition and to study arching effect within a stope.

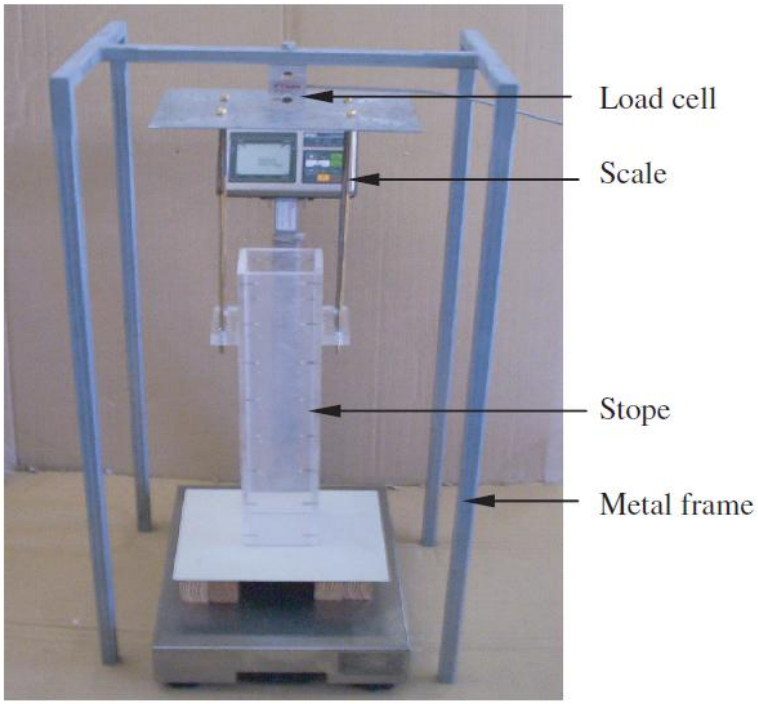

Figure 2.6. Apparatus to measure arching within minefills (Pirapakaran and Sivakugan 2006)

2.3 Summary and conclusion

A review of literature on techniques used to investigate the arching mechanism on stress distribution has been conducted, which includes analytical, numerical and laboratory/field modeling. Most of these researches are conducted with reference to vertical stope and there is limited research carried out for inclined stope. The current design approach for an inclined stope is based on the results obtained from vertical stope (allowing for some minor errors).

Backfilling is becoming increasingly important in underground mining operations for safety considerations. As mines get deeper, the need for improved precision on ground stability control and maximum resources recovery become more important for safe and economic mine operations. However, there is no universally recognized standard design practice in solving these problems. Generally, the mine operators have their unique set of engineering solutions to deal with ground stability and mine tailing disposal issues. A better understanding of the stress distribution within the minefill and a rational methodology to account for stope inclination with due consideration to arching will significantly improve the current state-of-the-art and design practices.

Chapter 3 Extension of Marston's Theory

3.1 General

Determination of the stress distribution, giving due consideration to the arching mechanism within minefill stopes, is of great importance because of its influence on the ground stability, ore recovery and cost effectiveness.

Simple analytical expression is very useful for the preliminary design and remains the principal tool among practicing engineers. Depending on the confinement of surrounding boundaries and the resulting arching action, some theoretical formulations have been developed for estimating vertical (σ_z) and horizontal (σ_x) stresses at any depth of a bin/silo structure or backfilled stope (Aubertin et al. 2003; Handy 1985; Li et al. 2003; Marston 1930; Marston and Anderson 1913; Pirapakaran and Sivakugan 2007a; Shukla et al. 2009a; Sperl 2005; Terzaghi 1943).

Most of these studies on the stress determination have been applied to vertical stopes, and there is a lack of research, especially analytical work, on inclined stopes. This chapter discusses the development of an analytical expression for calculating the stress distribution within an inclined backfilled stope, considering the arching effect along the interface between the rock wall and the fill. To validate the analysis, the proposed results are compared with existing solutions reported in the literature listed below.

Caceres Doerner (2005) developed an analytical equation (Eq. 2.12) for an inclined stope based on the shear plane method which involved the equilibrium of forces acting on a differential element across the span width. Instead of using the conventional *Jaky* earth pressure coefficient, K_o and *Rankine* earth pressure coefficients, K_a *and* K_p, he developed an empirical equation for K using data from numerical modeling.

$$\sigma_z(z) = \left(\frac{\gamma B}{2K tan\phi}\right) sin^2\beta \left[1 - \exp\left(-\frac{2Kz\, tan\phi}{B\, sin^2\beta}\right)\right] \qquad (2.12)$$

where $K = 1.4 \sin^2\phi - 2\sin\phi + 1$ and $0 \leq \phi \leq 40^o$.

Figure 3.1 shows the comparison of lateral stress ratio, K at different friction angles ϕ, for the cases of K_o, K_p, K_a and K determined by Caceres Doerner (2005). The value of K obtained by Caceres Doerner (2005) is consistent with K_a, until $\phi = 30^o$ and then becomes effectively constant as ϕ increase from 30^o to 40^o, which falls between K_o and K_a.

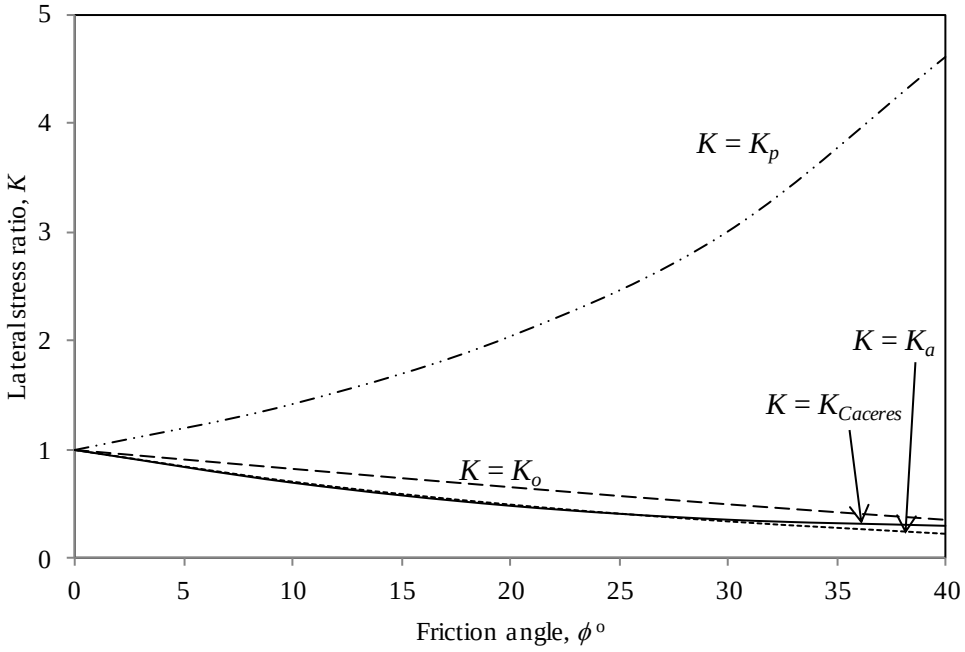

Figure 3.1. Comparison of lateral stress ratio, K at different friction angle, ϕ

Li and Aubertin (2009) developed a numerical model using FLAC without using interface elements between fill and rock mass. The backfill was assumed to follow the Mohr Coulomb failure criterion, surrounded by linear elastic rock mass. A multistep filling sequence was considered in the simulation. The results obtained were validated by Marston type equations and an experimental model (Li and Aubertin 2009).

3.2 Analytical expression for vertical stress within an inclined mine stope with parallel walls

The analytical formulation proposed herein is an extension of the classical arching theories proposed by Janssen (1895)(vide Sperl 2005), Marston (1930), Marston and Anderson (1913) and Terzaghi (1943) that consider a non-vertical or inclined wall in the trench situations, generally found in underground mines. The following assumptions are made in the analysis:

- The backfill is bounded between two parallel inclined walls,
- A two dimensional plane strain condition is assumed,
- The vertical normal stresses are uniformly distributed laterally at any depth, and
- The shear stresses along the interfaces of the backfill to hangingwall and footwall are considered the same at any depth.

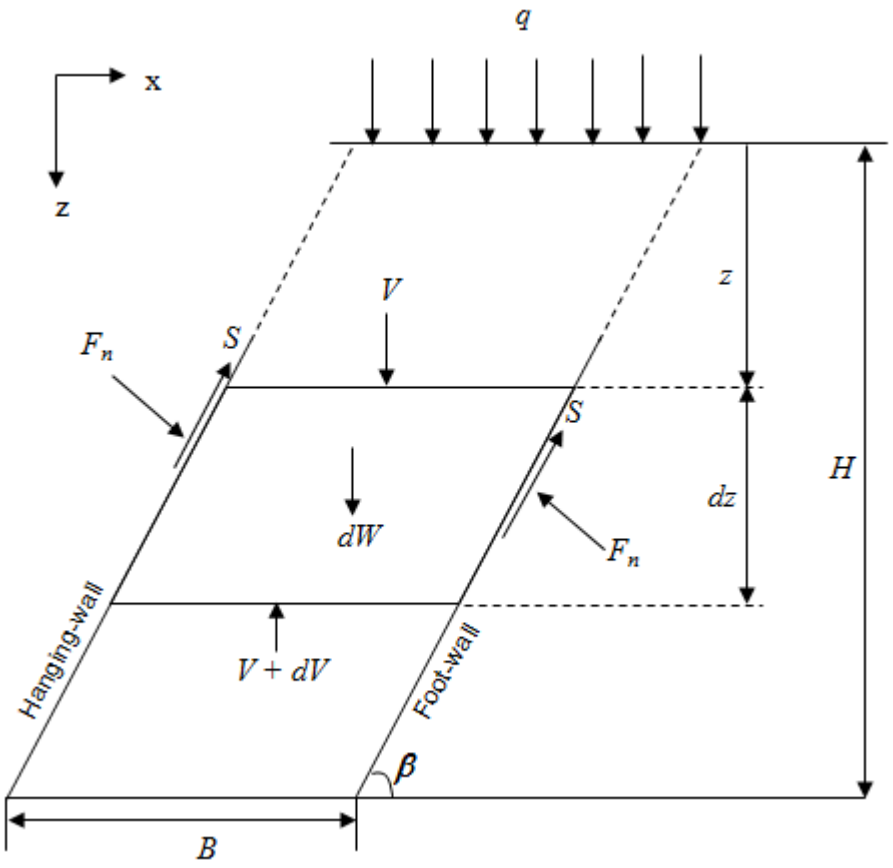

Figure 3.2. Schematic diagram of an inclined stope

Figure 3.2 shows a schematic diagram of a two-dimensional inclined backfilled stope of height *H* and width *B*, inclined at an angle, β to the horizontal. *V* is the vertical force acting on a horizontal element of thickness *dz* at a depth *z* below the top surface of the stope. For clarity, the thickness of the element "*dz"* is exaggerated. The forces are considered per unit length of the stope. Based on this diagram, a general plane strain equation as described below can be developed.

Self weight of the element is given by:

$$dW = \gamma B dz \tag{3.1}$$

Vertical force *V* acting on the layer at depth *z* is:

$$V = \sigma_z B \tag{3.2}$$

where σ_z is the vertical stress at depth z.

Vertical force acting upward at the bottom of the element at position $z + dz$ is:

$$V + dV = (\sigma_z + d\sigma_z)B \tag{3.3}$$

Shear force acting at the backfill-rock interface at depth z is:

$$S = \tau dz/sin\beta \tag{3.4}$$

where τ is the shear stress along the wall at depth z.

The maximum shear stress (τ) mobilized at the backfill-rock interface can be determined using the Mohr-Coulomb strength criterion as:

$$\tau = c + \sigma_n tan\delta \tag{3.5}$$

where c is the cohesion of the backfill, σ_n is the normal stress acting on the plane and δ is the interface friction angle.

Using the stress transformation concept commonly used in engineering mechanics (Das 1998), the normal stress on a plane can be found as

$$\sigma_n = \frac{\sigma_z+\sigma_x}{2} + \frac{\sigma_z-\sigma_x}{2} cos2\beta + \tau_{xz} sin2\beta \tag{3.6}$$

where σ_z, σ_x and τ_{zx} are the vertical, horizontal and shear stresses respectively. The relationship between the vertical and the horizontal stresses can be expressed as

$$\sigma_x = K\sigma_z \tag{3.7}$$

where K is the lateral pressure coefficient or the ratio of horizontal stress to vertical stress. Substituting Eq. 3.7 and Eq. 3.5 into Eq. 3.6 gives

$$\sigma_n = \sigma_z \left(\frac{1+K}{2} + \frac{1-K}{2} cos2\beta + Ktan\delta\ sin2\beta\right) + c\ sin2\beta \tag{3.8}$$

Let

$$K' = \frac{1+K}{2} + \frac{1-K}{2} cos2\beta + Ktan\delta\ sin2\beta \tag{3.9}$$

Substituting Eqs. 3.8 and 3.9 into Eq. 3.5 gives

$$\tau = \xi + K'\sigma_z \tan\delta \tag{3.10}$$

where

$$\xi = c(1 + \sin 2\beta \tan \delta) \tag{3.11}$$

The equilibrium of vertical forces acting on the element leads to

$$V + dV - V - dW + 2S\ sin\beta = 0$$

$$dV - dW + 2S\ sin\beta = 0 \tag{3.12}$$

Substituting Eqs. 3.1, 3.2, 3.4 and 3.10 into Eq. 3.12 gives

$$d\sigma_z B - \gamma B dz + 2(\xi + K'\sigma_z \tan\delta)dz = 0$$

$$d\sigma_z = \left(\gamma - \frac{2\xi}{B} - \frac{2K\prime\sigma_z tan\delta}{B}\right) dz$$

$$d\sigma_z = (P - Q\sigma_z)dz \tag{3.13}$$

where

$$P = \gamma - \frac{2\xi}{B} \tag{3.14a}$$

$$Q = \frac{2K\prime tan\delta}{B} \tag{3.14b}$$

At z = *0*, $\sigma_z = q$, Eq. 3.13 can be solved as

$$\int_q^{\sigma_z} \frac{d\sigma_z}{P - Q\sigma_z} = \int_0^z dz$$

$$\therefore \quad \sigma_z = \frac{P}{Q}(1 - e^{-Qz}) + qe^{-Qz}$$

which on substitution from Eq. 3.14 becomes

$$\sigma_z = \frac{\gamma B - 2\xi}{2K\prime tan\delta}\left(1 - e^{-\frac{2K\prime tan\delta}{B}z}\right) + qe^{-\frac{2K\prime tan\delta}{B}z} \tag{3.15}$$

where $(\gamma B - 2\xi) \geq 0$.

In non-dimensional form, Eq.3.15 can be expressed as:

$$\frac{\sigma_z}{\gamma B} = \frac{1 - 2\xi/\gamma B}{2K\prime tan\delta}\left(1 - e^{-2K\prime\frac{z}{B}tan\delta}\right) + \frac{q}{\gamma B}e^{-2K\prime\frac{z}{B}tan\delta} \tag{3.16}$$

The general expression for the vertical stress at any depth is given in Eq. 3.16. This equation can be further simplified as shown in Table 3.1 to address the special field situations as governed by the following criteria:

- For vertical stope, $\beta = 90^o$;
- In the absence of surcharge, $q = 0$; and
- For cohesionless soil, $c = 0$.

Table 3.1. Special cases of Eq. 3.16 for different field situations in terms of specific values of β, q and c; K' for cases 5,6 and 7 is given by Eq. 3.9

No	β^o	q	c	Expression	Eq.
1	90	0	0	$\frac{\sigma_z}{\gamma B} = \frac{1}{2K tan\delta}\left(1 - e^{-2K\frac{z}{B}tan\delta}\right)$	(3.17)
2	90	0	> 0	$\frac{\sigma_z}{\gamma B} = \frac{1-2c/\gamma B}{2K tan\delta}\left(1 - e^{-2K\frac{z}{B}tan\delta}\right)$	(3.18)
3	90	> 0	0	$\frac{\sigma_z}{\gamma B} = \frac{1}{2K tan\delta}\left(1 - e^{-2K\frac{z}{B}tan\delta}\right) + \frac{q}{\gamma B}e^{-2K\frac{z}{B}tan\delta}$	(3.19)
4	90	> 0	> 0	$\frac{\sigma_z}{\gamma B} = \frac{1-2c/\gamma B}{2K tan\delta}\left(1 - e^{-2K\frac{z}{B}tan\delta}\right) + \frac{q}{\gamma B}e^{-2K\frac{z}{B}tan\delta}$	(3.20)
5	< 90	0	0	$\frac{\sigma_z}{\gamma B} = \frac{1}{2K' tan\delta}\left(1 - e^{-2K'\frac{z}{B}tan\delta}\right)$	(3.21)
6	< 90	0	> 0	$\frac{\sigma_z}{\gamma B} = \frac{1-2\xi/\gamma B}{2K' tan\delta}\left(1 - e^{-2K'\frac{z}{B}tan\delta}\right)$	(3.22)
7	< 90	> 0	0	$\frac{\sigma_z}{\gamma B} = \frac{1}{2K' tan\delta}\left(1 - e^{-2K'\frac{z}{B}tan\delta}\right) + \frac{q}{\gamma B}e^{-2K'\frac{z}{B}tan\delta}$	(3.23)

Equation 3.17 in Table 3.1 is the same as the equation developed by Marston and Anderson (1913) and Aubertin et al. (2003), and Eqs. 3.18 and 3.20 are similar to the equations presented by Terzaghi (1943) in the absence of surcharge and when q is not equal to zero, respectively.

Figure 3.3 shows a comparison of vertical stress along the centreline using different K values (K_o, K_a and K_p as defined in Chapter 2) in the expression with $\delta = \frac{2}{3}\phi$ against the relevant solutions from the literature. The results shown here agree well with the observation

of Pirapakaran and Sivakugan (2007a) where the combination of $\delta = \frac{2}{3}\phi$ and $K = K_o$ is appropriate in estimating the vertical stress. In addition, considering that the wall is not yielding, it is reasonable to assume the backfill is at rest and hence $K = K_o$ is a realistic assumption. $K = K_p$ grossly underestimates the vertical stress, and $K = K_a$ overestimates the vertical stress. In design of retaining walls and piles, it is common to assume $\delta = \frac{2}{3}\phi$ at the soil-concrete interface. Therefore, $\delta = \frac{2}{3}\phi$ appears to be a realistic assumption. For these reasons, $K = K_o$ and $\delta = \frac{2}{3}\phi$ have been adopted for presenting specific results and discussion in the following section.

3.2.1 Comparison of results with solutions from literature

The solutions obtained from the proposed analytical expression Eq. 3.21, where $c = 0$ and $q = 0$, have been compared with the numerical results obtained by Li and Aubertin (2009) and the analytical equation proposed by Caceres Doerner (2005) for an inclined stope.

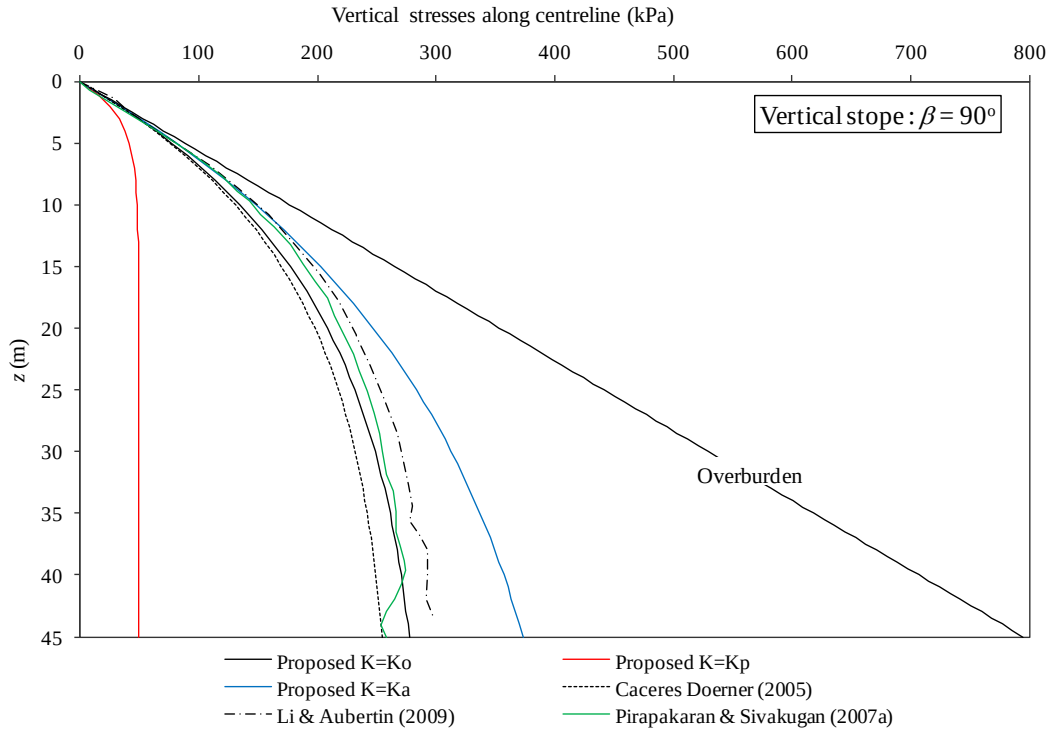

Figure 3.3. Comparison of vertical stresses along centreline of the stope ($B = 6$ m, $H = 45$ m, $\gamma = 18$ kN/m^3, $c = 0$, $\phi = 30^o$, $\delta = \frac{2}{3}\phi$, $q = 0$, $\beta = 90^o$)

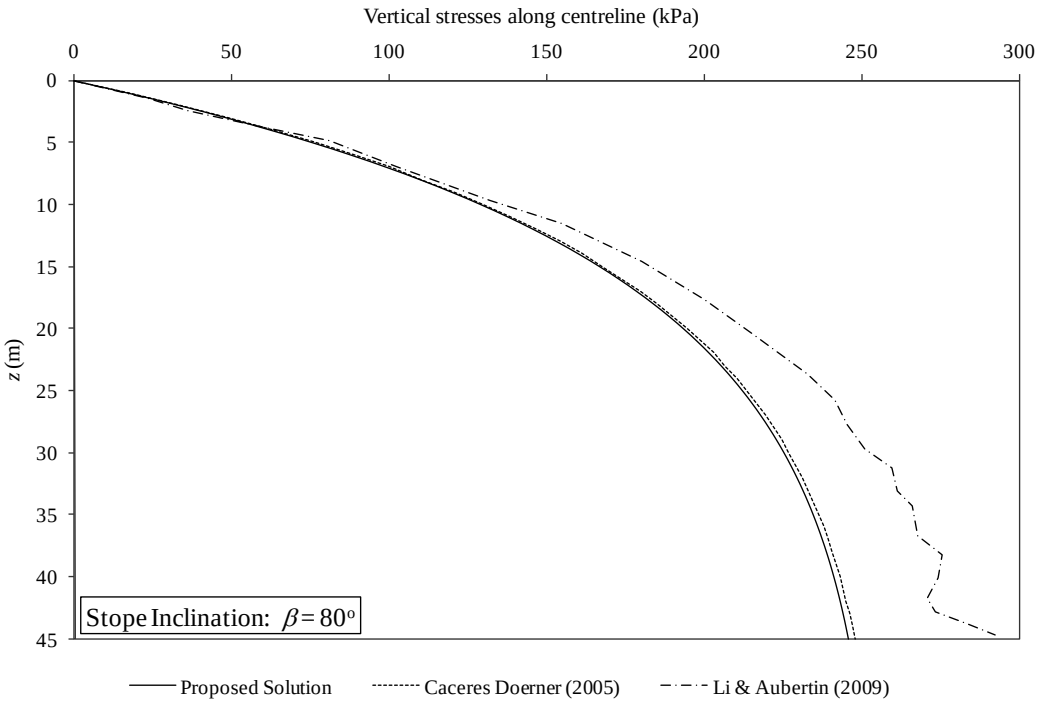

Figure 3.4. Comparison of vertical stresses along centreline of the stope *(B = 6 m, H = 45 m, γ =18 kN/m^3 , c = 0, ϕ = 30^o, δ = ⅔ϕ, q = 0, β = 80^o)*

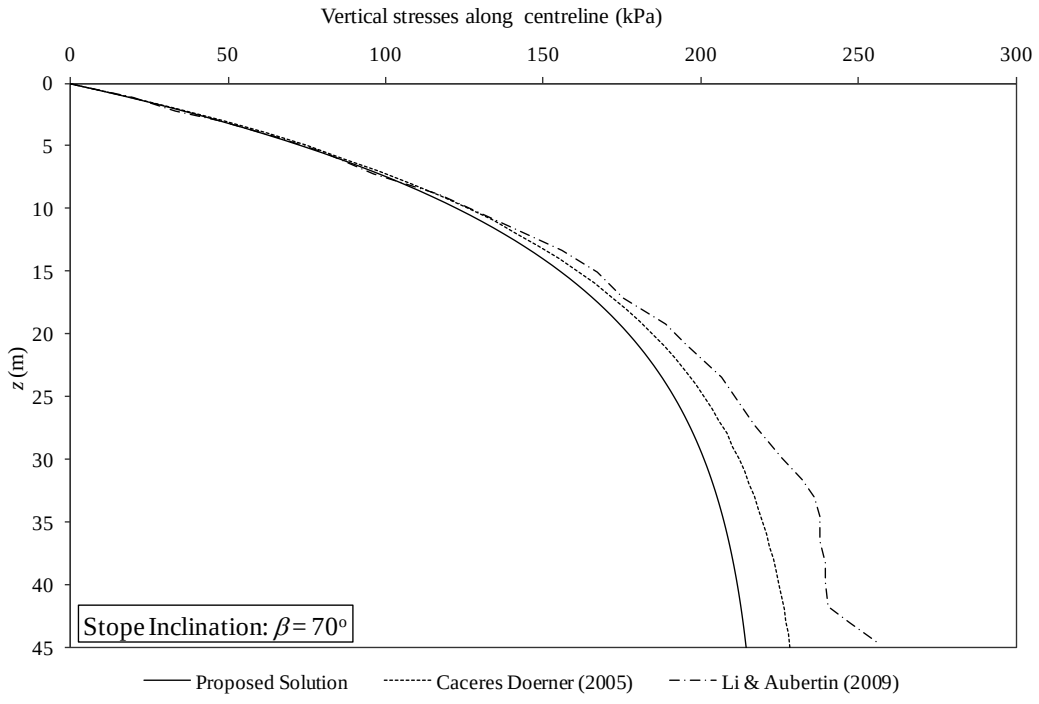

Figure 3.5. Comparison of vertical stresses along centre line of the stope *(B = 6 m, H = 45 m, γ = 18 kN/m^3 , c = 0, ϕ = 30^o, δ = ⅔ϕ, q = 0, β = 70^o)*

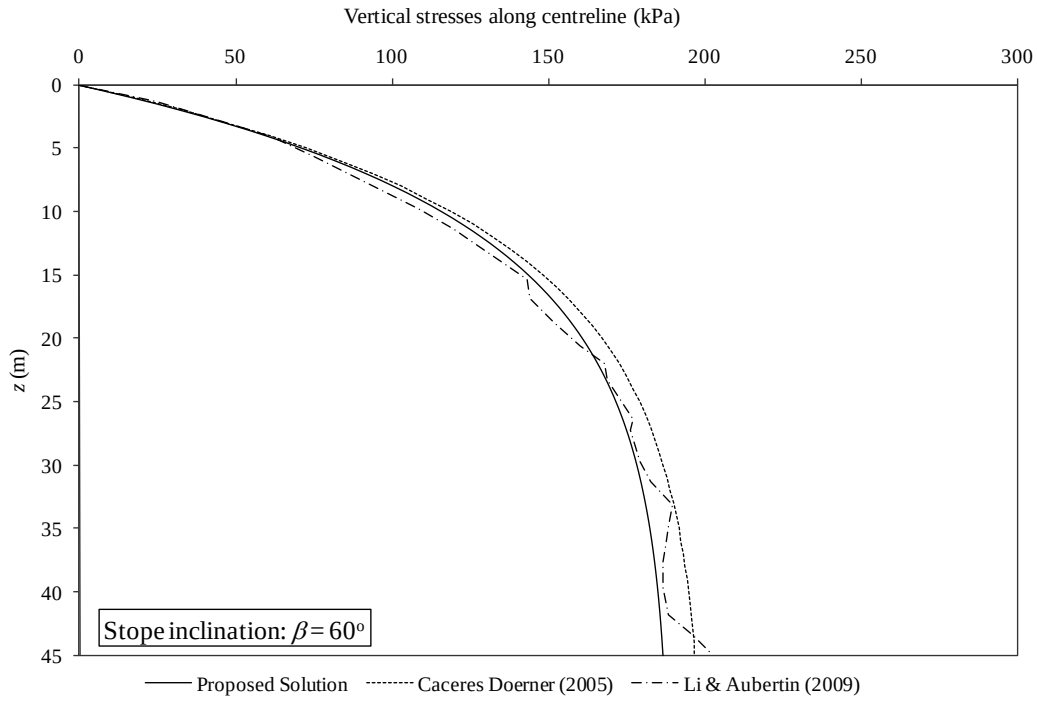

Figure 3.6. Comparison of vertical stresses along centreline of the stope *(B = 6 m, H = 45 m, $\gamma = 18$ kN/m^3 , c = 0, $\phi = 30^o$, $\delta = \frac{2}{3}\phi$, q = 0, $\beta = 60^o$)*

Figures. 3.3 to 3.6 show the comparison of vertical stresses along the centreline among the proposed solutions, Li and Aubertin's (2009) numerical results, and Caceres Doerner's (2005) analytical solutions for stope inclinations of 90°, 80°, 70° and 60° respectively. Overall, the proposed analytical solution gives lower values than the vertical stresses obtained from Li and Aubertin's (2009) numerical solution and a close agreement with Caceres Doerner (2005) for all three values of β. A close match of the results is observed among all three at $\beta = 60^o$.

3.2.2 Parametric studies

Now that the proposed solution with $\delta = \frac{2}{3}\phi$ and $K = K_o$ has been validated against two other independent methods, it is used in this section to carry out a parametric study on the effects of:

(a) Stope inclination,
(b) Aspect ratio (height : width), and
(c) Fill properties.

The parameters used are stated below each graph.

Effects of Stope Inclination

Figure 3.7 shows the vertical stresses estimated from the proposed analytical solution for narrow stopes with inclination from 60^o to 90^o, to the horizontal. By comparing the estimated vertical stresses with the overburden pressure, significant reductions of about 65-70% of vertical stresses are observed toward the base of the stope. This shows that arching is taking place in transferring most of the overburden pressure to the walls in the form of shear stresses. In addition, it is clearly seen that vertical stress decreases with the increase in stope inclination. Vertical stresses reduce about 20% for $\beta = 70^o$ and 30% for $\beta = 60^o$ when compared to the case of vertical stope. Jahns and Brauner (vide Robertson et al. 1986) stated that when the inclination was less than 30^o to vertical, the error in vertical stress due to stope inclination was less than 10%. They may have underestimated the influence of stope inclination on stress distribution especially for a narrow stope. The possible reason for this stress reduction may due to the effect of stope inclination which induces part of the overburden pressure being transferred directly to the footwall under gravity.

Effects of Aspect Ratio

The effect of aspect ratio (height to width ratio) is examined by keeping the height of stope, H constant at 45 m and varying the width of stope, B from 4.5 m to 22.5 m. Fig. 3.8 shows the effect of arching with respect to different stope geometries for cases where $\beta = 70^o$. The effect of arching is more significant in the case of narrow stopes with higher aspect ratio. Besides, at any depth where z is greater than $5B$, the vertical stresses remain approximately constant down to the base of the stope. In other words, the pressure exerted at the bottom of the stope is almost independent of the fill depth when $H > 5B$. This depth will be slightly different for the other values of β.

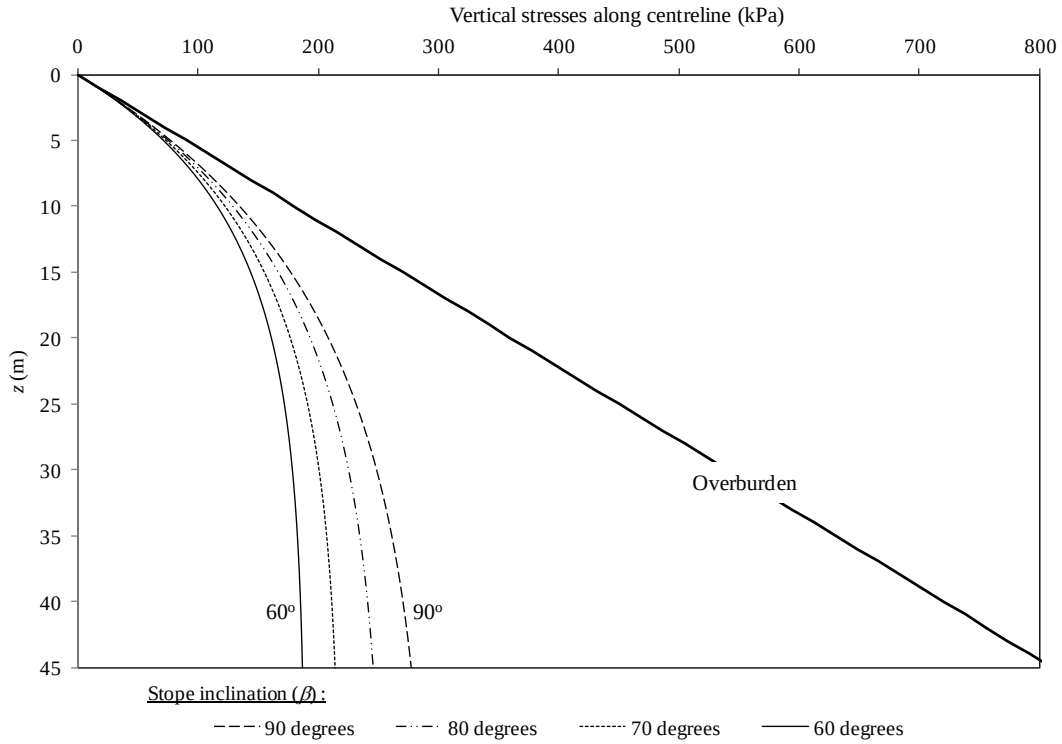

Figure 3.7. Comparison of vertical stresses along centreline for different stope inclinations *(B = 6 m, H = 45 m, $\gamma = 18$ kN/m^3 , c = 0, $\phi = 30^o$, $\delta = \frac{2}{3}\phi$, q =0)*

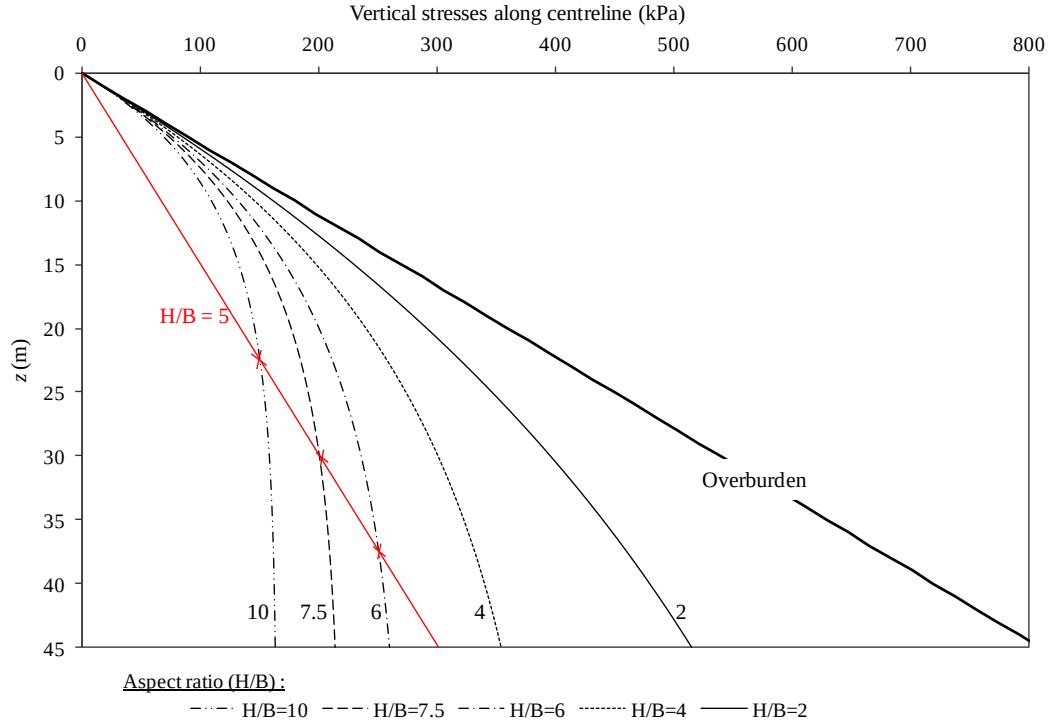

Figure 3.8. Comparison of vertical stresses along centreline for different aspect ratios *(H = 45 m, $\gamma = 18$ kN/m^3 , c = 0, $\phi = 30^o$, $\delta = \frac{2}{3}\phi$, q = 0^o, $\beta = 70^o$)*

Effects of Fill Properties

The effects of friction angle, ϕ, and cohesion, c, of the backfill on vertical stress distribution are shown in Figs. 3.9 and 3.10, respectively. The results obtained are compared with Li and Aubertin's (2009) numerical results. For the comparison of friction angle (see Fig. 3.9), similar trends are observed between the proposed solutions and Li and Aubertin's (2009) solutions. In both cases, the stress decreases with an increase in friction angle and it does not vary significantly when ϕ is greater or equal to 30^o. This indicates that arching is almost insensitive to ϕ for its practical range (30^o – 40^o), which also has been reported by Singh et al. (2010).

In comparison, the influence of fill cohesion on stress distribution is more pronounced than friction angle. Similar trends are observed for both the present study and Li and Aubertin's (2009) solutions as shown in Fig. 3.10. The vertical stress reduces considerably with increasing fill cohesion, c and approaches zero when c > 40 kPa for the case of γ = 18 kN/m^3 or when $(\gamma B - 2\xi)$ tends to zero, in general.

From Eqs. 3.11 and 3.15 where $q = 0$ and $z > 0$, $\sigma_z = 0$ when $(\gamma B - 2\xi) = 0$. Therefore, for $\sigma_z \geq 0$, $\gamma B - 2\xi \geq 0$.

$$\gamma B \geq 2\xi \quad \text{and} \quad \xi = c(1 + sin2\beta tan\delta)$$

gives $$c \leq \frac{\gamma B}{2(1+sin2\beta tan\delta)}$$

$$\therefore \quad 0 \leq c \leq \frac{\gamma B}{2(1+sin2\beta tan\delta)} \tag{3.24}$$

Therefore, if $c = \frac{\gamma B}{2(1+sin2\beta tan\delta)}$, vertical stress becomes zero and the entire fill load is taken by the walls. The effect of cohesion can be also seen from Eq. 3.18, which clearly shows that increase in cohesion reduces the vertical stress within the fill, as more fill load is being transferred to the wall.

Figure 3.11 shows the stress variation along the stope centerline for a cohesionless material by varying the unit weight from14 kN/m^3 to 22 kN/m^3. It is observed that the vertical stresses increase proportionally with increasing unit weight. Similar results are also reported in Pirapakaran and Sivakugan (2006) for a vertical stope. It can be seen for all cases in Table 3.1 that σ_z is proportional to the unit weight γ, which is reflected in Fig. 3.11.

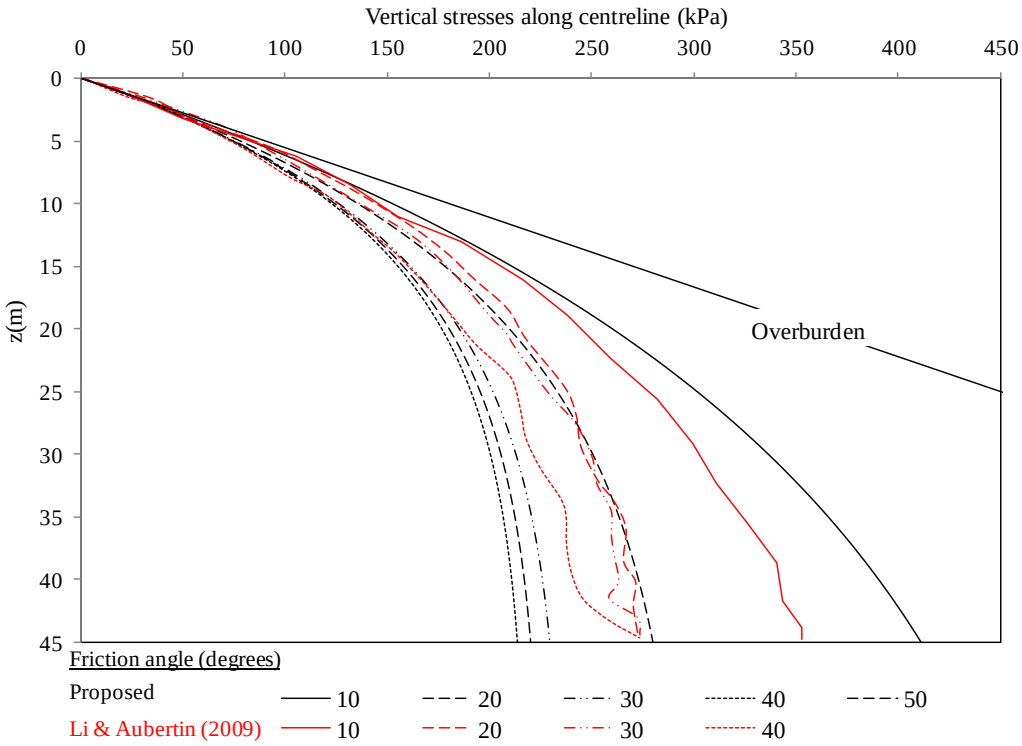

Figure 3.9. Comparison of vertical stresses along centreline for different friction angles ϕ (H = 45 m, B = 6 m, γ =18kN/m^3 , $K = K_o$, c = 0, $\delta = \frac{2}{3}\phi$, $q = 0^o$, $\beta = 75^o$)

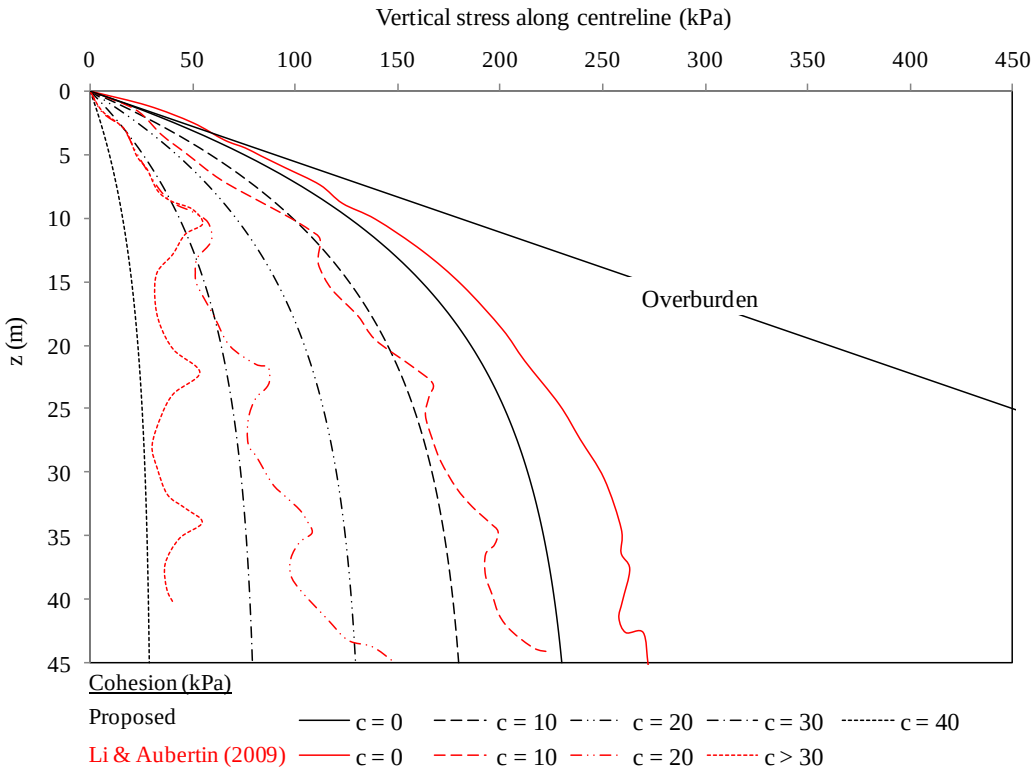

Figure 3.10. Comparison of vertical stresses along centreline for different fill cohesions c (H = 45 m, B = 6 m,γ = 18 kN/m^3 , $K = K_o$, $\phi = 30^o$, $\delta = \frac{2}{3}\phi$, $q = 0^o$, $\beta = 75^o$)

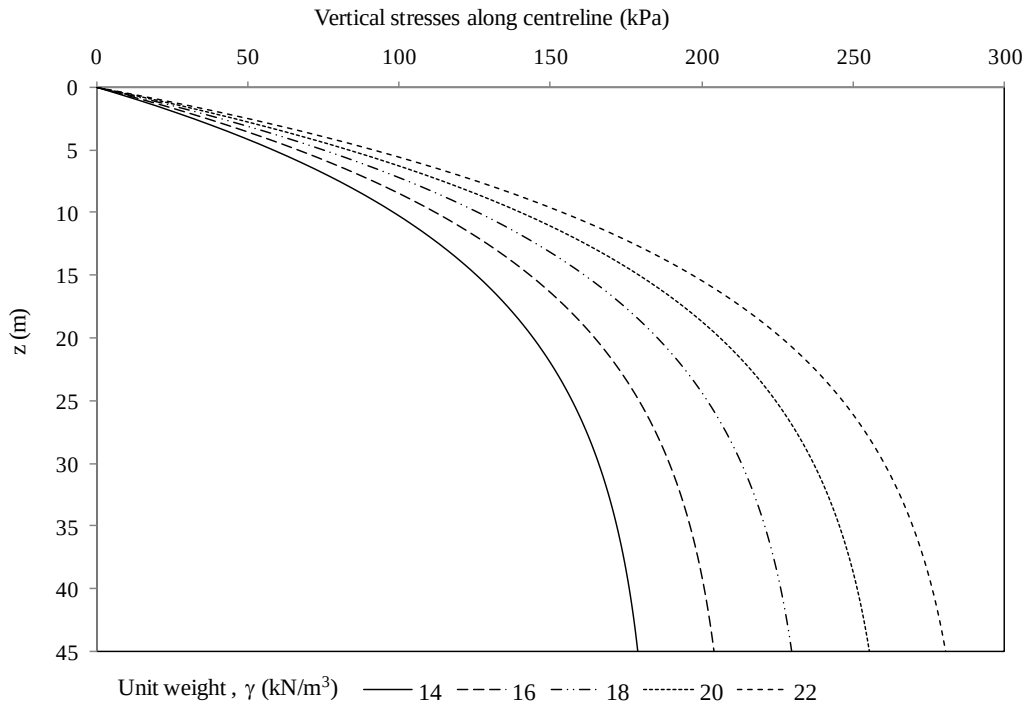

Figure 3.11. Comparison of vertical stresses along centreline for different backfill unit weights γ *(H = 45 m, B = 6 m, $K = K_o$, c = 0, $\phi = 30^o$, $\delta = \frac{2}{3}\phi$, $q = 0^o$, $\beta = 75^o$)*

3.2.3 Discussion

As uniformly distributed vertical stress across the horizontal plane has been assumed in the analytical model proposed herein, the average vertical stress at any depth, z will be constant across the span of the stope. This assumption differs from the non-uniform and asymmetrical vertical stress profile obtained from numerical results, where a lower vertical stress is observed close to the hanging wall and footwall due to arching action. Further analytical work is required to consider non-uniformly distributed load, across the span of the stope.

In addition, K is estimated solely based on material properties without any consideration of the stress state experienced by the backfill across the span. As estimated from numerical results (Chapter 6), the difference in K value from hangingwall to footwall increases as the stope inclination increases. Higher value is observed at hangingwall. K value also influences the prediction of lateral stress significantly ($\sigma_x = K\sigma_z$). For instance, a comparison of lateral stresses along the centreline of 6 m x 45 m stope of different inclinations is shown in Fig. 3.12. The lateral stresses estimated from the proposed solution ($\sigma_x = K\sigma_z$ where $K = K_o$) are higher than results of Li and Aubertin (2009) and Caceres Doerner (2005). It decreases as

the inclination increases. Similar trends are observed in Caceres Doerner's (2005) solutions. However, as seen in Fig. 3.12, the lateral stresses obtained from numerical analysis of Li and Aubertin's (2009) are insensitive to inclination. The expression of *K* appears to be one of the important contributing factors to this variation. Therefore, more attention should be discussed on these issues in future studies.

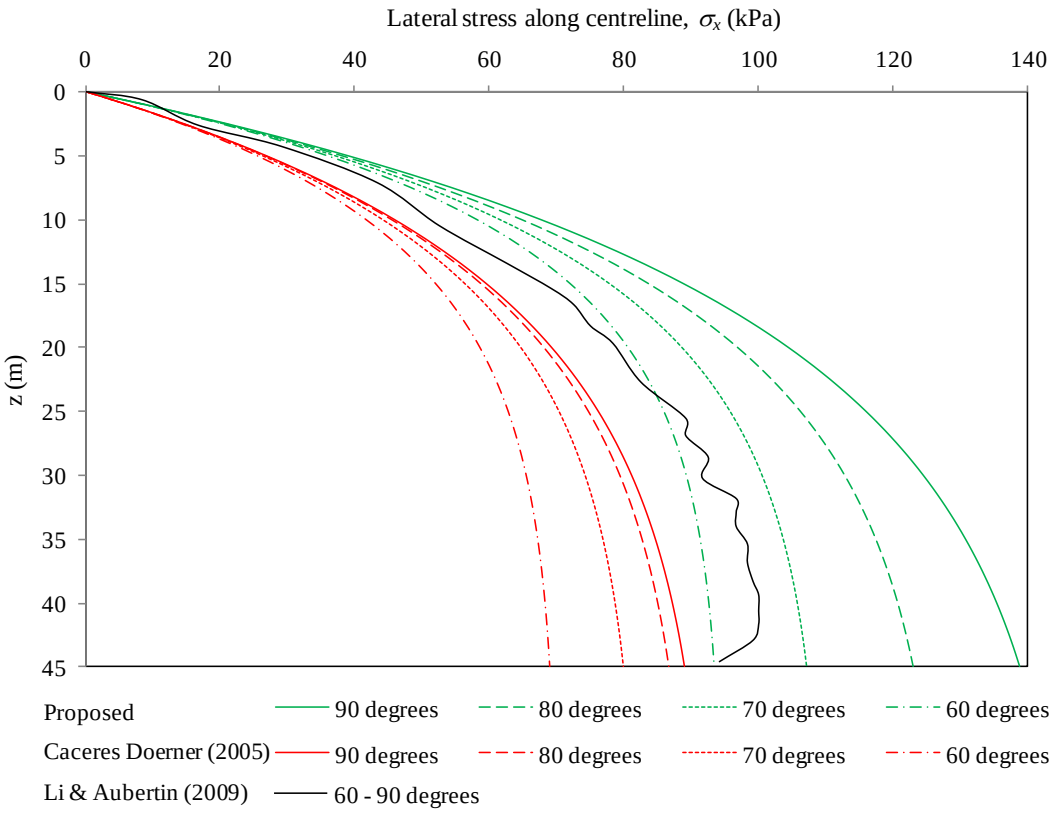

Figure 3.12. Comparison of lateral stresses along centreline *(H = 45 m, γ = 18 kN/m^3 , c = 0, ϕ = 30^o, $\delta = \frac{2}{3}\phi$, q = 0)*

3.2.4 Simple design charts

In mine stopes containing granular backfills such as hydraulic fills where it is uncommon to have any surcharge, $c = 0$ and $q = 0$. Eq. 3.16 can be used to develop simple design charts for different combinations of ϕ, δ, β and z/B *to* minimize the computation efforts in the calculation of average vertical stress at any depth. Common range of ϕ, δ, β and z/B for mining purposes is stated below (Rankine et al. 2006):

$$\frac{\sigma_z}{\gamma B} = f\left(K' tan\delta, \frac{z}{B}\right) ; \qquad (3.25)$$

$$K' = f(\phi, \delta, \beta); \;\; K = K_o \; or \; K_a$$

ϕ : 5^o - 50^o

δ : (1/3, 2/3, 1) of ϕ

β : 50^o, 60^o, 70^o, 80^o and 90^o

z/B: 1 – 10, 20, 50-100

Figures 3.13 and 3.14 show separate design charts for $K = K_o$ and $K = K_a$ respectively. These design charts enable quick estimates of the average vertical normal stress at any depth of a granular backfill contained within an inclined stope. This will be a valuable tool for practicing engineers working with minefills. The use of the design charts is illustrated through a simple numerical example below.

Given: A plane strain stope with B =10 m, z = 30 m, c = 0, $\delta = \phi = 30^o$, γ = 18 kN/m^3, β = 80^o, $K = K_o$.

Required: σ_v at z = 30 m depth.

Solution: From Fig. 3.13 (graph of $K'\tan\delta$ vs ϕ), $\delta/\phi = 1$ and $\phi = 30^o$, $K'tan\delta = 0.35$. Using $K'tan\delta = 0.35$, from the graph of $\sigma_v/\gamma B$ vs $K'tan\delta$, z/B = 3, $\sigma_v/\gamma B$ = 1.24. Therefore, σ_v = 223.2 kN/m^2. The results obtained using Eq. 3.16, where $K'tan\delta$ = 0.3544, and $\sigma_v/\gamma B$ = 1.2426 is that σ_v = 223.67 kN/m^2. They are almost identical with an error 0.21%.

These design charts can be used for finding σ_z at any depth within the stope but not necessarily at the bottom of stope. Referring to Figs 3.13 and 3.14, at $K'tan\delta = 0$, there is no arching effect; therefore σ_z is at its maximum value. As $K'tan\delta$ increases from 0 to 1, $\sigma_v/\gamma B$

reduces exponentially towards a minimum constant value of 0.5 as $K'tan\delta$ approach 1 for any depth z/B. Comparing Figs 3.13 and 3.14 for any value of β and ϕ, $K'tan\delta$ is always higher when $K = K_o$, indicating that there is higher arching and therefore a smaller σ_z value for $K = K_o$. This can be explained by the larger horizontal stress when $K = K_o$, implying larger shear stress thus enabling a larger fraction of the fill load to be carried by the wall.

As noted by Singh et al. (2010) that the product of K' and $tan\delta$, $K'tan\delta$, is the main factor that contributes to the variation of average vertical stress at any depth within the granular backfill. It can be seen from Figs 3.13 and 3.14 that, within the range 25^o- 50^o, ϕ has little influence on the development of $K'tan\delta$ for a vertical stope. $K'tan\delta$ becomes more sensitive with increasing wall inclination especially for very rough walls, where δ get closer to ϕ. The variation of $\sigma_z/\gamma B$ becomes very small and tends to be constant with $K'tan\delta$ greater than 0.3. This explains the results given in Fig. 3.9 where there is very little difference in σ_v as ϕ varies from 30^o to 50^o. This also supports the observation of Singh et al. (2010) that arching is almost insensitive to ϕ for the practical friction angle range.

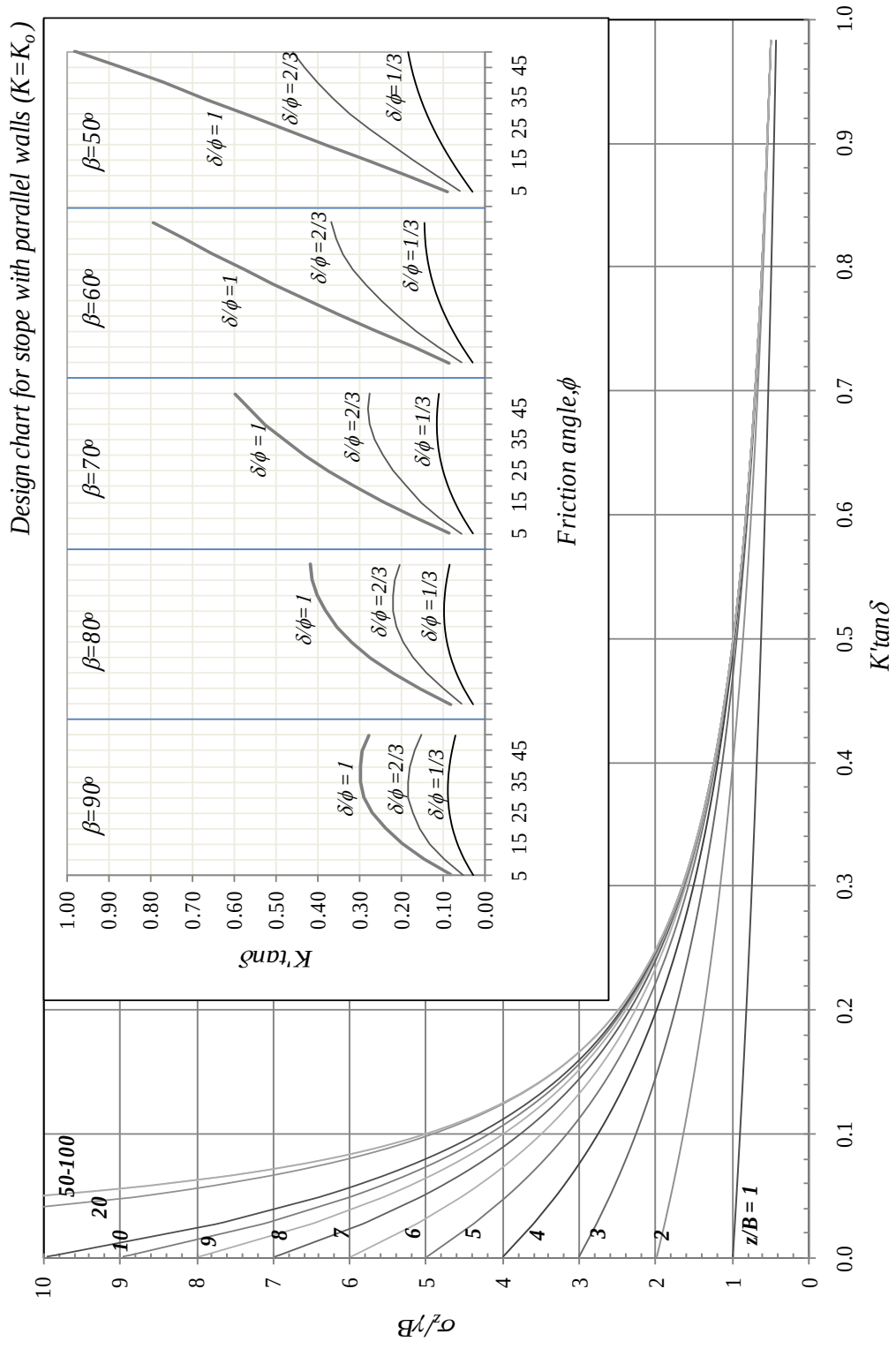

Figure 3.13. Design charts for estimating average vertical stress at any depth of stope for $K = K_o$

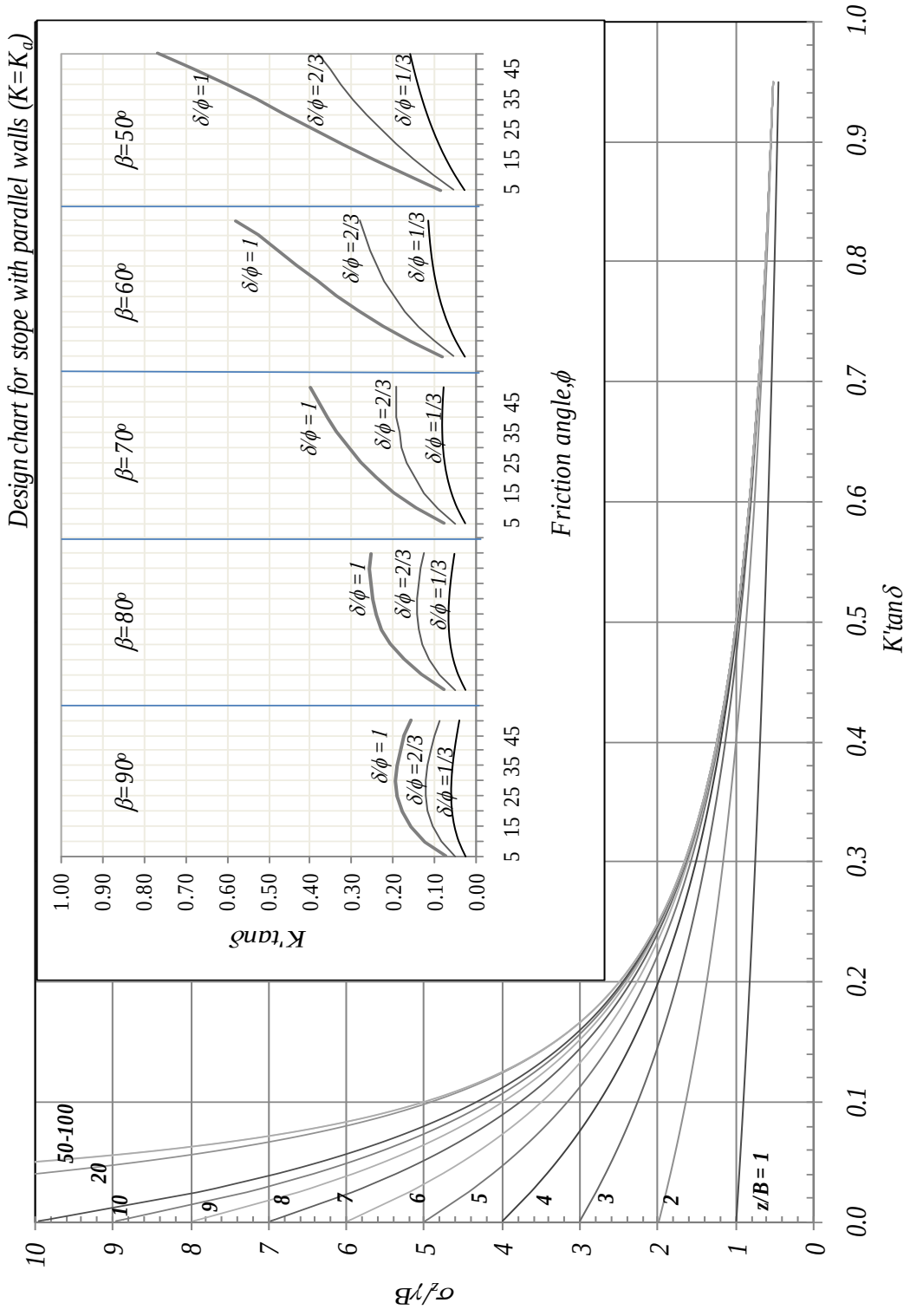

Figure 3.14. Design charts for estimating average vertical stress at any depth of stope for $K = K_a$

3.3 Analytical expression for vertical stress within an inclined mine stope with non-parallel walls

In reality, it is rare to find stope with exactly parallel walls. Most of them are stopes with non-parallel walls. They are usually trapezoids with both walls inclining at different angle. Shukla et al. (2009a) derived an equation to estimate the vertical stress of soils for a cone-shaped structure by considering arching effects as an axi-symmetric problem. An attempt is made in this section to develop an analytical expression for vertical stress in a backfilled stope with non-parallel walls with both slopes leaning to the same side as shown in Fig. 3.15. The following assumptions are made in the analysis:

- The backfill is bounded between two non-parallel inclined walls with both walls are leaning to the same side at different angles, α and β, to the horizontal.
- Top and bottom widths of the stope should be greater than or equal to zero.
- A two dimensional plane strain condition is considered.
- At any depth, the vertical normal stresses are uniformly distributed laterally across the stope width.
- As the wall-fill interface is very rough for actual stope condition, the shear plane is taken few grains away from the wall, and hence the interface friction angle, δ, is taken as friction angle of backfill, ϕ.

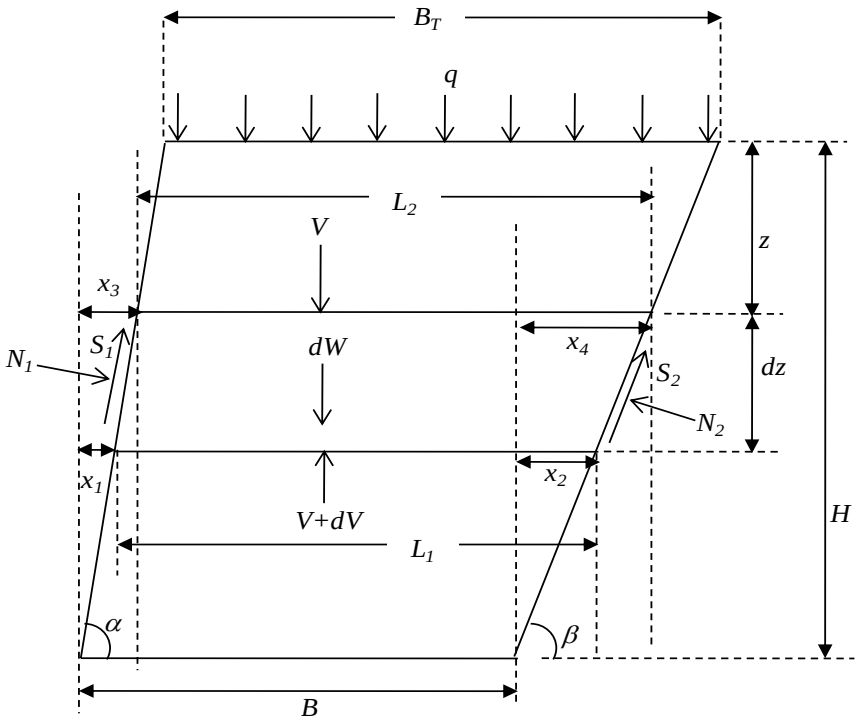

Figure 3.15: Schematic diagram of an inclined stope with non-parallel walls ($B < B_T$)

The geometry of the stope is shown in Fig. 3.15 with the necessary dimensions and angles where B = stope width at base, B_T = stope width at top, H = height of the stope, α = wall inclination at hangingwall wall, β = wall inclination at footwall, S_1 = shear force acting along hangingwall, S_2 = shear force acting along footwall, N_1 = normal force acting on hangingwall, N_2 = normal force acting on footwall and q = surcharge on top of fill material. The thickness dz of the infinitesimal element is shown larger for clarity. Based on the geometry of Fig. 3.15, dimension of x_1, x_2, x_3, x_4, L_1 and L_2 can be defined as follows:

$$tan\alpha = \frac{H-z-dz}{x_1} \Rightarrow x_1 = \frac{H-z-dz}{tan\alpha} \tag{3.26}$$

$$tan\beta = \frac{H-z-dz}{x_2} \Rightarrow x_2 = \frac{H-z-dz}{tan\beta} \tag{3.27}$$

$$tan\alpha = \frac{H-z}{x_3} \Rightarrow x_3 = \frac{H-z}{tan\alpha} \tag{3.28}$$

$$tan\beta = \frac{H-z}{x_4} \Rightarrow x_4 = \frac{H-z}{tan\beta} \tag{3.29}$$

$$L_1 = B + x_2 - x_1 \Rightarrow L_1 = B + \frac{(H-z-dz)(tan\alpha-tan\beta)}{tan\beta tan\alpha} \tag{3.30}$$

$$L_2 = B + x_4 - x_3 \Rightarrow L_2 = B + \frac{(H-z)(tan\alpha-tan\beta)}{tan\beta tan\alpha} \tag{3.31}$$

Area of the differential element,

$$A_{strip} = \left[\frac{L_1+L_2}{2}\right]dz \Rightarrow A_{strip} = \left[B + \frac{(2H-2z-dz)(tan\alpha-tan\beta)}{2tan\beta tan\alpha}\right]dz \tag{3.32}$$

As derived in Section 3.2, Eq. 3.8, 3.9, 3.10 and 3.11 can be used again to express normal stress on the wall, σ_n, and shear stress, τ, acting at the wall when wall inclination is involved.

$$\sigma_{n1} = K_1\sigma_z + c\ sin2\alpha \tag{3.33}$$

$$K_1 = \frac{1+K}{2} + \frac{1-K}{2}cos2\alpha + Ktan\phi\, sin2\alpha \tag{3.34}$$

$$\tau_1 = \zeta_1 + K_1\sigma_z tan\phi \tag{3.35}$$

$$\zeta_1 = c(1 + sin2\alpha\ tan\phi) \tag{3.36}$$

$$\sigma_{n2} = K_2\sigma_z + c\ sin2\beta\ ; \tag{3.37}$$

$$K_2 = \frac{1+K}{2} + \frac{1-K}{2} cos2\beta + Ktan\phi\, sin2\beta \quad (3.38)$$

$$\tau_2 = \zeta_2 + K_2\sigma_z tan\phi; \quad (3.39)$$

$$\zeta_2 = c(1 + sin2\beta\, tan\phi) \quad (3.40)$$

where σ_{ni} = normal stress on the wall, τ_i = shear stress acting at the wall, K_i = lateral stress ratio incorporating wall inclination and ζ_i = fill cohesion incorporating wall inclination. The subscripts i = 1 and i =2 denote the hangingwall (left) and footwall (right) respectively.

Self weight, dW of the element is given by substituting Eq. 3.32 into A_{strip} :

$$dW = \gamma A_{strip}$$

i.e., $$dW = \gamma \left[B + \frac{(2H-2z-dz)(tan\alpha-tan\beta)}{2tan\beta\, tan\alpha}\right] dz \quad (3.41)$$

Vertical force, V acting on the layer of depth z (refer Eq. 3.31 for L_2) is:

$$V = \sigma_z L_2$$

i.e., $$V = \sigma_z \left[B + \frac{(H-z)(tan\alpha-tan\beta)}{tan\beta tan\alpha}\right] \quad (3.42)$$

Vertical force, $V+dV$ acting on the layer of depth $z+dz$ (refer Eq. 3.30 for L_1) is:

$$V + dV = (\sigma_z + d\sigma_z)L_1$$

i.e., $$V + dV = (\sigma_z + d\sigma_z)\left[B + \frac{(H-z-dz)(tan\alpha-tan\beta)}{tan\beta tan\alpha}\right] \quad (3.43)$$

Shear force, S_1 and S_2 acting at the backfill-rock interface at depth z on the hangingwall and footwall respectively are given by:

$$S_1 = \frac{\tau_1 dz}{sin\alpha} \quad (3.44)$$

$$S_2 = \frac{\tau_2 dz}{sin\beta} \quad (3.45)$$

Normal force, N_1 and N_2 acting at the backfill-rock interface at depth z are:

$$N_1 = \frac{\sigma_{n1} dz}{sin\alpha} \quad (3.46)$$

$$N_2 = \frac{\sigma_{n2} dz}{sin\beta} \quad (3.47)$$

For equilibrium of vertical forces on the element

$$(V + dV) - V - dW + S_1 sin\alpha + S_2 sin\beta + N_2 cos\beta - N_1 cos\alpha = 0 \qquad (3.48)$$

Substituting Eq. 3.41 through Eq. 3.47 into Eq. 3.48, gives

$$(\sigma_z + d\sigma_z)\left[B + \frac{(H-z-dz)(tan\alpha-tan\beta)}{tan\beta tan\alpha}\right] - \sigma_z\left[B + \frac{(H-z)(tan\alpha-tan\beta)}{tan\beta tan\alpha}\right] -$$
$$\gamma\left[B + \frac{(2H-2z-dz)(tan\alpha-tan\beta)}{2tan\beta tan\alpha}\right]dz + \frac{\tau_1 dz}{sin\alpha}sin\alpha + \frac{\tau_2 dz}{sin\beta}sin\beta + \frac{\sigma_{n2}dz}{sin\beta}cos\beta - \frac{\sigma_{n1}dz}{sin\alpha}cos\alpha = 0$$

i.e.,

$$-\left[\frac{\sigma_z(tan\alpha-tan\beta)}{tan\beta tan\alpha} + \gamma B + \frac{\gamma(2H-2z-dz)(tan\alpha-tan\beta)}{2tan\beta tan\alpha}\right]dz + \left[B + \frac{(H-z-dz)(tan\alpha-tan\beta)}{tan\beta tan\alpha}\right]d\sigma_z +$$
$$\tau_1 dz + \tau_2 dz + \sigma_{n2}\cot\beta\, dz - \sigma_{n1}\cot\alpha\, dz = 0 \qquad (3.49)$$

Substituting Eq. 3.33, 3.35, 3.37 and 3.39 into Eq. 3.49,

$$-\left[\frac{\sigma_z(tan\alpha-tan\beta)}{tan\beta tan\alpha} + \gamma B + \frac{\gamma(2H-2z-dz)(tan\alpha-tan\beta)}{2tan\beta tan\alpha}\right]dz + \left[B + \frac{(H-z-dz)(tan\alpha-tan\beta)}{tan\beta tan\alpha}\right]d\sigma_z$$
$$+(\zeta_1 + K_1\sigma_z tan\phi)dz + (\zeta_2 + K_2\sigma_z tan\phi)dz + (K_2\sigma_z + c\, sin2\beta)cot\beta dz$$
$$-(K_1\sigma_z + c\, sin2\alpha)cot\alpha dz = 0$$

i.e. $\left(B + \frac{H(tan\alpha-tan\beta)}{tan\beta tan\alpha}\right)d\sigma_z - \frac{(tan\alpha-tan\beta)}{tan\beta tan\alpha}zd\sigma_z - \frac{(tan\alpha-tan\beta)}{tan\beta tan\alpha}dzd\sigma_z =$

$$\left(\gamma B - \zeta_1 - \zeta_2 - c\, sin2\beta cot\beta + c\, sin2\alpha cot\alpha + \frac{\gamma H(tan\alpha-tan\beta)}{tan\beta tan\alpha}\right)dz - \frac{\gamma(tan\alpha-tan\beta)}{tan\beta tan\alpha}zdz -$$
$$\frac{\gamma(tan\alpha-tan\beta)}{2tan\beta tan\alpha}(dz)^2 + \left[\frac{(tan\alpha-tan\beta)}{tan\beta tan\alpha} - K_1 tan\phi - K_2 tan\phi - K_2 cot\beta + K_1 cot\alpha\right]\sigma_z dz \qquad (3.50)$$

Let

$$P = B + \frac{H(tan\alpha-tan\beta)}{tan\beta tan\alpha} \qquad (3.51)$$

$$Q = \frac{(tan\alpha-tan\beta)}{tan\beta tan\alpha} \qquad (3.52)$$

$$R = \gamma B - \zeta_1 - \zeta_2 - c\, sin2\beta cot\beta + c\, sin2\alpha cot\alpha + \frac{\gamma H(tan\alpha-tan\beta)}{tan\beta tan\alpha} \qquad (3.53)$$

$$S = \frac{\gamma(tan\alpha-tan\beta)}{tan\beta tan\alpha} \qquad (3.54)$$

$$T = \frac{(tan\alpha-tan\beta)}{tan\beta tan\alpha} - K_1 tan\phi - K_2 tan\phi - K_2 cot\beta + K_1 cot\alpha \qquad (3.55)$$

Then

$$Pd\sigma_z - Qzd\sigma_z - Qdzd\sigma_z = Rdz - Szdz - S(dz)^2 + T\sigma_z dz \quad (3.56)$$

The product of two infinitesimal small numbers tends to zero,

$$Pd\sigma_z - Qzd\sigma_z = Rdz - Szdz + T\sigma_z dz$$

i.e., $$\frac{d\sigma_z}{dz} - \left(\frac{T}{P-Qz}\right)\sigma_z = \frac{R-Sz}{P-Qz} \quad (3.57)$$

Equation 3.57 is a 1st order differential equation, which on solving, gives

$$(P-Qz)^{T/Q}\sigma_z = -\frac{(R-Sz)(P-Qz)^{T/Q}}{T} - \frac{S}{T}\int (P-Qz)^{T/Q}dz + C$$

$$\sigma_z = -\frac{(R-Sz)}{T} + \frac{S(P-Qz)}{T(T+Q)} + \frac{C}{(P-Qz)^{T/Q}} \quad (3.58)$$

At $z = 0$, $\sigma_z = q$. This will give the value of C, the constant of integration, which will be substituted in the above to get final expression. C is determined as:

$$C = qP^{T/Q} + \frac{RP^{T/Q}}{T} - \frac{SP^{\frac{T}{Q}+1}}{T(T+Q)} \quad (3.59)$$

The final expression for the vertical stress at depth z becomes:

$$\sigma_z = -\frac{(R-Sz)}{T} + \frac{S(P-Qz)}{T(T+Q)} + \left(qP^{T/Q} + \frac{RP^{T/Q}}{T} - \frac{SP^{\frac{T}{Q}+1}}{T(T+Q)}\right)(P-Qz)^{-T/Q} \quad (3.60)$$

where B and B_T should be greater than or equal to zero.

Eq. 3.60 is developed on the basis of known base width B (see Fig. 3.15). Sometimes it is useful to have the expression in terms of the top width B_T. An alternative expression (Eq. 3.61) is developed to counter the situation as shown in Fig 3.16 where the width of base is unknown and the top width, B_T of stope is used in the calculation. In other words, the expression is modified to present σ_z in terms of B_T instead of B, along with other parameters.

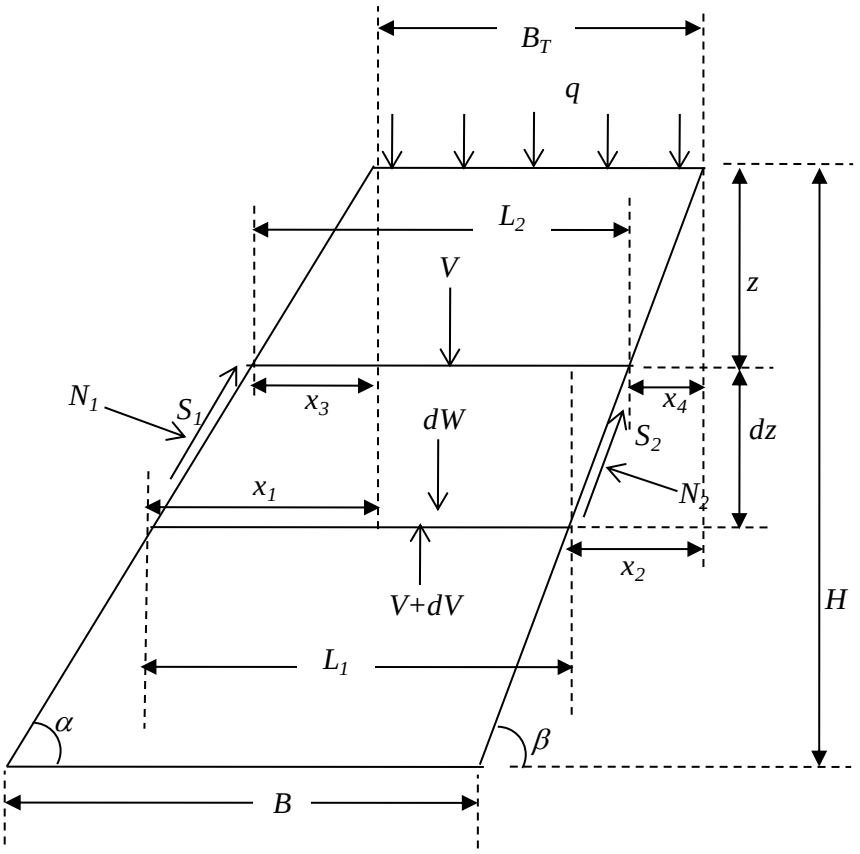

Figure 3.16. Schematic diagram of an inclined stope with non-parallel walls ($B > B_T$)

$$\sigma_z = \frac{(-R+Sz)}{T} - \frac{S(B_T+Qz)}{T(T+Q)} + \left(qB_T^{T/Q} + \frac{RB_T^{T/Q}}{T} + \frac{SB_T^{\frac{T}{Q}+1}}{T(T+Q)} \right)(B_T + Qz)^{-T/Q} \qquad (3.61)$$

where

$$Q = \frac{(tan\beta - tan\alpha)}{tan\beta tan\alpha} \qquad (3.62)$$

$$R = -\gamma B_T + \zeta_1 + \zeta_2 + c\ sin2\beta cot\beta - c\ sin2\alpha cot\alpha \qquad (3.63)$$

$$S = \frac{\gamma(tan\beta - tan\alpha)}{tan\beta tan\alpha} \qquad (3.64)$$

$$T = \frac{(tan\beta - tan\alpha)}{tan\beta tan\alpha} + K_1 tan\phi + K_2 tan\phi + K_2 cot\beta - K_1 cot\alpha \qquad (3.65)$$

and K_1, K_2, ζ_1 and ζ_2 as above, B and B_T should be greater than or equal to zero.

3.3.1 Special cases

The general solutions presented above, Eqs. 3.60 and 3.61, are not applicable for the cases when the walls are parallel ($\alpha = \beta$) or when the fill is bounded between a vertical wall and an inclined wall (α = 90° or β = 90°). The solutions can be modified to address these particular cases. This can also be seen as a verification exercise for those solutions proposed for non-parallel walls.

Special case 1: Cohesionless material bounded between parallel walls

When $\alpha = \beta$, the values of Q (computed from Eqs. 3.52 and 3.62) and S (computed from Eqs. 3.54 and 3.64) will be zero. Therefore, Eqs. 3.60 and 3.61 will be independent of z, making these equations invalid.

In this case, when $\alpha = \beta$, Eq. 3.57 can be redefined by simplifying Eqs. 3.33 to 3.40:

$$\sigma_{n1} = \sigma_{n2}\ ; \quad K_1 = K_2 = K'; \quad \zeta_1 = \zeta_2 = \zeta; \quad \tau_1 = \tau_2 = \tau$$

and Eqs. 3.51 to 3.55 become

$$P = B;\ Q = 0\ ;\ R = \gamma B;\ S = 0 \text{ and } T = -2K'tan\phi$$

$$\frac{d\sigma_z}{dz} - \left(\frac{T}{P-Qz}\right)\sigma_z = \frac{R-Sz}{P-Qz} \tag{3.57}$$

i.e., $$\frac{d\sigma_z}{dz} + \left(\frac{2K'tan\phi}{B}\right)\sigma_z = \gamma \tag{3.66}$$

Let $$A = \frac{2K'tan\phi}{B} \tag{3.67}$$

then $$\frac{d\sigma_z}{dz} + A\sigma_z = \gamma \tag{3.68}$$

Integrating Eq. 3.68 gives:

$$e^{Az}\sigma_z = \frac{\gamma}{A}e^{Az} + C \tag{3.69}$$

where C is a constant of integration, which can be determined by applying the boundary conditions. At $z=0$, $\sigma_z=q$. Therefore,

$$e^{Az}\sigma_z - e^0 q = \frac{\gamma}{A}e^{Az} - \frac{\gamma}{A}e^0$$

i.e., $\sigma_z = \frac{\gamma}{A}(1 - e^{-Az}) + qe^{-Az}$ (3.70)

Substituting Eq. 3.67 into Eq. 3.70, gives

$$\sigma_z = \frac{\gamma B}{2K'tan\phi}\left(1 - e^{-\frac{2K'tan\phi}{B}z}\right) + qe^{-\frac{2K'tan\phi}{B}z} \quad (3.71)$$

Eq. 3.71 is the same as Eq. 3.15 where $c = 0$ and $\delta = \phi$, which is the case of granular fills with very high wall roughness.

Special case 2: Cohesionless material bounded between a vertical wall and an inclined wall

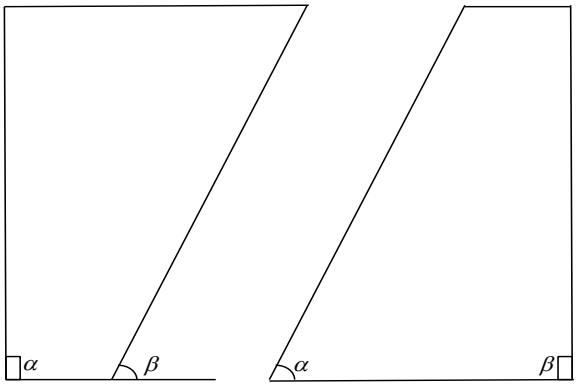

(a) (b)

Figure 3.17. Stope with one vertical slope and one inclined slope

Figure 3.17 shows two stopes where one of the two walls is vertical. These are special cases of the more general stope as shown in Figure 3.15. Tangent 90^o being ∞, some of the expressions become undefined in computing σ_z using Eqs. 3.60 and 3.61. Two analytical expressions (Eqs. 3.72 and 3.73) are derived here in the attempt to overcome these situations by substituting α or β with 90^o into Eq. 3.60. To avoid numerical problems, 89.999^o is used in Eq. 3.60 to represent the vertical wall. The results are plotted in Figs 3.18 and 3.19. The numbers (for example 90-70) shown in plot legends indicate the slope angle of the walls, α and β, respectively.

For vertical hangingwall and inclined footwall, where $\alpha = 90^o, \beta < 90^o$ as shown in Fig 3.17(a), Eq. 3.51 to Eq. 3.55 become

$$P = B + \frac{H(tan\alpha - tan\beta)}{tan\beta tan\alpha} = B + \frac{H(\infty - tan\beta)}{\infty\, tan\beta} = B + H$$

$$Q = \frac{(tan\alpha - tan\beta)}{tan\beta tan\alpha} = \frac{(\infty - tan\beta)}{\infty\, tan\beta} = 1$$

$$S = \frac{\gamma(tan\alpha - tan\beta)}{tan\beta tan\alpha} = \frac{\gamma(\infty - tan\beta)}{\infty\, tan\beta} = \gamma$$

$$R = \gamma B - \zeta_1 - \zeta_2 - c\, sin2\beta cot\beta + \frac{\gamma H(\infty - tan\beta)}{\infty\, tan\beta} = \gamma(B + H) - \zeta_1 - \zeta_2 - c\, sin2\beta cot\beta$$

$$T = \frac{(\infty - tan\beta)}{\infty\, tan\beta} - K_1 tan\phi - K_2 tan\phi - K_2 cot\beta = 1 - K_1 tan\phi - K_2(tan\phi + cot\beta)$$

Hence, Eq. 3.60 becomes

$$\sigma_z = -\frac{R - \gamma z}{T} + \frac{\gamma(B + H - z)}{T^2 + T} + \left(q(B + H)^T + \frac{R(B + H)^T}{T} - \frac{\gamma(B + H)^{T+1}}{T^2 + T}\right)[(B + H) - z]^{-T} \quad (3.72)$$

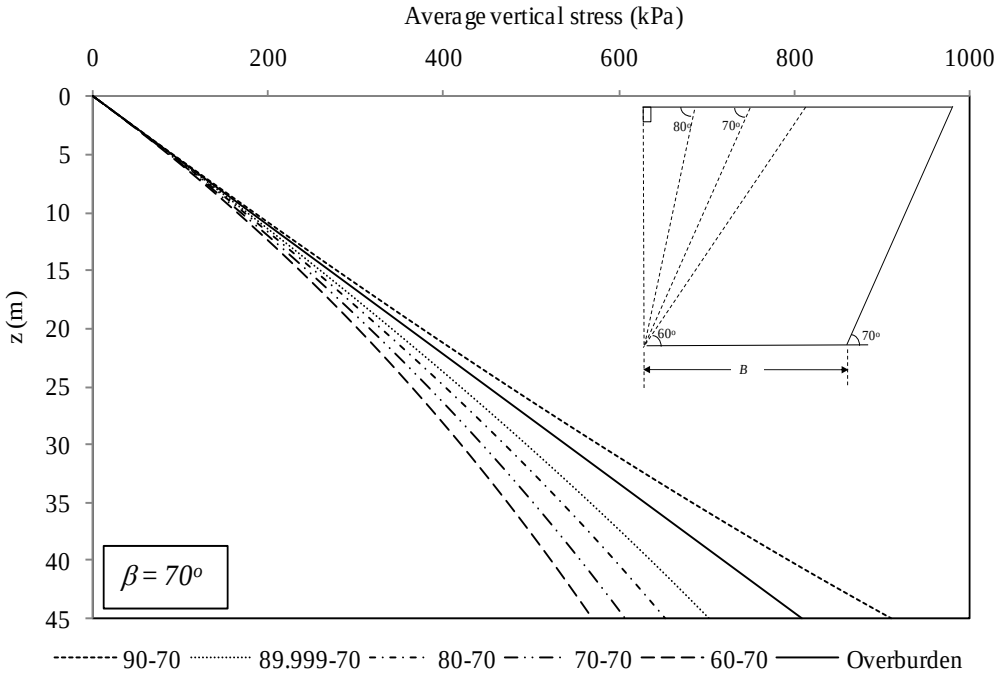

Figure 3.18. Average vertical stress calculated from Eq. 3.60 for $\alpha < 90^o$ and Eq. 3.72 for $\alpha = 90^o$ while β is fixed at 70^o *($B = 46$ m, $H = 45$ m, $\phi = 30^o$, $\gamma = 18 kN/m^3$, $c = 0$, $K = K_a$)*

For inclined hangingwall and vertical footwall, where $\alpha < 90^o$ and $\beta = 90^o$ as shown in Fig 3.17(b), Eq. 3.51 to Eq. 3.55 become

$$P = B + \frac{H(tan\alpha - tan\beta)}{tan\beta tan\alpha} = B + \frac{H(tan\alpha - \infty)}{\infty\, tan\alpha} = B - H$$

$$Q = \frac{(tan\alpha - tan\beta)}{tan\beta tan\alpha} = \frac{(tan\alpha - \infty)}{\infty\, tan\alpha} = -1$$

$$R = \gamma B - \zeta_1 - \zeta_2 + c\, sin2\alpha cot\alpha + \frac{\gamma H(tan\alpha - \infty)}{\infty\, tan\alpha} = \gamma(B - H) - \zeta_1 - \zeta_2 + c\, sin2\alpha cot\alpha$$

$$S = \frac{\gamma(tan\alpha - tan\beta)}{tan\beta tan\alpha} = \frac{\gamma(tan\alpha - \infty)}{\infty\, tan\alpha} = -\gamma$$

$$T = \frac{(tan\alpha - \infty)}{\infty\, tan\alpha} - K_1 tan\phi - K_2 tan\phi + K_1 cot\alpha = -1 - K_2 tan\phi - K_1(tan\phi - cot\alpha)$$

Hence, Eq. 3.60 becomes

$$\sigma_z = -\frac{R + \gamma z}{T} - \frac{\gamma(B - H + z)}{T^2 - T} + \left(q(B - H)^{-T} + \frac{R(B - H)^{-T}}{T} + \frac{\gamma(B - H)^{1-T}}{T^2 - T}\right)[(B - H) + z]^T \tag{3.73}$$

where $B > H$.

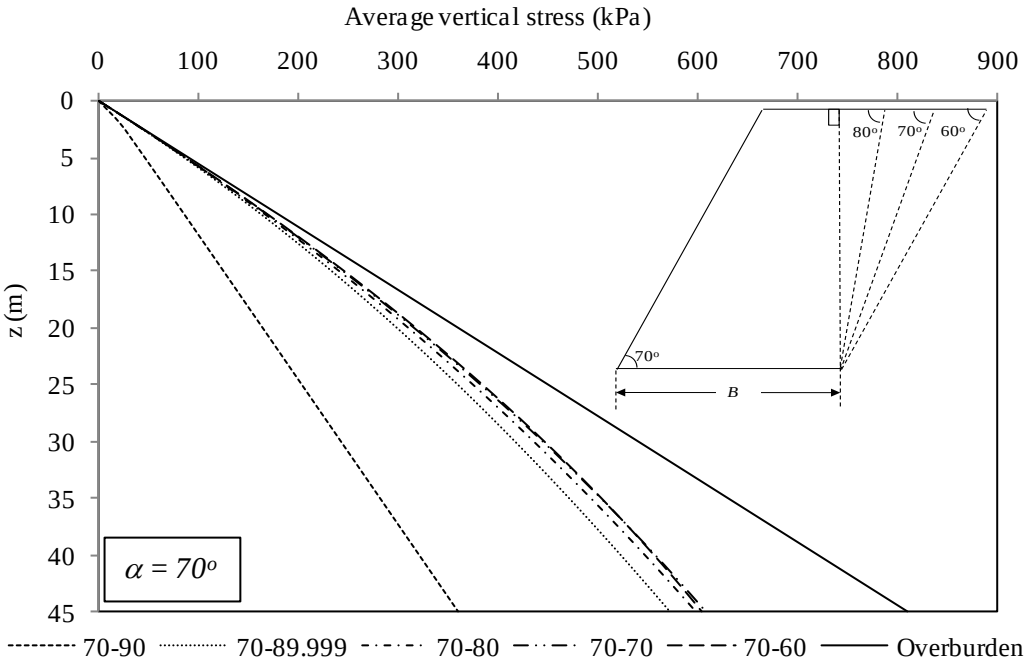

Figure 3.19. Average vertical stress calculated from Eq. 3.60 for $\beta < 90^o$ and Eq. 3.73 for $\beta = 90^o$ while α is fixed at70^o *(B = 46 m, H = 45 m, $\phi = 30^o$, $\gamma = 18kN/m^3$, c = 0, $K = K_a$)*

In Fig 3.18, β is fixed at 70^o while α varies from 60^o to 90^o. When α decreases from 89.999^o to 60^o, the average vertical stresses calculated based on Eq. 3.60 show a decreasing trend and all values fall below overburden pressure. As expected, for $\beta = 70^o$, the vertical stress at any depth is the maximum when the hangingwall is vertical. When $\alpha = 90^o$, the average vertical stress calculated from Eq. 3.72 deviates from the trend of vertical stress when $\alpha < 90^o$ and also exceed the overburden pressure, which is unlikely to happen.

Similarly, in Fig 3.19 where α is fixed at 70^o while β decreases from 90^o to 60^o, the average vertical stress calculated from Eq.3.60 show a slight increase from $\beta = 89.999^o$ to 80^o, and appears to converge towards values when $\beta = 60^o$. However, when $\beta = 90^o$, the average vertical stress calculated using Eq. 3.73 shows no continuity from values obtained when $\beta < 90^o$ and is significantly less than the value obtained for $\beta = 80^o$ which is unlikely.

The loss of continuity found in both cases when α or β is taken as 90^o (see Figs 3.18 and 3.19) indicates that Eq. 3.72 and 3.73 are not valid. This is because as the angle tends toward 90^o, tangent grows without bound, which may cause unexpected changes in parameters. Therefore, 89.999^o (instead of 90^o) should be used in Eq. 3.60 when dealing with stope bounded between vertical and inclined walls to avoid any numerical explosions. This has been confirmed by numerical simulation using FLAC as shown in Fig. 3.20. Fig 3.20 shows the comparison between stress distributions derived using Eq. 3.60 with 89.999^o to represent vertical wall and the results from numerical modeling simulated using 90^o to represent vertical wall. The analytical results obtained are consistent with the numerical results.

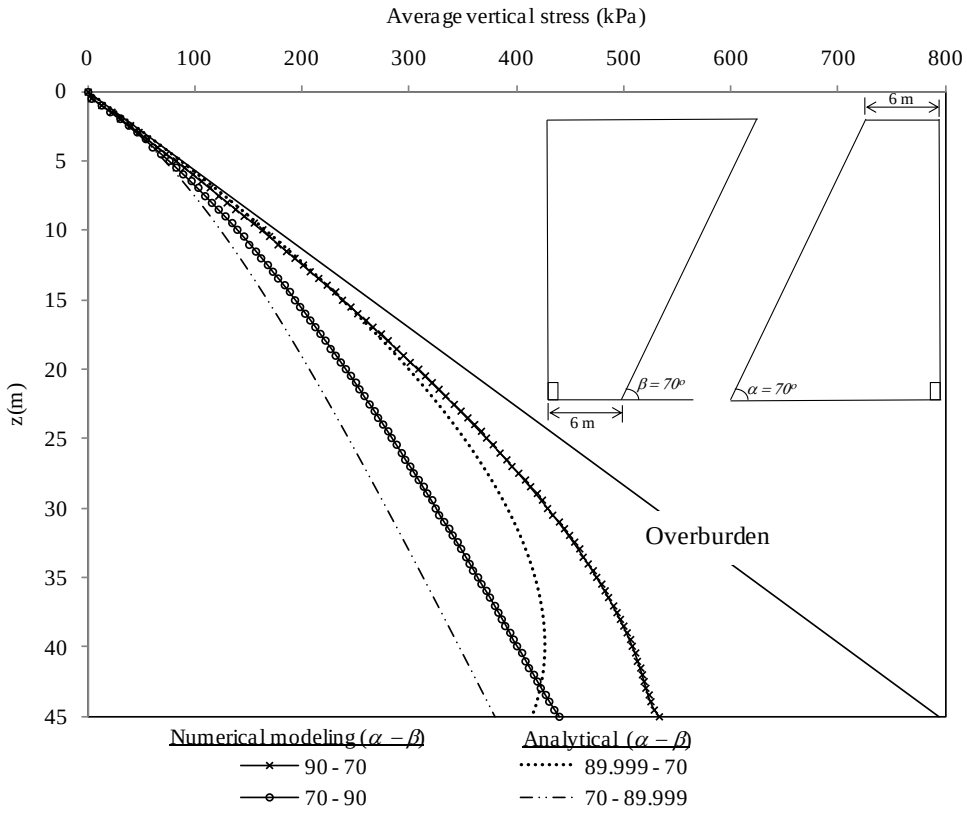

Figure 3.20. Average vertical stress for stope bounded between vertical and inclined walls *(B = 6 m for model $90^o - 70^o$ and B_T = 6 m for model $70^o - 90^o$, H = 45 m, $\phi = 30^o$, γ = 18kN/m^3, c = 0)*

3.3.2 Comparison to results from numerical modeling

Different combinations of α–β are examined in the following section using Eq. 3.60 for non-parallel walls situation and Eq. 3.71 is used to calculate the vertical stress for a stope with parallel walls. As concluded in Chapter 4, the combination of ($K = K_o$ and $\delta = \frac{2}{3}\phi$) or ($K = K_a$ *and* $\delta = \phi$) provide very good agreement with the results obtained from elasto-plastic numerical modeling where the Mohr-Coulomb constitutive model was used for the fill. Hence, $K = K_a$ is used in conjunction with $\delta = \phi$ in this section. The input parameters used in the calculations are: $K = K_a$, γ =18 kN/m^3, $c = 0$ and $\delta = \phi = 30^o$, $H = 45$ m, $B = 6$ m when $\alpha \geq \beta$ and $B_T = 6$ m when $\alpha < \beta$. For comparison with numerical solutions, same parameters and stope dimensions are used in modeling and the results are plotted in Figs 3.21 and 3.22. The detail of numerical modeling approach will be discussed in Section 6.5 (Chapter 6). The input parameters and constitutive models for rock mass and backfill materials used in the modelling are tabulated in Table 6.2.

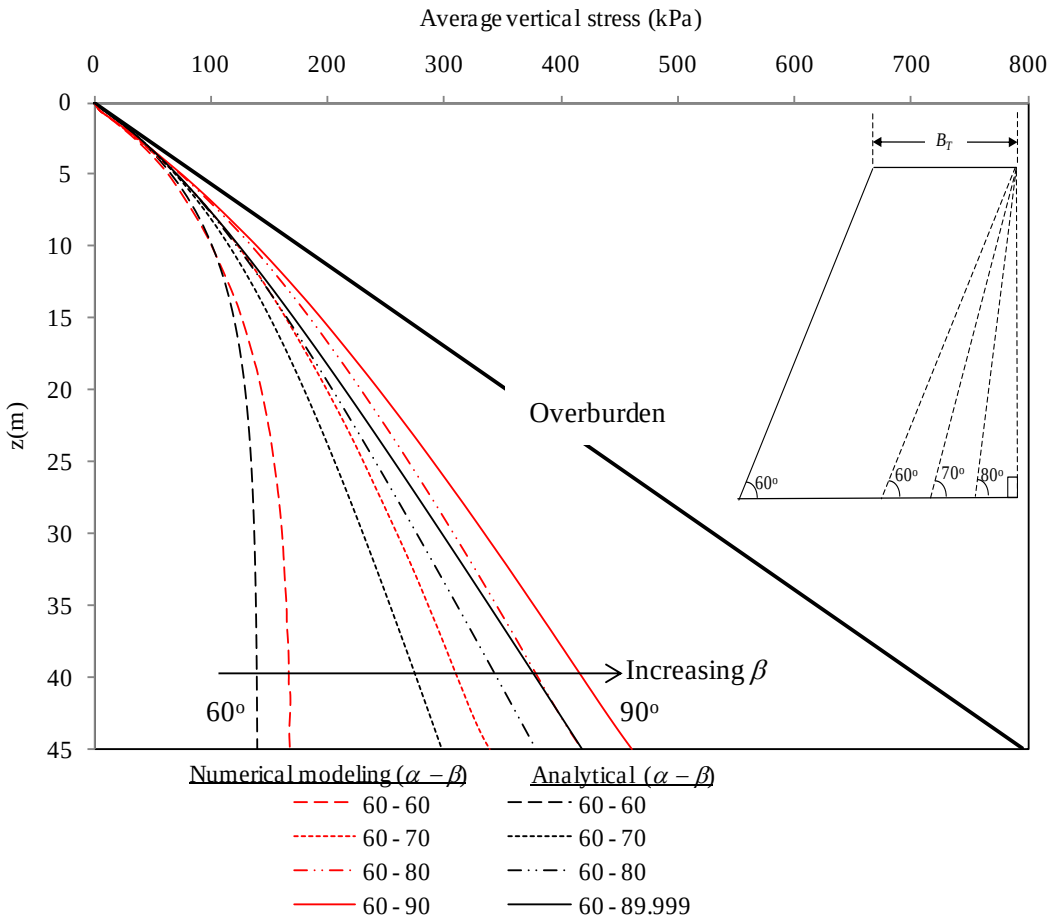

Figure 3.21. Vertical stress for stope with non-parallel walls where $\alpha < \beta$, $B_T = 6\,m$

The good agreement between numerical and analytical solutions is achieved for cases where $\alpha < \beta$. As shown in Fig.3.21, the vertical stresses estimated using Eq. 3.60 (analytical solutions) are slightly lower than those from numerical modeling. With B_T fixed at 6 m, the average vertical stress experienced by fill materials increases with the increase of angle β for all solutions. However, the stress increment decreases when β approaches 90° where the footwall becomes vertical and the effect of arching is less effective due to lower aspect ratio.

For both analytical and numerical solutions where $\alpha > \beta$ as shown in Fig 3.22, the average vertical stress increases gradually with depth and with the increase of α. Instead of maximum vertical stress occurring at the bottom of stope, the maximum vertical stresses estimated from analytical expression occur at a depth above the bottom of the stope and the plots start to curve inward, indicating a reduction of vertical stress experienced by the fill material, which is unlikely. For example, with β fixed at 60° (see Fig. 3.22), the maximum vertical stress estimated from analytical expression occurs at aspect ratio z/*B* = 5 to z/*B* = 6

when α increases from 70° to 90° respectively. No such inward curve observed in the results of numerical modeling and the maximum vertical stress occurs at the base of the stope. Further investigation is needed to overcome this limitation.

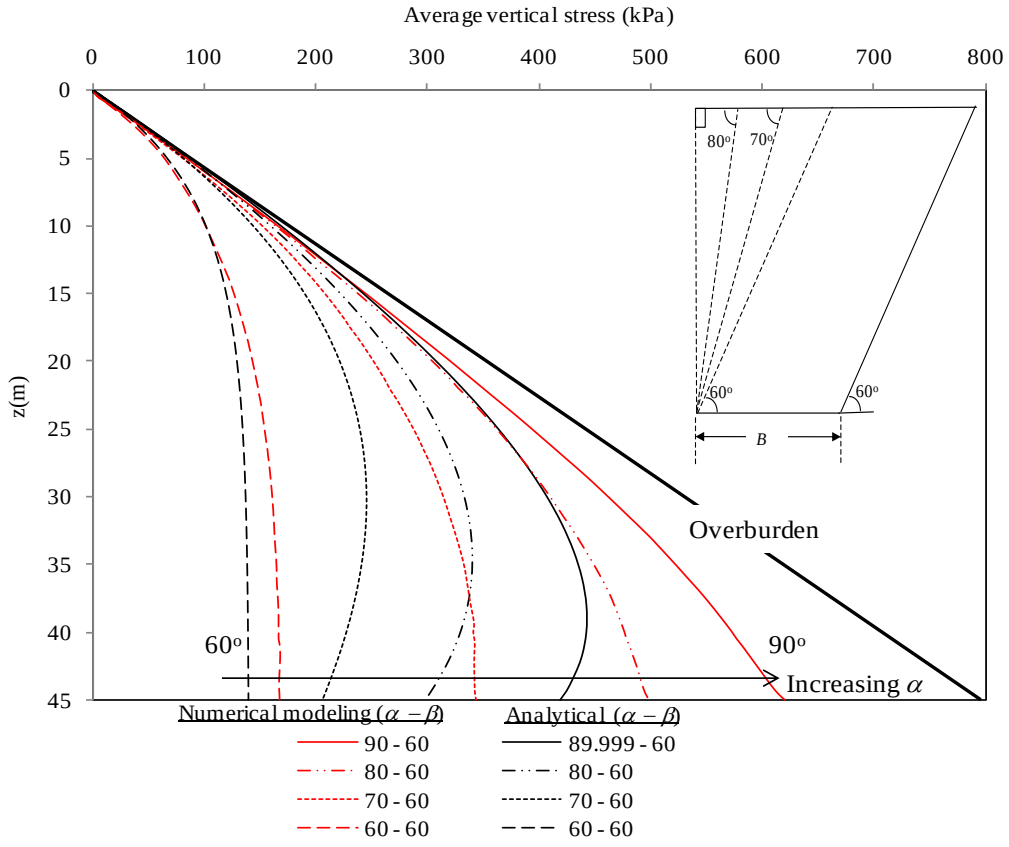

Figure 3.22. Vertical stress for stope with non-parallel walls where $\alpha > \beta$, $B = 6\ m$

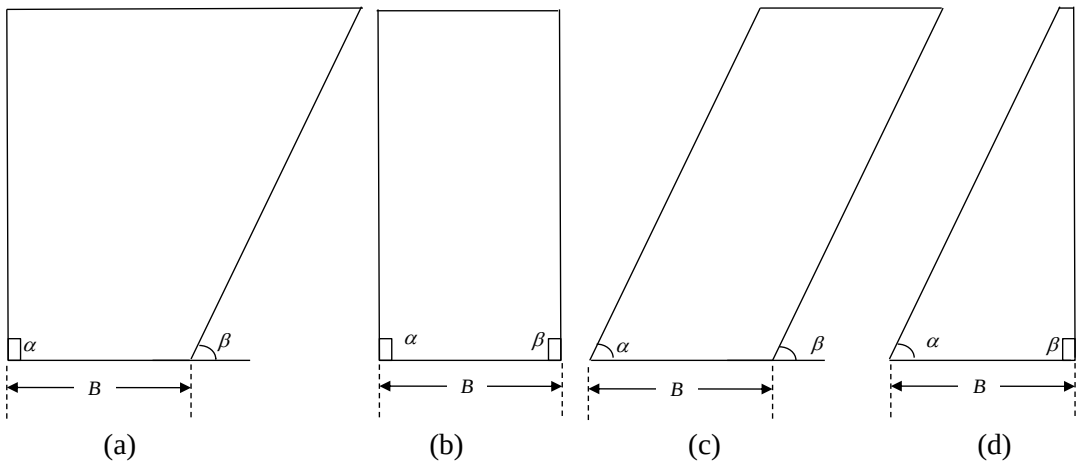

Figure 3.23. Stopes with different combination of wall inclination (α and β)

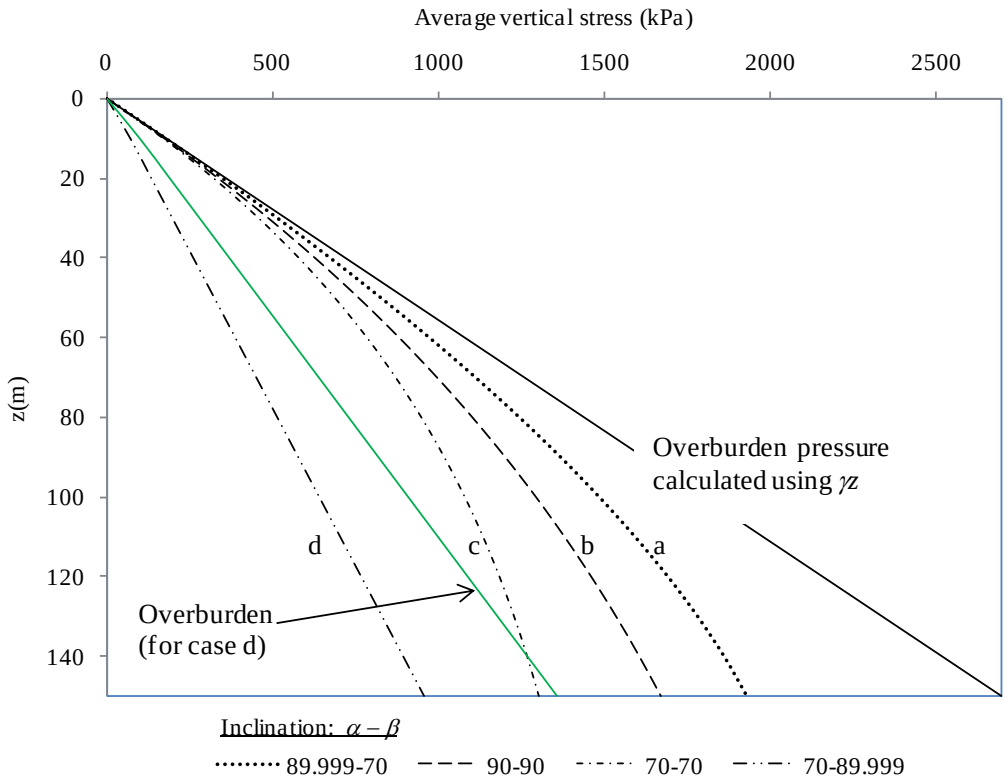

Figure 3.24. Comparison of average vertical stresses with depth for different combination of wall inclinations α–β, estimated from analytical equations *(H = 150 m, B = 55 m, $K = K_a$, c = 0, $\phi = \delta = 30^o$,γ =18 kN/m^3)*

Figures 3.23 (a - d) shows the diagrams of stope geometry with different combination of wall inclination (α and β). The corresponding results are presented in Fig.3.24. In all four cases, B = 55 m and H = 150 m. As the overburden pressure at any depth z in case (d) is significantly less compared to that of calculated using γz, a separate overburden line (shown in green) is plotted in Fig 3.24 to give better comparison for case (d). The line is computed by dividing the product of unit weight and area (γ*Area) with stope width at depth z:

$$Overburden\ pressure\ for\ case\ (d) at\ depth\ z = \frac{\gamma * Area\ at\ depth\ z}{Stope\ width\ at\ depth\ z} \qquad (3.74)$$

It can be observed from the Fig. 3.24 that arching takes place in all situations and more in case (c) than the other three. Case (a) shows the lowest level of arching. With same overburden pressure γz and base width B, the stress magnitude experienced by fill material at any depth z can be significantly varied due to the change in wall inclination.

3.4 Maximum vertical stress in inclined backfilled stope

One of the main findings reported in Chapter 5 (see Fig 5.9) from the laboratory model tests is that the vertical stress is at its maximum when the stope is inclined at 80^o to the horizontal. The attempt of this section is to check whether this is correct using the analytical expressions developed in this chapter.

The vertical stress at any depth *z* for an inclined stope with $c = 0$ and $q = 0$ is given by

$$\sigma_z = \frac{\gamma B}{2K\prime tan\delta}\left(1 - e^{-\frac{2K\prime tan\delta}{B}z}\right) \tag{3.21}$$

where $K' = \frac{1+K}{2} + \frac{1-K}{2}cos2\beta + Ktan\delta\ sin2\beta$ (3.9)

Let $u = \frac{2K\prime tan\delta}{B}$; (3.75)

then $\sigma_z = \frac{\gamma}{u}(1 - e^{-uz})$ (3.76)

Differentiating σ_z with respect to β to determine maximum or minimum value of σ_z,

$$\frac{d\sigma_z}{d\beta} = \frac{d\sigma_z}{du} \cdot \frac{du}{d\beta} = 0 \tag{3.77}$$

$$\Longrightarrow \quad \frac{d\sigma_z}{du} = 0\ or\ \frac{du}{d\beta} = 0$$

and

$$\frac{du}{d\beta} = 2\frac{tan\delta}{B}\frac{dK\prime}{d\beta} = 0 \quad \Longrightarrow \quad \frac{dK\prime}{d\beta} = 0 \tag{3.78}$$

As $\frac{1-e^{-uz}}{u}$ is a monotonically decreasing function and has no extremum (See Appendix A1), $\frac{d\sigma_z}{du} \neq 0$ and therefore $\frac{d\sigma_z}{d\beta}$ becomes zero when $\frac{du}{d\beta} = 0$. That is, when $\frac{dK\prime}{d\beta} = 0$.

$$\frac{dK\prime}{d\beta} = (K-1)sin2\beta + 2Ktan\delta\cos 2\beta\ = 0 \tag{3.79}$$

i.e., $(K-1)tan2\beta + 2Ktan\delta\ = 0$

$$\tan 2\beta = \frac{2Ktan\delta}{1-K} \tag{3.80}$$

$$\beta = \frac{1}{2}tan^{-1}\left(\frac{2Ktan\delta}{1-K}\right), \text{ and } 0 < \beta < \pi/2 \tag{3.81}$$

Note: The location where $d\sigma_z/dz = 0$ is independent of z.

The extremum of Eq. 3.81 as a maximum or minimum can be identified through second order differentiation. From Eq. 3.77,

$$\frac{d\sigma_z}{d\beta} = \frac{d\sigma_z}{du} \cdot \frac{du}{d\beta} = 0$$

$$\frac{d^2\sigma_z}{d\beta^2} = \frac{d}{d\beta}\left(\frac{d\sigma_z}{du}\right) \cdot \frac{du}{d\beta} + \frac{d\sigma_z}{du} \cdot \frac{d^2u}{d\beta^2} = 0$$

At the extremum, $\frac{du}{d\beta} = 0$, so

$$\frac{d^2\sigma_z}{d\beta^2} = \frac{d\sigma_z}{du} \cdot \frac{d^2u}{d\beta^2}$$

$$\frac{d\sigma_z}{du} = \frac{uze^{-uz} - 1 + e^{-uz}}{u^2}$$

$$= \frac{(uz+1)e^{-uz} - 1}{u^2} \; < 0, \; z \neq 0 \text{ (See Appendix A1)} \tag{3.82}$$

Next,

$$\frac{d^2u}{d\beta^2} = 2\frac{tan\delta}{B}\frac{d^2K\prime}{d\beta^2} = 2[(K-1)cos2\beta - 2Ktan\delta \; sin2\beta] \tag{3.83}$$

From Eq. 3.79, at the extremum $\frac{dK\prime}{d\beta} = 0$,

$$\cos 2\beta = -\frac{(K-1)sin2\beta}{2Ktan\delta} \;, \tag{3.84}$$

Substituting Eq. 3.84 into Eq.3.83, gives

$$\frac{d^2K\prime}{d\beta^2} = -2\frac{\left[(K-1)^2 + 4K^2tan^2\delta\right]}{2Ktan\delta} sin2\beta$$

Noting that $(K-1)^2 + 4K^2tan^2\delta > 0$, $K \geq 0$, $tan\,\delta > 0$,

$$\frac{d^2K\prime}{d\beta^2} < 0, \text{ and therefore } sin2\beta > 0. \tag{3.85}$$

Now, $sin2\beta > 0$ when $0 < 2\beta < \pi$. That is, $0 < \beta < \pi/2$. So, the vertical stress σ_z is a minimum when

$$\beta = \frac{1}{2}tan^{-1}\left(\frac{2Ktan\delta}{1-K}\right), \text{ and } 0 < \beta < \pi/2 \tag{3.81}$$

This analysis concludes that no maximum vertical stress falling within the range of $0 < \beta < \pi/2$, contradicting with the observation of the laboratory model tests, which gives the highest vertical stress around $\beta = 80^o$. The reason for this inconsistency is not clear at this stage, whether it is due to experimental anomalies or some factors that are not captured in the analytical model. Further investigation is required to assess this fact.

3.5 Summary and conclusion

This chapter develops analytical equations for the vertical stress at any depth, giving consideration to arching mechanism within inclined minefill stopes. The research undertaken can be divided into two major parts.

The first part of the study extends Marston's theory to include generalized plane strain inclined stopes with parallel walls. Comparatively, the results obtained from this study agree well with other limited analytical and numerical results reported in the literature (e.g. Caceres Doerner (2005) and Li and Aubertin (2009)). A parametric study is undertaken to investigate the effect of various parameters involved in the proposed analytical expression. The results obtained reveal that stope geometry, fill properties and stope inclination are critical factors in predicting the stress distribution in mine stopes.

The second part of the study relates to developing an analytical expression for plane strain inclined stopes with non-parallel walls where both walls leaning to the same side. The results reveal that the analytical expression developed is capable of estimating stress distribution within an inclined stope when $\alpha < \beta$. For the case where $\alpha > \beta$, stress reduction occurs at a depth above the bottom of the stope, which is unlikely. Further investigation is required to assess this limitation. This part of the study also show that, with the same overburden pressure γz, and base width B, the stress distribution experienced within a stope can be significantly varied due to the change in wall inclination.

An analysis on stress optimization is also being carried out in this section. The result reveals that there is no maximum vertical stress within the range of $0 < \beta < \pi/2$ (practical range) using the analytical method, contradicting with the observation of the laboratory model tests.

Chapter 4 A simple analytical method to determine vertical stresses within a granular material contained in right vertical prisms and inclined mine fill stopes

4.1 General

In large and tall storage containers/structures such as silos, hoppers and mine stopes, the average vertical stress at a depth within the vertical prism/stope can be significantly less than what is given by the product of unit weight and depth due to arching within the backfills. Here, a significant fraction of the self weight of the backfills is transferred to the walls in the form of friction, thus reducing the vertical stress at any level (Aubertin et al. 2003; Pirapakaran and Sivakugan 2006, 2007a, 2007b; Singh et al. 2010; Take and Valsangkar 2001).

There are few analytical expressions available in the literature, as discussed in Chapter 2, to determine the vertical stresses considering arching effects based on equilibrium considerations. These expressions have been used extensively in computing the vertical stresses in underground mine fill stopes, with K assumed as K_a or K_o, and δ assumed as $2/3\ \phi$ or ϕ where ϕ is the friction angle (Aubertin et al. 2003; Pirapakaran and Sivakugan 2007a; Singh et al. 2010).

In spite of their simplicity and independence from the constitutive behaviour of the fill material, Marston's model and it's modifications have come a long way to date in geotechnical applications. Recent work by Li and Aubertin (2008, 2009), Li et al. (2005) and Pirapakaran and Sivakugan (2007a, 2007b) suggest that these simple methods are the primary tools for computing the average vertical stresses within backfilled stopes, especially the ones where the walls are vertical, and they compare well with the values derived from sophisticated numerical models and laboratory measurements.

The purpose of this chapter is to propose an alternate analytical method that can be used to compute the average vertical stress within the granular material contained within a long container or stope, assuming plane strain conditions, which represents a storage structure in mining, civil and chemical engineering disciplines. The method is extended to accommodate a surcharge at the top of the granular material (section 4.4) and to storage structures with

sloping walls (section 4.5). Marston's based equations listed below, as discussed in Chapter 2, will be used to compare the results obtained from present study for vertical right containments.

For a stope with rectangular cross section in plan (Pirapakaran and Sivakugan 2007a):

$$\sigma_z = \frac{\gamma B - 2c}{2K tan\delta}\left(\frac{L}{L+B}\right)\left[1 - exp\left\{-\frac{2Kz\ tan\delta}{B}\left(\frac{L+B}{LB}\right)\right\}\right] \quad (2.3)$$

For square or circular stope (Pirapakaran and Sivakugan 2007a):

$$\sigma_z = \frac{\gamma B - 2c}{4K tan\delta}\left[1 - exp\left\{-\frac{4Kz\ tan\delta}{B}\right\}\right] \quad (2.4)$$

For plane strain model (Marston 1930):

$$\sigma_z = \frac{\gamma B}{2K\ tan\delta}\left[1 - \exp\left(-\frac{2Kz\ tan\delta}{B}\right)\right] \quad (2.5)$$

where B = breadth (or diameter) of the stopes, L = length of the stope in plan, H = height of the fill, γ = unit weight of the fill, c = cohesion of the fill, δ = friction angle between the fill and the wall, K = lateral earth pressure coefficient, σ_x/σ_z at the wall, and σ_x = horizontal normal stress.

4.2 Derivations

Initially, the derivation is carried out for stopes or containments where the walls are vertical. Later this is extended to inclined walls.

4.2.1 Pascal's triangle

The analytical method proposed herein uses the Pascal's triangle to develop a series solution. Let's divide the granular fill of height H and width B in Fig. 4.1 into M equal horizontal layers where each layer has thickness h and self weight V_0. In the first layer (m = 1), a fraction of the self weight V_0 is transferred to the bottom of the layer (V_1) and the rest is transferred to the wall (F_1) in the form of shear force. Let's assume that the fraction transferred to the wall is x, and the one transferred to the second layer is 1-x, as shown in Fig. 4.1. Here, $0 < x < 1$.

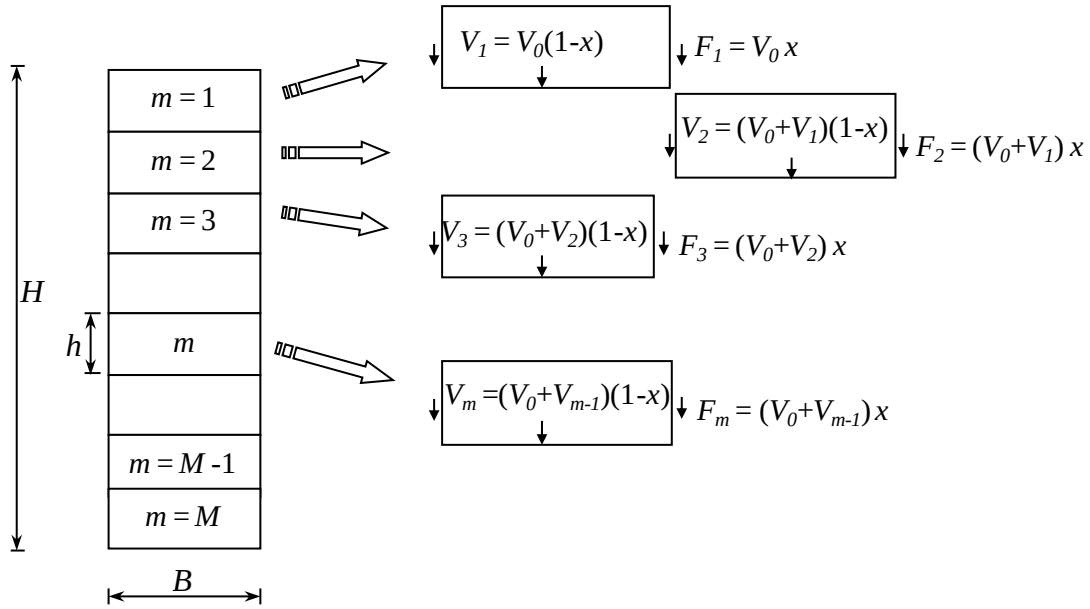

Figure 4.1. Granular fill layers and the loads transferred to the bottom and the wall

Table 4.1. Loads at the bottom of layers 1 to 7

Layer No., m	Load V_m acting at the bottom of the m^{th} layer
1	$V_1 = V_0\,(1 - x)$
2	$V_2 = (V_0 + V_1)\,(1 - x) = V_0(1 - x)(\mathbf{2 - x})$
3	$V_3 = (V_0 + V_2)\,(1 - x) = V_0(1 - x)(\mathbf{3 - 3x + x^2})$
4	$V_4 = (V_0 + V_3)\,(1 - x) = V_0(1 - x)(\mathbf{4 - 6x + 4x^2 - x^3})$
5	$V_5 = (V_0 + V_4)\,(1 - x) = V_0(1 - x)(\mathbf{5 - 10x + 10x^2 - 5x^3 + x^4})$
6	$V_6 = (V_0 + V_5)\,(1 - x) = V_0(1 - x)(\mathbf{6 - 15x + 20x^2 - 15x^3 + 6x^4 - x^5})$
7	$V_7 = (V_0 + V_6)\,(1 - x) = V_0(1 - x)(\mathbf{7 - 21x + 35x^2 - 35x^3 + 21x^4 - 7x^5 + x^6})$

The second layer (m = 2) carries its self weight V_0 and the load V_1 transferred from the upper layer. Therefore the load V_2 transferred to the bottom of the second layer is $(V_0 + V_1)(1 - x)$, and the load F_2 transferred to the wall is $(V_0 + V_1)x$. It can be deduced that, in the m^{th} layer, the loads transferred to the bottom of the layer (V_m) and to the wall (F_m) are given by:

$$V_m = (V_0 + V_{m-1})(1 - x) \qquad (4.1)$$

$$F_m = (V_o + V_{m-1})x \tag{4.2}$$

The loads acting at the bottom of the top seven layers are summarised in Table 4.1.

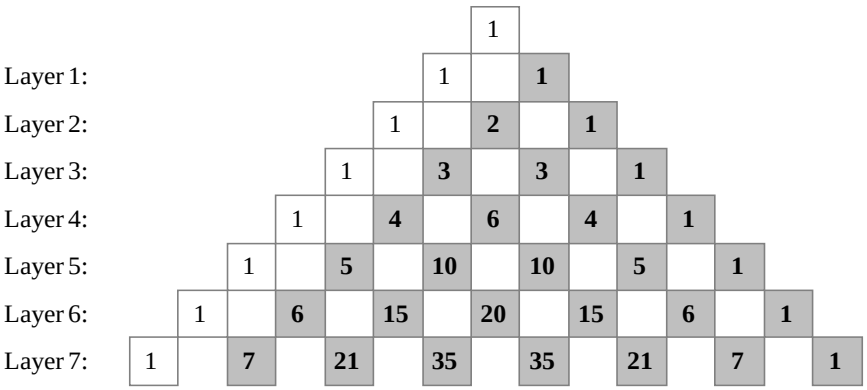

Figure 4.2. Pascal's triangle

It can be seen that the coefficients of the last term in Table 4.1, shown in bold, are the same as the entries in Pascal's triangle shown in Fig. 4.2, which is a triangular arrangement of the binomial coefficients (Chrystal 1964). These coefficients can be determined from the general expression of binomial coefficient involving factorials given by (Riley et al. 2002):

$$\binom{m}{i} = \frac{m!}{i!(m-i)!} \tag{4.3}$$

From Table 4.1, the load transferred at the bottom of layer m can be written as:

$$V_m = V_o(1-x)[a_1 + a_2x + a_3x^2 + a_4x^3 + a_5x^4 + \cdots + a_{m-1}x^{m-2} + a_mx^{m-1}] \tag{4.4}$$

where, $a_i = (-1)^{i+1}\binom{m}{i}$ for i = 1, 2,..., m. Eq. 4.4 can be written as:

$$V_m = V_0(1-x)\sum_{i=1}^{m}\left[(-1)^{i+1}\binom{m}{i}x^{i-1}\right] \tag{4.5}$$

For example, from Eq. 4.4, the vertical load at the bottom of the 7th layer (m = 7) can be written as:

$$V_7 = V_0(1-x)[a_1 + a_2x + a_3x^2 + a_4x^3 + a_5x^4 + a_6x^5 + a_7x^6]$$

where, $a_1 = (-1)^{1+1}\binom{7}{1} = 7$, $a_2 = (-1)^{2+1}\binom{7}{2} = -21$, $a_3 = (-1)^{3+1}\binom{7}{3} = 35$, $a_4 = (-1)^{4+1}\binom{7}{4} = -35$, $a_5 = (-1)^{5+1}\binom{7}{5} = 21$, $a_6 = (-1)^{6+1}\binom{7}{6} = -7$, and $a_7 = (-1)^{7+1}\binom{7}{7} = 1$.

In other words,

$$V_7 = V_0(1-x)[7 - 21x + 35x^2 - 35x^3 + 21x^4 - 7x^5 + x^6\,],$$

which is the same expression given at the bottom of Table 4.1.

Binomial expansion

The binomial theorem states that (Riley et al. 2002):

$$(a+b)^m = \sum_{i=0}^{m}\binom{m}{i} a^i b^{m-i} \tag{4.6}$$

Substituting a = -x and b = 1 in Eq. 4.6,

$$(1-x)^m = \sum_{i=0}^{m}\binom{m}{i}(-x)^i(1)^{m-i}$$

$$= \sum_{i=0}^{m}\binom{m}{i}(-1)^i x^i$$

$$= (-1)^0\binom{m}{0}x^0 + \sum_{i=1}^{m}(-1)^i\binom{m}{i}x^i$$

$$= 1 + \sum_{i=1}^{m}(-1)^i\binom{m}{i}x^i = 1 + \sum_{i=1}^{m}(-1)^i(-1)\binom{m}{i}(-1)xx^{i-1}$$

Therefore,

$$(1-x)^m = 1 - x\sum_{i=1}^{m}(-1)^{i+1}\binom{m}{i}x^{i-1}$$

$$\sum_{i=1}^{m}(-1)^{i+1}\binom{m}{i}x^{i-1} = \frac{1-(1-x)^m}{x} \tag{4.7}$$

Substituting Eq. 4.7 into Eq. 4.5, the vertical normal load at the bottom of m^{th} layer can be written as:

$$V_m = V_o\frac{(1-x)}{x}[1-(1-x)^m] \tag{4.8}$$

Therefore, in a plane strain situation shown in Fig. 2.5(b), the vertical normal stress at the bottom of the m^{th} layer is given by:

$$\sigma_z = \frac{V_m}{B} = \frac{V_o}{B}\frac{(1-x)}{x}[1-(1-x)^m] \quad (4.9)$$

Substituting $V_0 = \gamma Bh$, Eq. 4.9 becomes:

$$\sigma_z = \gamma h\frac{(1-x)}{x}[1-(1-x)^m] \quad (4.10)$$

The above equation is the same for rectangular, square and circular stopes without any taper, where the cross section remains the same at all depths.

4.2.2 Mathematical proof

The equation 4.8 can be proved mathematically from first principles as follows. Assuming the layers are of uniform thickness of weight V_o, the load acting at the base of layer-1, V_1 is

$$V_1 = V_o(1-x) \quad (4.11)$$

In the m^{th} layer, where $m = 2,\ldots,M$, the load V_m is given by

$$V_m = (V_o + V_{m-1})(1-x)$$

$$= V_o(1-x) + V_{m-1}(1-x) \quad (4.12)$$

This is a linear, non-homogeneous first order difference equation with constant coefficients for V_m. This can be solved by finding the solution to the homogeneous equation, then adding on a particular solution. The initial condition Eq. 4.11 can then be used to evaluate the arbitrary constant and fully define the solution.

The homogeneous equation is

$$V_m^{(H)} - (1-x)V_{m-1}^{(H)} = 0 \quad (4.13)$$

Assuming a solution of the form

$$V_m^{(H)} = A\lambda^m \quad (4.14)$$

the homogeneous Eq. 4.13 becomes

$$A\lambda^m - (1-x)A\lambda^{m-1} = A\lambda^{m-1}(\lambda-(1-x)) = 0 \quad (4.15)$$

For non-trivial solutions,

$$\lambda = 1 - x \tag{4.16}$$

and

$$V_m^{(H)} = A(1-x)^m \tag{4.17}$$

For a particular solution, try $V_m^{(P)} = p$ where p is a constant. Substituting into Eq. 4.12,

$$p = V_o(1-x) + p(1-x)$$

$$p = V_o(1-x) + p - px$$

$$p = \frac{V_o(1-x)}{x} \tag{4.18}$$

Therefore, the general solution is

$$V_m = V_m^{(H)} + V_m^{(P)}$$

$$= A(1-x)^m + \frac{V_o(1-x)}{x} \tag{4.19}$$

Now, using the initial condition Eq. 4.11 with $m = 1$, the solution specific to this problem is

$$V_1 = V_o(1-x)$$

$$= A(1-x)^1 + \frac{V_o(1-x)}{x} \tag{4.20}$$

Cancelling the common factor (1-x),

$$V_o = A + \frac{V_o}{x}$$

$$A = -\frac{V_o}{x}(1-x) \tag{4.21}$$

Hence, the load in layer-m is

$$V_m = -\frac{V_o}{x}(1-x)(1-x)^m + \frac{V_o(1-x)}{x}$$

$$V_m = \frac{V_o(1-x)(1-(1-x)^m)}{x} \tag{4.22}$$

which is the same as Eq. 4.8.

4.2.3 Determination of *x*, fraction of load transferred to the walls

1. *Long narrow stopes under plane strain conditions*

In plane strain situation, considering unit width, the vertical normal stress at the bottom of the m^{th} layer is given by:

$$\sigma_z = \frac{V_m}{B} = \frac{(V_o+V_{m-1})(1-x)}{B} \tag{4.23}$$

The horizontal normal stress at the wall is $K\sigma_z$. Assuming that the frictional coefficient at the wall-fill interface is tan δ, the maximum shear stress mobilized at the wall can be determined using the Mohr-Coulomb strength criterion as $K\sigma_z \tan\delta$, and can be written as:

$$\tau_m = K\ tan\delta\ \frac{(V_o+V_{m-1})(1-x)}{B} \tag{4.24}$$

The shear load is divided between the two walls, and the shear stress at the wall can also be derived from F_m as:

$$\tau_m = \frac{F_m}{2h} = \frac{(V_o+V_{m-1})x}{2h} \tag{4.25}$$

Equating Eqs. 4.24 and 4.25,

$$x = \frac{2Kh\ tan\delta}{B}\ (1-x)$$

Therefore,

$$x = \frac{\psi}{1+\psi} \tag{4.26}$$

where $\psi = \frac{2Kh\ tan\delta}{B}$.

2. *Stopes with rectangular or square cross-sections*

Consider a stope with *M* equal layers with height *H*, length, *L* and width *B*. The height of each layer is assumed as *h*, where *h = H/M*.

Weight of each layer,

$$V_o = \gamma BLh \tag{4.27}$$

The shearing force or load transferred to the walls for a rectangular model is

$$F_m = (V_o + V_{m-1})x = 2(B + L)\tau_m h \quad (4.28a)$$

and

$$\tau_m = K\sigma_{z-m} tan\delta \quad (4.28b)$$

The vertical stress acting at the base of layer-*m* gives

$$\sigma_{z-m} = \frac{V_m}{LB} = \frac{(V_o+V_{m-1})(1-x)}{LB} \quad (4.29)$$

Substituting Eq.4.29 into Eq.4.28

$$(V_o + V_{m-1})x = 2(B + L)\left(K\frac{(V_o+V_{m-1})(1-x)}{LB} tan\delta\right)h$$

$$x = 2(B + L)\left(K\frac{(1-x)}{LB} tan\delta\right)h$$

$$x = \frac{\psi_R}{1+\psi_R} \quad (4.30)$$

where $\psi_R = \frac{2(B+L)Kh\ tan\delta}{BL}$

For square cross-sectional, at which *L* = *B*,

$$V_o = \gamma B^2 h \quad (4.31)$$

$$x = \frac{\psi_s}{1+\psi_s} \quad (4.32)$$

where $\psi_s = \frac{4Khtan\delta}{B}$

3. *Stopes with circular cross-sections*

Consider a stope with *M* equal layers with height *H* and radius *R*. The height of each layer is assumed as *h*, where *h* = *H/M*.

Weight of each layer is,

$$V_o = \gamma\pi R^2 h \quad (4.33)$$

The shearing force or load transferred to the walls for a circular model is

$$F_m = (V_o + V_{m-1})x = 2\pi R\tau_m h \quad (4.34)$$

The vertical stress acting at the base of layer-*m* gives

$$\sigma_{z-m} = \frac{V_m}{\pi R^2} = \frac{(V_o + V_{m-1})(1-x)}{\pi R^2} \tag{4.35}$$

Thus, $(V_o + V_{m-1})x = 2\pi R\left(K\frac{(V_o+V_{m-1})(1-x)}{\pi R^2}tan\delta\right)h$

$$x = 2\left(K\frac{(1-x)}{R}tan\delta\right)h$$

$$x = \frac{\psi_c}{1+\psi_c} \tag{4.36}$$

where $\psi_c = \frac{2Kh\,tan\delta}{R}$ or with $B = 2R$, ψ_c becomes $\psi_c = \frac{4Kh\,tan\delta}{B}$.

The summary of *ψ-equation* is tabulated in Table 4.2.

Table 4.2. Expressions of *ψ-equation* for different cross-sectional shape

Model	Width	Length	Radius	Diameter	Area	V_o	ψ
Plane strain	*B*	-	-	-	*B*	γBh	$\frac{2hKtan\delta}{B}$
Square	*B*	*B*	-	-	B^2	γB^2h	$\frac{4hKtan\delta}{B}$
Rectangular	*B*	*L*	-	-	*BL*	γBLh	$\frac{2(B+L)hKtan\delta}{BL}$
Circular	-	-	*R*	*B*	πR^2	$\gamma\pi R^2h$	$\frac{2hKtan\delta}{R}$ or $\frac{4hKtan\delta}{B}$

4.3 Results and discussion

The use of the above method is illustrated through a simple numerical example below.

Given: A plane strain stope with B = 10 m, H = 60 m, c = 0, $\phi = 30^\circ$, γ = 18 kN/m^3

Solution: Let's assume $\delta = \phi = 30^\circ$, $K = K_0$ and divide the fill into 100 layers (i.e. M = 100 and h = 0.6 m).

From Jaky (1948), K_0 = 1 - sinϕ = 0.5.

Therefore, V_o =108 kN, $\psi = \frac{2Kh\,tan\delta}{B}$ = 0.03464, and from Eq. 4.26, x = 0.03348. Substituting these values in Eq. 4.9, for M = 100, σ_z = 301.4 kPa at the bottom of the fill.

Using Marston's equation Eq. 2.5 (with $K = K_o$ and $\delta = \phi$) separately, σ_z = 302.0 kPa, which is in very good agreement with the value predicted by the alternate method proposed herein. The predictions are better for larger values of M (i.e. more slices) and the computations are not any harder as the equations are the same. With 100 slices (M = 100), the predictions are within 1% of the values obtained from the Marston's equation. The variation of σ_z with depth, when the above fill is divided into 10, 50 and 100 layers, is shown in Fig. 4.3. It is quite clear that there is very little improvement by dividing the fill into more than 50 layers. Nevertheless, the computational effort is the same for any number of layers.

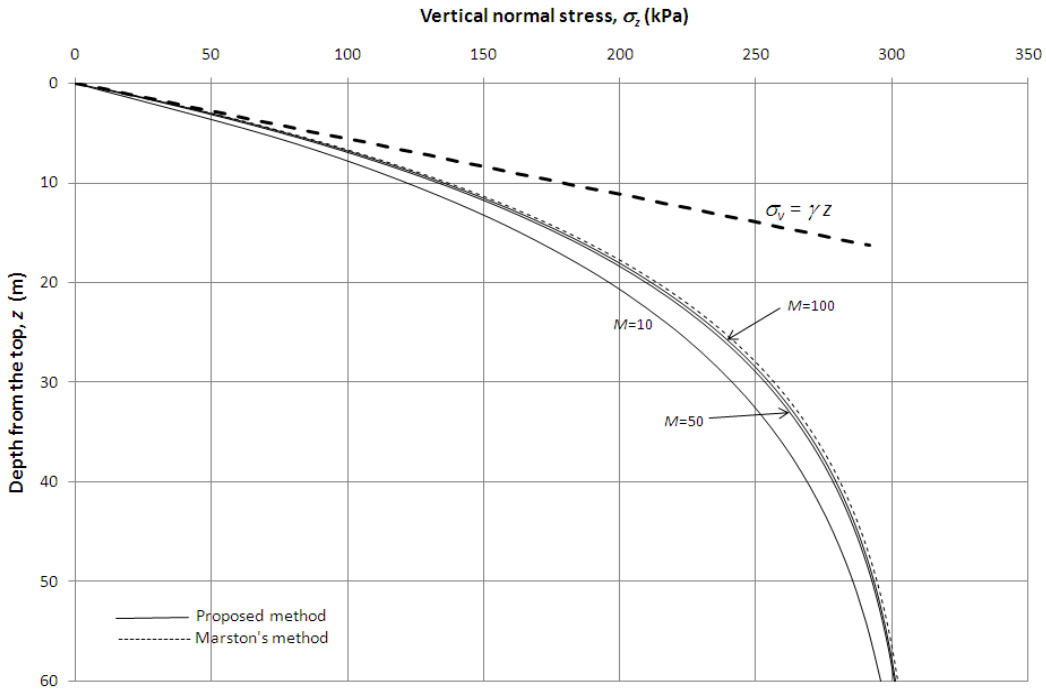

Figure 4.3. Variation of vertical normal stress with depth in a strip stope compared with Marston's method for several number of slices (M) in the proposed method, where B = 10 m, H = 60 m, γ = 18 kN/m^3, c = 0, $\delta = \phi$ = 30°

The vertical normal stresses estimated from the proposed method and the Marston's equation calculated using Eqs. 2.4 and 2.5 are shown in Fig. 4.4, for long strip, square and circular stopes of B = 10 m, H = 60 m, c = 0, γ = 18 kN/m^3, $\phi = \delta = 30^\circ$, M = 100. In square and circular stopes, since the walls are present right around the entire perimeter, there is substantial stress reduction taking place due to arching. The stress at the bottom of a square or circular stope is approximately half that in a long strip.

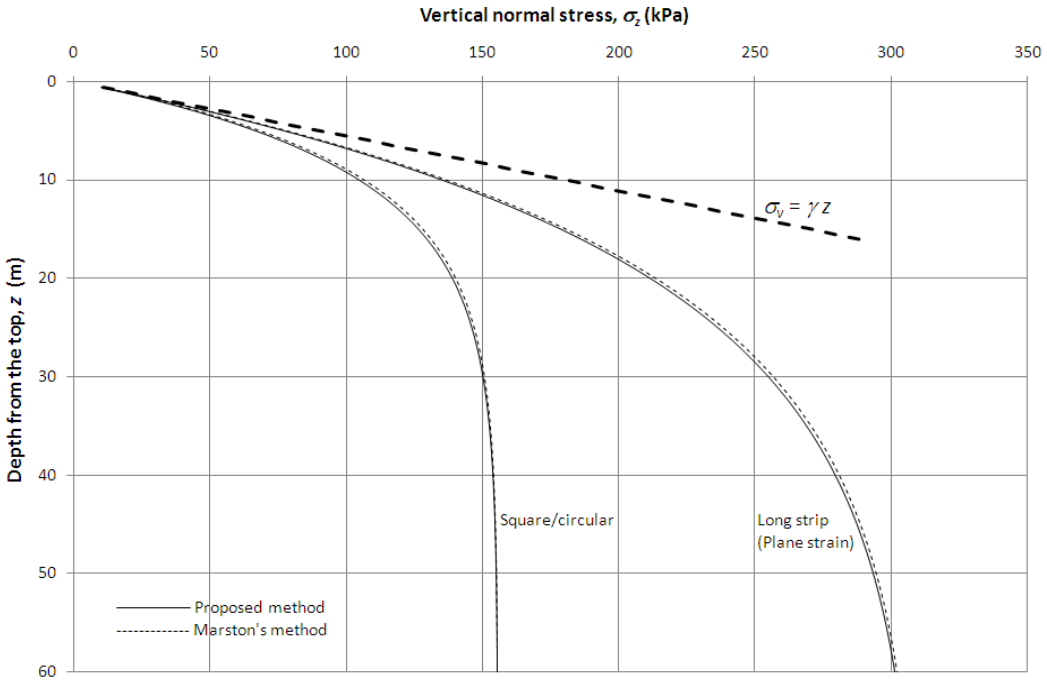

Figure 4.4. Variation of vertical normal stress within a strip, square and circular stopes where B = 10 m, H = 60 m, γ = 18 kN/m^3, c = 0, $\delta = \phi = 30^\circ$, M = 100

The solutions obtained from the proposed method are compared with the numerical results obtained by Li and Aubertin (2009) and Pirapakaran and Sivakugan (2006, 2007a) for strip (plane strain), circular (axi-symmetric) and square models in Figs. 4.5 (a - b). The numerical modeling by both Li and Aubertin (2009) and Pirapakaran and Sivakugan (2006) are carried out using an explicit finite difference code FLAC/FLAC^{3D} where the backfill is assumed to be an elasto-plastic material following the Mohr-Coulomb failure criterion.

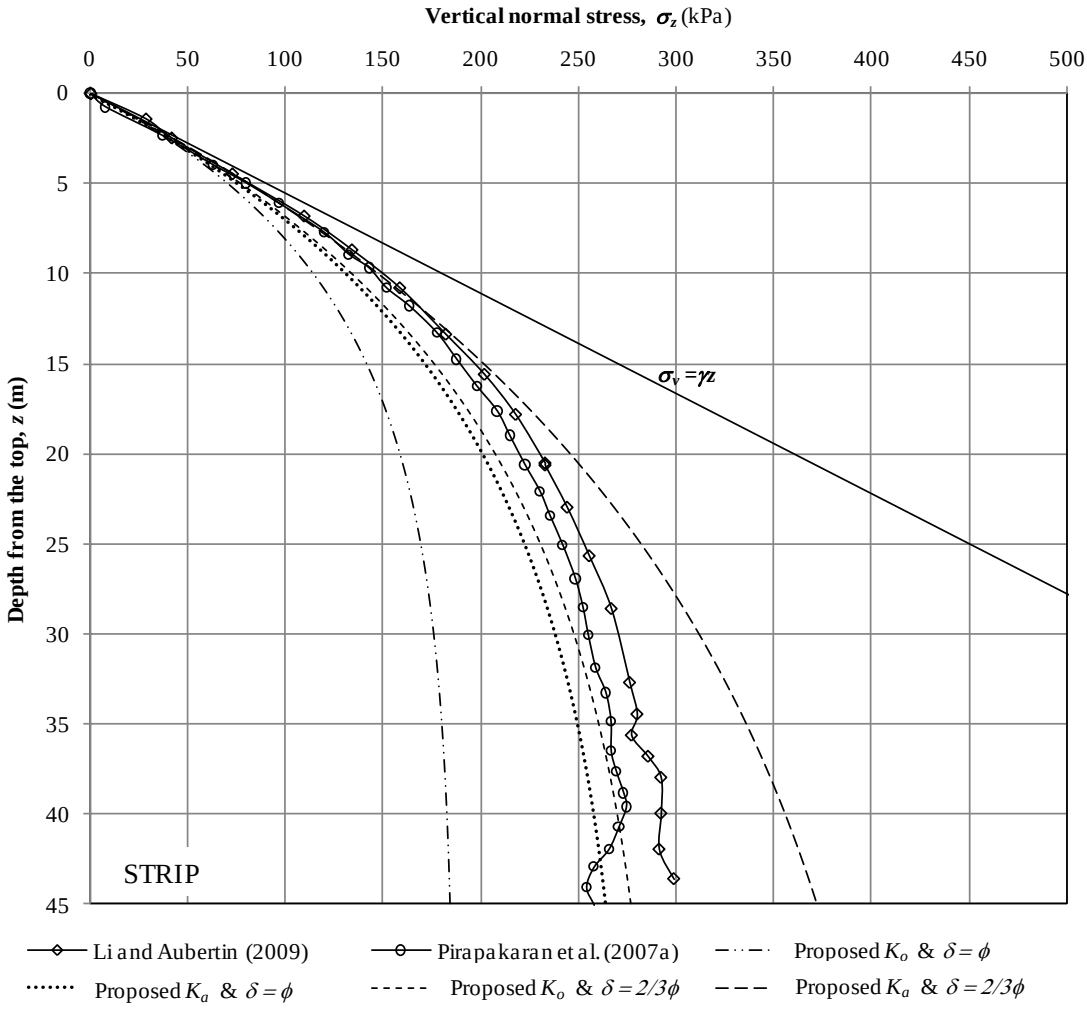
Vertical normal stress, σ_z (kPa)
0
50
100
150
200
250
300
350
400
450
500
0
5
10
15
20
25
30
35
40
45
Depth from the top, z (m)
$\sigma_v = \gamma z$
STRIP
Li and Aubertin (2009)
Pirapakaran et al. (2007a)
Proposed K_o & $\delta = \phi$
Proposed K_a & $\delta = \phi$
Proposed K_o & $\delta = 2/3\phi$
Proposed K_a & $\delta = 2/3\phi$

(a)

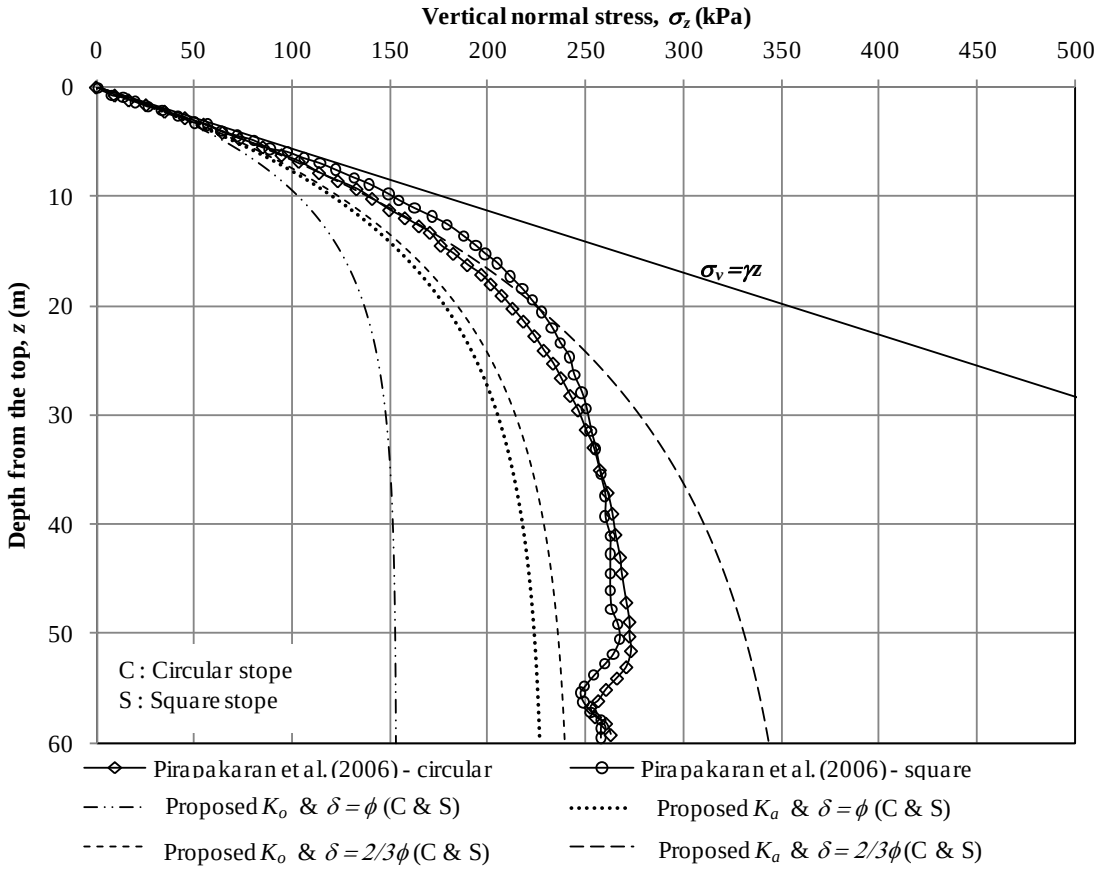

(b)

Figure 4.5. Variation of vertical normal stress: (a) within a strip stope with B = 6 m, H = 45 m, γ = 18 kN/m^3, c = 0, ϕ = 30°; and (b) within square and circular stopes with B = 10 m, H = 60 m, γ = 17.66 kN/m^3, c = 0, ϕ = 30°

Four different combinations of K (K_o or K_a) and δ (ϕ or $2/3$ of ϕ) have been used in the proposed analytical expression for comparison with the results from the elasto-plastic numerical model. It can be seen from Fig. 4.5 that good agreement is observed between numerical results and the proposed solutions for two of the four combinations: (a) $K = K_o$ and $\delta = 2/3\ \phi$ and (b) $K = K_a$ and $\delta = \phi$. These K-δ combinations agree well with the comments of:

- Li and Aubertin (2008) where they stated that the stress state is best described by considering the backfill is close to an active state ($K = K_a$) and the wall-fill interface is very rough and hence $\delta = \phi$, and
- Pirapakaran and Sivakugan (2007a) where they stated that $K = K_o$ and $\delta = 2/3\ \phi$ gives a very close match to numerical results.

4.4 Proposed method with surcharge at the top

It is not common to have a surcharge at the top of the mine fill within a stope or on top of the granular material within a silo. Nevertheless, the analytical method proposed herein can be extended to incorporate the surcharge load Q at the top of the fill. Here, Eq. 4.5 becomes:

$$V_m = V_o(1-x)\sum_{i=1}^{m}\left[(-1)^{i+1}\binom{m}{i}x^{i-1}\right] + Q\sum_{\boldsymbol{j=0}}^{\boldsymbol{m}}\left[(-1)^{\boldsymbol{j}}\binom{m}{i}x^{j}\right] \quad (4.37)$$

From binomial expansion,

$$(1-x)^m = \sum_{j=0}^{m}\binom{m}{j}(-1)^j x^j \quad (4.38)$$

Substituting Eqs. (4.7), (4.38) into Eq. (4.37),

$$V_m = V_o\frac{(1-x)}{x}[1-(1-x)^m] + Q(1-x)^m \quad (4.39)$$

Assuming that the surcharge load (Q) is in the form of a uniformly distributed pressure q at the top, the general expression for vertical stress at the bottom of a stope of any cross section is given by:

$$\sigma_z = \gamma h\frac{(1-x)}{x}[1-(1-x)^m] + q(1-x)^m \quad (4.40)$$

It is only the value of x that depends on the cross section. The way to compute x was discussed before in section 4.2.3.

4.5 Proposed method for stopes and containments with inclined walls

The analytical solution presented above can be extended to evaluate the vertical stress within an inclined stope as well. Herein, an attempt is made to extend this to inclined stopes with parallel walls, assuming a plane strain model. As Eq. 4.8 is dependent only on self weight of layer, V_o and fraction of load transferred to the wall, x, therefore, for stope with parallel walls (hanging and foot walls), Eq. 4.8 can be used to estimate the vertical normal load at the bottom of mth layer. Modification of the function of x is required to incorporate the wall inclination which will be discussed in this section.

From the basic stress transformation of soil mechanics (Das 1998), as discussed in Chapter 3, Eqs. 3.9-3.11 can be used to calculate the shear stress τ_m acting at the inclined walls with slope angle β to the horizontal. For granular fill where $c = 0$, these equation can be reduced to

$$\tau_m = K'\sigma_z tan\delta \tag{4.41}$$

where

$$K' = \frac{1+K}{2} + \frac{1-K}{2} cos2\beta + Ktan\delta sin2\beta \tag{3.9}$$

From section 4.2.3, Eq. 4.23 gives

$$\sigma_z = \frac{V_m}{B} = \frac{(V_0+V_{m-1})(1-x)}{B} \tag{4.23}$$

Hence, Eq. 4.24 becomes

$$\tau_m = K'tan\delta \frac{(V_o+V_{m-1})(1-x)}{B} \tag{4.42}$$

Since the walls are inclined, the shear load will not be shared by the two walls equally. However, the shear stress between the walls cannot be separated. Therefore, the average shear stress, τ_m at the two walls is used.

F_m is the total shear load carried by the two walls at m_{th} layer. The shear load, F_m is divided between the two walls for a plane strain model, and can be expressed as:

$$F_m = (V_o + V_{m-1})x = 2h\tau_m \tag{4.43}$$

Hence,

$$x = \frac{2K'h\ tan\delta}{B}\ (1-x)$$

$$x = \frac{\psi}{1+\psi} \tag{4.26}$$

where $\psi = \frac{2K'h\ tan\delta}{B}$.

It can be seen that all derivations and expressions are very similar to those for vertical walls, except for *K'* which replaces *K*.

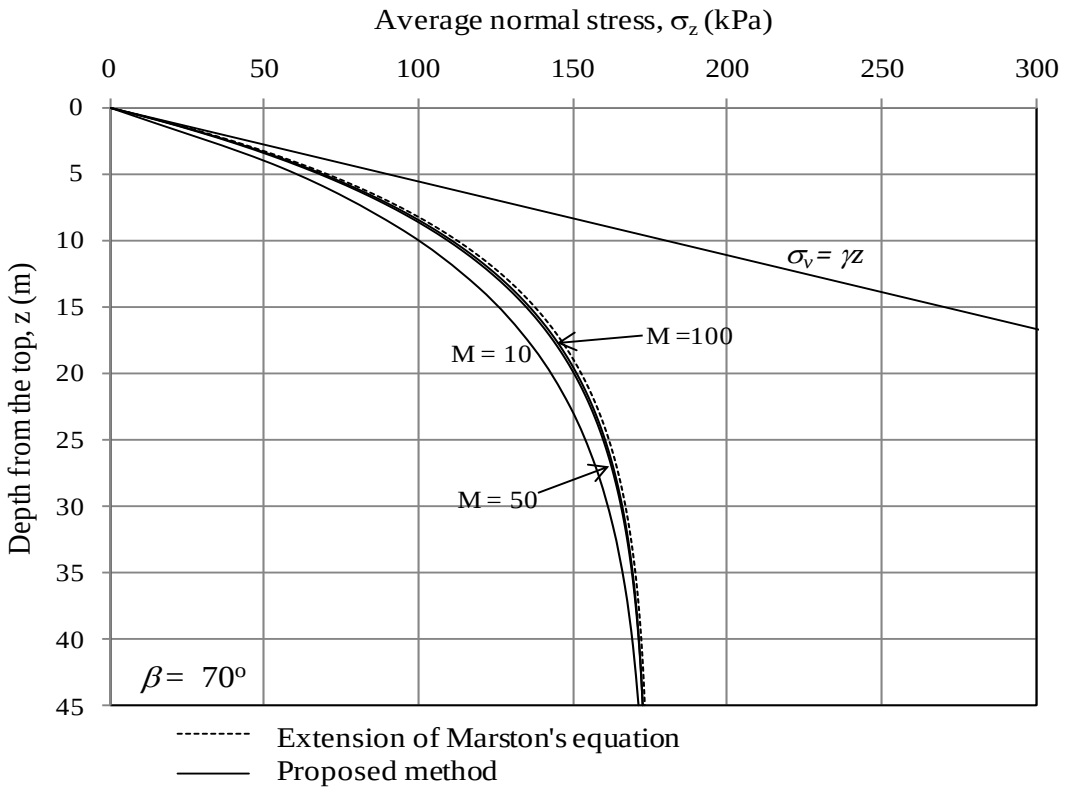

Figure 4.6. Variation of vertical normal stress with depth in a strip inclined stope compared with extension of Marston's equation (Eq. 3.15) for several number of slices (*M*) in the proposed method, where *B = 6 m, H = 45 m,* γ *= 18kN/m*^{3}*, c = 0 and* $\delta = \phi = 30^o$*,* $\beta = 70^o$

The prediction with the method proposed herein is compared with the expression developed in Chapter 3 (Eq.3.15) for an inclined stope. Fig. 4.6 shows the variation of σ_z with depth, with M = 10, 50 and 100. Similar conclusions as for vertical case can be drawn where very little or no significant improvement is observed with M > 50, indicating the convergence of σ_z for large M. Comparison of vertical normal stresses for different stope inclinations, estimated from the proposed method and Eq.3.15, is shown in Fig. 4.7. Both equations show very good agreement. Therefore, by replacing *K* with *K'*, Eq. 4.10 can still be used to estimate the vertical stress at any depth of an inclined stope in a plane strain situation.

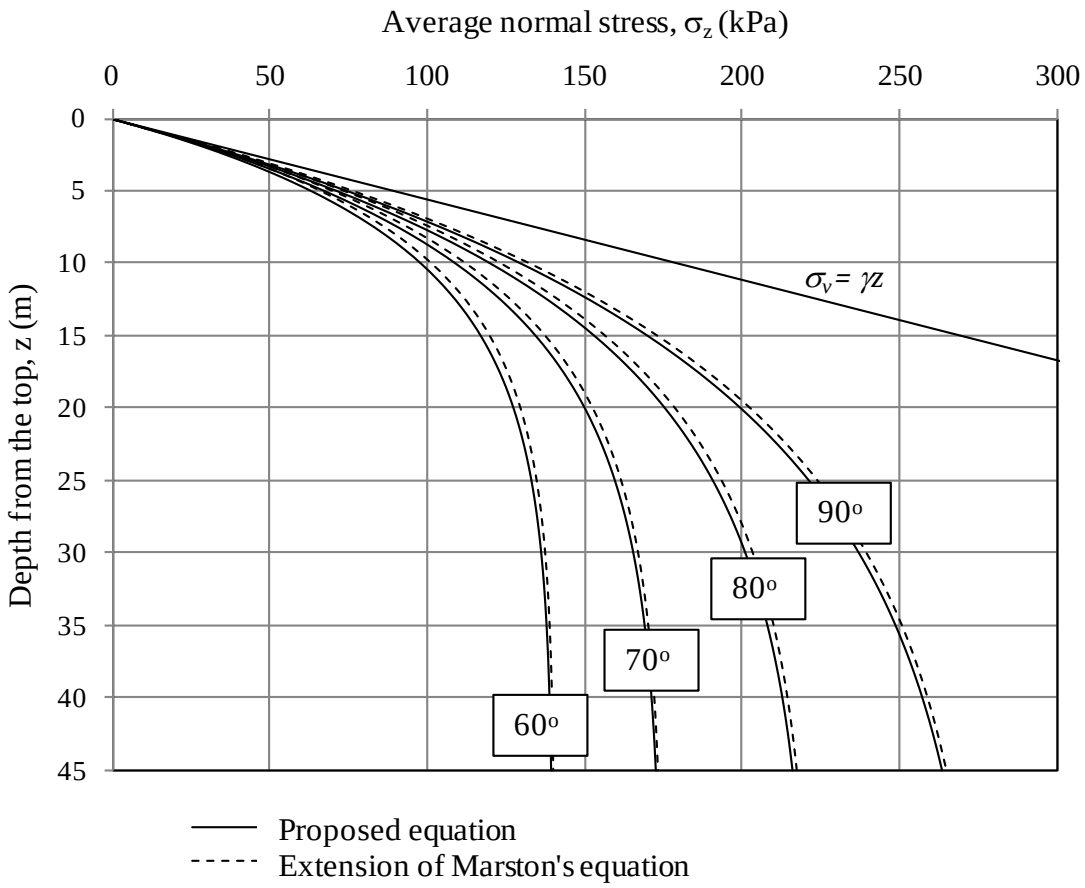

Figure 4.7. Comparison of vertical stresses for different stope inclination *where B = 6 m, H = 45 m, $\gamma = 18$ kN/m^3 ,K = K_a, c = 0, $\phi = \delta = 30^o$, q = 0, M = 45*

4.6 Summary and conclusions

A simple analytical method to compute the vertical stresses within a right vertical or inclined containment, filled with a granular material, is proposed. This situation occurs in underground mine stopes backfilled with granular mine fills such as hydraulic fills, and silos storing grains, sugar, etc. Due to the wall friction, a significant fraction of the fill weight is carried by the wall. The normal vertical stress at the bottom of the stope, irrespective of the cross sectional shape, is given by:

$$\sigma_z = \gamma h \frac{(1-x)}{x}[1-(1-x)^m] + q(1-x)^m \qquad (4.40)$$

where the fill is divided into *m* layers of thickness *h*, and *q* is the surcharge pressure at the top of the fill. The value of *x* is given by general equation,

$$x = \frac{\psi}{1+\psi} \qquad (4.29)$$

where $\psi = \frac{2(B+L)Kh\tan\delta}{BL}$ for rectangular stopes and $\psi = \frac{4Kh\ tan\delta}{B}$ for square and circular stopes. For long strips, a special case of a rectangular stopes, $\psi = \frac{2Kh\ tan\delta}{B}$ for vertical stope and $\psi = \frac{2K'h\ tan\delta}{B}$ for inclined stope.

The values of vertical normal stresses computed for a long strip, square and circular cross sections are in excellent agreement with those computed from Marston's theory. Recent research has shown that Marston's expression and its extensions still remain the main analytical tool for estimating the average vertical stress at any depth within a mine fill. Validation of these analytical methods against numerical and laboratory model tests have been found to be satisfactory. Comparison with elasto-plastic numerical modeling results also show that, the proposed method is in very good agreement, provided the K and δ values are taken as follows: (a) $K = K_0$ and $\delta = 2/3\phi$, or (b) $K = K_a$ and $\delta = \phi$.

Here, the analytical model is calibrated against numerical results by changing the combination of K and δ. It would be recommended in the future research that a friction force factor, $k_{friction}$ is introduced in the equation to allow for the cases in which the maximum friction force is not reached while choosing K and δ based on physical situation rather than calibration requirements. For example, if $K = K_o$ and $\delta = \phi$ are more appropriate to be used from the physical conditions of a stope, these values will be used in the analytical model by finding an appropriate $k_{friction}$ value such that the vertical normal stress σ_z computed from the analytical model agrees well with the corresponding numerical results.

The developed analytical expressions are of particular interest in mining geomechanics, where it is necessary to determine the vertical stresses within the mine stopes that can be approximated as right vertical/inclined prisms and silos used for storing flour, sugar and grains. More than the expressions, the method itself would pave the way for its extended application to inclined stopes with different cross sectional shape and hoppers.

Chapter 5 Laboratory model of an inclined stope

There are three major techniques, namely analytical modeling, numerical modeling and laboratory/field measurements, that have been undertaken in the past to investigate the stress distribution within the backfill inside vertical and inclined stopes (Aubertin et al. 2003; Caceres Doerner 2005; DeSouza and Dirige 2002; Fahey et al. 2009; Knutsson 1981; Li and Aubertin 2008, 2009; Li et al. 2005, 2007; Pierce 2001; Pirapakaran and Sivakugan 2006, 2007a). So far, the only laboratory model tests conducted are to study the stress distribution within a vertical stope by Pirapakaran and Sivakugan (2007b) and no model tests have been developed to study the effects of stope inclination on stress distribution. Most of the present studies on inclined stopes are based on numerical modeling and there is limited work on analytical modeling. At present, these models are compared against each other. Therefore, a physical model that can exhibit arching effect and simulate the filling process within an inclined backfill stope, enabling vertical stress measurements, is very valuable.

The objective of this study is to extend the laboratory model of Pirapakaran and Sivakugan (2007b) to a plane strain inclined stope in order to study the vertical stress variation with depth within inclined backfill stopes. This also serves as a validation tool for comparing with analytical and numerical modeling results. Pore water pressure is not considered in the model, and the fill can be assumed dry.

5.1 Properties of backfilled material

The purpose of this exercise is to develop a small-scale laboratory model, using which a series of tests can be carried out that can be compared against the value derived from the analytical or numerical models. It is not necessary that real hydraulic fills be used in the model tests. It is only required that the same properties be used in the numerical and analytical studies for a meaningful comparison. Having this in mind, it is decided to use ordinary river sand which is very similar to hydraulic fills in the entire laboratory test program. From past studies, it is observed that the factors such as density, friction angle, etc, that influence the vertical stress distribution are the same for this sand and common hydraulic fills used as backfills in mines (see Table 5.1). Some hydraulic fills can have relatively higher densities due to their larger specific gravity values, which are attributed to the mineral compositions. In dry condition, both materials are similar in their physical and mechanical characteristics. In arching study, the influencing factors are usually related to

the confinement of fill material, stope geometry and relative interface characteristics. They may differ in the magnitude of the results due to the differences in unit weight. However, both should give similar arching behavior and stress profile. Further, this sand has been used at James Cook University Geomechanics laboratory for several years and the parameters determined can be cross checked. In addition, for future research at James Cook University, where they will use the same sand, a meaningful comparison can be made with the data reported herein.

As reported by Li and Aubertin (2009) and Singh et al. (2010), the vertical stress within the granular fill contained in a stope or silo is insensitive to the friction angle, provided the friction angle is greater than 30^o. The numerical and analytical studies show the same results. Therefore, no attempt is made to carry out the laboratory model tests at too many different relative densities, *Dr* (or friction angles, ϕ). Tests are carried out only at 30% and 60% relative densities for a uniformly graded sand with effective grain size D_{10} = 0.13 mm and uniformity coefficient C_u = 3.1. The same properties are used in analytical and numerical studies for comparison in Chapter 6.

Table 5.1. Material properties for sand and minefill (Geotechnical info.com 2011; Rankine et al. 2006)

Properties	Sand	Fill
Dry density, ρ_d (kg/m^3)	1345 - 2370	1800 - 4400
Friction angle, ϕ (^{o})	30 - 45	30 - 45
Cohesion, c	0	0 in dry condition
Poisson's ratio, ν	Depends on % of relative density	0.15~0.40
Relative density, *Dr* (%)	Depends on degree of compaction	45-80 on placement

A series of laboratory tests were carried out to determine the properties of the granular backfill material as per Australian standards listed in Table 5.2. The interfacial friction angle was determined using modified direct shear test (Pirapakaran 2008) where the conventional direct shear box test was modified by replacing the lower half of the apparatus with Perspex flat box with different roughness surfaces. The same grade of sandpaper

mounted onto the model stope wall was used here to provide the roughness. The low wall roughness in Table 5.4 implies Perspex walls with no sandpaper attached.

The sand specimens were prepared with relative densities ranging from loose to dense conditions in order to establish a relationship between the material parameter (friction angle, interfacial friction angle and elastic modulus) and relative density (see Appendix B1). The physical properties were summarized in Table 5.3. The friction angles and interfacial friction angles tabulated in Tables 5.3 and 5.4 were adjusted for the plane strain condition within the stope (Sivakugan and Das 2010). Figure 5.1 showed the particle size distribution of the sandy backfill material used in the study.

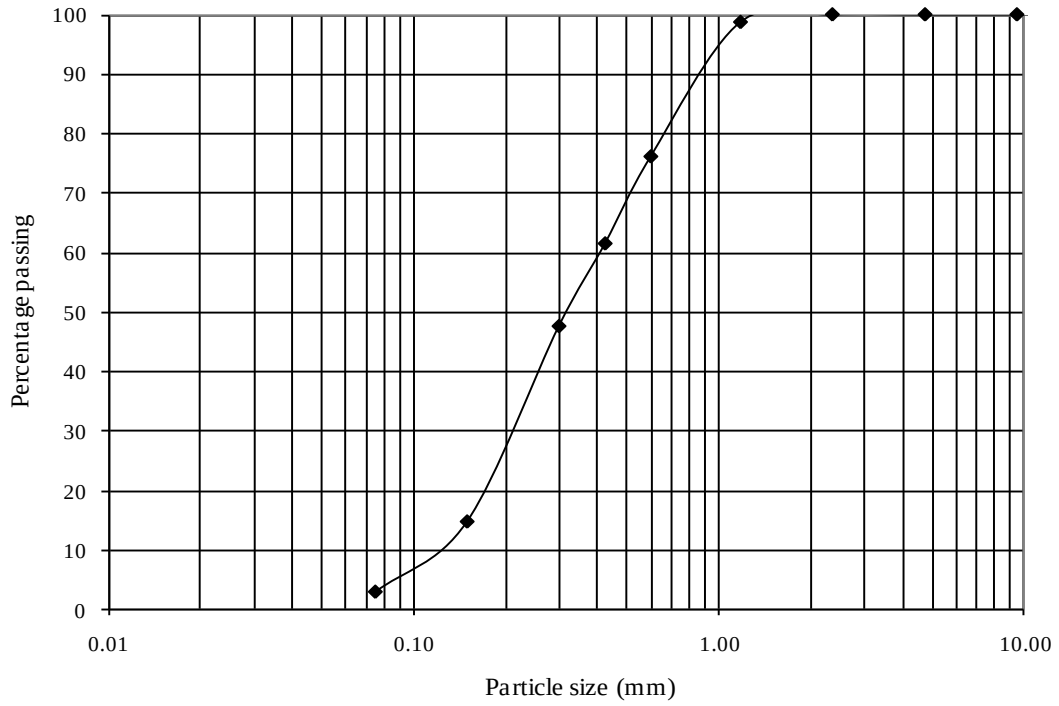

Figure 5.1. Particle size distribtuion curve of granular backfill material

Table 5.2. Laboratory test program for the granular soil

Properties	Method /Australian Standard used
Grain size distribution	AS1289.3.6.2-1995 (Standards Australia 1995)
Specific gravity	AS 1289.3.5.1-2006 (Standards Australia 2006)
Maximum and minimum density	AS1289.5.5.1- 1998 (Standards Australia 1998a)
Friction angle and dilation angle of sand	AS1289.6.2.2-1998 (Standards Australia 1998b) Plane strain friction angle, $\phi_{ps} = tan^{-1}(1.2tan\phi_{ds})$ where ϕ_{ds} is the friction angle from direct shear (Sivakugan and Das 2010). Dilation angle, $\varphi = 1.25\left(\phi_{peak} - \phi_{cv}\right)$ where ϕ_{peak} and ϕ_{cv} are the peak and residual friction angle respectively (Bolton 1986).
Interface friction angle	Modified direct shear test (Pirapakaran 2008)
Elastic modulus	AS1289.6.6.1-1998 (Standards Australia 1998c) Oedometer modulus, $D = \frac{(1-\nu)}{(1+\nu)(1-2\nu)}E$ and $E = \frac{(1+\nu)(1-2\nu)}{(1-\nu)}D$ where E = Young's modulus and ν = Poisson's ratio ranging from 0.2 in loose state to 0.4 in dense state

Table 5.3. Physical properties of backfilled granular material

Properties	Relative density	
	(30%)	(60%)
Initial moisture content, w (%)	0.24	0.24
Specific gravity, G_s	2.58	2.58
Young's Modulus, E (kPa)	420	420
Minimum dry density, $\rho_{d,min}$ (kg/m^3)	1430	1430
Maximum dry density, $\rho_{d,max}$ (kg/m^3)	1676	1676
Dry density, ρ_d (kg/m^3)	1496	1568
Peak friction angle, ϕ_{peak} (^{o})	40	41
Residual friction angle, ϕ_{cv} (^{o})	38	38
Dilation angle, φ (^{o})	2.5	3.75

Table 5.4. Summary of interface friction angle for different wall roughness

Properties	Relative density	
	(30%)	(60%)
Interface friction angle – high wall roughness, δ_R (^{o})	39	40
Interface friction angle – medium wall roughness, δ_M (^{o})	32.5	33.6
Interface friction angle – low wall roughness, δ_S (^{o})	27	28

5.2 Laboratory model

Based on a concept similar to that of the experimental model developed by Pirapakaran and Sivakugan (2007b), a small scaled inclined plane strain model with additional strain gauges attached to the outer side of the long wall of framework was developed to study stresses within the granular fill as well as stresses acting on the hangingwall and footwall. The model of Pirapakaran and Sivakugan (2007b) replicated vertical stopes without using strain gauges. To separate the self weight of the fill carried by the hangingwall and the footwall, it was necessary to use strain gauges. This was not the case with the vertical walls, where they were the same and hence the wall load was simply apportioned equally to both walls. A brief description of the new model for the inclined stope was provided below.

5.2.1 Apparatus

Fig. 5.2(a) shows the diagram of the complete setup to scale, and Fig. 5.2(b) is a photograph of the same. The connections and the dimensions that cannot be shown in Fig. 5.2 are shown through Fig. 5.3. The apparatus consists of the following components:

- A model stope, made of Perspex, which can be adjusted to inclination of 90^o, 80^o, 75^o and 70^o to the horizontal by placing it on the appropriate base (Fig. 5.3);
- A metal frame from which the stope is suspended as shown in Figs. 5.2(a) and 5.2(b);
- A 60 kg-balance located below the stope with a clearance of less than 1 mm between the base of the stope and the balance, to measure the weight of backfill transferred to the base;
- A high precision load cell connected to a digital readout unit, to measure the backfill weight transferred to both the walls of the stope;
- 8 strain gauges (4 on each side) mounted at equal spacing along the centerline of outer side of stope, which are connected to a data logger TDS-602 unit, to measure the deformation experienced by the walls due to the loading on both walls (hangingwall and footwall) separately. These readings are used as the basis to apportion the wall load between the two walls; and
- A funnel with adjustable opening, which is used to place the backfill material onto the stope. The relative density can be controlled by varying the mass of falling material through the opening (depositional intensity). Due to the space limitation, the deposition of the sand into the box is done from a prescribed height. As the depth of the soil is substantial, differences in relative density may occur through the height of the specimen. Therefore, the relative density used throughout the text is referred to as average relative density within the stope.

The stope with length (L) to width (B) ratio of 5 and height of the model to width ratio of 9 is adopted. Pirapakaran (2008) carried out numerical modeling of 3-dimensional stopes of different L/B ratios and concluded that the stress profiles remain approximately constant for $L/B > 4$. Therefore, a model with $L/B = 5$ is suitable to model plane strain condition. The dimensions of the model stope used in this study are:

- Shortest width of the model (between hangingwall and footwall): 100 mm

- Length of the model: 500 mm
- Height of the model: 900 mm

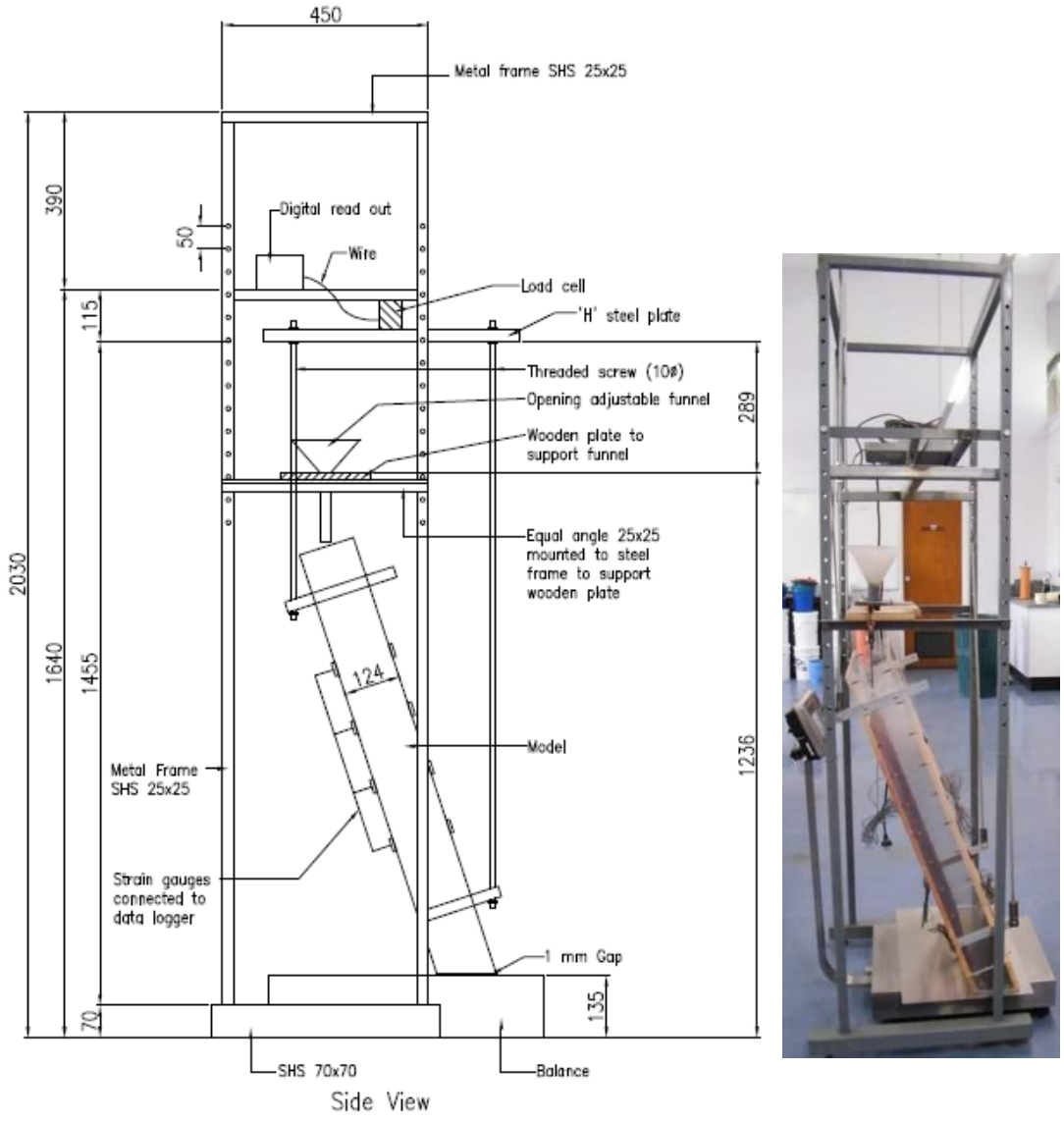

(a) (b)

Figure 5.2. (a) The diagram of the apparatus to scale and (b) a photograph of the laboratory experimental model

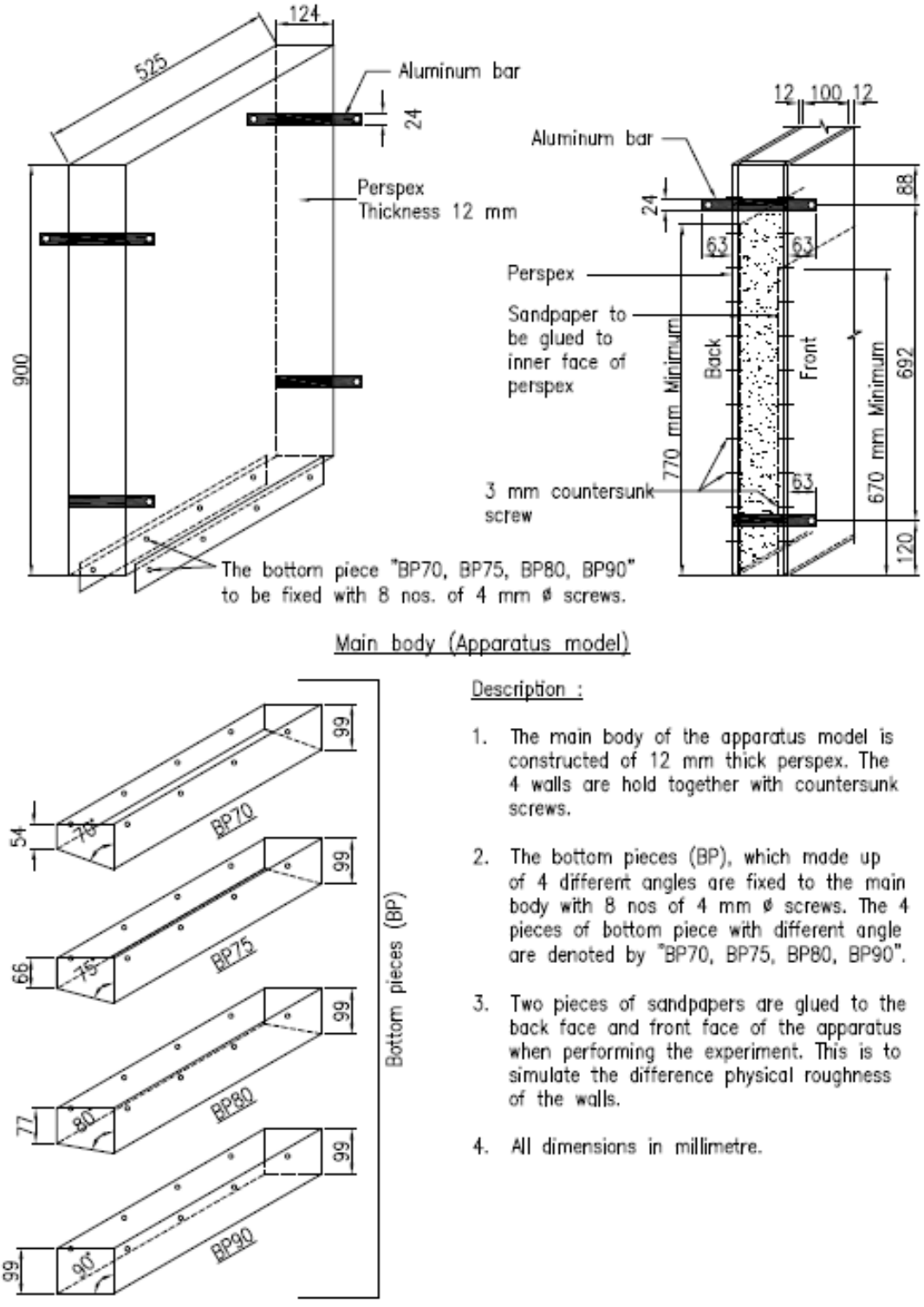

Figure 5.3. Further details of the model stope

Depending on the surface roughness required, sandpapers of two different grades are glued to the inner wall surface of Perspex model stope to represent medium and high roughness of the wall. The low wall roughness is represented by the original smooth surface of framework. Table 5.5 lists the material used for different surface roughness and their trade names. Selleys KWIK GRIP contact adhesive is used to attach the sandpaper to the wall.

Table 5.5. Sandpaper used to represent different wall roughness

Wall roughness modeled	Material	Grade of sandpaper
Low	Original surface of Perspex	No sandpaper
Medium	Sandpaper	KMCA P1200 Wet/Dry S85 Silicon Carbide electro coated water proof abrasive paper
High	Sandpaper	KMCA Garnet G62 P40 Garnet electro coated dry sanding abrasive paper

5.2.2 Strain gauges

In vertical stopes, the self weight of the fill carried by the stope walls is shared equally between the two walls. In the case of inclined stopes, the self weight carried by the two walls can be quite different; footwall will carry a larger fraction than the hangingwall. The high precision load cell simply measures the fraction of the self weight that is jointly carried by the two walls. To separate the components carried by the hangingwall and the footwall, strain gauges are employed (Dally and Riley 1991; Window and Holister 1982). When backfill material is loaded into the stope, there will be minor deformations on the Perspex walls. As the intention of this experiment is to determine the ratio of loads acting on footwall compared to hangingwall, single linear-position TML strain gauges (PFL-30-11-3L) are used for this purpose. CN CYANOACRYLATE adhesive is used to attach the TML strain gauge to the stope wall at four locations on both hanging and footwall walls. Fig. 5.4 and Table 5.6 show the location of strain gauges in the laboratory model. As it is difficult to deduce the stress experienced by the wall through single linearly positioned strain gauge, a simple method is introduced to apportion the total load into the fraction carried by the hangingwall and the footwall.

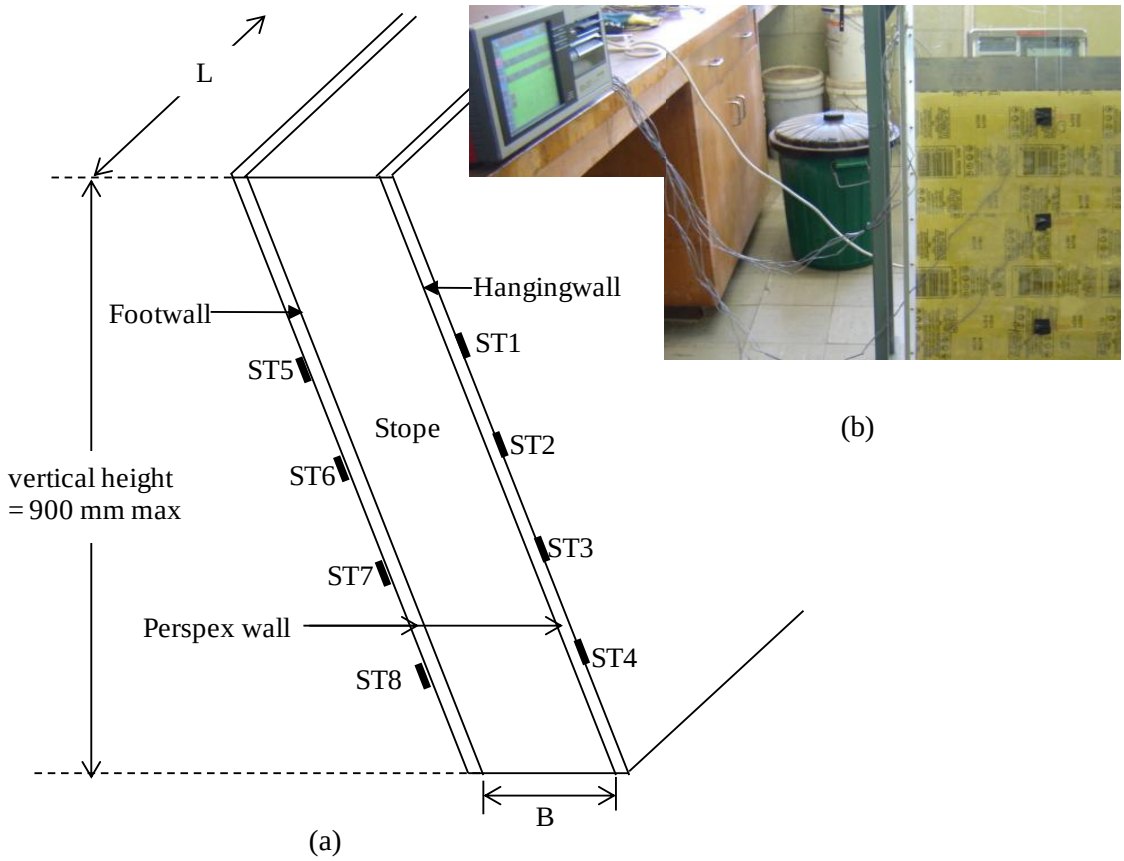

Figure 5.4. (a) Schematic diagram of strain gauges' positions (b) A close up view of strain gauge to show how it was installed

Table 5.6. Heights of strain gauges from the base of stope

Inclination to the horizontal (degrees)	Vertical height of strain gauge from base (mm)							
	Front (Hangingwall)				Rear (Footwall)			
	ST1	ST2	ST3	ST4	ST5	ST6	ST7	ST8
90	739.0	539.0	339.0	139.0	784.0	584.0	384.0	184.0
80	727.8	530.8	333.8	136.9	750.4	553.5	356.5	159.5
75	713.8	520.6	327.4	134.3	725.4	532.2	339.0	145.9
70	694.4	506.5	318.6	130.6	694.4	506.5	318.6	130.6

The wall loads carried by the hangingwall and footwall are related to the normal stresses acting on them. The normal stresses on the stope walls can be approximated as point loads distributed along the walls. These normal stresses (or the equivalent point loads) are measures of the wall loads. The strain gauge readings are therefore measures of these distributed point loads. The simplistic calibration is carried out on the empty stope lying flat on the two supports. Point loads are applied at the location of the strain gauges and the loads are plotted against the strain (see Fig 5.5). It is noted that, in all cases the strain gauge readings increase linearly with the applied loading. The average values of the four strain gauges are used as the basis for apportioning the total wall load (i.e. hangingwall plus footwall) measured by the load cell to the hangingwall and the footwall. The calibration technique used is simple and crude; however, it can be seen later (Table 5.8) that the apportioning carried out on the experimental results match the numerical values calculated using stress transformation concept of soil mechanics.

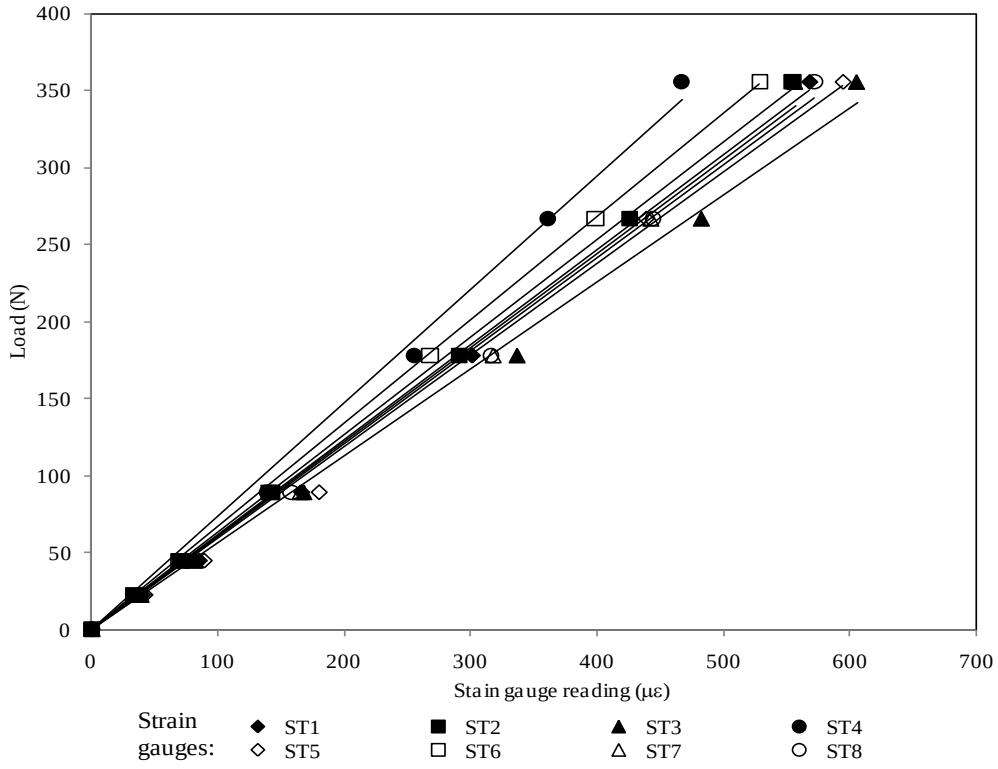

Figure 5.5. Calibration results of strain gauges for stope with inclination 80^{o} and low wall roughness (see Appendix B2 for medium and rough wall roughness)

5.2.3 Methodology and Interpretation

The following procedure had been used to perform the laboratory tests. To ensure reproducibility, the tests were carried out in triplicate and average values were used for each combination based on the inclination, surface roughness and relative density of the material.

1. For each test, the mass of backfill material for the desired relative density was determined in order to maintain the final aspect ratio of vertical-height/span-width = 7, and the material was then split evenly among 7 containers. The material in each container was further split into 6 equal portions, enabling the stope be filled in 42 equal layers (see Fig. 5.6).

2. The model as shown in Fig. 5.2 was setup with a small gap (less than 1 mm) between the stope and the weighing scale. As the granular material used in the test had particle size smaller than 1 mm, less than 100 g (about 7% - 8% of the material required for a single pour or 0.2% of the material required to complete the filling) of material will flow through the gap at the first stage of filling. As the influence was insignificant, this small fraction of material was neglected in the test.

3. Depending on the density required, the opening of funnel was adjusted to the desired depositional intensity, where the pouring rate was pre-calibrated for each model.

4. The stope was filled in equal layers (pours) with 6 equal layers from each container. Overall, 42 pours were required to complete filling the stope (see Fig 5.6). The readings of balance and load cell at the end of each pour were recorded. The readings of strain gauges were recorded directly by data logger.

5. At the end of the test, the height of fill material in the stope was taken, and the stope was emptied. The fill material was then recollected and weighed. From this, the relative density was determined.

Simple calculations had been performed to study the arching behavior of fill material based on the readings recorded from the weighing scale and load cell. When the stope was filled to a height of h above the base of the stope, part of the fill weight was transferred to the bottom of the stope, and the remaining weight was transferred to the walls due to arching effect.

When the stope was filled up to height *h*, the proportions of fill weight were defined as: W_w = the fill weight transferred to the wall of stope (recorded by load cell), W_b = the fill weight acting at the base of stope (recorded by scale), and W = the total fill weight.

The average vertical stress acting at the base of the stope at fill height of *h* was

$$\sigma_v = W_b/(BL) \tag{5.1}$$

and

$$W = W_w + W_b \tag{5.2}$$

The ratio of load acting at footwall (F_{FW}) to that of hangingwall (F_{HW}) was calculated as:

$$\frac{F_{FW}}{F_{HW}} = \frac{\sum_{i=1}^{4}\left(\frac{Strain\ gauge\ reading\ at\ footwall}{Strain\ gauge\ reading\ at\ hangingwall}\right)_i}{4} \tag{5.3}$$

where *i* represented the index of summation for the pairs of strain gauges (ST5, ST1)$_1$, (ST6, ST2)$_2$, (ST7, ST3)$_3$ and (ST8, ST4)$_4$. The average variation from the mean was less than 14%. The load cell reading was apportioned on the basis of this ratio determined from the strain gauge readings.

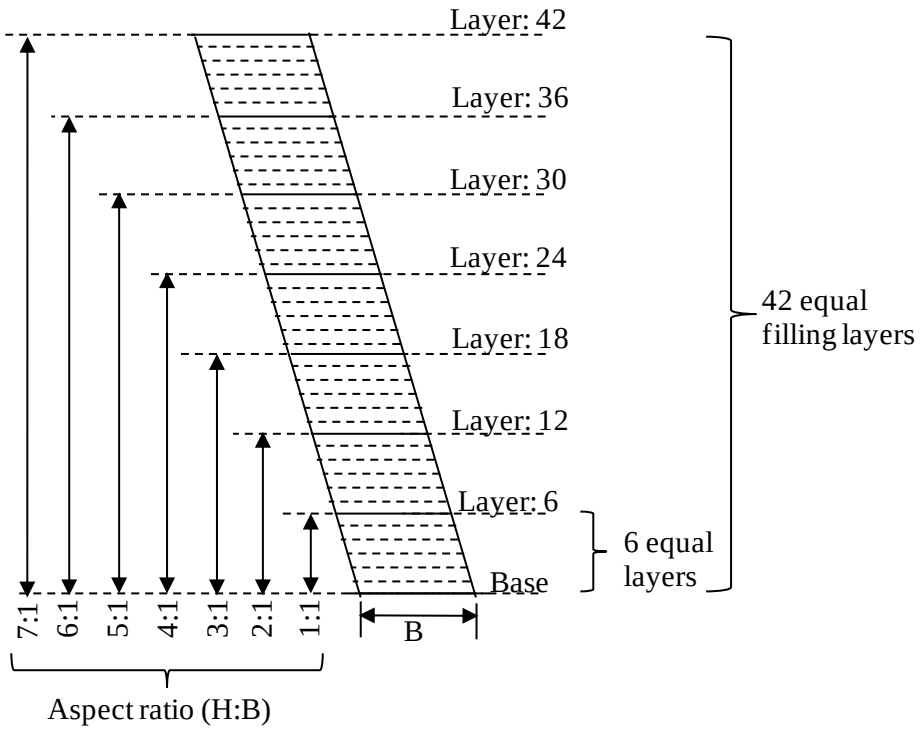

Figure 5.6. Schematic diagram of equal filling layers and corresponding aspect ratios

To investigate the stress developments within the stope, the following cases as shown in Table 5.7 were considered in the model.

- Four different slope angles (90^o, 80^o, 75^o, 70^o to the horizontal)
- Three different wall roughnesses (low, medium and high)
- Two different relative densities (30% and 60%). As similar trend of results were obtained for relative density of 30% and 60%, the results of 30% relative density were given in the Appendix B3.
- Aspect ratio (vertical-height/span-width) of 1 to 7 for all the cases above.

It should be noted that symbol such as 70R60 used in this study identified the test conducted in the laboratory model stope with 70° inclination to the horizontal having high wall roughness, and granular backfill with relative density of 60%. Using the readings obtained from the load cell and the balance, it was possible to separate the load transferred to the base and the wall, and hence computed the average vertical normal stress at the base of the stope. This could be done at every stage of filling and hence the plots of average vertical stress against the depth could be generated. In addition, the above data obtained from a single pour could also be used for developing $\sigma_v - z$ plots for stopes of other aspects ratios such as 1:1, 1:2...1:7 (see Fig. 5.6). The 42 stages of filling represented 42 different aspect ratios ranging from 0 to 7. Three tests, listed at the bottom of Table 5.7, were carried out where the roughness at the footwall and hangingwall were different.

Table 5.7. Description of the model test

Model	Slope angle (degrees)	Wall roughness	Aspect ratio	Relative density (%)
90R60	90	High	1-7	60
90R30	90	High	1-7	30
90M60	90	Medium	1-7	60
90M30	90	Medium	1-7	30
90S60	90	Low	1-7	60
90S30	90	Low	1-7	30
80R60	80	High	1-7	60
80R30	80	High	1-7	30
80M60	80	Medium	1-7	60
80M30	80	Medium	1-7	30
80S60	80	Low	1-7	60
80S30	80	Low	1-7	30
75R60	75	High	1-7	60
75R30	75	High	1-7	30
75M60	75	Medium	1-7	60
75M30	75	Medium	1-7	30
75S60	75	Low	1-7	60
75S30	75	Low	1-7	30
70R60	70	High	1-7	60
70R30	70	High	1-7	30
70M60	70	Medium	1-7	60
70M30	70	Medium	1-7	30
70S60	70	Low	1-7	60
70S30	70	Low	1-7	30
70RS60	70	Hangingwall (front): High Footwall (rear): Low	1-7	60
70SR60	70	Hangingwall (front): Low Footwall (rear) : High	1-7	60
90SR30	90	Hangingwall (front): Low Footwall (rear): High	1-7	30

5.3 Results and Discussion

The test results obtained with different aspect ratios (from 1 to 7), wall roughnesses (low, medium and high), and stope inclinations (90^o, 80^o, 75^o and 70^o to the horizontal) are depicted in Figs. 5.7-5.9, respectively. In these figures, dimensionless stress ratio, $\sigma_v/\gamma H$ is plotted against dimensionless depth, z/B, where σ_v is the average vertical stress acting at any depth z measured from top of the backfill. γ is the unit weight of the fill, H is the total height. Except Fig. 5.7, z is normalized with respect to B to express depth in terms of aspect ratio (e.g. $z = 5B$). In Fig 5.7, depth z is normalised with respect to H, mainly to illustrate the level of arching at a certain fraction of the total depth for various aspect ratios and wall roughnesses. It should be noted that the results plotted are the averages of three replicate tests, the maximum variability in relation to the mean of the measured value is less than 5.38% and the mean variation is about 1.68%. In Fig 5.7(a), the error bars indicating the standard deviation obtained from the test results are included in order to give a better indication of the reproducibility of the test results.

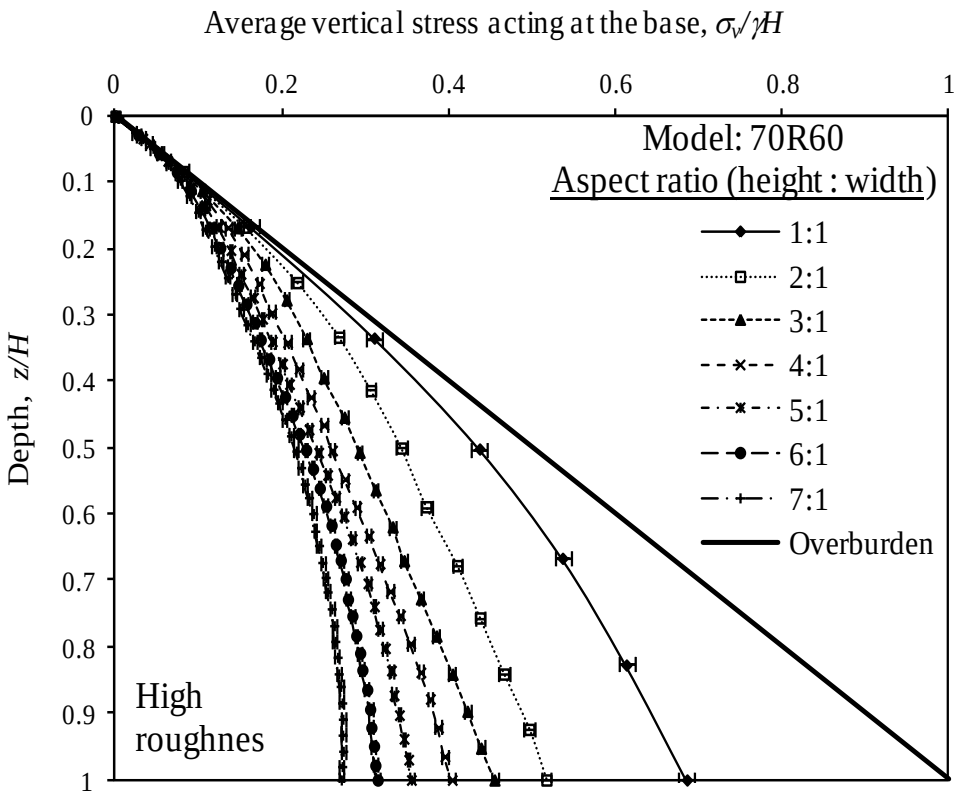

(a)

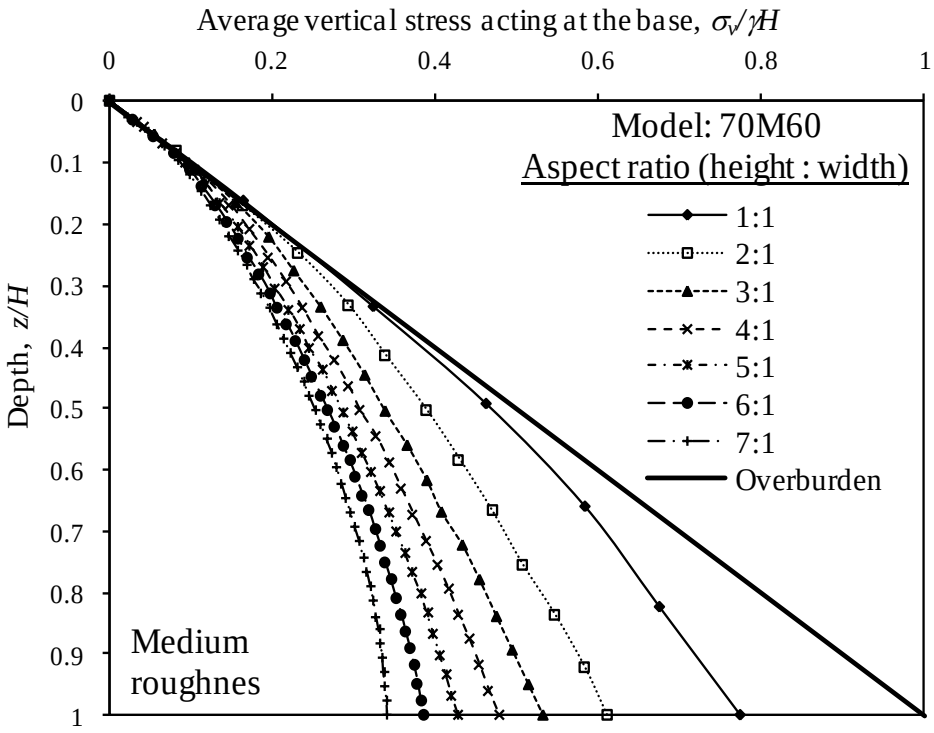
Average vertical stress acting at the base, $\sigma_v/\gamma H$
0
0.2
0.4
0.6
0.8
1
Depth, z/H
0
0.1
0.2
0.3
0.4
0.5
0.6
0.7
0.8
0.9
1
Model: 70M60
Aspect ratio (height : width)
1:1
2:1
3:1
4:1
5:1
6:1
7:1
Overburden
Medium
roughnes

(b)

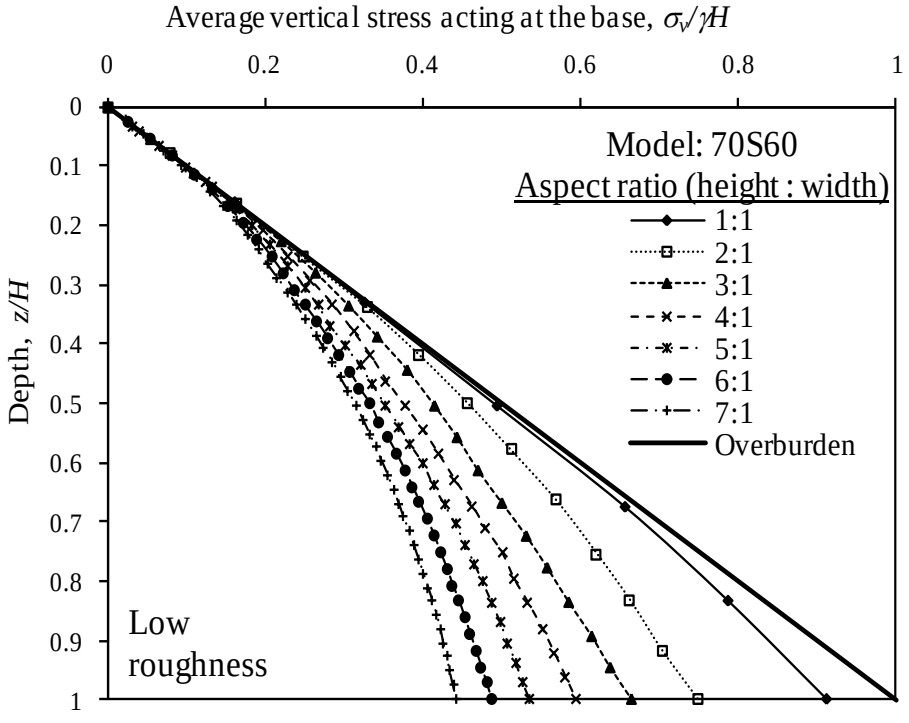
Average vertical stress acting at the base, $\sigma_v/\gamma H$
0
0.2
0.4
0.6
0.8
1
Depth, z/H
0
0.1
0.2
0.3
0.4
0.5
0.6
0.7
0.8
0.9
1
Model: 70S60
Aspect ratio (height : width)
1:1
2:1
3:1
4:1
5:1
6:1
7:1
Overburden
Low
roughness

(c)

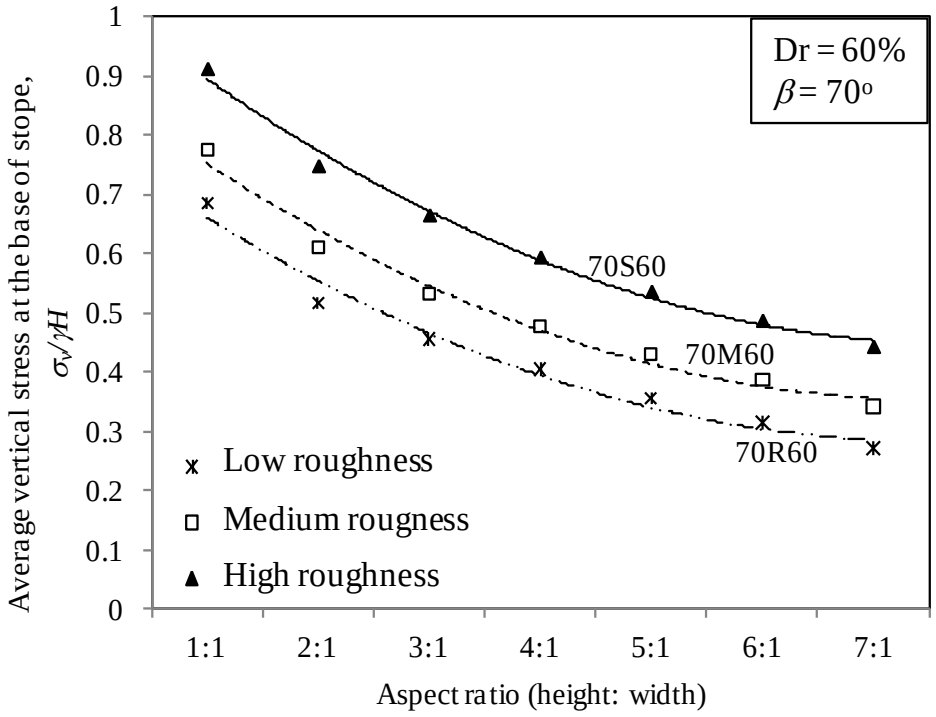

(d)

Figure 5.7. Average vertical stress at the base of stope with inclination 70^{o} to the horizontal for different aspect ratios: (a) high wall roughness, (b) medium wall roughness, (c) low wall roughness and (d) vertical stress acting at the base vs aspect ratio

5.3.1 Effect of stope aspect ratio (height to width)

Figure 5.7 (a-c) shows the variation of average vertical normal stress acting at the base of stope against the dimensionless fill height, determined from the laboratory model tests, for rough, medium and low roughness of walls where the stope is inclined at 70° to the horizontal and the relative density of the fill is 60%. Here, the fill height is normalised with respect to the stope height *H*. The straight line in the figures shows the variation of the overburden pressure ($\sigma_v = \gamma z$) with depth, a situation which arises when the wall is perfectly smooth and does not contribute in carrying the fill weight. As the filling progresses, the aspect ratio increases from 0 at the beginning to 7 when the filling stops. As shown in Fig. 5.7, the vertical stress decreases significantly when the aspect ratio increases from 1 to 7. This can be explained by the increase in the wall contact areas for the stopes with larger aspect ratios. The magnitude of stress transferred to the base of stope varies depending on the wall roughness and inclination. For model 70R60, 70M60 and 70S60, the vertical stress decreases from 69% to 27% , 77% to 34% and 91% to 44%, respectively of the overburden

pressure when aspect ratio increases from 1 to 7. Rough wall contributes more in carrying the fill weight and therefore, the average vertical stress at the base is smaller. It can be seen in the figure that this is true for any aspect ratio and at any depth. The effects of wall roughness at different aspect ratios are highlighted in Fig 5.7(d). It is evident from the figure that the arching effect increases with wall roughness for all aspect ratios. For a given wall roughness, the arching effect increases with the aspect ratio, transferring a larger fraction of the fill load to the wall. Similar trends as shown in Figs. 5.7(a - d) are obtained for vertical stope and slope angle of 80^o to the horizontal (see Appendix B4).

5.3.2 Effect of wall roughness

The effects of wall roughness are illustrated in Figs. 5.8(a) through 5.8(c), where $\sigma_v/\gamma H$ is plotted against z/B for stopes having inclination to the horizontal of 70°, 80° and 90° respectively, with walls of low, medium and high roughnesses. All these plots are for relative density of 60%. For all three wall roughnesses, it is evident that the rougher the wall surface, the lower is the vertical normal stress at any depth. The difference becomes more and more pronounced with depth.

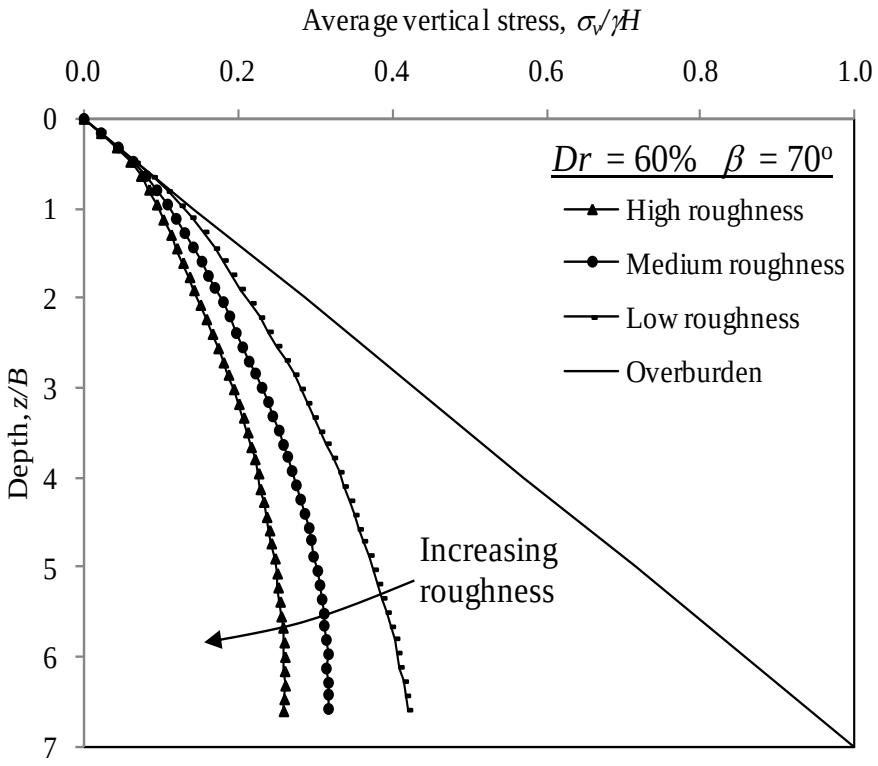

(a)

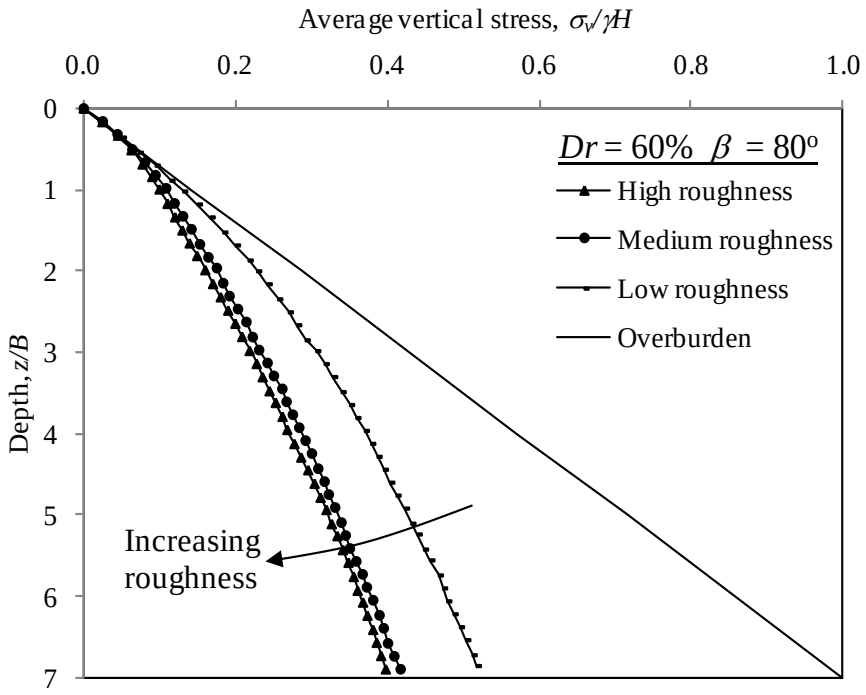

(b)

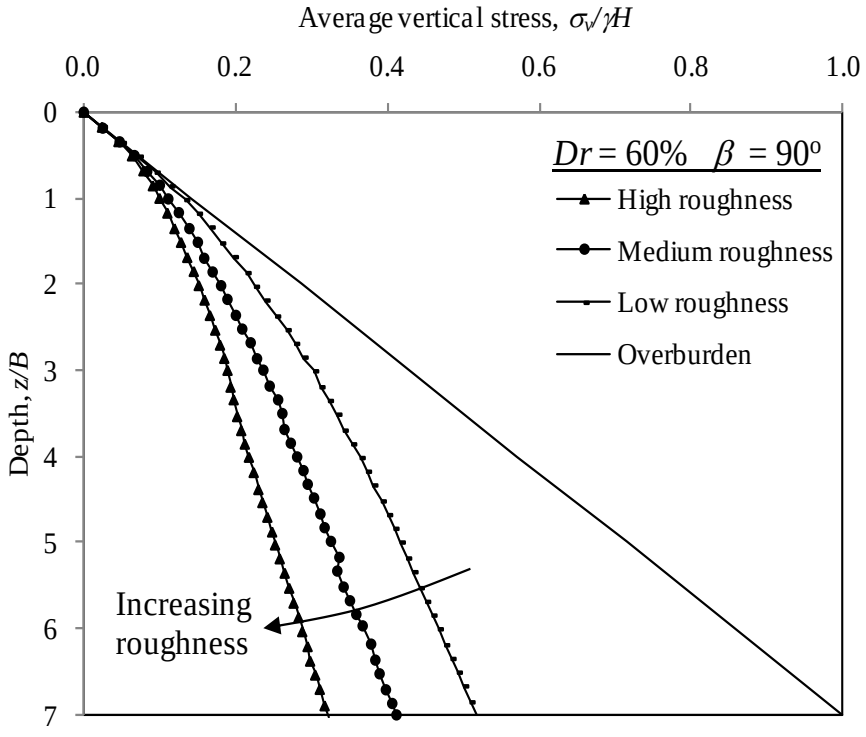

(c)

Figure 5.8. Average vertical stress acting at the base of stope for different wall roughnesses: (a) stope inclination, $\beta = 70^{\circ}$ to the horizontal, (b) stope inclination, $\beta = 80^{\circ}$ to the horizontal and (c) stope inclination, $\beta = 90^{\circ}$ to the horizontal

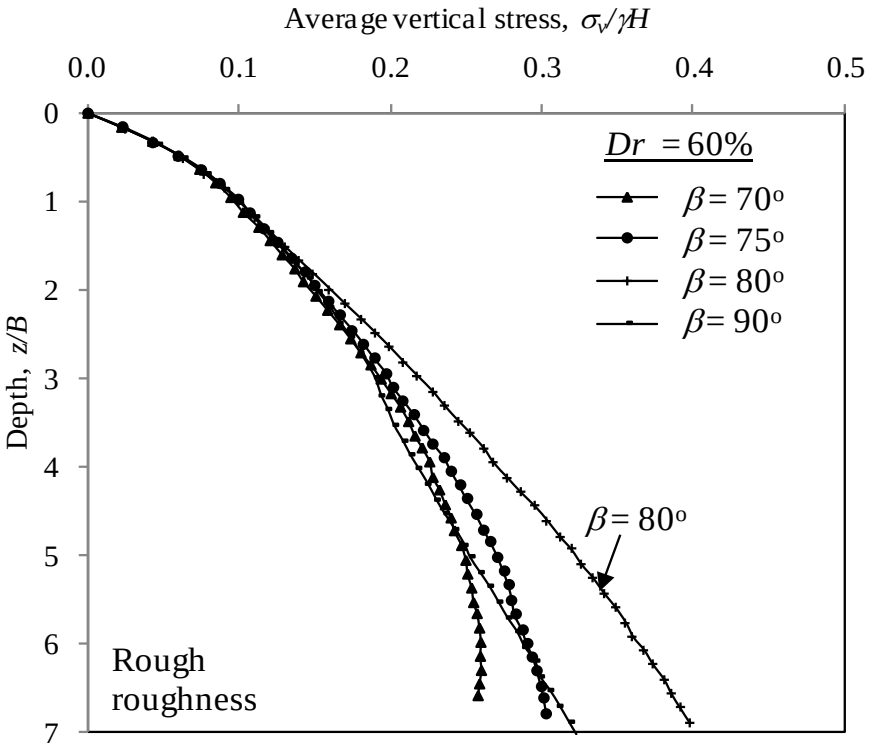
Average vertical stress, $\sigma_v/\gamma H$
0.0
0.1
0.2
0.3
0.4
0.5
0
1
2
3
4
5
6
7
Depth, z/B
Dr = 60%
β = 70°
β = 75°
β = 80°
β = 90°
β = 80°
Rough
roughness

(a)

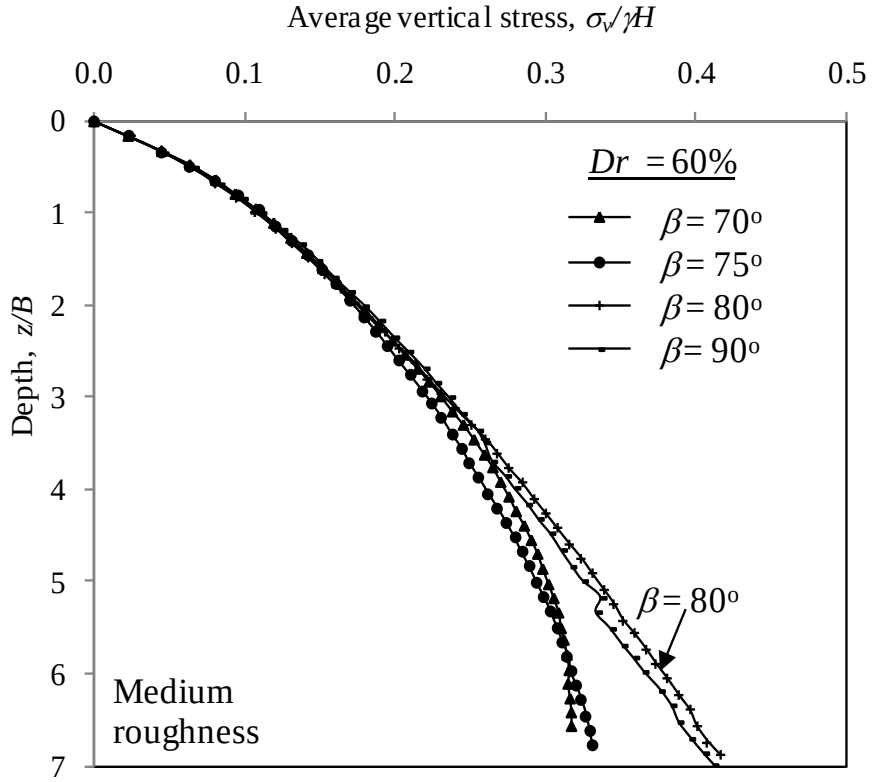
Average vertical stress, $\sigma_v/\gamma H$
0.0
0.1
0.2
0.3
0.4
0.5
0
1
2
3
4
5
6
7
Depth, z/B
Dr = 60%
β = 70°
β = 75°
β = 80°
β = 90°
β = 80°
Medium
roughness

(b)

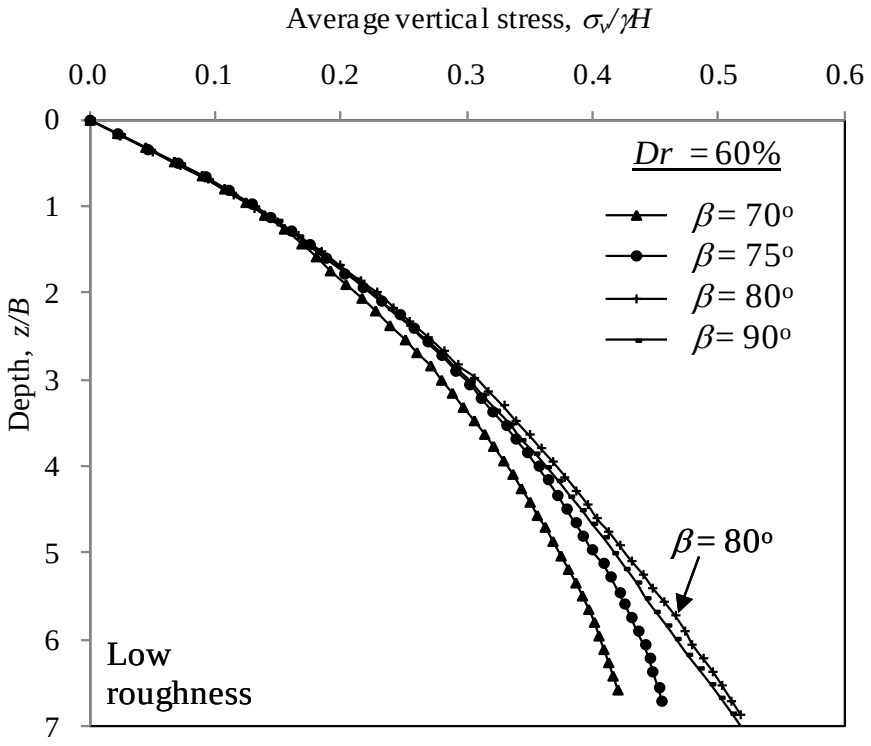

(c)

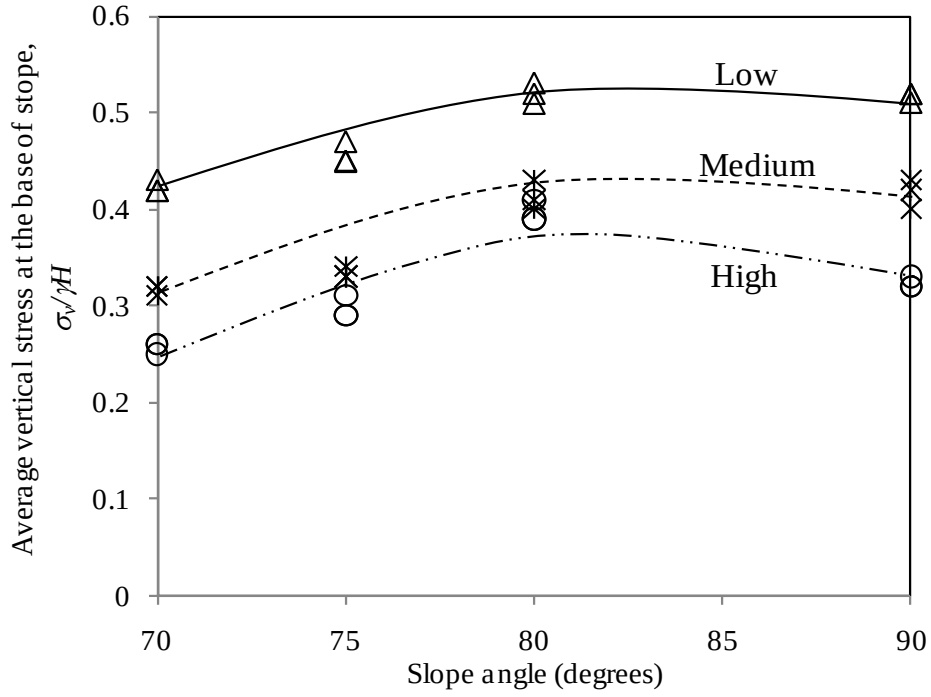

(d)

Figure 5.9. Average vertical stress acting at the base of stope for different inclinations: (a) high wall roughness, (b) medium wall roughness, (c) low wall roughness and (d) average vertical stress acting at the base of stope

5.3.3 Effect of stope inclination

Fig. 5.9 (a-c) shows the variation of $\sigma_v/\gamma H$ against z/B for stope inclination of 70°, 75°, 80° and 90° to the horizontal, for different grade of wall roughness (high, medium and low). An interesting observation here is that the maximum load is transferred to the base when the stope inclination to the horizontal is about 80° for all three grades of roughness considered. The vertical normal stress is increasing from 70^o to 80^o, and then relatively flat from 80^o to 90^o as highlighted in Fig. 5.9 (d). For relatively smooth wall-fill interface, the change of vertical stress is insignificant when there is very slight tilt to the vertical of less than 10^o. Only when the tilt is more than 10^o, there is noticeable reduction in the vertical stress.

It appears that with a slight deviation from vertical, there is significant loss of arching at the hangingwall, and hence reduction in the fill weight carried by the hangingwall which increases the vertical stress at the bottom of the stope. At the same time, there is a greater tendency for the footwall to carry greater load than when the wall is vertical. Depending on the relative magnitudes of these two components, the vertical stress at the bottom of the stope may increase or decrease, with the inclination of the stope wall. When the stope inclination to the horizontal is reduced from 90^o to 80^o, it appears that the vertical normal stress increases. With further reduction in the slope angle, the vertical stress decreases, due to increase in the load carried by the footwall. The relative reduction and increase depend on the changes in wall friction and slope angle.

The observation on the occurrence of maximum load for the stope inclination of 80^o to the horizontal is not consistent with the analytical studies (Chapter 3) and numerical modeling (Chapter 6) of inclined stope, where the vertical stope always gives the highest vertical stress with depth. However, the results obtained herein are consistent for all three grades of roughness and at all aspect ratios. The conflict observed among the results may be due to some parameters not being fully captured in the analytical or numerical modeling or due to some irregularity in the experimentation setting (e.g. placement conditions, rotating at the base, etc). The actual reason behind this slight disagreement will need to be investigated further in order to address this issue.

5.3.4 Stresses acting on hangingwall (HW) and footwall (FW)

The results of stresses acting on hangingwall and footwall in this section are compared with the results obtained from numerical modeling using FLAC as discussed in Section 6.3. From numerical modeling, the shear stress acting at footwall and hangingwall are calculated based on the following stress transformation equation (Hibbeler 2005).

$$\tau = -\frac{\sigma_x - \sigma_z}{2} sin2\beta + \tau_{xz} cos2\beta \quad (5.4)$$

where σ_z = vertical stress in *z*-direction, σ_x = horizontal stress in *x*-direction, τ_{xz} = shear stress in *x*-*z* direction, and β = stope inclination to the horizontal. The following example demonstrates the way to calculate shear stress acting at footwall and hangingwall using Eq. 5.4 for model 70M60 at depth z = 56.1 cm and β = 70°. From the results of numerical modeling,

At hangingwall : σ_x = -1.036 kPa, σ_z = -1.833 kPa and τ_{xz} = -0.77 kPa,

$$T_{HW} = -\frac{-1.036-(-1.833)}{2} \sin(2*70) + (-0.77)\cos(2*70)$$

$$= 0.3337\ kPa$$

At footwall: σ_x = -0.823 kPa, σ_z = -2.709 kPa and τ_{xz} = 0.04 kPa,

$$\tau_{FW} = -\frac{-0.823-(-2.709)}{2} \sin(2*70) + 0.04\cos(2*70)$$

$$= -0.6368\ kPa = 0.6368\ kPa \text{ (absolute value).}$$

The ratio of shear stress acting at footwall to that of hangingwall are computed as:

$$Ratio\ at\ depth\ z = \frac{Shear\ stress\ acting\ at\ footwall\ at\ depth\ z}{Shear\ stress\ acting\ at\ hangingwall\ at\ depth\ z} \quad (5.5)$$

Comparison with experimental results is based on average ratio obtained from Eq. 5.5 throughout the height of the stope. The results of stress ratio for both experimental and numerical models are tabulated in Table 5.8. It can be seen that all the numerical values are greater than or equal to 1.

The line in Fig 5.10 represents the condition that the numerical results are the same as experimental results. Data points on the graph are scattered close to the line showing that the experimental results are well correlated with numerical results with an average difference of less than 10%. It can be seen that the shear stresses experienced by both hangingwall (HW) and footwall (FW) are approximately equal for vertical stopes. When the walls are inclined, as expected intuitively, the load acting at FW is higher than HW due to the combined effect of gravity and arching action. The differences between loads acting on HW and FW increase significantly with the increase of stope inclination and wall roughness. As can be seen for model 70R60 where the ratio is about 2.0, indicating that 2/3 of the load

transferred to the walls is acting on the FW and only 1/3 is transferred to the HW. The influence of the relative densities of the fill materials seem to be insignificant in the split between hanging and foot walls. The results are in agreement with Singh et al. (2010) who observed that the friction angle of the fill and hence the relative density have negligible influence on the vertical stresses within the fill. They observe that the two influencing factors are the wall roughness (i.e., δ/ϕ) and the wall movement (i.e. whether $K = K_a$ or K_0).

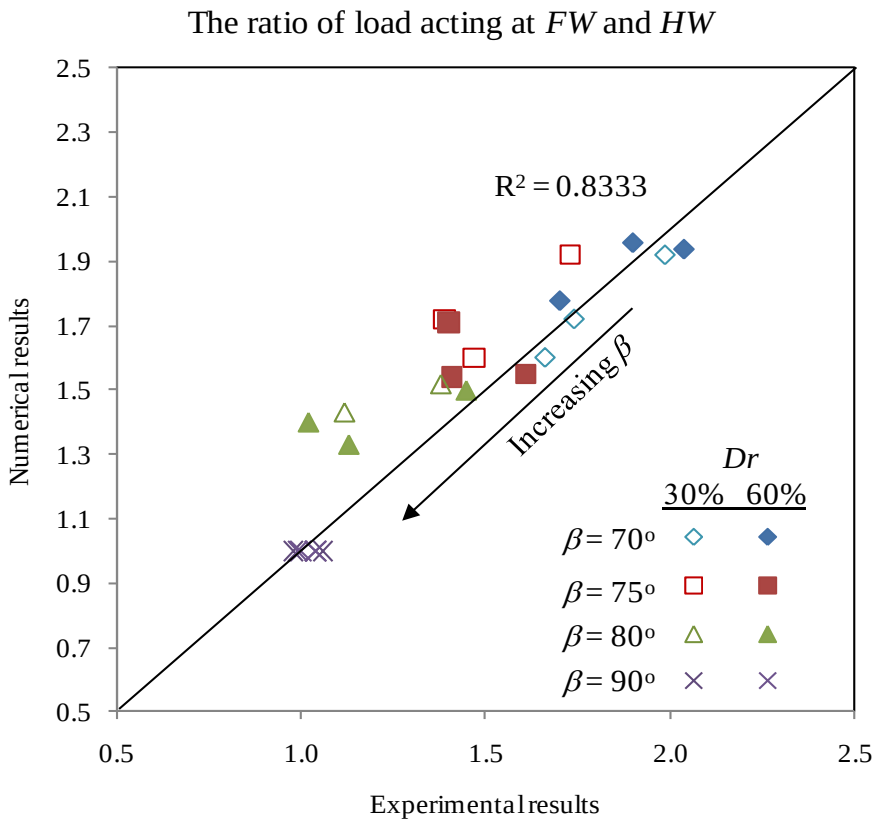

Figure 5.10. Comparison of the ratio of load acting at footwall and hangingwall – Experimental vs numerical results

Table 5.8. The ratio of load acting at footwall to that of hangingwall

Model	Experimental	Numerical	Difference (%)
70R30	1.99	1.91	4.2
70R60	2.04	1.94	5.2
70M30	1.74	2.05	15.1
70M60	1.90	1.96	3.1
70S30	1.66	1.88	11.7
70S60	1.70	1.78	4.5
75R30	1.73	1.92	9.9
75R60	1.61	1.55	3.9
75M30	1.39	1.72	19.2
75M60	1.40	1.71	18.1
75S30	1.47	1.60	8.1
75S60	1.41	1.54	8.4
80R30	1.38	1.52	9.2
80R60	1.45	1.50	3.3
80M30	1.12	1.43	21.7
80M60	1.02	1.40	27.1
80S30	1.33	1.38	3.6
80S60	1.13	1.33	15.0
90R30	1.04	1.00	4.0
90R60	1.04	1.00	4.0
90M30	0.98	1.00	2.0
90M60	1.00	1.00	0.0
90S30	1.06	1.00	6.0
90S60	0.99	1.00	1.0
[1] 70RS60	1.38	1.22	13.1
[2] 70SR60	2.35	2.78	15.5
[3] 90SR30	1.22	1.52	19.7

[1]Wall roughness: hangingwall-high and footwall-low

[2]Wall roughness: hangingwall-low and footwall-high

[3]Wall roughness: hangingwall (front)-low and footwall (rear)-high

The Models 90SR30, 70RS60 and 70SR60, which are modeled with dissimilar wall roughness characteristics as described in Table 5.8, show that more loads are transferred to the wall with higher friction compared to that of relative smooth wall. For vertical stope, the ratio deviates from 0.98 to 1.22 (experimental) for smooth surface at hangingwall and rough surface at footwall. For inclined stope, the ratios vary from 1.38 to 2.35 (experimental) by

changing the wall characteristics from 70RS60 to 70SR60. Apart from this, from the Figs 5.11 (a – b), it can be seen that the average vertical stress profile for 90M30 is similar to 90SR30, 70M60 is similar to 70RS60 and 70SR60 for both experimental and numerical results. Since δ_M is an approximate average value of δ_R and δ_S, it can be concluded that a reasonable estimate of vertical stresses can be obtained with an average interface friction angle of the two dissimilar surfaces. This result is comparable to the observations of Take and Valsangkar (2001). This result also enables the use of equations developed in Chapter 3 and 4 as well as those listed in Tables 2.2, 2.3 and 2.4, with a single average value of δ used to represent both wall characteristics.

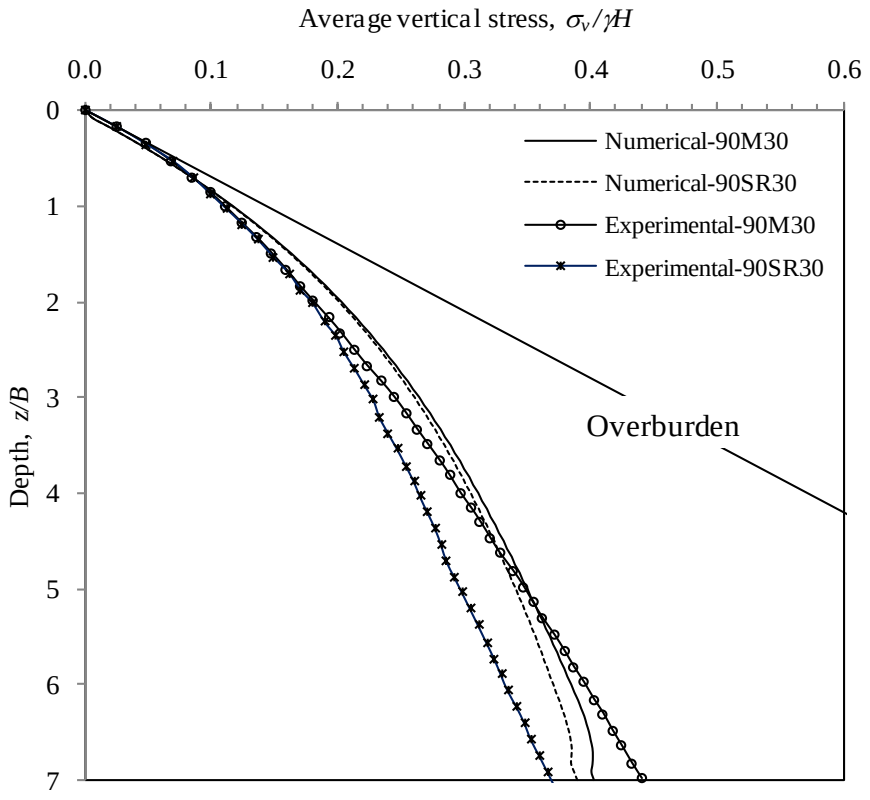

(a)

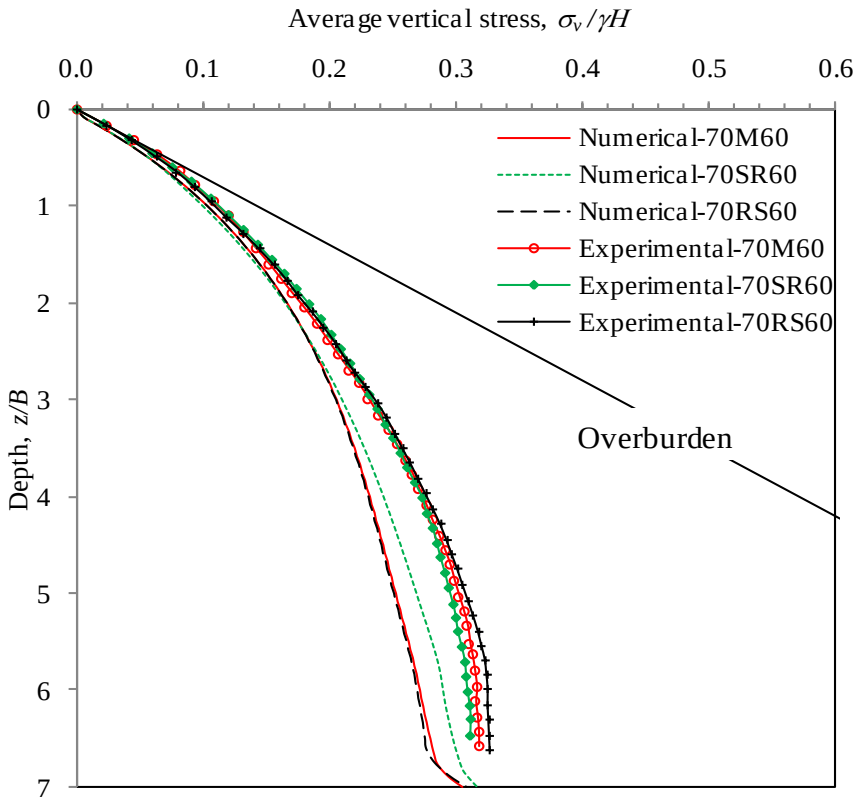

(b)

Figure 5.11. Average vertical stress acting at the base of stope for dissimilar wall characteristics: (a) vertical walls, (b) inclined walls

5.4 Summary and conclusions

This chapter describes the development of a plane strain laboratory model that simulates mine backfilling in an inclined stope, and enables determination of the average vertical stress at any depth within the fill. Sand is used as granular fill in the study. The material properties of this granular material are determined through a series of laboratory tests as per Australian standards.

The laboratory model is developed based on the similar concept of experimental model of Pirapakaran and Sivakugan (2007b) with additional strain gauges attached to the long wall of the framework to separate the self weight carried by hangingwall and footwall. Four different slope angles (90^o, 80^o, 75^o, 70^o to the horizontal), three different wall roughnesses (low, medium and high), seven aspect ratio (vertical-height to span-width) as well as two different relative fill densities are considered in the study.

The laboratory model test results clearly demonstrate the effects of arching within inclined stope filled with granular material. The model clearly demonstrates that a significant fraction of the fill weight is carried by the stope walls. This fraction gets larger with increasing wall roughness and aspect ratio.

The experimental results reveal that aspect ratio, stope inclination and wall roughness are critical factors in predicting stress distribution within a stope. The effect of arching is the least when the stope is inclined at about 80° to the horizontal, giving highest vertical stresses at any depth. However, this fact is not captured in both the mathematical and numerical models developed in the past and the ones discussed herein.

The observation from the reading of strain gauges also reveals that the load acting at footwall is higher than hanginwall for an inclined stope. Two of the contributing factors to this load fraction are stope inclination and wall roughness. In the case of walls with dissimilar frictional characteristics, the test results show that an average value of wall-fill friction angles can be used in analytical expression to represent both wall characteristics.

Chapter 6 Numerical modeling of inclined stopes using FLAC

6.1 General

Numerical modeling appears to be a useful tool in exploring and providing new insights to a system, which is too complex for an analytical solution and/or too cumbersome for laboratory modeling or simulation (Coulthard 1999). It is a process that can help one to fully understand the complex real physical system and to improve the judgement of engineers in making prediction (Lee Barbour and John Krahn 2004). Numerical models are also used as validation tools where the results can be compared with those from analytical and/or laboratory model studies. In geomechanics, numerical simulations have been used across the full range of geotechnical problems, such as analysis of ground conditions, mining, ground support, seismic studies, slope stability, foundation, tunnelling/caveability and fragmentation analysis. The focus of this dissertation is limited to the stress development within backfilled stopes. A review of past studies by researchers using numerical modeling on arching effect and stress development within backfilled stope has been discussed in Chapter 2.

This chapter develops a numerical model to simulate the stress development within the laboratory model for backfilled stope discussed in Chapter 5 using FLAC (version 5.00), which is a powerful numerical tool suited to solve complex geotechnical problems that consist of several stages, such as sequential excavations, backfilling and loading. The simulation results are compared to analytical and laboratory measurements of stresses, that are developed in Chapter 3 and 5 respectively. A similar approach is then extended to a full scale mine stope to investigate the stress distribution within the backfill. In the analyses throughout this chapter, the simulations are limited to static problem in plane-strain and the deformation is assumed to be time-independent.

A brief discussion of FLAC is given in the following section. The details are taken from FLAC user's manual and the official website of FLAC (CeAs 2011; Coetzee et al. 1998; ITASCA 2011).

6.2 Review of FLAC

FLAC (Fast Lagrangian Analysis of Continua) is a two-dimensional explicit finite difference program for engineering mechanics computation. It is a design tool for solving geotechnical, civil, and mining engineering problems. Materials are represented by a grid system that is adjustable by user to fit the shape of the object to be modelled. Each element behaves according to a prescribed linear or nonlinear stress/strain law in response to the applied forces of boundary restraints. The material can yield and flow, and the grid can deform (in large-strain mode) and move with the material that is represented. The explicit, Lagrangian calculation scheme and the mixed-discretization zoning technique used in FLAC ensure that plastic collapse and flow are modelled very accurately. FLAC is suited to model the geotechnical continuum problems that consist of several stages (such as sequential excavations, backfilling and loading), non-linear material behaviour and unstable systems even if yield/failure occurs over a large area or if total collapse occurs.

The program is equipped with built-in constitutive models which include isotropic elastic model and a wide range of plasticity models such as Mohr-Coulomb, Drucker-Prager, modified Cam-Clay, ubiquitous joint, double yield, strain-hardening/softening and Hoek-Brown. Groundwater flow and consolidation (fully coupled) model are also available in FLAC. Another main feature in FLAC is the built-in programming language, FISH (short for FLACish). FISH enables the users to write their own functions and user-defined constitutive models to suit their specific needs.

FLAC uses an explicit, time-marching solution scheme where no matrix is required for solving problems with large amount of elements. Hence, it requires relatively low computer resources (in terms of memory and processor speed) in handling computation analyses of large and complex problem. The full dynamic equations of motion are used in FLAC to model both static and dynamic problems, which enable FLAC to model unstable system effectively without numerical distress. The disadvantage of FLAC is that large numbers of steps must be taken due to the small time-step used in explicit solution scheme and the problem of damping. Compared to other equivalent numerical programs, FLAC is less efficient in linear simulations.

6.3 Numerical modeling of arching in laboratory stope

In this section, stopes with similar geometries (vertical-height to width-ratio: 7) and the same material properties as in the laboratory models were adopted for numerical simulation using FLAC. A typical inclined backfilled stope (laboratory model) with dimension of 100 mm width and 700 mm vertical height was modelled as shown in Fig. 6.1.

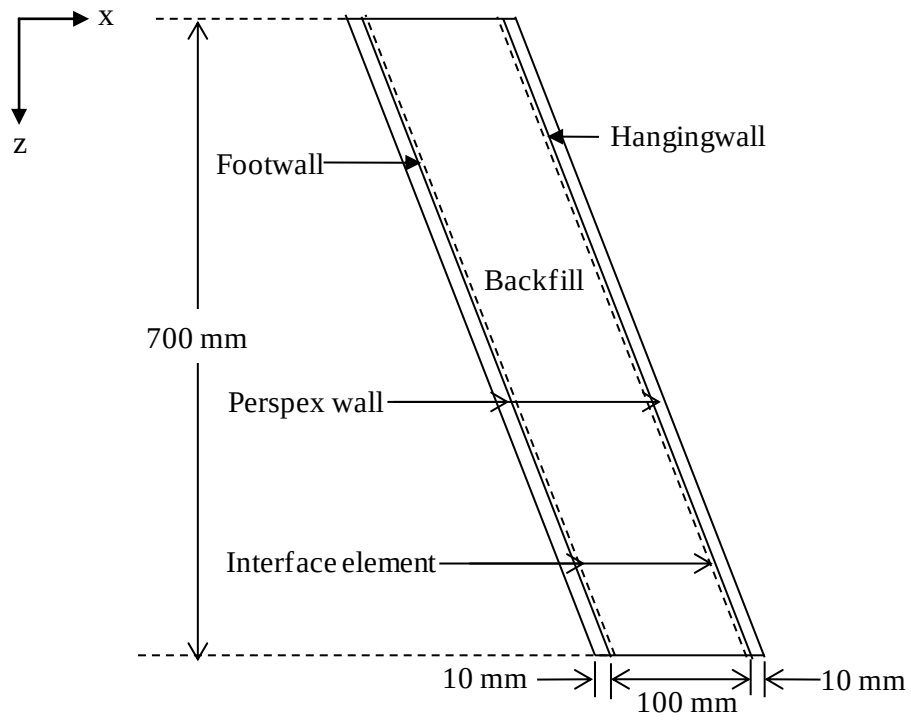

Figure 6.1. Schematic diagram of inclined laboratory stope used in numerical modeling

6.3.1 Modeling approach

The wall was considered to be a homogeneous, isotropic, and linearly elastic material, whereas the granular backfill was assumed to follow the Mohr-Coulomb failure criterion with linear elastic behaviour prior to failure. Fixed boundary conditions were applied to the walls and vertical displacement was fixed at the bottom of the stope. Interface elements between the walls and fill material were incorporated in the numerical simulation, to allow relative slip between the wall and the backfill. The choice of boundary conditions, mesh density and interface properties were established prior to the investigation in the study through a sensitivity analysis as discussed in Section 6.3.2. Filling was performed in 42 layers to simulate the 42 pours used in the experimental model. The default mode of FLAC is a two-dimensional plane-strain model; therefore, the assumption of plane-strain loading

conditions was made in analysing the stress-strain behaviour. The FLAC code of the model can be found in Appendix C1.

6.3.2 Sensitivity analysis

Sensitivity analysis was conducted for all important parameters in the numerical simulation in order to evaluate the effect of each parameter so as to avoid incorrect specification and uncertainty associated with the model.

Constitutive models

In numerical modeling, the Perspex walls were assumed to be homogeneous, isotropic and linear elastic, which was confirmed by Fig. 5.5 where the loads were proportional to the displacements. The material properties of typical Perspex were used in the numerical modeling: Young's modulus, E = 3.2 GPa; Poisson's ratio, ν = 0.3; and density, ρ = 1190 kg/m^3. The sand backfill was assumed to follow Mohr-Coulomb failure criterion (Vermeer and de Borst 1984). The required material properties for the sand were given in Table 5.3. These were assumed in the numerical model.

Initial condition

There was always an in-situ state of stress prior to any excavation or filling, which might influence the behaviour of the model. To reproduce this in-situ state, the model was allowed to achieve its equilibrium and steady state under the gravitational stresses before any filling occurs.

Boundary conditions

The wall thickness was modelled as 10 mm in thickness which was 1/10 of the stope width. To avoid the occurrence of premature failures during simulation with inclined stope, fixed boundary conditions were applied to the perimeter walls of the model. Laboratory model tests with full bracing along the outer walls of model were conducted. Bracing was referred to the insertion of metal bars along the perimeter of the model at fixed interval along the depth of the model to prevent any possible deformation. Fig 6.2 showed the comparison of stress profiles for model 70M60 between unbraced and braced models. The dotted lines (tests 1-3) showed the results obtained from the standard laboratory model (unbraced) as discussed in Chapter 5, whereas, the straight continuous lines (tests 1-2) showed the results obtained from laboratory model with bracing along hangingwall and footwall. The results showed that the minor displacements as reflected by the strain gauges did not influence the

stress profile within the backfill. Therefore, it was appropriate to provide fixed boundary conditions to the model in the numerical simulations.

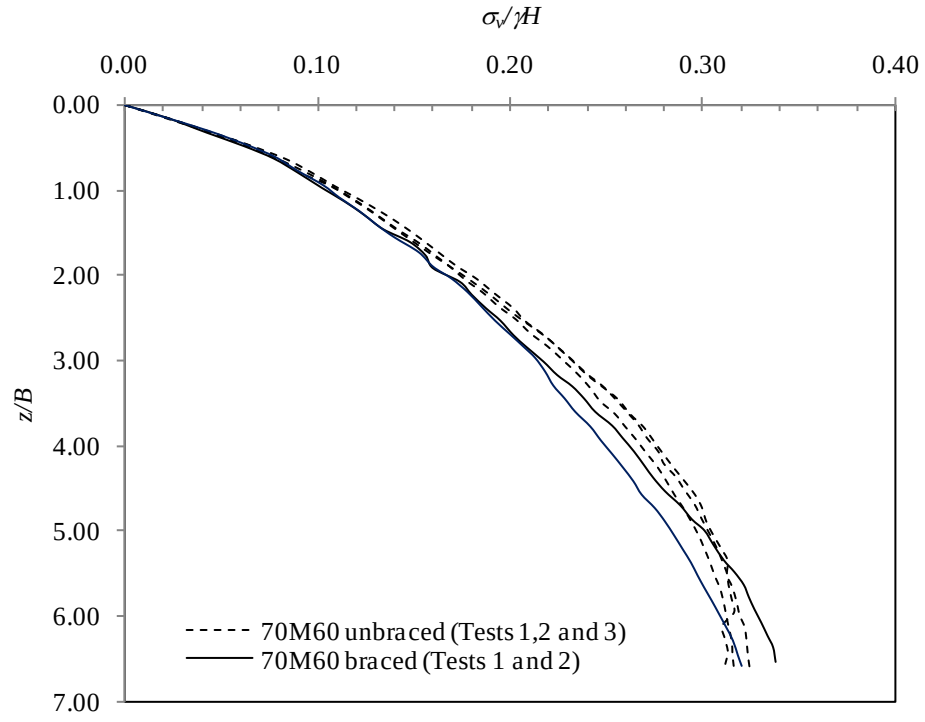

Figure 6.2. Comparison of stress profiles between unbraced and braced model for 70M60

Mesh density

The mesh density was established by refining the grid from 14 elements (10 mm/grid) to 38 elements (3.33 mm/grid) in *x*-direction (horizontal) and from 84 elements (8.33 mm/grid) to 210 elements (3.33 mm/grid) in *z*-direction (vertical) as shown in Table 6.1. Vertical stress along centreline and shear stress along hangingwall at depth, z = 600 mm (B = 100 mm) were used as indicators in the selection of optimum grid size to be used in the model. As shown in Fig 6.3 and 6.4, the stresses remained almost the same for all the combination. Therefore, a square grid was preferred in the simulation. Because higher mesh density required longer simulation time and higher computer specification, grid 26 x 126 (3276 elements) which was equivalent to grid size 5 mm/grid in *x*-direction and 5.6 mm/grid in *z*-direction was selected in this exercise.

Table 6.1. Grid size, number of element, and stresses variation at *z/B = 6* in FLAC at 600 mm depth

Stresses at *z/B = 6*			
Elements in direction *x – z*	No of element	Vertical stress along centreline (kPa)	Shear stress along hangingwall (kPa)
14 x 84	1176	3.033	0.5855
26 x 84	2184	3.039	0.6199
26 x 126	**3276**	**3.026**	**0.5945**
38 x 168	6384	2.988	0.5819
38 x 210	7980	2.990	0.5769

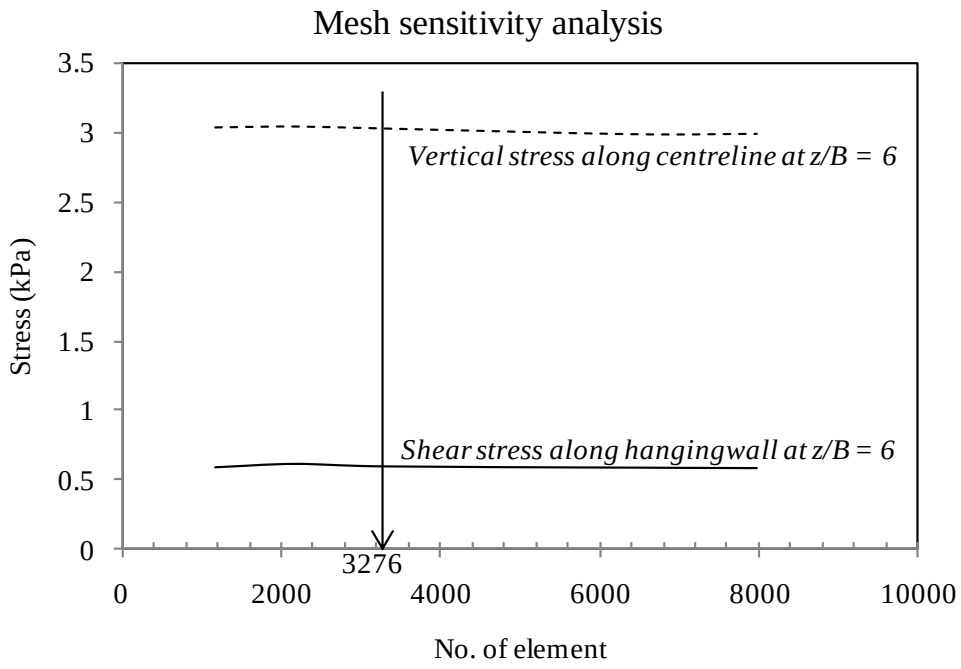

Figure 6.3. Stresses variation against number of element modelled in FLAC

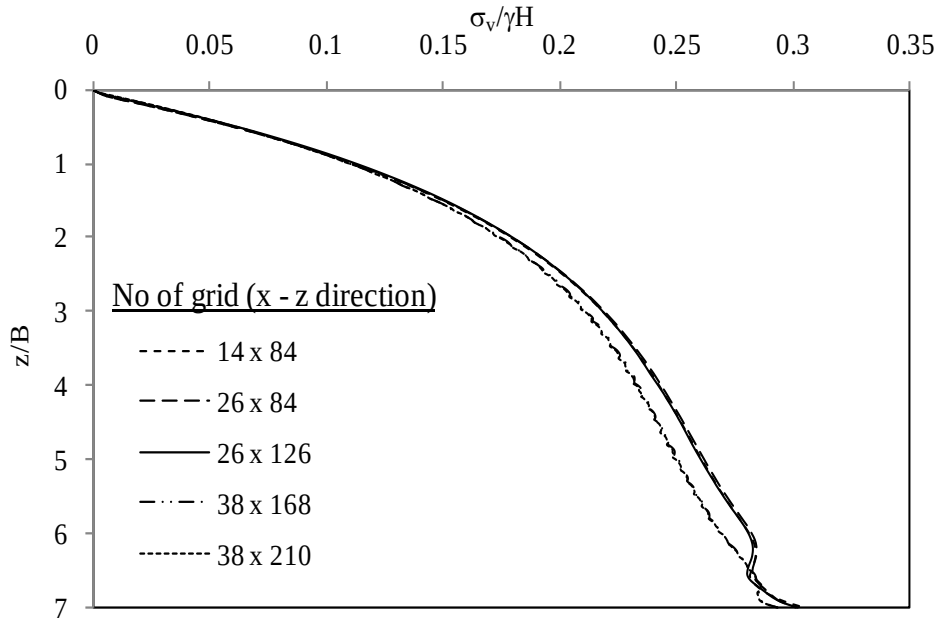

Figure 6.4. Vertical stress along centreline with depth at different grid sizes

Interfacial frictional properties

Interface elements were included in the model to represent the slip plane between two relative bodies, the backfilled material and the Perspex walls, and to model different surface roughnesses of the walls. A detailed discussion on the selection of interface element could be found in Pirapakaran (2008) and FLAC user's manual (Itasca 2005). The material properties assigned to an interface included interfacial friction angle, dilation angle, normal (k_n) and shear stiffnesses (k_s) between contact regions. The properties of interfacial friction and dilation angles were obtained from Tables 5.3 and 5.4. As high value of normal and shear stiffnesses tend to slow the solution convergence, it was recommended by Itasca (2005) to use the lowest stiffnesses that were consistent with small interface deformation in the modeling. A good rule-of-thumb was to set the k_n and k_s ten times the equivalent stiffness of the neighbouring zone, which was

$$k_n = k_s = 10 * max\left[\frac{\left(K_b + \frac{4}{3}G\right)}{\Delta z_{min}}\right] \quad (6.1)$$

where Δz_{min} was the smallest width of an adjoining zone or element in the normal direction, and K_b and G were the bulk and shear moduli respectively. With variation of stiffness on both side of interface, Eq. 6.1 should be applied to the softer side to ensure that the interface had minimal influence on the system. Because there was uncertainty in the selection of

appropriate stiffnesses, a sensitivity analysis was carried out to examine the influence of the stiffnesses on stress profile as well as to improve the solution efficiency.

Assuming $k_n = k_s$, a range of values from 10^6 Pa/m to 10^{10} Pa/m were tried for normal and shear stiffnesses. Corresponding variations of the shear stresses along the two walls of a vertical stope with depth were shown in Fig 6.5 for $k_n = k_s = 10^6$ Pa/m, 10^7 Pa/m, 10^8 Pa/m, 10^9 Pa/m, and 10^{10} Pa/m. As could be seen in Fig 6.5, 10^8 Pa/m had the least oscillation and gave identical results for both hangingwall and footwall. It was clear that, with further increase in k_n and k_s, the stresses remained approximately constant at all depth and the trend of the plots started to oscillate and deviate between hangingwall and footwall. Therefore, $k_n = k_s = 10^8$ Pa/m was selected for the numerical simulation of the laboratory stope.

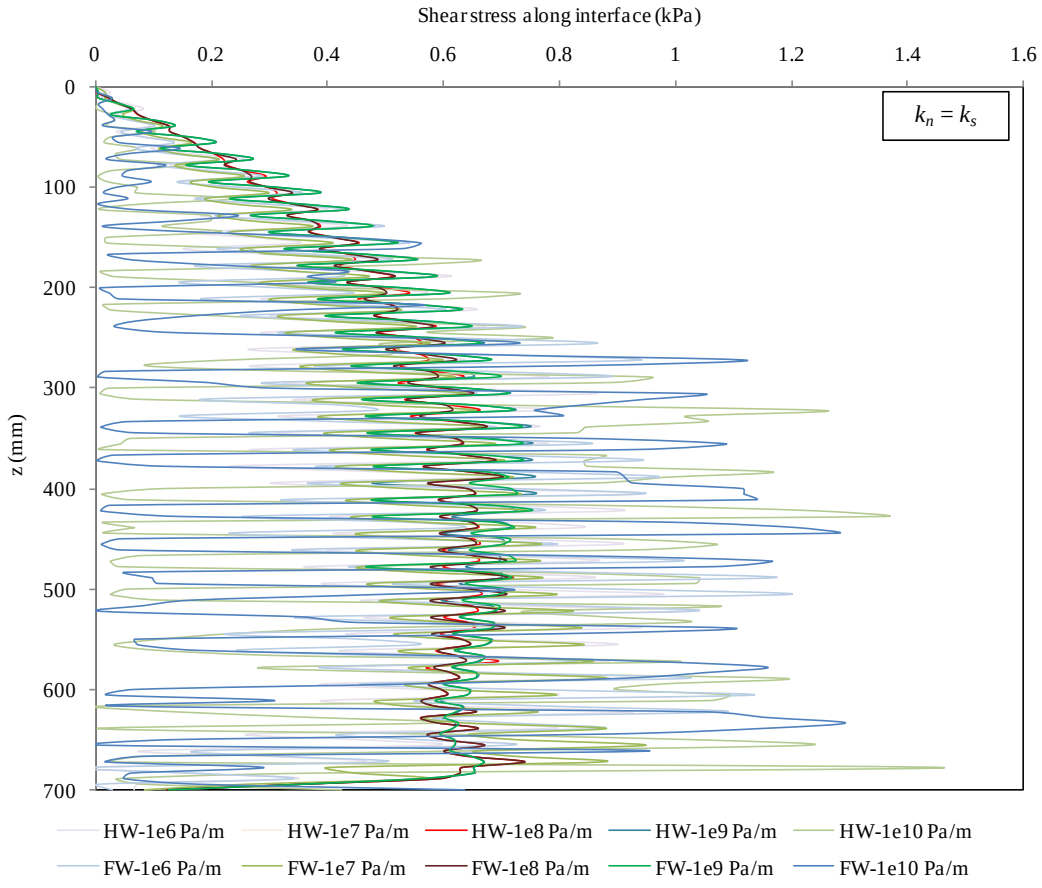

Figure 6.5. Shear stresses at interfaces along hangingwall (*HW*) and footwall (*FW*) with depth for different normal (k_n) and shear (k_s) stiffnesses

6.4 Comparison of analytical, experimental and numerical results

The experimental results obtained from Chapter 5 had been validated by comparing these with the stresses calculated from numerical and analytical models. Equation 3.15 was used in this study as an analytical tool for determining the average vertical stress at any depth where, K was taken as K_o or K_a. The value of δ was taken in accordance to the wall roughness as listed in Table 5.4. For relative fill density of 60%, δ was taken as 40^o, 33.6^o and 28^o for high, medium and low wall roughness respectively. The average vertical normal stress was also determined from the numerical model. These three were compared against each other.

The comparisons of results among the three different approaches (experimental, numerical and analytical) were presented in Figs. 6.6-6.8. The overburden pressure ($\sigma_v = \gamma z$) shown in the figures was the situation where the wall was assumed to be perfectly smooth and no arching was taking place. In these figures, dimensionless stress ratio $\sigma_v/\gamma H$ was plotted against dimensionless depth, z/B, where σ_v was the average vertical stress acting at any depth z measured from top of the backfill. γ was the unit weight of the fill, H was the total fill height. Here the depth was normalized with respect to the stope width B. These figures showed the variations of normalized average vertical normal stress against normalized depth for different wall roughness and slope angles.

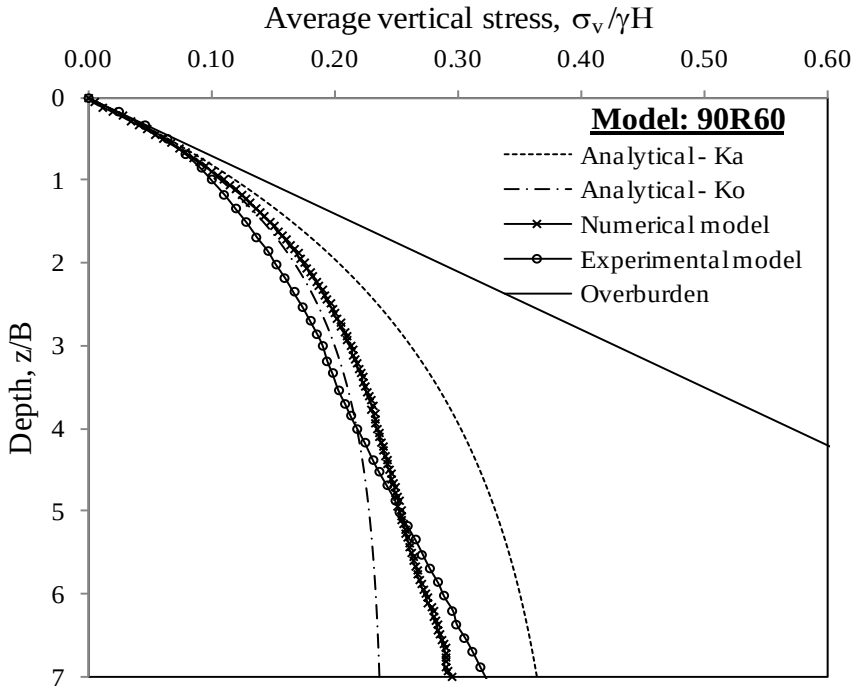

(a)

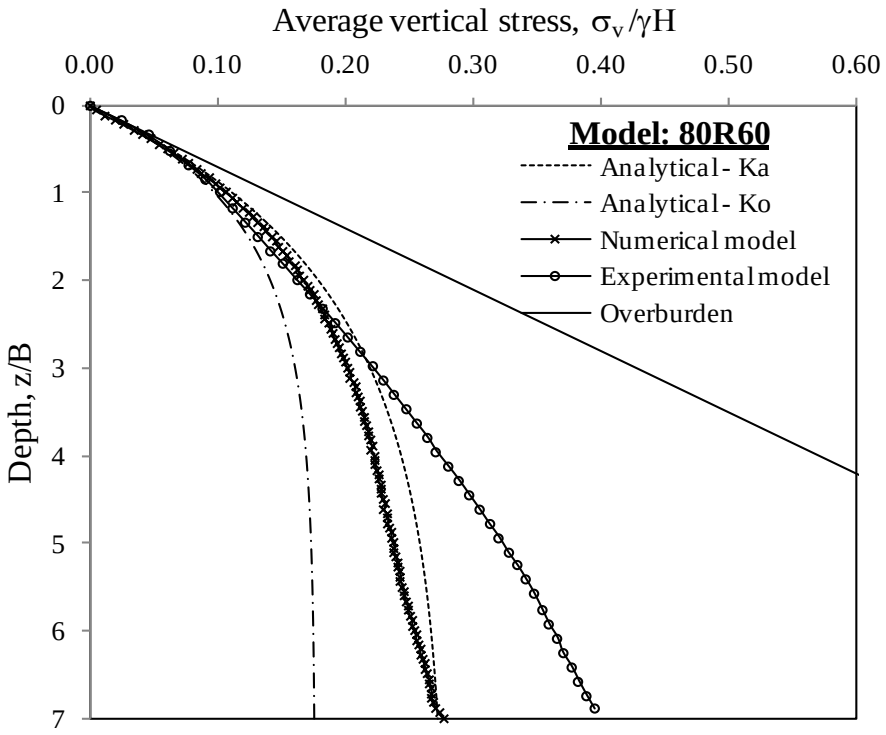
Average vertical stress, σv/γH
0.00
0.10
0.20
0.30
0.40
0.50
0.60
Depth, z/B
0
1
2
3
4
5
6
7
Model: 80R60
Analytical- Ka
Analytical- Ko
Numerical model
Experimental model
Overburden

(b)

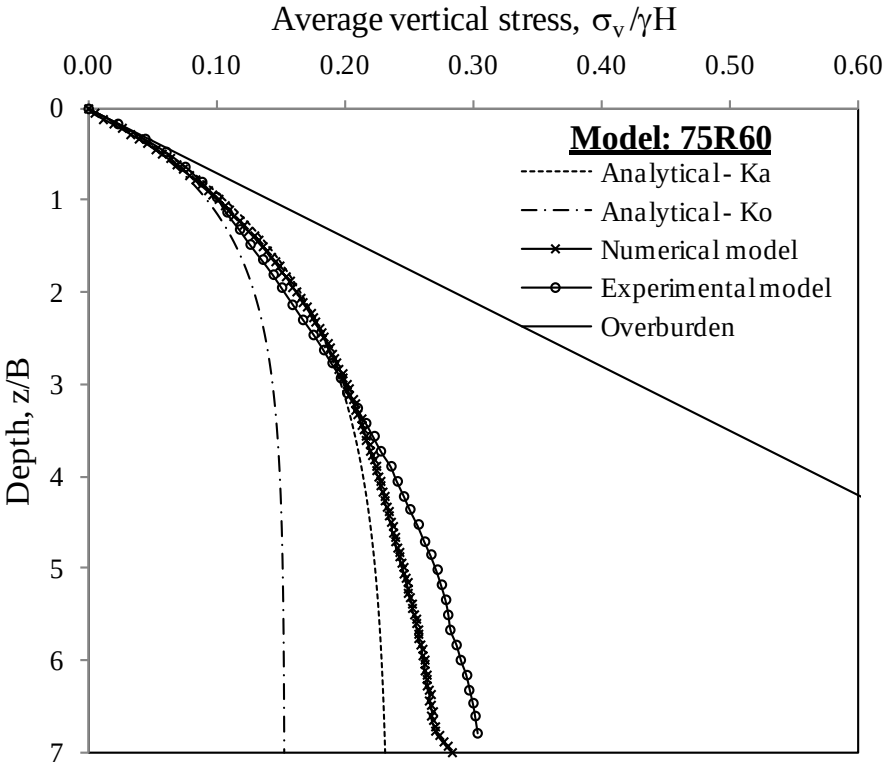
Average vertical stress, σv/γH
0.00
0.10
0.20
0.30
0.40
0.50
0.60
Depth, z/B
0
1
2
3
4
5
6
7
Model: 75R60
Analytical- Ka
Analytical- Ko
Numerical model
Experimental model
Overburden

(c)

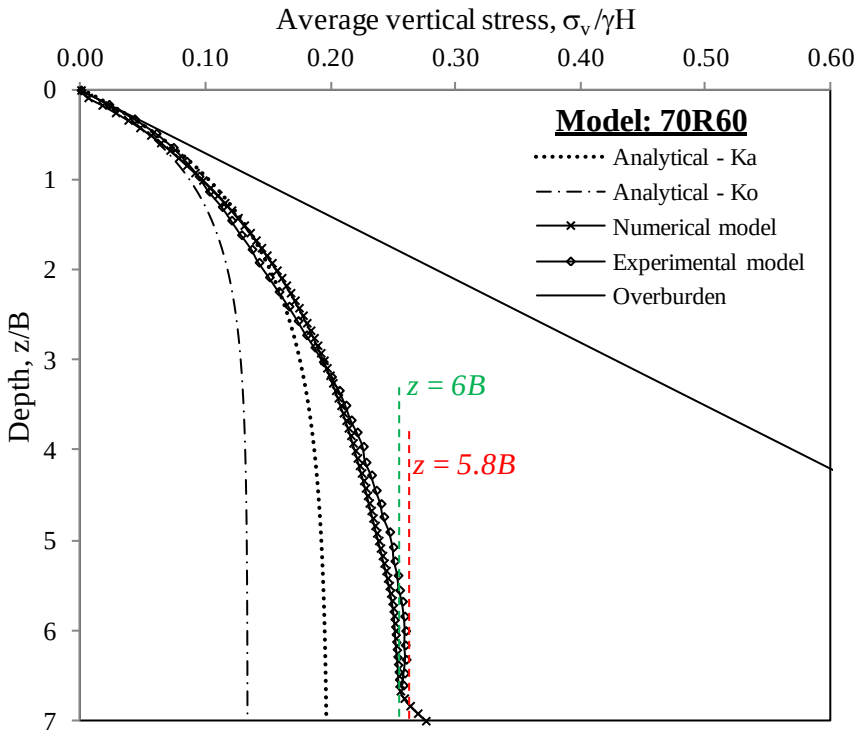

(d)

Figure 6.6. Comparison between the solutions of experimental, numerical and analytical modeling for different slope angle with high wall roughness: (a) model 90R60, (b) model 80R60, (c) model 75R60 and (d) model 70R60

The value of σ_v derived from the analytical expression showed a clear trend of reaching an asymptotic value at a certain depth for multiples of *B*. The asymptotic value and the exact depth at which it was reached depended on the stope inclination and the *K*-value assumed. In the case of laboratory model tests and numerical model the asymptotic value was not reached even at depth of 7*B*, except for the stope with $\beta = 70^o$ (see Figs 6.6d and 6.7d). The experimental and numerical modeling values were in good agreement for all cases except for the one where $\beta = 80^o$. As expected, the smoothness in the stress profiles seen in the numerical and analytical models was not seen from the laboratory model test data. A steady decline in σ_v with increasing tilt from vertical of the stope walls was quite clear from the analytical and numerical solutions. This trend was not very clear from Fig 6.6 for experimental modeling data.

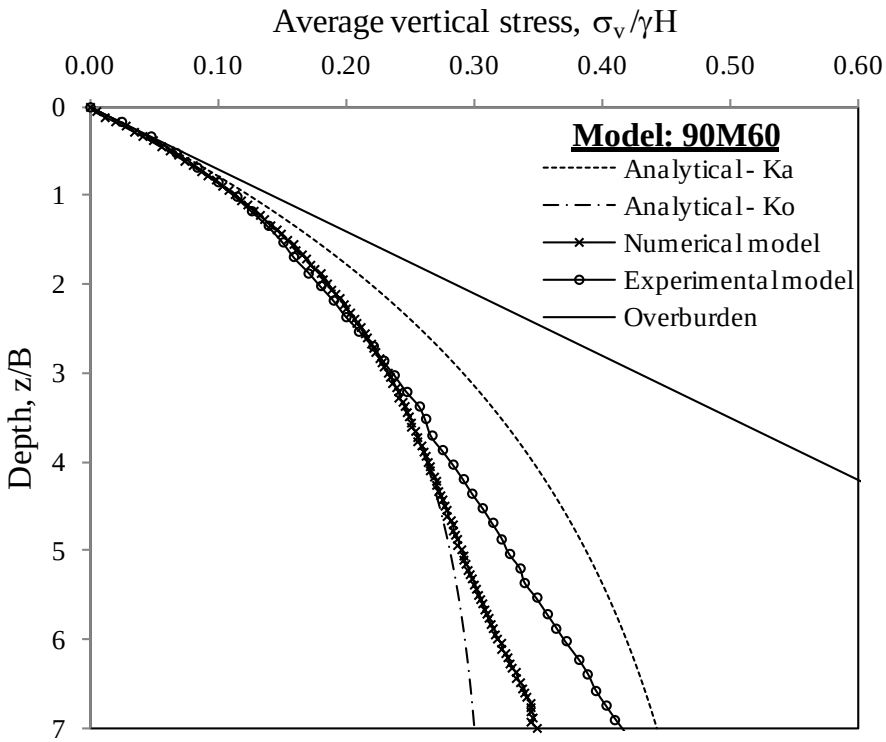
Average vertical stress, σv/γH
0.00
0.10
0.20
0.30
0.40
0.50
0.60
Depth, z/B
0
1
2
3
4
5
6
7
Model: 90M60
Analytical - Ka
Analytical - Ko
Numerical model
Experimental model
Overburden

(a)

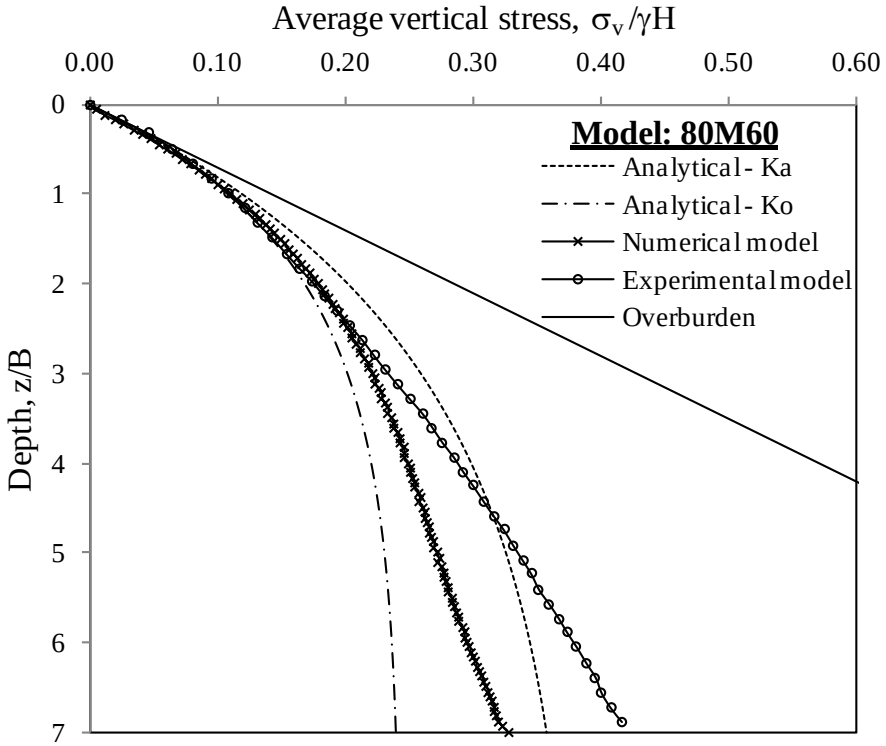
Average vertical stress, σv/γH
0.00
0.10
0.20
0.30
0.40
0.50
0.60
Depth, z/B
0
1
2
3
4
5
6
7
Model: 80M60
Analytical - Ka
Analytical - Ko
Numerical model
Experimental model
Overburden

(b)

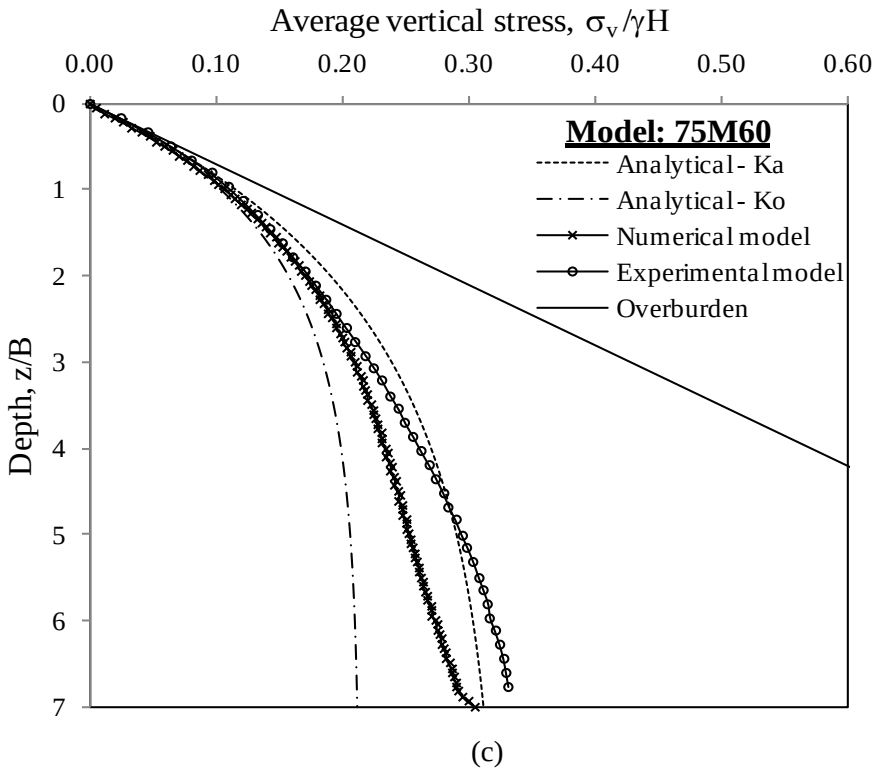

(c)

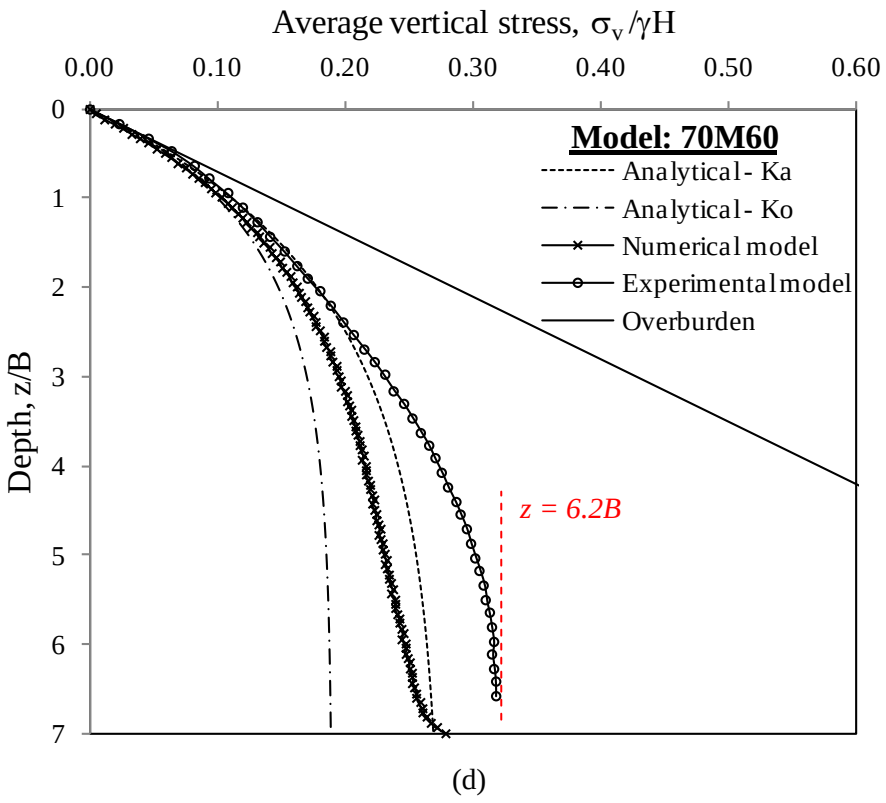

(d)

Figure 6.7. Comparison between the solutions of experimental, numerical and analytical modeling for different slope angle with medium wall roughness: (a) model 90M60, (b) model 80M60, (c) model 75M60 and (d) model 70M60

The trend for stope walls with medium roughness are similar to what is seen for walls of high roughness. In this case, for $\beta = 75^{o}$ and 70^{o}, the asymptotic value of σ_v is reached in the laboratory models as well. A trend that is evident for walls of high and medium roughness is that σ_v – z profile shows an increasing tendency to reach the asymptotic value with increasing tilt of the walls.

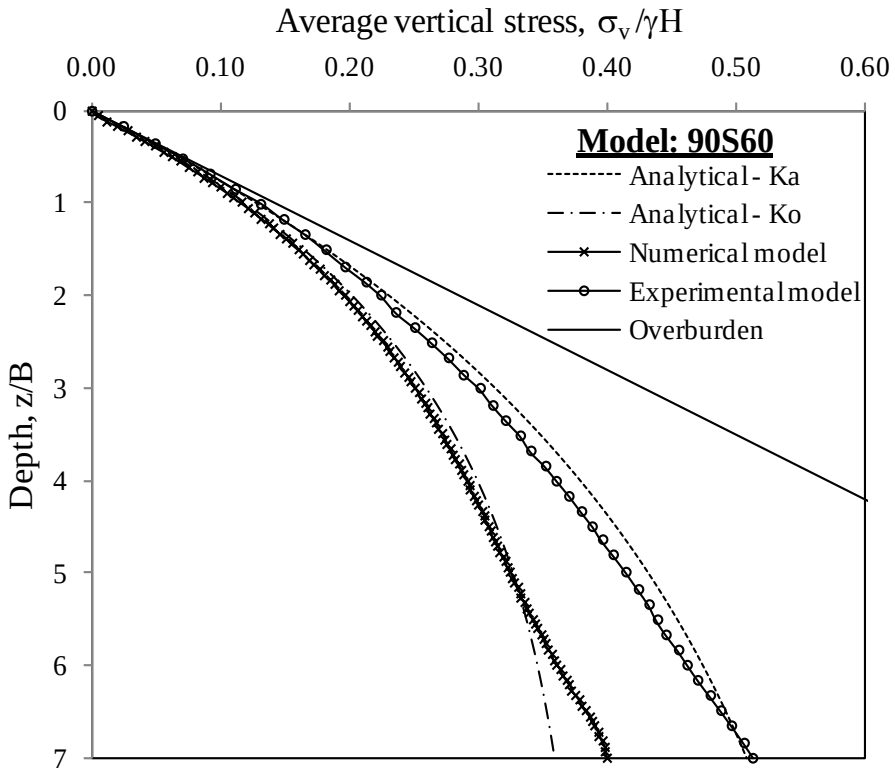

(a)

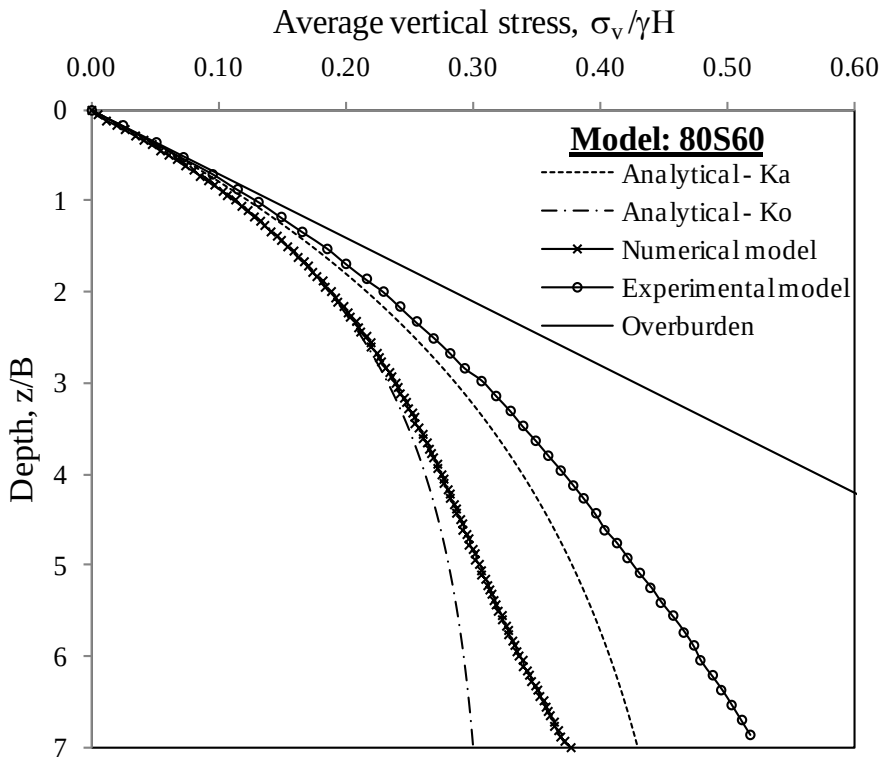
Average vertical stress, σv /γH
0.00
0.10
0.20
0.30
0.40
0.50
0.60
Depth, z/B
0
1
2
3
4
5
6
7
Model: 80S60
Analytical - Ka
Analytical - Ko
Numerical model
Experimental model
Overburden

(b)

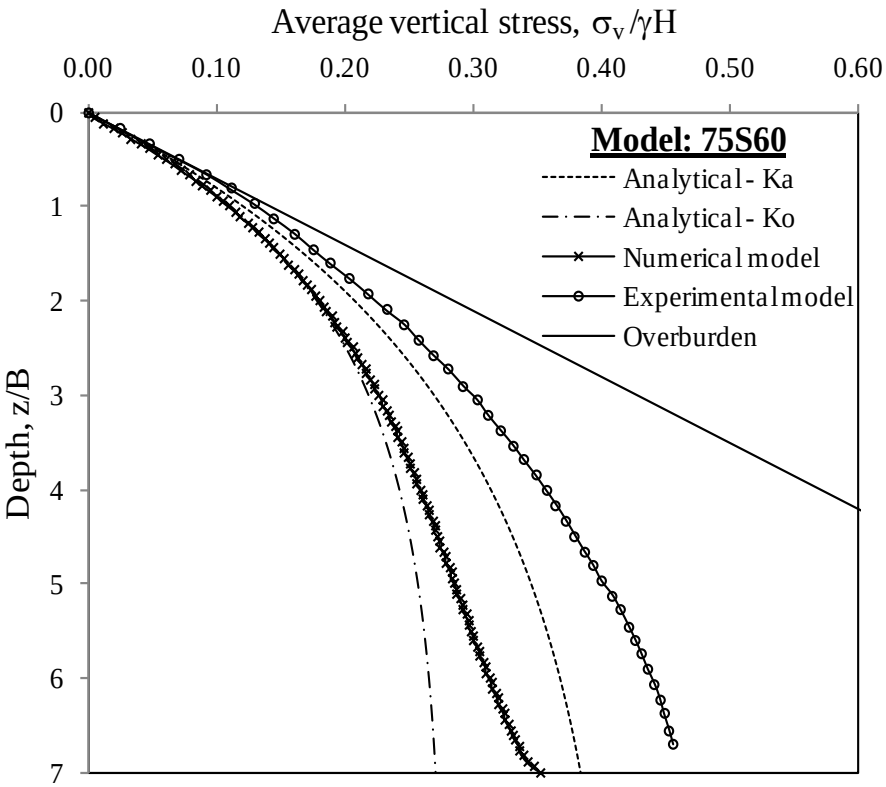
Average vertical stress, σv /γH
0.00
0.10
0.20
0.30
0.40
0.50
0.60
Depth, z/B
0
1
2
3
4
5
6
7
Model: 75S60
Analytical - Ka
Analytical - Ko
Numerical model
Experimental model
Overburden

(c)

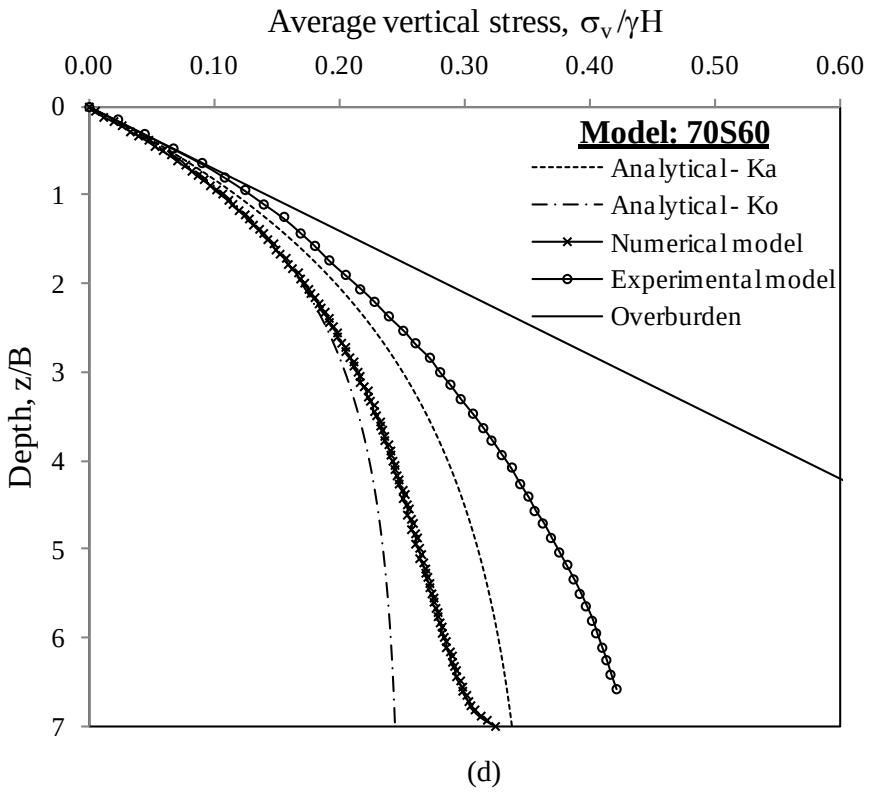

(d)

Figure 6.8. Comparison between the solutions of experimental, numerical and analytical modeling for different slope angle with low wall roughness: (a) model 90S60, (b) model 80S60, (c) model 75S60 and (d) model 70S60

For walls of low roughness, the trend was similar to what was seen for walls of high and medium roughnesses (See Fig. 6.8). The observation from Figs 6.6-6.8 showed that the asymptotic value of fill depth at which the average vertical stress did not increase with depth was dependent on wall-fill interfacial characteristics, stope inclination and the assumed *K*-value. This value decreased with the increase of wall roughness and stope inclination. Higher asymptotic value was observed for $K = K_a$, compared to $K = K_o$. This asymptotic value of depth implied that any increase in fill weight had negligible influence on load distribution beyond this depth.

As can be seen from Figs 6.6, 6.7 and 6.8, the results obtained from the laboratory tests agreed well with those obtained from numerical model for medium and high wall roughness, for all slope angles except for 80^o. Unlike the experimental results, the vertical stresses obtained from numerical and analytical solutions reduced gradually when the stope tilts from vertical. For low roughness wall-fill interface, slightly higher stresses were obtained from experimental results compared to those of numerical results as well as analytical solutions. This deviation might be due to the use of the higher interface friction angle δ_s for

low wall roughness obtained from modified direct shear test in the stress determination. δ_s used in numerical and analytical modeling may be higher than actual δ_s due to the fluctuating value of stress-strain profile obtained from modified direct shear test. In all cases, the value of K_a was always less than K_0 and therefore, the corresponding lateral earth pressure and the fill weight transferred to the wall were less when K was assumed as K_a. Therefore, assuming $K = K_a$ implied larger vertical normal stresses at any depth, which was evident from Figs. 6.6-6.8. When using the analytical equation (Eq 3.15), it could be seen that, in all cases, the results obtained by using $K = K_o$ tend to overestimate stresses transferred to the walls due to arching effect. It could also be seen from the figures (Figs 6.6-6.8) that the stress state within the backfill tended to shift from at-rest state to active state with increasing stope inclination and wall roughness. For vertical stope, the results obtained from numerical and experimental modeling fell between those obtained from Eq.3.15 using $K = K_o$ and $K = K_a$. For inclined wall, the solutions obtained from numerical modeling were well correlated with analytical solutions using $K = K_a$ except for the cases of low wall roughness where the numerical prediction of the average normal stress fell between those analytical solutions predicted using $K = K_o$ and $K = K_a$. This result revealed that both stope inclination and wall roughness might have significant influence on the stress state change within the backfill. However, for a typical inclined minefill stope, where $\delta = \phi$, $K = K_a$ was reasonably appropriate to describe the stress development within the stope.

6.5 Numerical modeling of arching in a full scale stope backfilled with granular material

Now that the numerical model has been validated against the laboratory model test data and the analytical expression, it is time to apply the model to solve a real-life mining problem. Numerical modeling of stresses within a prototype mine stope with due consideration to the surrounding environment is carried out in this section to investigate the stress state in the backfilled stope.

6.5.1 Modeling approach

Using approach similar to what was discussed in previous section; a numerical model of typical plane strain inclined stope was developed assuming idealized mining characteristics and processes as shown in Fig 6.9 (see Appendix C2 for FLAC code). The vertical height of the model, H was 45 m and the width, B was 6 m (i.e. aspect ratio of width to height is 1:7.5). The reason of selecting these stope dimensions was to compare the numerical

modeling results with those from Professor Aubertin's group with similar dimensions (Aubertin et al. 2003; Li and Aubertin 2008, 2009; Li et al. 2003, 2007). The same material properties were used for the calculations in FLAC.

In Fig 6.9, *b* was the minimum distance between rock boundaries and stope walls; *d* was the depth of rock below the base of stope and also the depth of rock above the stope; h_v was the gap between the rock roof and fill material which was typically 0.5 m to 1 m and was taken as 0.5 m in this research. β was the angle of stope inclination to the horizontal.

In the simulation, top of the stope was assumed to be located approximately 200 m below the ground surface. *b* and *d* were selected such that they were far enough from the area of interest and did not influence the system being modelled and the accuracy of the results. This was because using larger *b* and *d* value in the simulation would result in increasing number of elements, and therefore increased the simulation time. Modeling with *b* ranging from 10 to 30 m and *d* ranging from 10 to 30 m had been conducted in a sensitivity study and *b* was taken as 20 m and *d* was taken as 10 m in this dissertation. The remaining 190 m depth of rock mass on top of stope from ground surface was converted to equivalent overburden pressure *q* acting on the top boundary of the model as shown in Fig 6.9. The value of *q* was calculated as 5.0325 x 10^6 kPa.

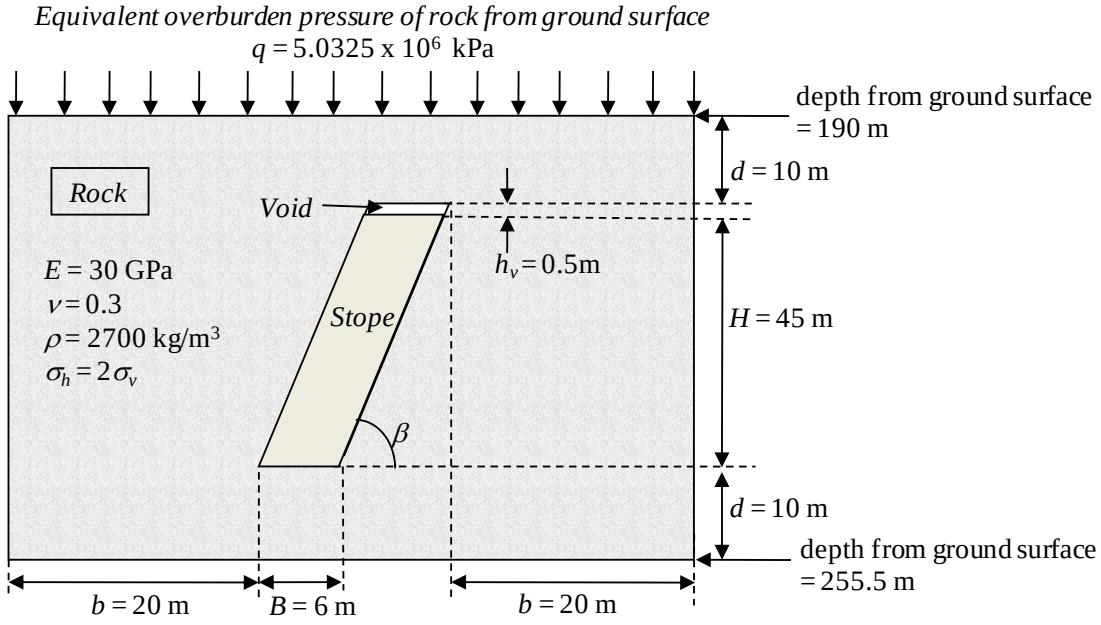

Figure 6.9. Schematic diagram of an idealized mine stope

6.5.2 Sensitivity analysis

Based on the sensitivity analysis similar to what was done in Section 6.3.2, the following modeling criteria had been established.

Mesh Density

Mesh density ranging from 1 m/grid to 0.25 m/grid had been carried out to determine the grid size used in the simulation. It could be seen from the Fig 6.10 that stresses levelled off at grid size 0.5 m/grid at all elevations. Mesh density with grid size 0.5 m/grid produced reasonably good results rather quick without sacrificing the accuracy. Therefore, 0.5 m/grid in both *x*- and *y*-direction were selected in the modeling, with a total of 12408 elements.

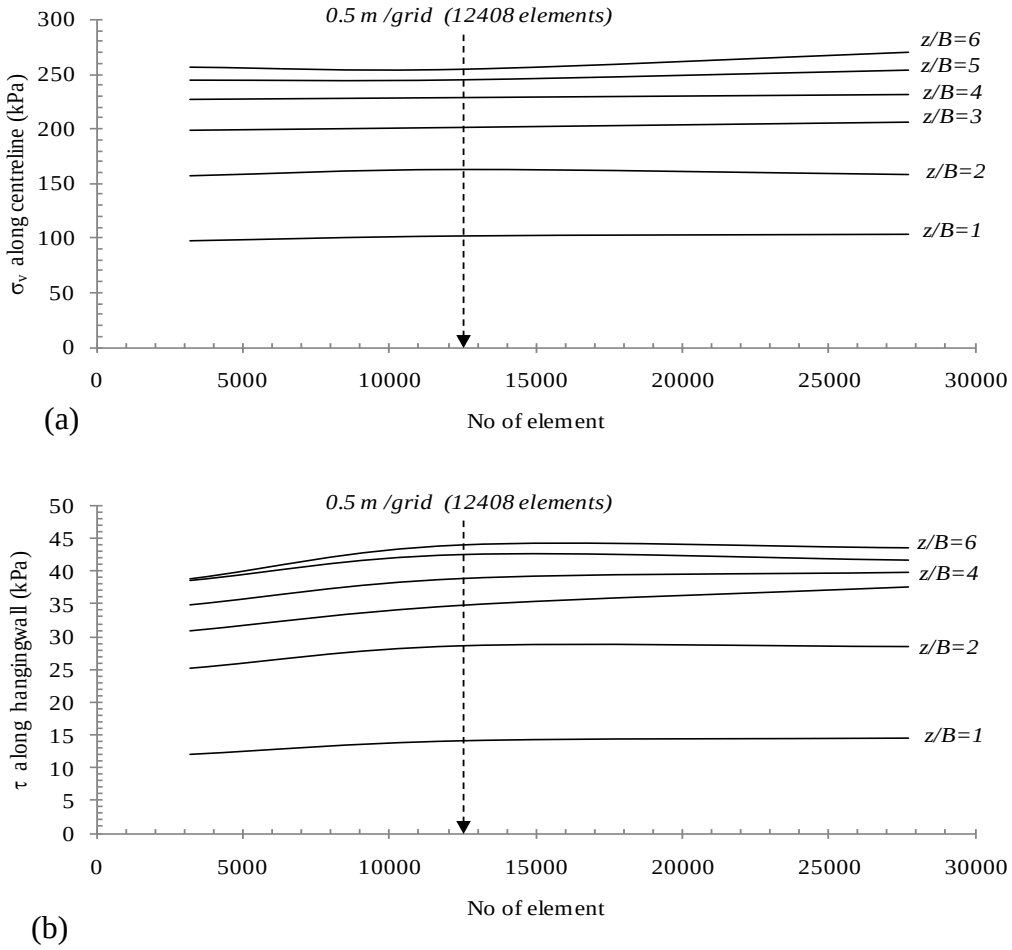

Figure 6.10. Stresses variation against number of element at different depth modelled in FLAC (a) Vertical stress along centreline (b) Shear stress along hangingwall

Constitutive models

The FLAC built-in constitutive models were used in the simulation. The rock mass was assumed to be homogeneous, isotropic and linear elastic whereas backfill materials was modelled to follow Mohr-Coulomb failure criterion. Table 6.2 showed the summary of input parameters and constitutive models for rock mass and backfills used in FLAC for basic calculation. These parameters were typical of rock surroundings and the various hydraulic fills studied at James Cook University Geomechanics laboratory.

Table 6.2. Input parameters and constitutive models for rock mass and backfill materials

Model input parameters	Rock mass	Backfills
Constitutive model	Linear elastic	Mohr Coulomb
Young's modulus, E (GPa)	30	0.3
Poission's ratio, ν	0.3	0.2
Density, ρ (kg/m^3)	2700	1800
Cohesion, c (kPa)	-	0
Friction angle, ϕ (^{o})	-	30
Interfacial friction angle, δ (^{o})	-	30
Dilation angle, φ (^{o})	-	0

Boundary conditions

The boundary conditions along the far left and right ends of rock region were fixed in *x*-direction and the base of rock regions was fixed in both *x*- and *y*-direction. Simulations had been conducted with and without using interface elements between the fill and rock mass. Almost identical results among models with and without interface elements were obtained when interfacial friction angle, δ was taken as fill friction angle, ϕ. However, when δ was taken as less than ϕ, higher vertical stresses were developed due to less arching induced along rock-fill interfaces. The interfacial elements where $\delta < \phi$ allowed slip between the fill and the rock mass that enabled a greater load to be transferred to the base. In this dissertation, interface elements were included along the walls between the rock mass and fill material and the k_n *(=* k_s*)* was taken as 10^{10} kPa/m based on the similar approach discussed in Section 6.3.2.

Initial conditions

The initial stress distribution of the model was modelled in accordance with typical mining situations. The natural in-situ vertical stress of rock mass was taken by considering the self weight of rock mass surrounding the stope and the overburden pressure on top of the model. The natural in-situ lateral stress was taken as twice of the vertical stress (i.e. K_o = 2 which was common in rocks). The system was allowed to reach its steady state under gravitational stresses before excavation and filling were carried out. The stope was then excavated and once again, the system was allowed to reach its equilibrium state before commencing the filling process.

Lift/filling rate

The filling process was conducted by placing the fill in several layers. Number of filling layers ranging from 5, 10, 18 and 45 were modelled and almost identical results were obtained. As the solution time increased with increasing number of layers, 10 layers were selected in the simulation for the present model.

6.5.3 Results and discussion

Vertical stress distribution

Figure 6.11 showed the comparison of vertical stress along centreline against depth between proposed model and Li and Aubertin's (2009) model. There was very good agreement between the two results. The author's results gave slightly lower values for stopes with inclination of 90^o and 80^o and very close match at $\beta = 70^o$ and 60^o. The models developed by Li and Aubertin (2009) were simulated without using interface element. However, as discussed in section 6.5.2 (boundary condition), with $\delta = \phi$, the results were almost identical for models with and without using interface elements. Therefore, they should be comparable to each other.

.

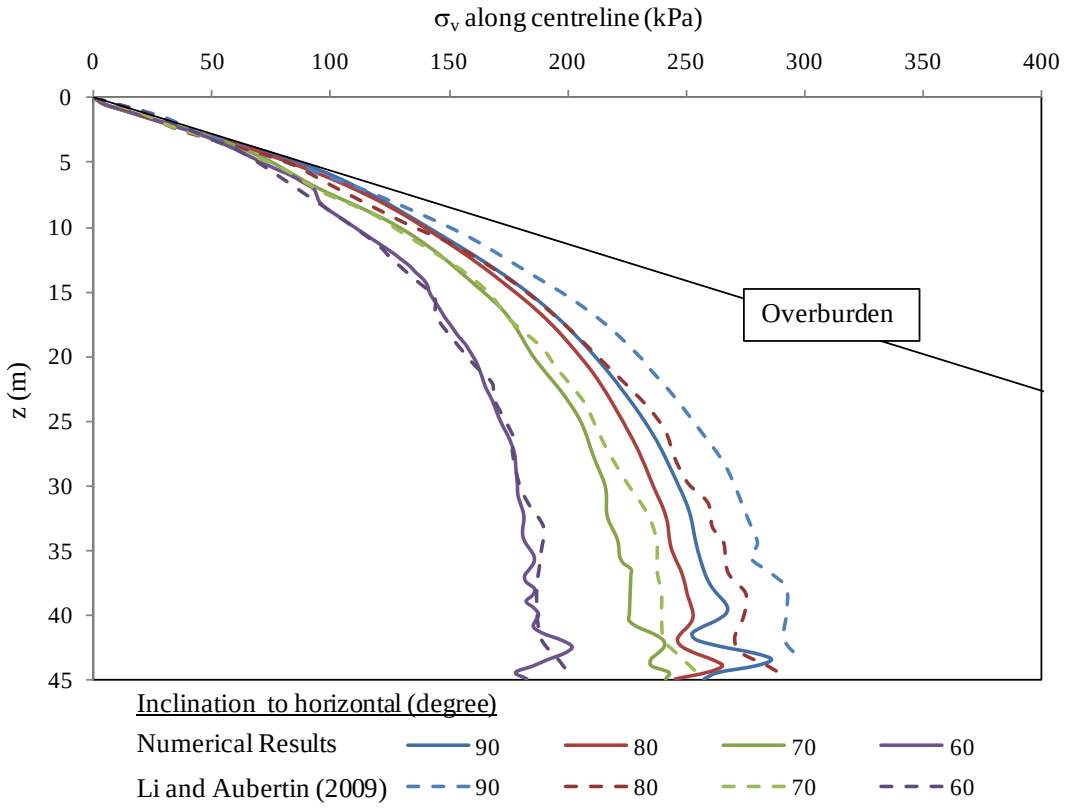

Figure 6.11. Comparison of vertical stress along centreline with Li and Aubertin's (2009) model

Figure 6.12 showed the vertical stress contours within the backfill and surroundings rock mass for different stope inclination. The stresses within the backfill were smaller along the walls compared to those at the centre of the stope at any elevation, clearly showing that arching occurred within the fill. As stope inclined from vertical, the peak stress deviated from centreline towards footwall and the stress profile quickly became asymmetric. Higher stresses were observed along the footwall compared to those along hangingwall at a given elevation. It was clearly shown in the Figs 6.11-6.13 that the stress experienced by the fill decreased when the wall became more inclined. The reason for this behaviour might be due to the combined action of arching and gravitational effects.

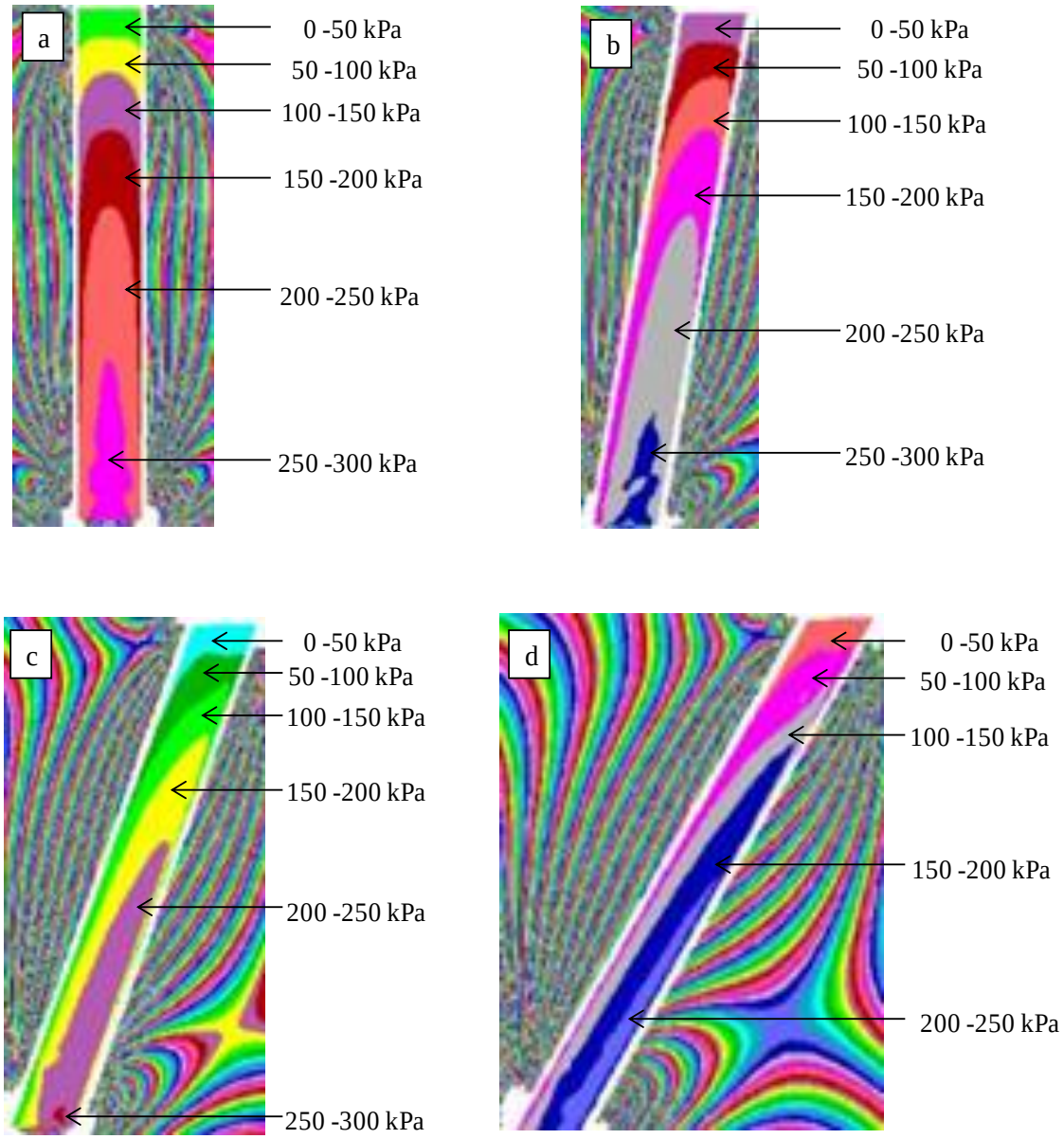

Figure 6.12. Vertical stress distribution profiles within backfill and surroundings rock region for stope inclination of (a) 90^{o} (b) 80^{o} (c) 70^{o} and (d) 60^{o} to the horizontal

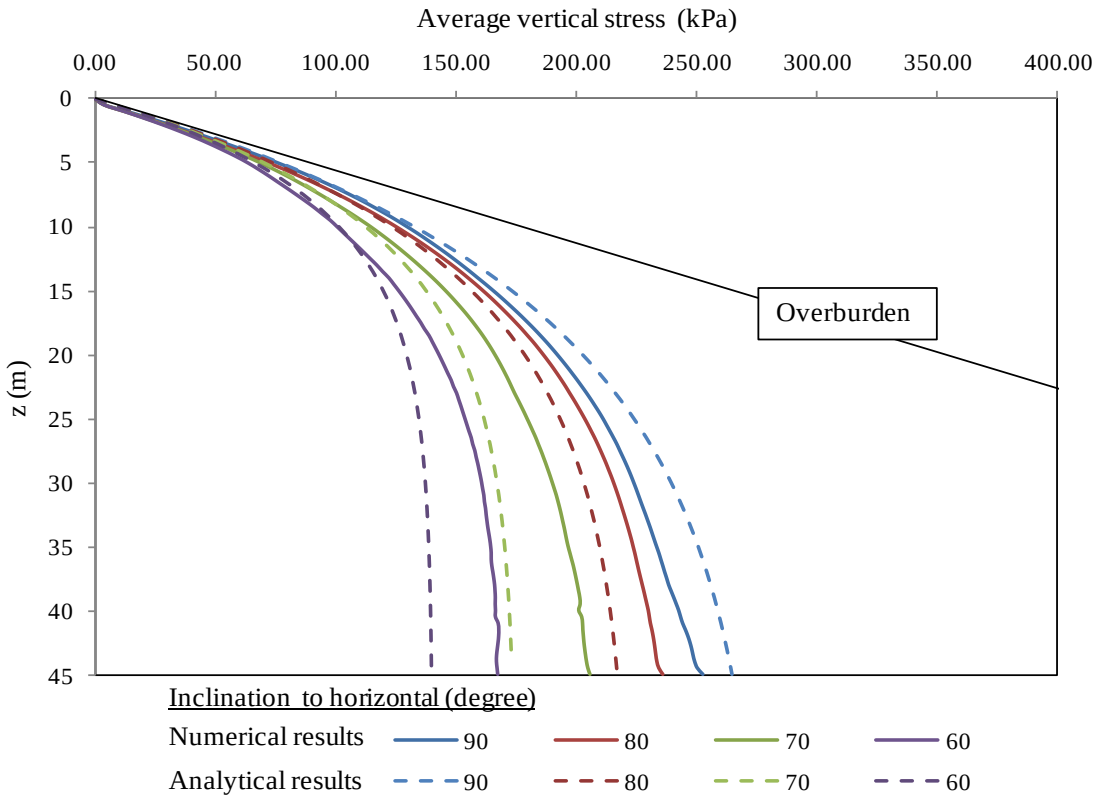

Figure 6.13. Comparison of average vertical stress against depth among numerical and analytical solutions

Figure 6.13 showed the comparison of average vertical stresses between numerical results and analytical solutions computed using Eq. 3.15 with $q = 0$, $K = K_a$ and $\delta = \phi$. There was good agreement between the two methods, proving that Eq. 3.15 with $q = 0$, $K = K_a$ and $\delta = \phi$ was capable of estimating vertical stress within backfill for a mine stope realistically. In general, the average vertical stress tend to decrease with the increase of stope inclination. It could be seen from numerical results that the stress increment was nonlinear. The difference increased with increasing tilt. Slight decrease in stress magnitude was observed when slope angle varied from 90^o to 80^o. The decrease of stress magnitude became more significant when slope angle was less than 80^o. This result was consistent with the results obtained from laboratory model where the variation of stress magnitude was small for slope angle between 90^o and 80^o.

It should be noted, $q = 0$ was used in the Eq. 3.15, indicating that no surcharge was applied to the model. This condition was not consistent with the numerical model where the stope was located 245 m below earth surface with 200 m rock overburden on top of it. The reasons

for the good agreement between the two models could be attributed to the gap left on top of the stope, the stiff and arching action of surrounding rock mass. The 0.5 m gap on top of the fill avoided the immediate contact between the fill and the overlying rock mass, justifying q = 0. With stiffness of rock mass two orders of magnitude larger than fill materials, the displacement of rock walls was expected to be very small. In the case of narrow stope, the effect of arching enabled stress redistribution and transmission of overburden pressure on top of the stope into both the hangingwall and footwall or around the openings to the surroundings rock mass.

Horizontal stress distribution

Figure 6.14 showed the comparison of lateral stress against depth along centreline between proposed numerical results and Li and Aubertin's (2009) results. The results agreed well with the comments by Li and Aubertin (2009) that the lateral stress was not sensitive to the stope inclination. This behaviour could not be shown in analytical solution (refer to Fig 3.12), where with a constant value of K (K_a or K_o), the lateral stress varied in accordance to the magnitude of vertical stress ($\sigma_h = K\sigma_v$). No such constant K was assumed in numerical modeling, allowing K to vary throughout the fill.

Figures 6.15 (a - d) showed the lateral stress profiles within backfill for different stope inclinations. The stress magnitude varied from 0 kPa to 110 kPa from top of the stope down to the base of the stope with a stress contour interval of 10 kPa. As the stope became more inclined, the stress distribution became asymmetric. Higher lateral stresses were observed along hangingwall compared to that of footwall with the highest stress located at the bottom region of hangingwall. From the equation $\sigma_h = K\sigma_v$, it was expected that σ_h would increase when σ_v increased. However, based on numerical modeling results, it was shown that σ_h increased when σ_v decreased. It could be due to the variation of K across the span. Therefore, a preliminary analysis of K was carried out below.

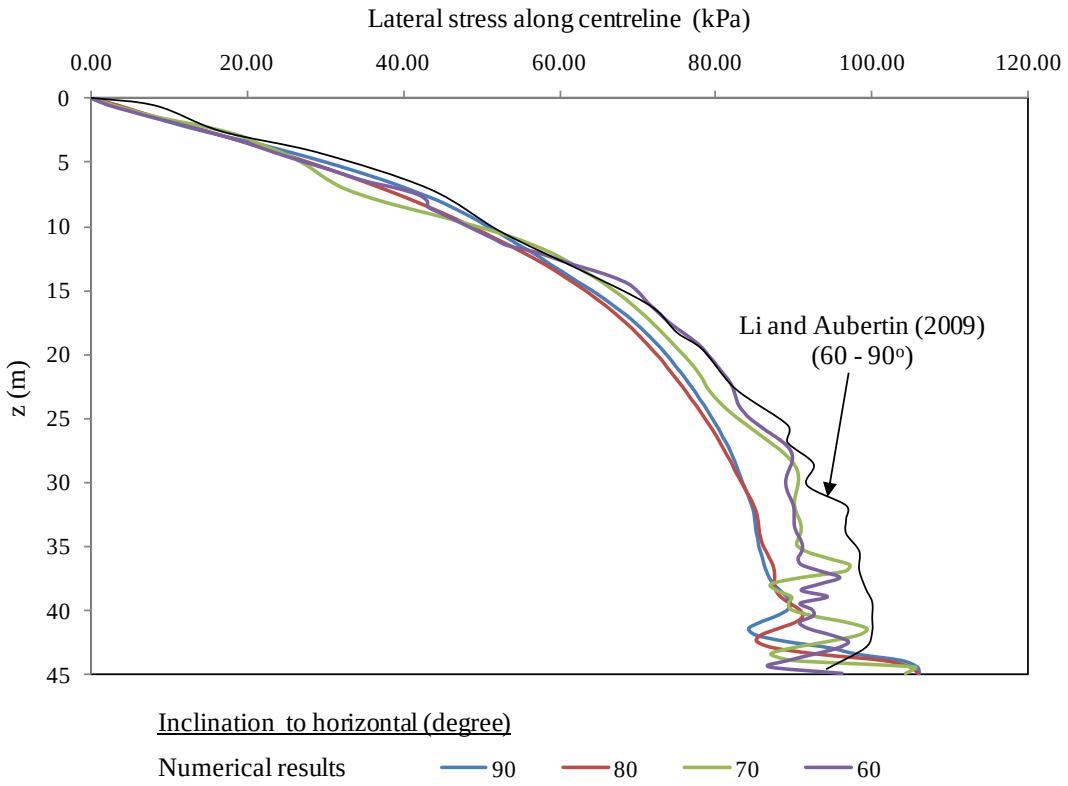

Figure 6.14. Comparison of lateral stress with Li and Aubertin's (2009) model

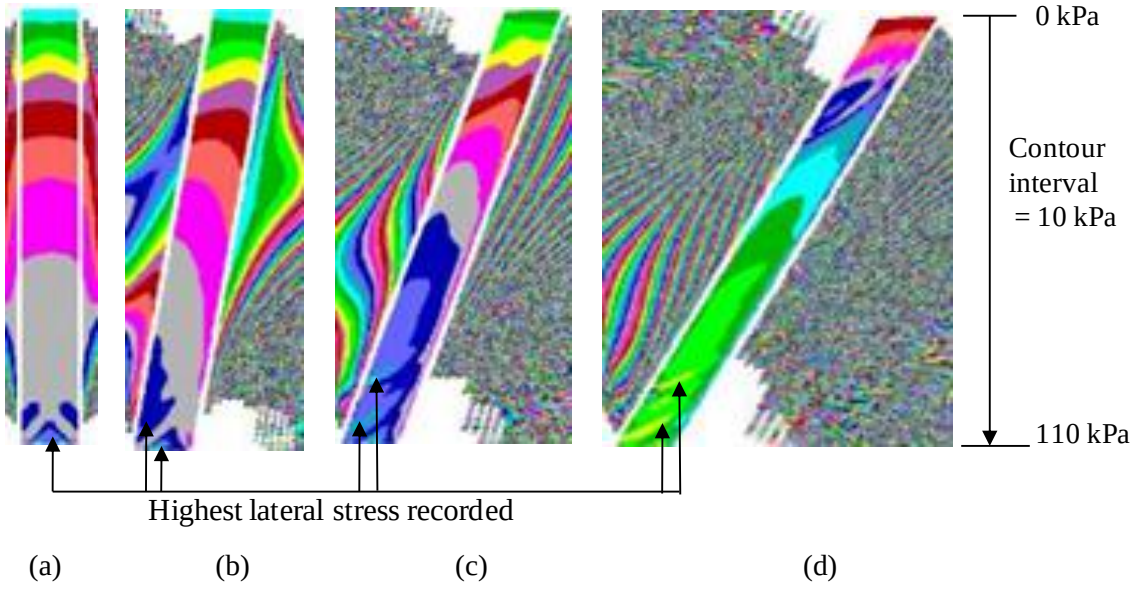

Figure 6.15. Lateral stress profiles within backfill and surroundings rock region for stope inclination of (a) 90° (b) 80° (c) 70° and (d) 60° to the horizontal

Figures 6.16 (a – d) showed the value of *K* across the span at elevation, *z* = 10, 20, 30 and 40 m for stope varied from 90° to 60° to the horizontal respectively, where *z* was measured from the top of the fill. Here, *K* was calculated using equation $K=\sigma_x/\sigma_z$, where the vertical stress, σ_z and the horizontal stress, σ_x were obtained from numerical results. It could be seen from the figures that *K* was insensitive to the elevation. As shown in Fig 6.17, with the assumed $\phi = 30^o$, $K_o = 0.5$ and $K_a = 0.33$, when the stope became more inclined, the value of *K* increased along hangingwall and decreased gradually across the span towards footwall. The *K*-values for vertical stope lied between these two and showed symmetry as expected. The value of *K* was almost identical at footwall for all three different stope inclinations considered except for vertical stope, which gave slightly higher value of *K* at footwall. This combination of higher *K* and lower σ_z or vice versa would result in constant σ_x across the span. This behaviour could not be captured in simple analytical solutions and therefore further investigation was required to address this issue.

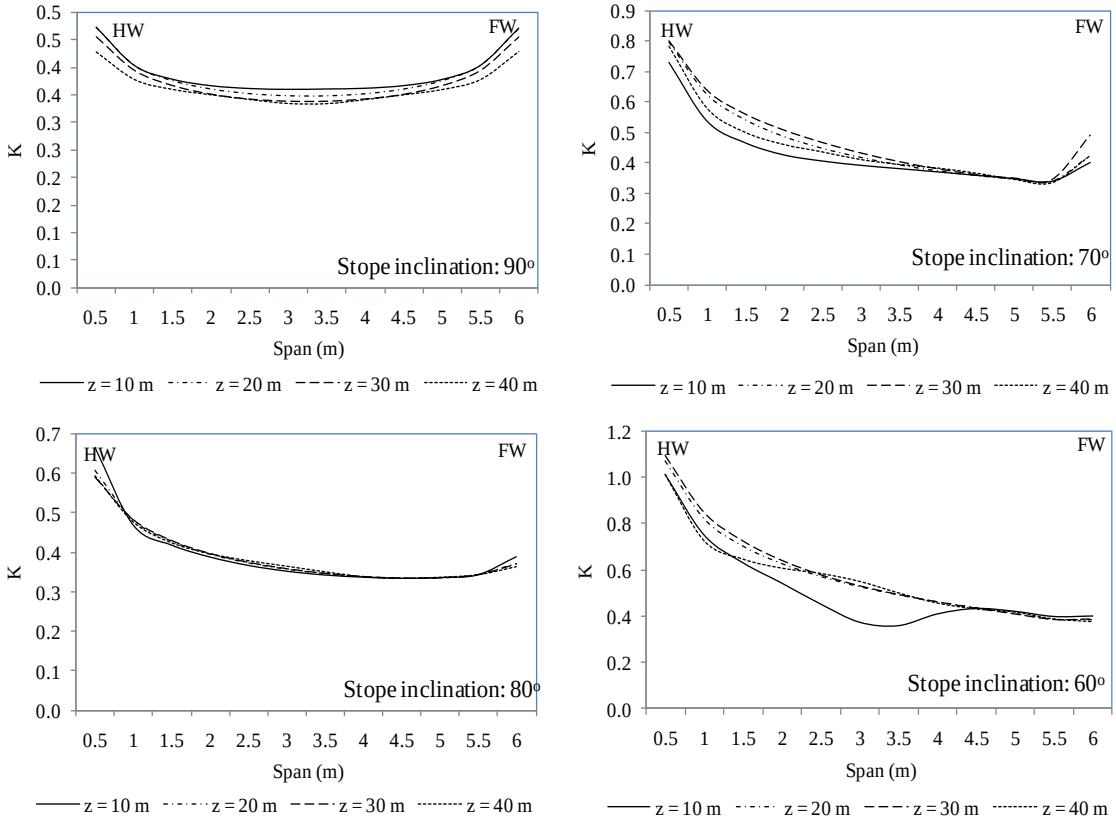

Figure 6.16. Variation of *K* across the span for stope inclination of 90°, 80°, 70° and 60° to the horizontal at elevation z = 10, 20, 30 and 40 m

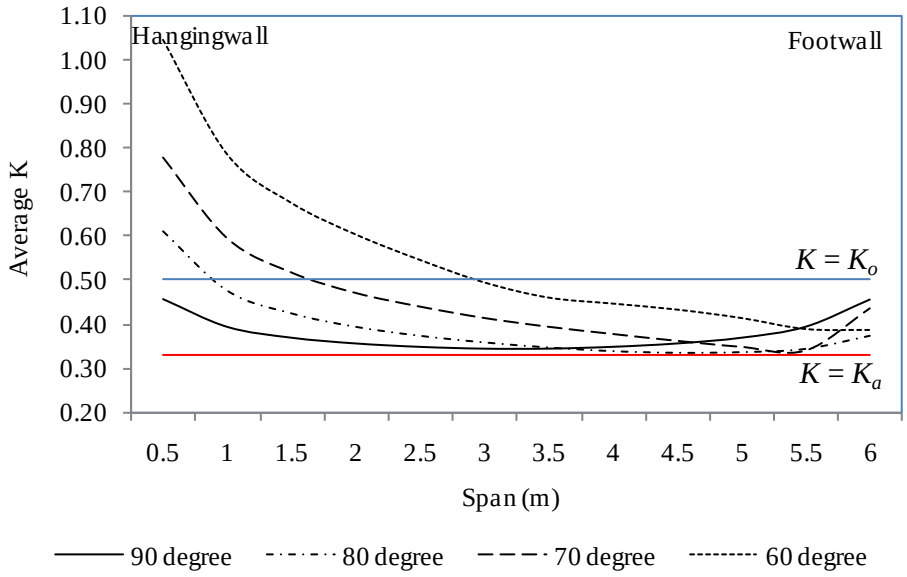

Figure 6.17. Variation of average *K* value across the span for different stope inclination

For this typical example (shown in Fig 6.17 with material properties listed in Table 6.2), *K* varied, along the hangingwall, from 1.05 to 0.45 as slope angle varied from 60^o to 90^o respectively. At footwall, *K* was computed as 0.45 for vertical stope and 0.4 for inclined stope (β = 60^o to 80^o). The theoretical values of K_p, K_o and K_a were calculated as 3, 0.5 and 0.33 respectively. It could be observed from the figure that the stress state experienced by the fills changed across the span from slight passive state to at rest state and finally active state except for vertical stope, which was almost constant throughout the span. The plots in Fig. 6.17 also showed that *K* value fell between K_o and K_a and $K = K_a$ was more appropriate for describing the stress state within a stope.

Shearing stress distribution

Figure 6.18 showed the variation of shear stresses along hangingwall and footwall with depth for different stope inclination. The shear stress was calculated based on the following stress transformation equation.

$$\tau = -\frac{\sigma_x - \sigma_z}{2} sin2\beta + \tau_{xz} cos2\beta \qquad (5.4)$$

As shown in the figure, the magnitude of shear stress for a vertical stope was the same along hangingwall and footwall. For an inclined stope, the shearing stress along footwall increased from vertical to stope inclination of 80^o and remained unchanged for slope angle of 70^o and

60^{o} (to the horizontal). Conversely, the shearing stress along the hangingwall decreased significantly when the stope became more inclined. The difference of stresses between hangingwall and footwall became more pronounced with the increase of stope inclination. Table 6.3 showed the ratio of shear stress acting at footwall to that of hangingwall. The ratio varied from 1 to 2.6 when the stope inclined from vertical to 60^{o} to the horizontal respectively.

This stress behaviour could be explained by the combined action of arching and gravitational effects. The shear component along footwall was assumed to be fully mobilized when the stope inclined more than 10^{o} to the vertical. At the same time, the fills within the stope settled under gravitational force and transferred part of their weight to the rock mass in the vicinity through the footwall.

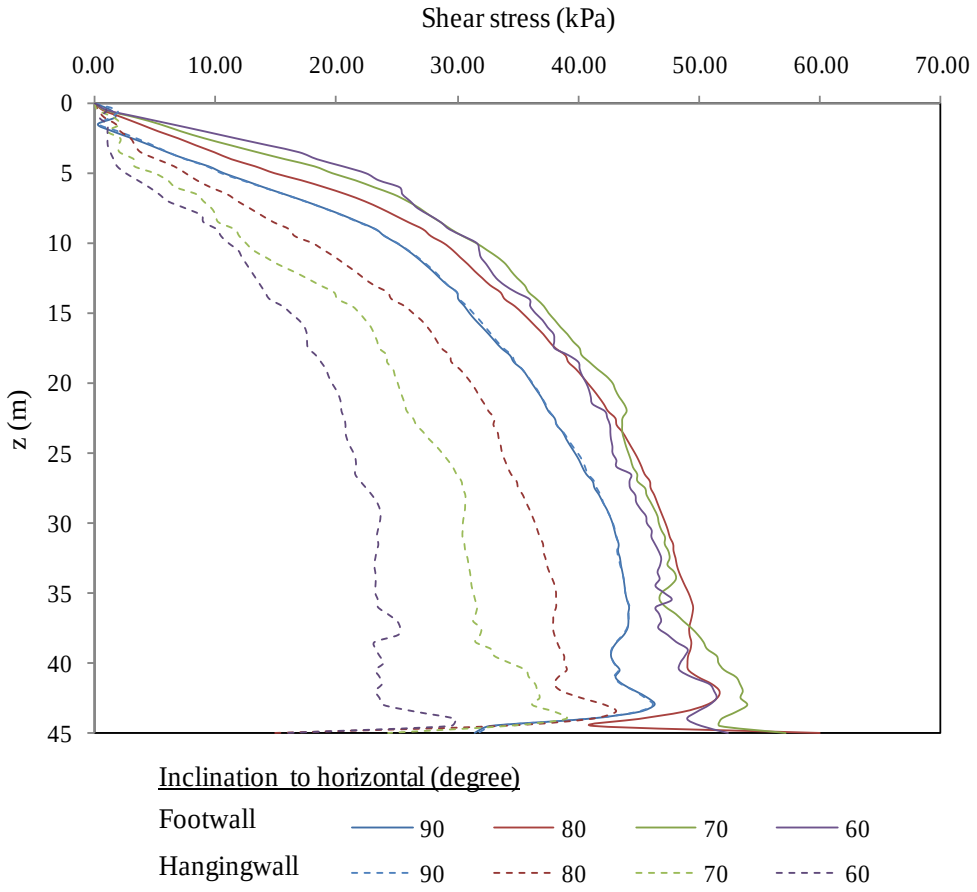

Figure 6.18. Variation of shear stresses with depth along hangingwall and footwall for different stope inclination

Table 6.3. The ratio of shear stress acting at footwall to that of hangingwall

Slope angle to horizontal	Numerical results
90	1
80	1.51
70	2.11
60	2.60

6.6 Numerical modeling for a full scale laboratory stope surrounded by rock

With similar approach as described in section 6.3, a numerical model with width, $B = 6\ m$ and vertical height, $H = 42\ m$ (*aspect ratio* $H/B = 7$) was modelled to scale up the laboratory model (100 x 700 mm). Scaling up of this model would better represent the mining condition. The model was simulated with sand as fill material bounded between Perspex walls with rough wall characteristics. The material properties used in the modeling was listed in Table 6.4 (sand and Perspex).

The numerical results of both models (6 x 42 m and 100 x 700 mm) for different stope inclinations were plotted in Figs 6.19 (a - c) along with analytical and experimental results. In these figures, normalized stress was plotted against normalized depth. It could be shown in the plots that scaling effect was insignificant as long as the aspect ratio at any depth remained constant and normalized values were used in comparison. Marston's equation for vertical stopes and its extension for inclined stopes (Eq 3.16) clearly showed that normalized stress ($\sigma_v/\gamma B$) was a function of normalized depth (z/B). This implied that $\sigma_v/\gamma H$ was a function of z/H and H/B (aspect ratio), and hence $\sigma_v/\gamma H$ variation with z/H would be the same for a specific aspect ratio, irrespective of the stope width B. In addition, as discussed in Chapter 3 and 5, the vertical stress within a stope was influenced by the lateral earth pressure coefficient, aspect ratio, stope inclination and relative interface characteristics, therefore, the model with dimension of 6 m width and 42 m vertical height (aspect ratio = 7) could be used to describe the stress profile within the model of 100 x 700 mm.

Table 6.4. Input parameters and constitutive models for sand, Perspex and rock mass used in numerical modeling

Properties	Sand	Perspex	Rock mass
Constitutive model	Mohr Coulomb	Linear elastic	Linear elastic
Young's Modulus, E	420 kPa	3.2 GPa	-
- Model 100 x 700 mm			
Young's Modulus, E	0.1 GPa	3.2 GPa	30 GPa
- Model 6 x 42 m			
Poission's ratio, ν	0.2	0.3	0.3
Density, ρ (kg/m^3)	1568	1190	2700
Cohesion, c (kPa)	-	-	-
Friction angle, ϕ (^{o})	41	-	-
Dilation angle, φ (^{o})	3.75	-	-
Interface friction angle, δ_R (^{o})	40	-	-

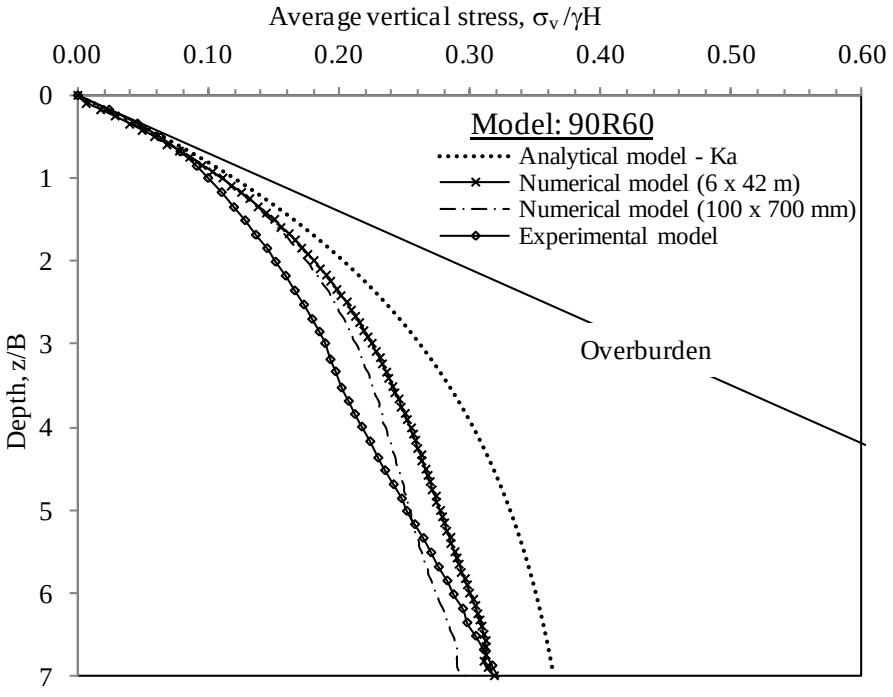

(a)

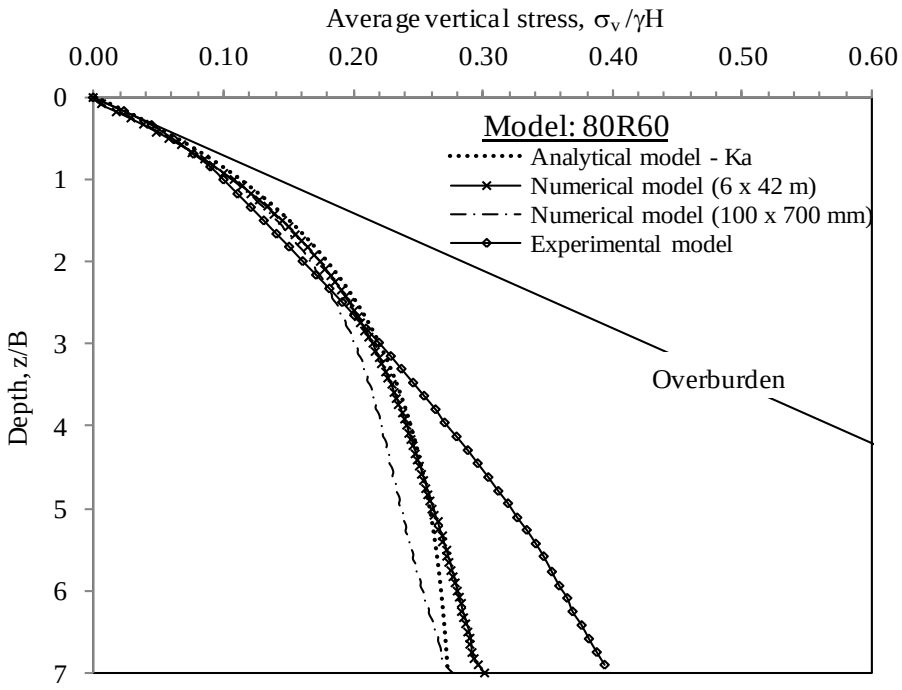

(b)

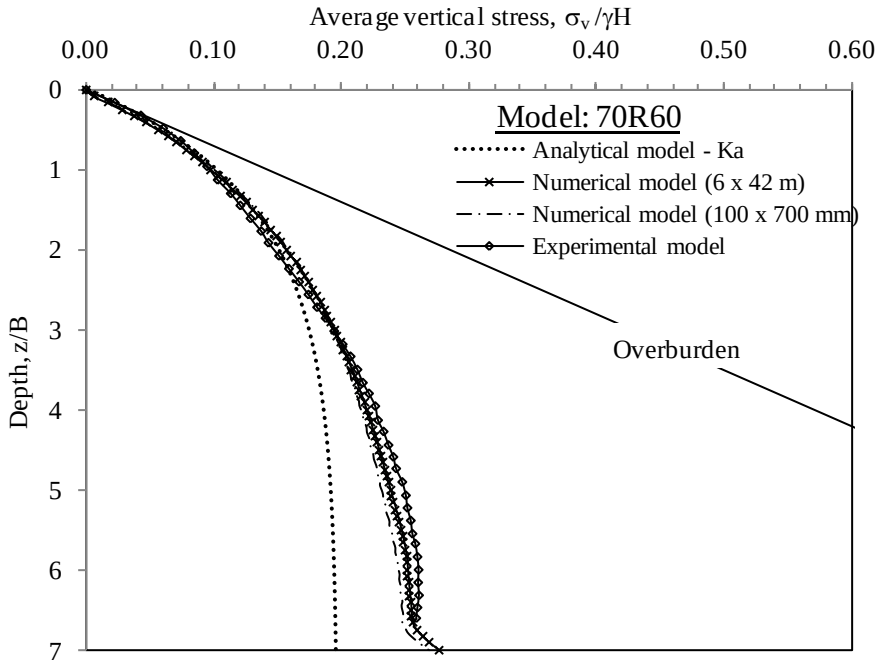

(c)

Figure 6.19. Normalized average vertical stress estimated from analytical equation using $K=K_a$, numerical model with stope dimension 6 x 42 m, numerical model with stope dimension 100 x 700 mm and experimental model (100 x 700 mm) for models (a) 90R60 (b) 80R60 and (c) 70R60

The full-scale 6 x 42 m model was extended to simulate the mining situation by incorporating the model into rock mass condition while the fill material remained as sand, which was shown in Fig. 6.9. The material properties used was listed in Table 6.4 (sand and rock mass). The results obtained for different stope inclinations were plotted together with the results obtained from laboratory model, analytical model and the numerical model with Perspex wall (see Fig 6.20 (a - c)). In general, the results of the four models were in reasonable agreement, justifying the use of laboratory model introduced in Chapter 5 to study stress distribution within minefill stope.

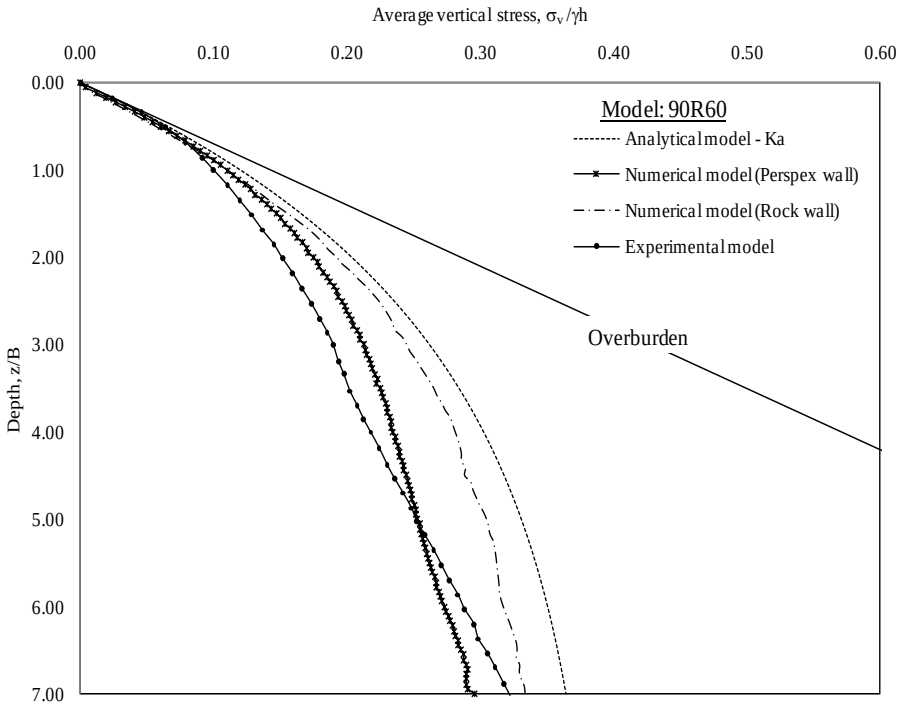

(a)

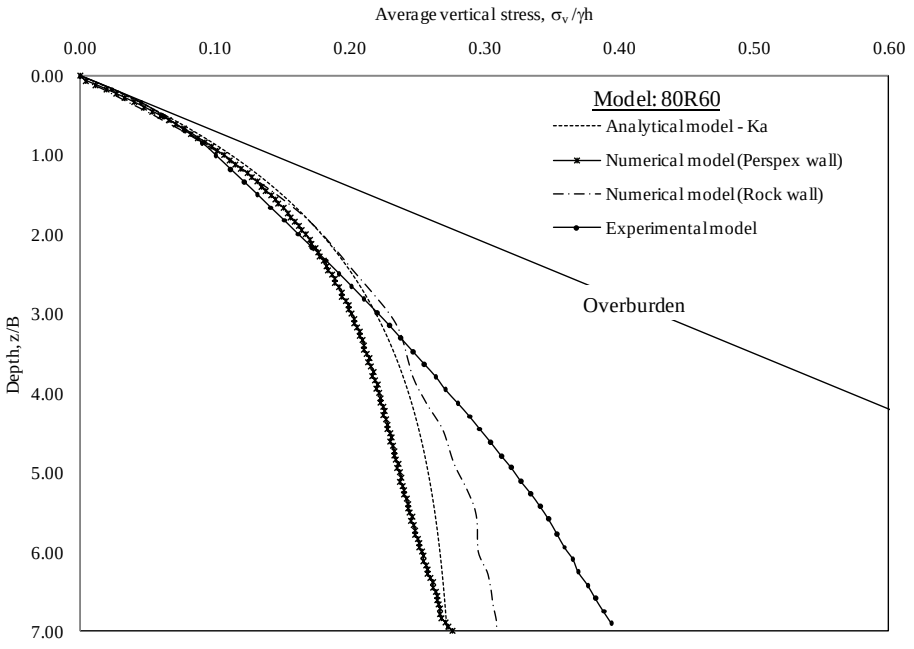

(b)

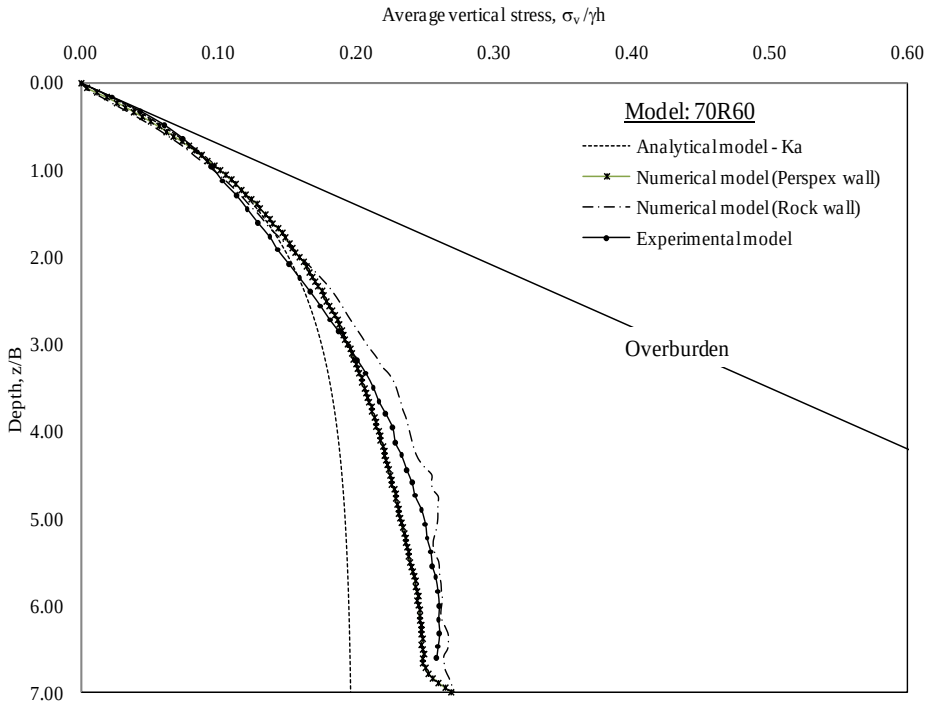

(c)

Figure 6.20. Normalized average vertical stress estimated from analytical equation using $K=K_a$, numerical model with Perspex walls (6 x 42 m), numerical model with rock walls (6 x 42 m) and experimental model (100 x 700 mm) for models (a) 90R60 (b) 80R60 and (c) 70R60

6.7 Summary and conclusions

Numerical modeling has been used in this chapter to simulate the stress distribution within an inclined stope. The effects of the input parameters of the numerical modeling are determined using sensitivity analysis. The simulation undertaken can be divided into three parts.

The first part simulates laboratory model developed in Chapter 5. The simulation results are compared with the results from the analytical equation developed in Chapter 3 and the laboratory measurements in Chapter 5. Comparable results are obtained among the three different techniques. In this section, it can be concluded that the proposed laboratory model is capable of quantifying arching effect and will be a useful tool in validating the solutions obtained from analytical and numerical modeling. The results also show that the fill depth to which increment of fill weight has insignificant influence on load distribution is dependent on assumed *K*-value, wall roughness and stope inclination.

The second part of the study is to simulate minefill stope under a typical underground mining condition. In this case, the simulation results are compared to the analytical equations developed in Chapter 3 and numerical solutions reported in the literature. This section confirms the applicability of analytical equations developed in Chapter 3 in estimating vertical stress distribution within an inclined stope. A brief discussion of stress distributions within an inclined stope are also carried out in this section.

The third part of this chapter scales up the 100 x 700 mm laboratory model to a full-scale 6 x 42 m model and incorporates it into mining conditions, where sand is used as fill material with surrounding rock mass. This section concludes that scaling factor is insignificant if the aspect ratio remains constant and the laboratory model introduced in Chapter 5 is capable to be used to study stress distribution within minefill stope.

Chapter 7 Summary, Conclusions and Recommendations

This chapter presents a summary of the research carried out in this dissertation as well as conclusions, and recommendations for future research.

7.1 Summary

The objective of this thesis is to investigate the stress distribution within an inclined stope, with due consideration to the arching effect within the stope.

Arching is a universal phenomenon in soil mechanics where it occurs in minefills contained in underground voids, backfills in ditches and behind retaining walls. Previous studies have shown that arching occurred in mine backfilling, where part of overburden weight of fill material was transferred to adjacent rock wall in the form of shear stress. A review of previous research was conducted on backfill technology related to underground mining, with emphasis on techniques used to investigate the arching mechanism on stress distribution, which included analytical, numerical and laboratory/field work. The review showed that the current design approach for an inclined stope was based on the results obtained from vertical stope by allowing some minor errors. The research conducted on stress analysis for an inclined stope was largely based on numerical modeling, and there was a lack of research conducted in analytical and laboratory methods. Therefore, a realistic and simple analytical solution for an inclined stope taking into consideration arching effects; and a physical model that can exhibit arching effect and simulate filling process within an inclined stope are crucial to improve the current state-of-the-art.

Three major modeling techniques were carried out in this research, which included analytical, experimental and numerical methods. All three techniques were performed concurrently and the outcomes were compared among each other to verify that the results were in close agreement. The research could be divided into three major parts based on the techniques applied in the analysis.

The first part of the study developed analytical expressions for inclined stope using Marston's theory. Two separate equations were developed for the stope with parallel and non-parallel walls respectively. For stope with parallel walls, the final analytical expression developed was similar to Marston's and Terzaghi equations. The only difference was the expression of lateral stress coefficient, K, where K was replaced by K' (Eq. 3.9) in current

derivation by incorporating stope inclination and interfacial friction angle. A significant reduction of vertical stresses was observed toward the base of the stope, showed that arching was taking place. The results obtained compared well with limited analytical and numerical results reported in the literature. Noting that K was typically assumed as or equal to K_o or K_a, simple design charts for $K = K_o$ and $K = K_a$ were also developed. One can use these charts and interpolate for any K values in between K_o and K_a. Besides, parametric study was carried out to study the effects of various parameters related to the proposed analytical expression, which included stope inclination, aspect ratio and fill properties. The vertical stress was observed to reduce with the increase of stope inclination. The arching effect was more significant for higher aspect ratios and the pressure exerted at the bottom of the stope was almost independent of the fill depth when $H > 5B$ (for the case $\beta = 70^o$) where the vertical normal stress reached a constant asymptotic value. The results revealed that the vertical stress increased with an increase in unit weight and reduced when fill cohesion increased. Within practical range ($30^o - 40^o$), friction angle had insignificant influence on the stress development. Any increase in friction angle led to reduction in the earth pressure coefficient, and hence lowered normal stress on the wall. The net effect was negligible on the wall friction.

For the analysis of inclined stope with non-parallel walls, different combinations of wall inclinations were examined using the analytical expression developed. The results of the analysis showed that the proposed analytical expression was capable in estimating the vertical stress within stope where the inclination of the hangingwall to the horizontal, α is less than that the footwall, β. For the case where $\alpha > \beta$, an unrealistic stress reduction occurred at a depth close to the bottom of the stope where the vertical normal stress decreased beyond a certain depth. The results from equation limitation study suggested that 89.999^o should be used to represent 90^o in proposed analytical expression, to avoid numerical explosion from division by zero. An important behavioural trend for the stress distribution in stopes was observed where with the same overburden pressure γz and base width B, the stress magnitude experienced by fill material at any depth z could be significantly different depending on the wall inclination. With increasing tilt from vertical, there was significant stress reduction at any depth. No maximum vertical stress was observed within the range of $0 < \beta < \pi/2$ using the analytical method, which was inconsistent with the observation of the laboratory model. The analytical model and the numerical model later showed that the vertical stress at any depth was the maximum when the wall was vertical.

A new analytical approach is introduced in this study to serve as an alternate method in predicting the vertical stress distribution within vertical and inclined stopes. The analytical expression was developed using Pascal's triangle and binomial series by dividing the fill into M layers. The solution was found converging when the fill was divided into large number of layers (e.g. M > 50) and the computation effort was the same for any number of layers. The results obtained compared very well with the Marston type equations derived in this dissertation (Chapter 3) and numerical results from published literature. The results suggested that lateral earth pressure coefficient, K and interfacial friction angle, δ could be taken as either ($K = K_0$ and $\delta = 2/3\phi$) or ($K = K_a$ and $\delta = \phi$) to better describe the stress state at mining conditions in inclined stopes.

The second part of the study involved the development of a small scaled plane strain inclined laboratory model based on the similar concept of experimental model of Pirapakaran and Sivakugan (2007b). Stope inclination, wall roughness, relative density and aspect ratio were varied independently to study their influence on the stress distribution and arching effects within the stope. The results obtained from the studies revealed that aspect ratio, wall roughness and stope inclination were critical factors in predicting the stress distribution within a backfill stope. Vertical stress decreased with increase of aspect ratio and wall roughness. On the other hand, vertical stress increased from 70^o to 80^o and remained relatively same from 80^o to 90^o. The highest vertical stress was observed near 80^o to the horizontal. This observation was not consistent with the results of extension of Marston's Theory (Chapter 3) or numerical modeling (Chapter 6) where it was clear that the vertical stress was the maximum when the walls were vertical. Analysis of the stresses acting on hangingwall and footwall were conducted. The observations showed that, the load acting on the footwall was higher than the load acting on the hangingwall for an inclined stope. Models with different wall roughness characteristics were also tested. The laboratory model results showed that more loads were transferred to the wall with higher friction. In the case of walls with dissimilar frictional characteristics, the results showed that an average value of the wall-fill friction angles could be used in analytical expression for a reasonable estimate of the vertical stress at any depth. This overcame the limitation of analytical equations which had only a single value of δ to represent both rock-fill interfaces.

In the final part of the study, approximate solutions were developed for the stress distribution within inclined stopes based on FLAC simulation. Three separate models were conducted in the numerical simulation; laboratory model stope, a full-scale minefill stope surrounded by rock, and a full-scale laboratory stope surrounded by rock as in typical mine stopes. Sensitivity analysis and interface element were applied in each model. The

application of interface elements in the numerical model allowed for possible relative slip between the fill and the wall. The numerical results were validated with experimental results in Chapter 5 and the stresses determined from analytical expression (Chapter 3) as well as other numerical results from the literature. Stresses distribution within an inclined stope were also studied. At any depth, the vertical normal stresses near the hangingwall and footwall were less than that at the central part of the stope, showing that arching occurred and parts of the stresses were being transferred to the surrounding rock walls. The shearing stress along hangingwall decreased significantly with the increase of stope inclination. At footwall, the shearing stress increased with increasing stope inclination and remained constant when slope angle was greater than 80^o. The difference of stresses between hangingwall and footwall became more pronounced with the increase of stope inclination. The results indicated that the lateral stress was insensitive to stope inclination. Higher stresses were observed along hangingwall, which was not proportional to vertical stress with constant value of K in accordance to $\sigma_h = K\sigma_v$. The numerical modeling showed that K varied within the stope laterally, and it was better described by K_a for minefill stope. The results also confirmed the applicability of analytical expressions and laboratory model proposed in this dissertation in predicting vertical stress distribution within an inclined stope.

7.2 Conclusions

The main conclusions of the study are summarized below in corresponding to the chapters of the thesis.

Analytical modeling - Extension of Marston's Theory

- Two analytical expressions are proposed to estimate the vertical stress at any depth within the inclined backfilled stopes for parallel and non-parallel walls, taking into consideration the arching phenomenon within the fill materials. These expressions are applicable for two-dimensional plane strain problems where the length of the mining stope is much greater than the width. But, further investigation is required for case when $\alpha > \beta$. These expressions allow for a uniform surcharge pressure at the top of the stope.
- With the same overburden pressure and base width, the stress magnitude experienced by fill material significantly differs depending on the wall inclination. The vertical stress reduces with the increase in stope inclination.
- The arching effect is more significant for stope with higher aspect ratio.

- The vertical stress increases with the increase of unit weight and reduces with increasing fill cohesion. The analytical expression shows that the effect of friction angle is insignificant on the stress development within the practical range.

New analytical approach developed from Pascal's triangle and Binomial series

- A simple analytical method to compute the vertical stresses within a vertical or inclined containment for granular material is proposed.
- The model is capable of estimating normal vertical stress at any depth of the stope, irrespective the cross sectional shape.
- Lateral earth pressure coefficient, K and interfacial friction angle, δ can be taken as either ($K = K_0$ and $\delta = 2/3\phi$) or ($K = K_a$ and $\delta = \phi$) to better describe the stress state at mining conditions in inclined stopes.

Laboratory model of an inclined stope

- The proposed laboratory model is capable of quantifying arching effect, and enables estimation of stress profile within inclined stopes for a wide range of aspect ratios.
- Aspect ratio, wall roughness and stope inclination are critical factors in predicting the stress distribution within a backfill stope.
- The effect of arching is the least when the stope is inclined at 80^o to the horizontal, giving the highest vertical stresses at any depth, which is inconsistent with the results obtained from analytical and numerical modeling.
- The shear stress experienced by the footwall increases with an increase in stope inclination and wall roughness and more load is transferred to the wall with higher friction.
- The average interface friction angle can be used to predict the vertical stress within a stope with different wall characteristics.

Numerical modeling of inclined stopes using FLAC

- The results confirmed the applicability of:
  a. The proposed laboratory model developed in Chapter 5 in quantifying arching effect and enabling validation of the numerical and analytical modeling results from an inclined stope.
  b. The analytical equation developed in Chapter 3 as a preliminary design tool to estimate the vertical stress within an inclined stope.
- The study on stress distribution reveals that:

a. Arching occurs within the fill,
b. The lateral stress is insensitive to stope inclination and higher horizontal stress is observed along hangingwall than the footwall,
c. Shear stresses on hangingwall and footwall increase as stope inclination increases. The shear component along footwall is fully mobilized when the stope inclines more than 10^o to vertical.

- *K* is insensitive to the depth of the stope. For inclined stopes, the stress state experienced by the fills varies across the span from hangingwall to footwall.
- Active state is more appropriate than at rest state for describing the stress state within an inclined stope, with the interfacial friction angle δ being equal to the friction angle of the fill ϕ.
- The asymptotic value of fill depth to which the increment of fill load has insignificant influence on vertical stress distribution is dependent on assumed *K*-value, wall characteristic and stope inclination.
- Scaling effect is insignificant as long as the aspect ratio remains constant and normalized (e.g. $\sigma_v/\gamma H$, z/B) values are used.

7.3 Recommendations for future research

Based on works carried out in this dissertation, the following recommendations are made for future research. They are summarized in the sequence of the chapters in this dissertation.

Analytical modeling - Extension of Marston's Theory

- Refine the analytical expression for stope with parallel walls with the consideration of factors such as Young's modulus, Poisson's ratio and dilation angle.
- Refine the analytical expression developed for stope with non-parallel walls to overcome the limitation of:
    - Stope with parallel walls
    - Stope where slope angle of hangingwall is greater than angle of footwall
    - Enable the use of 90^o instead of 89.999^o in modeling vertical wall
- For stope with non-parallel walls and $\alpha > \beta$, examine the depth of onset of the inward curve, z_{cutoff} by observing the first derivative of the normal vertical stress with respect to depth, z (Eqs. 3.60 and 3.61) in order to condition the use of the equation for $z \geq z_{cutoff}$.

New analytical approach developed from Pascal's triangle and Binomial series

- Introduce and calibrate a friction force factor, $k_{friction}$ in the analytical equation to allow for the cases in which the maximum friction force is not reached while choosing K and δ based on physical situation.
- Extension of the proposed equation to include:
    - Vertical stope with irregular shape
    - Inclined stope with different cross sectional shape
    - Hopper
- Extension of the proposed equation to incorporate cohesion

Laboratory model of an inclined stope

- Modification of the model by conducting tests on wet minefills and cemented fills to better represent the field situations
- Investigation of the effects of fill properties by using a wide range of fill materials
- Investigation into the position and orientation of strain gauges so that stresses acting at the walls can be estimated directly from the readings of strain gauges.
- Investigate the inconsistency of maximum load at 80^o obtained from the experimental model which may be caused by experimental errors, such as systematic and intrinsic errors.
- The small-scaled models can lead to quite erroneous conclusion regarding soil-interaction effects. A full scale experiment or in-situ measurement is recommended to verify the results obtained from laboratory model.

Numerical modeling of inclined stopes using FLAC

- Modeling that incorporate the effect of pore water pressure and cementitious for cemented fill to better represent mine conditions is recommended
- Extension of the model from 2-dimension to 3-dimension, including square and rectangular stopes with tilt
- Study of the stability of an inclined stope is recommended when the neighboring stopes are excavated and refilled
- Further investigation on lateral stress ratio, K
- Validations of the model with in-situ data

References

Aubertin, M., Li, L., Arnoldi, S., and Simon, R. (2003). "Interaction between backfill and rock mass in narrow stopes." *Soil and Rock America 2003: 12th Panamerican Conference on Soil Mechanics and Geotechnical Engineering and 39th U.S. Rock Mechanics Symposium,*, Boston, Massachusetts, USA, 1157-1164.

Barrette, P.D. and Sayed, M. (2007). "Experimental and Numerical Investigation of Two-Dimensional Granular Flow through Bins." *Proceedings of the 9th International Symposium in Mining with Backfill*, Montreal, Canada.

Barrett, J. R., Coulthard, M. A., and Dight, P. M. (1978). "Determination of Fill Stability." *Mining with Backfill - 12th Canadian Rock Mechanics Symposium, Canadian Institute of Mining and Metallurgy*, Quebec, 85-91.

Belem, T., and Benzaazoua, M. (2004). "An overview on the use of paste backfill technology as a ground support method in cut-and-fill mines. ." *Proceedings of the 5th Int. Symp. on Ground support in Mining and Underground Construction*, Perth, Western Australia, Australia, 637 – 650.

Bloss, M., Cowling, R., and Meek, J. (1993). "A Procedure for the Design of Stable Cemented Fill Exposures." *Minefill 93*, Johannesburg, SAIMM.

Boldt, C. M. K., Atkins, L. A., and Jones, F. M. (1993). "The Backfilling Research Being Conducted by th U.S. Bureau of Mines." *Minefill' 93*, Johnnesburg, SAIMM., 389-395.

Bolton, M. D. (1986). "The strength and dilatancy of sands." *Geotechnique*, 36(1), 65-78.

Bosscher, P. J., and Gray, D. H. (1985). "Soil arching in sandy slopes." *Journal of Geotechnical Engineering, ASCE*, 112(6), 626-635.

Caceres Doerner, C. A. (2005). "Effect of Delayed Backfill on Open Stope Mining Methods. ." *MASc Thesis*, University of British Columbia.

CeAs. (2011). http://www.ceas.it/eng/schede_pdf/software/03_FLAC_INGLESE.pdf. (Last accessed: Sept 17, 2011)

Christopher, C.B., Rankine, K.J., and Sivakugan, N. (2007). "Materials properties of barricade bricks for mining applications." *Geotechnical and Geological Engineering*, 25(4), 449-471.

Chrystal, G. (1964). *Algebra - An Elementary Text Book (Part I)*, Chelsea Publishing Company, New York.

Coetzee, M. J., Hart, D. R. D., Varona, P. M., and Cundall, D. P. A. (1998). *FLAC Basics: An introduction to FLAC and a guide to its practical application in geotechnical engineering*, Itasca Consulting Group, Inc., Minneapolis, Minnesota.

Coulthard, M. A. (1999). "Applications of numerical modeling in underground mining and construction." *Geotechnical and Geological Engineering*, 17, 373-385.

Dally, J. W., and Riley, W. F. (1991). *Experimental Stress Analysis, 3rd Edition*, McGraw-Hill, Inc., New York.

Dalvi, R. S., and Pise, P. J. (2008). "Effect of Arching on Passive Earth Pressure Coefficient." *The 12th International Conference of International Association for Computer Methods and Advances in Geomechanics (IACMAG)*, Goa, India., 236-243.

Das, B. M. (1998). *Principles of Geotechnical Engineering (4th edition)*, PWS Publishing Company, Boston.

DeSouza, E., and Dirige, A. P. E. (2002). "Arching Effects and Sillmat Behaviour." *Proceedings of the 104th Annual General Meeting of the Canadian Institute of Mining, Metallurgy and Petroleum*, Vancouver, B.C., 102-107.

DeSouza, E., and Dirige, A. P. E. (2003). "Economics and Perspectives of Underground Backfill Practices in Canadian Mines." *Proceedings of the 105th Annual General Meeting of the Canadian Institute of Mining, Metallurgy and Petroleum.* Montreal: CIM.15.

Dhar, B. B., Shanker, K. V., and Sastry, V. R. (1983). "Hydraulic filling - An effective way of ground support." *Proceedings of the International Symposium on Mining with Backfill*, Lulea, 113-120.

Drescher, A. (1991). *Analytical mehtods in bin-load analysis*, Elsevier Science Publishers B.V., Amsterdam.

Fahey, M., Helinski, M., and Fourie, A. (2009). "Some aspects of mechanics of arching in backfilled stopes." *Can. Geotech. J.*, 46, 1322-1336.

Fourie, A.B., Helinski, M., and Fahey, M. (2007). " Using Effective Stress Theory to Characterize the Behavior of Backfill." *Proceedings of the 9th International Symposium in Mining with Backfill*, Montreal, Canada.

Geotechnical info.com. (2011). http://geotechnicalinfo.com/geotechnical_materials.html (Last accessed: Sept 17, 2011)

Goel, S., and Patra, N. R. (2008). "Effect of Arching on Active Earth Pressure for Rigid Retaining Walls Considering Translation Mode." *International Journal of Geomechanics*, 8(2), 123-133.

Grice, T. (1998). "Underground mining with backfill." *The 2nd Annual Summit - Mine Tailings Disposal Systems*, Brisbane.

Handy, R. L. (1985). "The Arch in Soil Arching." *Journal of Geotechnical Engineering*, 111(3), 302-318.

Harrop-williams, K. O. (1989). "Geostatic Wall Pressures." *Journal of Geotechnical Engineering-ASCE*, 115(9), 1321-1325.

Hassani, F. P., Mortazavi, A., and Shabani, M. (2008). "An investigation of mechanisms involved in backfill-rock mass behaviour in narrow vein mining." *The Journal of The Southern African Institute of Mining and Metallurgy.*, 106, 463-472.

Helinski, M. (2007). “Mechanics of Mine Backfill.” *PhD Thesis*, The University of Western Australia, Perth, Australia.

Hibbeler, R. C. (2005). *Mechanics of Materials (Sixth Edition in SI Units).* Prentice Hall and Pearson Education South Asia Pte Ltd, Singapore.

Itasca. (2005). *FLAC Fast Lagrangian Analysis of Continua (Theory and Background),* Itasa Consulting Group, Inc, Minnepolis, Minnesota, USA.

ITASCA. (2011). http://www.itascacg.com. (Last accessed: Sept 17, 2011)

Jaky, J. (1948). "Earth pressures in silos." *Proceedings of the second international conference on soil mechanics and foundation engineering*, Rotterdam, 103-107.

Janssen, H. A. (1895). " Versuche uber Getreidedruck in Silozellen." *Z. Ver. deut. Ingr., 39, p. 1045 (partial English translation in Proceedings of the Institute of Civil Engineers, london, England, 1986, p.553)*

Knutsson, S. (1981). "Stresses in the hydraulic backfill from analytical calculations and in-situ measurements." *Proceedings of the conference on the application of rock mechanics to cut and fill mining*, Lulea, Sweden, 261-268.

Krynine, D.P. (1945). Discussion of “Stability and Stiffness of Cellular Cofferdams.” by Karl Terzaghi. *Transactions, ASCE,* 110, 1175-1178.

Ladanyi, B. and and Hoyaux, B. (1969). “A study of the trap-door problem in a granular mass.” *Canadian Geotechnical Journal*, 6(1), 1-14.

Lee Barbour, S. And Krahn, J (2004). “Numerical Modeling – Prediction or Process?” *Geotechnical News, December 2004*, BiTech Publishers, 44-52.

Li, L., and Aubertin, M. (2008). "An improved analytical solution to estimate the stress state in subvertical backfilled stopes." *Canadian Geotechnical Journal*, 45(10), 1487-1496.

Li, L., and Aubertin, M. (2009). "Numerical Investigation of the Stress State in Inclined Backfilled Stopes." *International Journal of Geomechanics, ASCE*, 9(2), 52-62.

Li, L., Aubertin, M., Simon, R., Bussiere, B., and Belem, T. (2003). "Modeling arching effects in narrow backfilled stopes with FLAC." *Proc. 3rd International FLAC Symposium* Rotterdam, 211-218.

Li, L., Aubertin, M., and Belem, T. (2005). "Formulation of a three dimensional analytical solution to evaluate stresses in backfilled vertical narrow openings." *Canadian Geotechnical Journal*, 42(6), 1705-1717.

Li, L., Aubertin, M., Shirazi, A., Belem, T., and Simon, R. (2007). "Stress distribution in inclined backfilled stopes." *Proceedings of the 9th International Symposium in Mining with Backfill*, Montreal, Canada.

Marston, A. (1930). "The theory of external loads on closed conduits in the light of latest experiments." *Bulletin No.96, Iowa Engineering Experiment Station, Ames, Iowa*, USA.

Marston, A., and Anderson, A. O. (1913). "The Theory of Loads on Pipes in Ditches and Tests of Cement and Clay Drain Tile and Sewer Pipes." *Bulletin No.31, Iowa Engineering Experiment Station, Iowa State College, Ames, Iowa*, USA.

McNulty, J. W. (1965). "An Experimental Study of Arching in Sand.," University of Illinois., Urbana, USA.

Mitchell, R. J. (1989). "Model studies on the stability of confined fills." *Canadian Geotechnical Journal*, 26, 210-216.

Mitchell, R. J., Olsen, R. S., and Smith, J. D. (1982). "Model studies on cemented tailings used in mine backfill." *Canadian Geotechnical Journal*, 19, 14-28.

Ono, K., and Yamada, M. (1993). "Analysis of the arching action in granular mass." *Geotechnique*, 43(1), 105-120.

Paik, K. H., and Salgado, R. (2003). "Estimation of active earth pressure against rigid retaining walls considering arching effects." *Geotechnique*, 53(7), 643-653.

Pakalnis, R., Tenny, D., and Lang, B. (1991). "Numerical modeling as a tool in stope design." *CIM Bulletin July1991*, 84(195), 64–73.

Pierce, M. E. (2001). "Stability analysis of paste backfill exposures at Brunswick Mine." *Proceedings of the Second International FLAC Symposium*, France.

Pirapakaran, K. (2008). "Load-Deformation Characteristics of Minefills with particular reference to Arching and Stress Developments." *PhD Thesis*, James Cook University, Townsville, Australia.

Pirapakaran, K., and Sivakugan, N. (2006). "Numerical and experimental studies of arching effects within mine fill slopes." *Physical Modeling in Geotechnics - 6th ICPMG'06*, London, 1519-1525.

Pirapakaran, K., and Sivakugan, N. (2007a). "Arching within hydraulic fill stopes." *Geotech. Geol. Eng.*, 25(1), 25-35.

Pirapakaran, K., and Sivakugan, N. (2007b). "A Laboratory Model to Study Arching within a Hydraulic Fill Stope." *Geotechnical Testing Journal, ASTM*, 30(6), 496-503.

Potvin, Y., Thomas, E., and Fourie, A. (2005). *Handbook on Mine Fill*. ACG Australian Centre For Geomechanics, Nedlands, Western Australia.

Potts, V. J. And Zdravkovic, L. (2008). "Finite Element Analysis of Arching Behaviour in Soils." *The 12th International Conference of International Association for Computer Methods and Advances in Geomechanics (IACMAG)*, Goa, India.

Qiu, Y., and Sego, D.C (2001). "Laboratory properties of mine tailings." *Canadian Geotechnical Journal*, 38(1), 183-190.

Rankine, K. J. (2005). "An Investigation into the drainage characteristics and behaviour of hydraulically placed mine backfill and permeable minefill barricades." *PhD Dissertation*, James Cook University, Townsville, Australia.

Rankine, K. J., Sivakugan, N., and Cowling, R. (2006). "Emplaced geotechnical characteristics of hydraulic fills in a number of Australian mines." *Geotechnical and Geological Engineering*, 24(1), 1-14.

Rankine, R., Pacheco, M., and Sivakugan, N. (2007). "Underground mining with backfills." *Soils and Rocks.*, 30(2), 93-101.

Rankine, R. M. (2004). "The geotechnical characterisation and stability analysis of BHP Billinton's Cannington Mine Paste fill." *PhD Dissertation*, James Cook University, Townsville, Australia.

Riley, K. F., Hobson, M. P., and Bence, S. J. (2002). *Mathematical Methods for Physics and Engineering.* , Cambridge University Press, New York.

Robertson, A., Moss, A., and Niemi, W. R. (1986). "A Simple Tool to Measure Stress in Mine Backfill." *Proceeding of the Fifth Conference on Ground Control in Mining (ICGCM)* Morgantown, West Virginia.

Sabiti, S., Van der Meiji,R., and Leoni, M. (2007). "Piled Embankments: Literature Review and Required Further Research using Numerical Analysis." *August 2007- Institutsbericht 34*, Institute for Geotechnical Engineering, University of Stuttgart, German.

Sainsbury, D. P., and Urie, R. (2007). "Stability Analysis of Horizontal and Vertical Paste Fill Exposures at the Raleigh Mine." *Minefill 2007*, Montreal, Canada.

Shelke, A., and Patra, N. R. (2008). "Effect of Arching on Uplift Capacity of Pile Groups in Sand." *International Journal of Geomechanics. ASCE*, 8(6), 347-354.

Shukla, S. K., Gaurav, and Sivakugan, N. (2009a). "A simplied extension of the conventional theory of arching in soils." *International Journal of Geotechnical Engineering.*, 3(3), 353-359.

Shukla, S. K., Loughran, J. G., and Sivakugan, N. (2009b). "Stress within a cohesionless granular fill in a storage vessel with sloping walls during initial static loading." *Powder Technology*., 192 (3), 389-393.

Singh, S. (2009). "Drainage and Settlement Characteristics of Hydraulic Fills." *PhD Thesis*, James Cook University, Townsville, Australia.

Singh, S., Shukla, S.K. and Sivakugan, N. (2011). "Arching in Inclined and Vertical Mine Stopes." *Geotechnical and Geological Engineering*, 29(5), 685-693.

Singh, S., Sivakugan, N., and Shukla, S. K. (2010). "Can soil arching be insensitive to ϕ?" *International Journal of Geomechanics, ASCE*, 10(3), 124-128.

Sivakugan, N., and Das, B. M. (2010). *Geotechnical Engineering: A practical problem solving approach.*, J. Ross Publishing, Inc.

Sivakugan, N., Rankine, R.M., Rankine, K.J. and Rankine, K.S. (2006). "Geotechnical considerations in mine backfilling in Australia." *Journal of Cleaner Production*, 14(2006), 1168-1175

Spangler, M.G., and Handy, R.L. (1982). "Vertical Soil Arching and TerraFax (Ref: Soil Engineering, 4th Edition, Harper & Row)." *GeoTech System Corp: Discussion of Soil Arching.*

Sperl, M. (2005). "Experiments on Corn Pressure in Silo Cells – Translation and Comment of Janssen's Paper from 1895." *Granular Matter*, 8(2), 59-65.

Standards Australia (1995). *AS1289.3.6.2-1995, Methods of testing soils for engineering purposes – Soil classification tests – Determination of the particle size distribution of a soil – Analysis by sieving in combination with hydrometer analysis (Subsidiary method)*

Standards Australia (1998a). *AS1289.5.5.1- 1998, Methods of testing soils for engineering purposes - Soil compaction and density tests - Determination of the minimum and maximum dry density of a cohesionless material - Standard method*

Standards Australia (1998b). *AS1289.6.2.2-1998, Methods of testing soils for engineering purposes - Soil strength and consolidation tests - Determination of shear strength of a soil - Direct shear test using a shear box.*

Standards Australia (1998c). *AS1289.6.6.1-1998, Methods of testing soils for engineering purposes - Soil strength and consolidation tests - Determination of the one-dimensional consolidation properties of a soil - Standard method.*

Standards Australia (2006). *AS 1289.3.5.1-2006, Methods of testing soils for engineering purposes - Soil classification tests - Determination of the soil particle density of a soil - Standard method*

Take, W. A., and Valsangkar, A. J. (2001). "Earth pressures on unyielding retaining walls of narrow backfill width." *Canadian Geotechnical Journal*, 38(6), 1220-1230.

Terzaghi, K. (1943). *Theoretical Soil Mechanics*, John Wiley & Sons.

Tien, H.J. (1996). "A Literature Study of Arching Effect." *SM Thesis*, Massachusetts Institute of Technology, 40-184.

Udd, J. E. (1989). "Backfill research in Canadian Mines." *Proceedings of the 4th International Symposium on Mining with Backfill.*, Hassani, et. al., ed., Rotterdam, Balkema, Montreal, 3-13.

Udd, J. E., and Annor, A. (1993). "Backfill Research in Canada." *Minefill' 93*, Glen, H. W., ed., South African Institute of Mining and Metallurgy, Johannesburg, 361-368.

Vermeer, P. A., and de Borst, R. (1984). "Non-Associated Plasticity for Soils, Concrete and Rock." *Heron*, 29(3), 3-64.

Walters, J. K. (1973). "A theoretical analysis of stresses in silos with vertical walls." *Chemical Engineering Science*, 28, 13-21.

Window, A. L., and Holister, G. S. (1982). "Strain Gauge Technology." Applied Science Publishers, London and New Jersey.

Yumlu, M. (2007). "Paste backfill bulkhead failures and pressure monitoring at Cayeli Mine." *Digging Deeper (September 2007)*, AMC Consultants.

Appendix A

Differentiation of σ_z against u, $d\sigma_z/du$

The function

$$\sigma_z = \frac{\gamma}{u}(1 - e^{-uz}) \tag{A1.1}$$

can be shown to be monotonically decreasing (and thus has no turning points) by showing that the first derivative is always less than zero (Note: strict inequality applies). From Eq. 3.82

$$\frac{d\sigma_z}{du} = \frac{(uZ+1)e^{-uz}-1}{u^2} \tag{A1.2}$$

Note that

$$(uz + 1)e^{-uz} - 1 < 0 \implies \frac{d\sigma_z}{du} < 0, \tag{A1.3}$$

as $u^2 > 0$ when $u \neq 0$. The case $u = 0$ is a special case and will be treated later.

Letting $y = uz$, we need to show that

$$(y + 1)e^{-y} - 1 < 0, \quad y \neq 0. \tag{A1.4}$$

We know that

$$y + 1 < e^{y}, \quad y \neq 0, \tag{A1.5}$$

with equality occurring when $y = 0$. Multiplying the expression through by e^{-y} and subtracting 1, we obtained the required result.

When u = 0,

$$\begin{aligned}
\lim_{u\to 0} \frac{d\sigma_z}{du} &= \lim_{u\to 0} \frac{(uz+1)e^{-uz}-1}{u^2} \\
&= \lim_{u\to 0} \frac{ze^{-uz}-z(uz+1)e^{-uz}}{2u} \\
&= \lim_{u\to 0} \frac{-uz^2e^{-uz}}{2u} \\
&= -\frac{z^2}{2} < 0, \quad z \neq 0.
\end{aligned} \tag{A1.6}$$

Note that $\sigma_z = 0$ when $z = 0$, as expected. Hence the function in equation (A1.1) is monotonically decreasing ($z \neq 0$) or identically zero ($z = 0$). In either case, there are no relative optima.

Appendix B1

Laboratory results of material properties

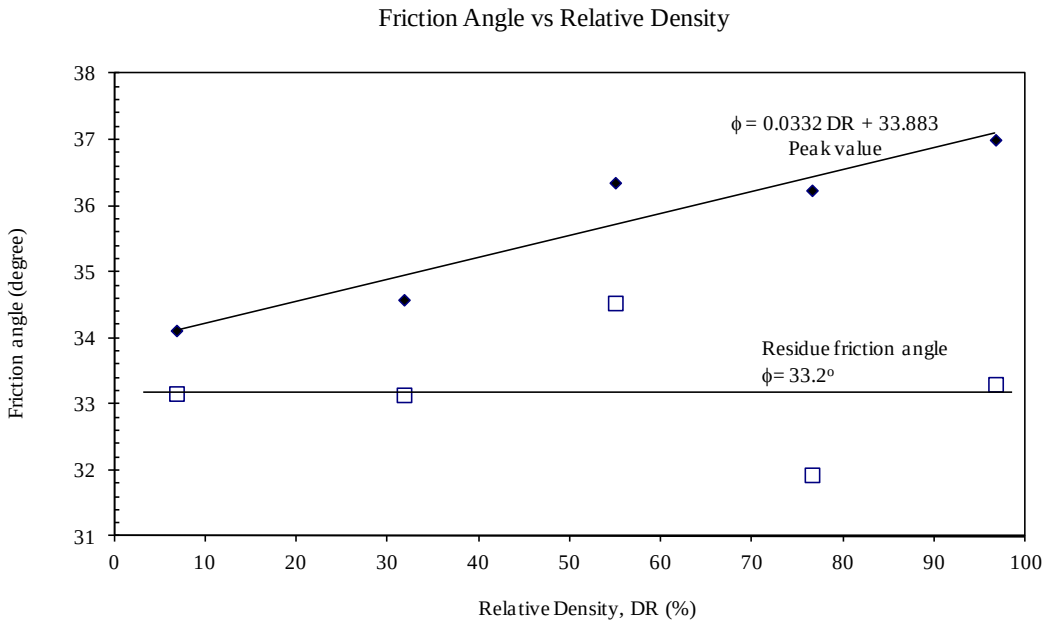

Figure B1. 1. Variation of friction angle with fill relative density

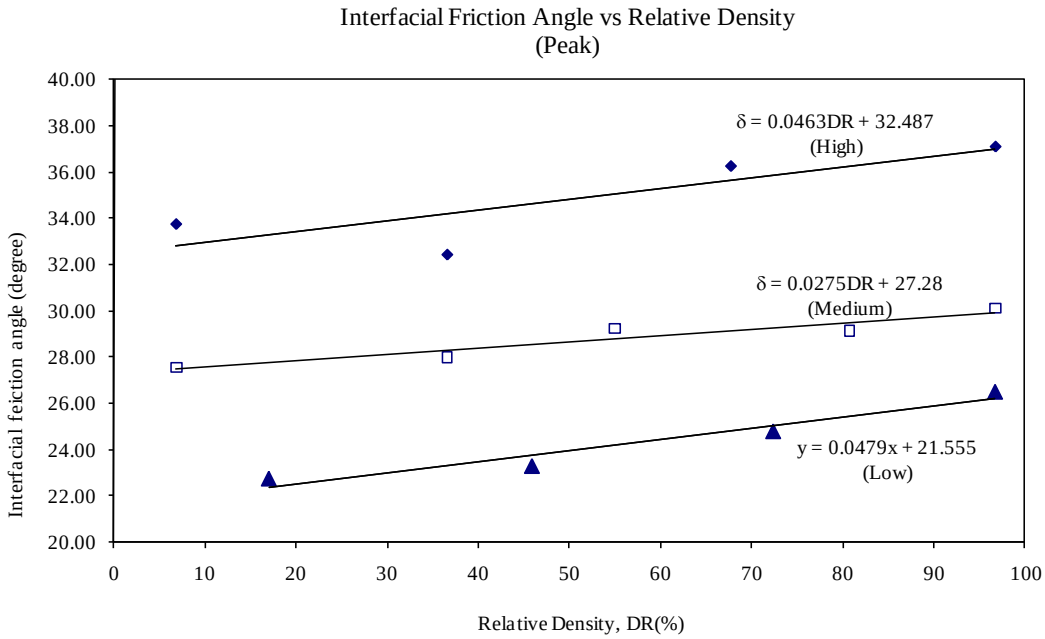

Figure B1. 2. Variation of interfacial friction angle with fill relative density

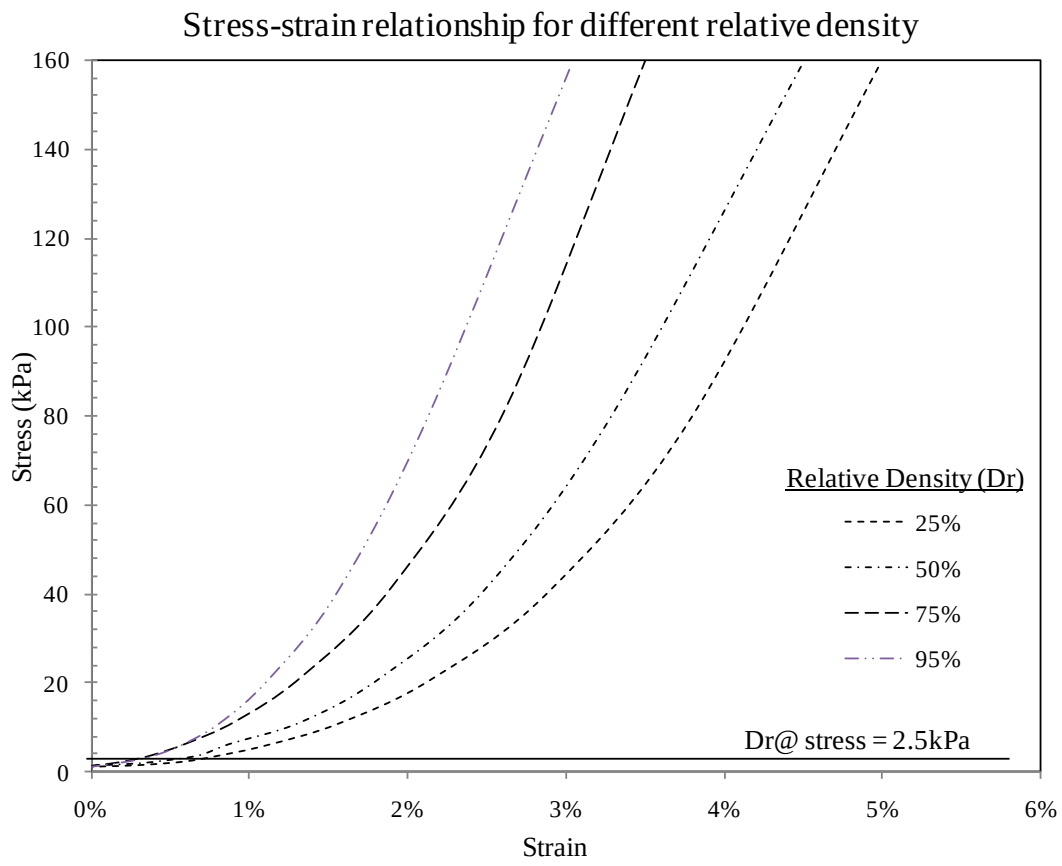

Figure B1.3. Stress-strain plots for different fill relative density (from one-dimension Oedometer test)

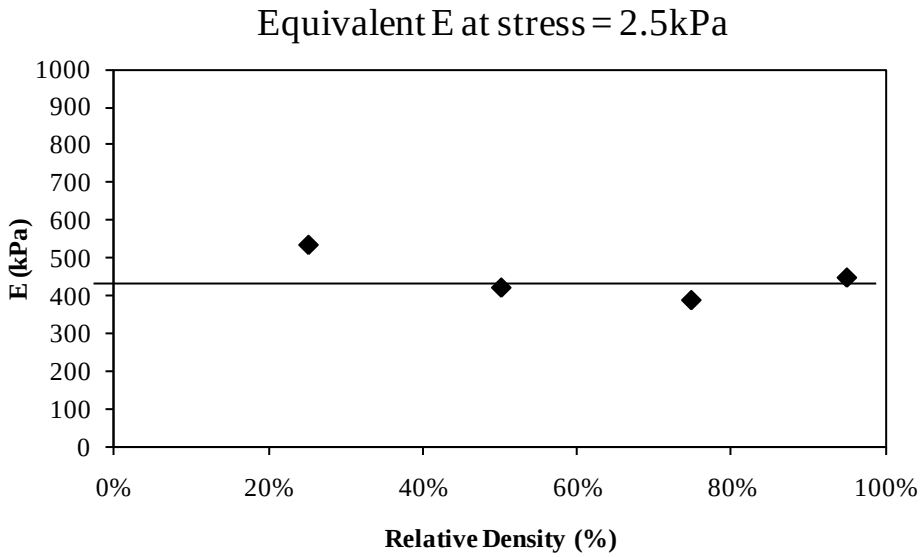

Figure B1.4. Variation of Young's modulus, E with fill relative density

Appendix B2

Calibration results of strain gauges

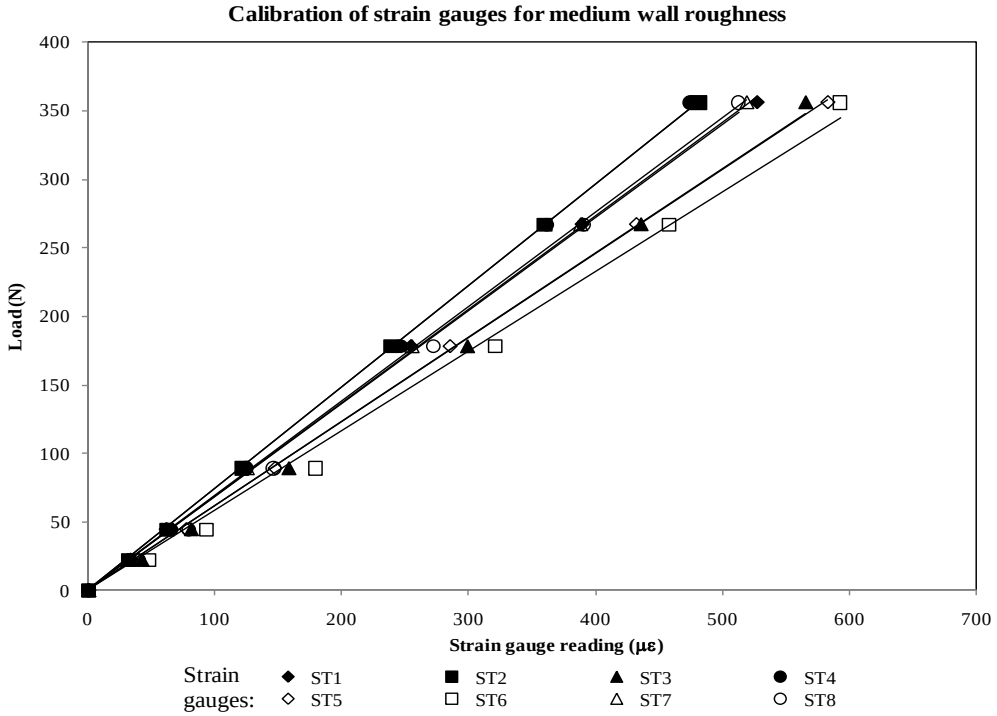

Figure B2. 1. Calibration results of strain gauges for stope with inclination 80^{o} and medium wall roughness

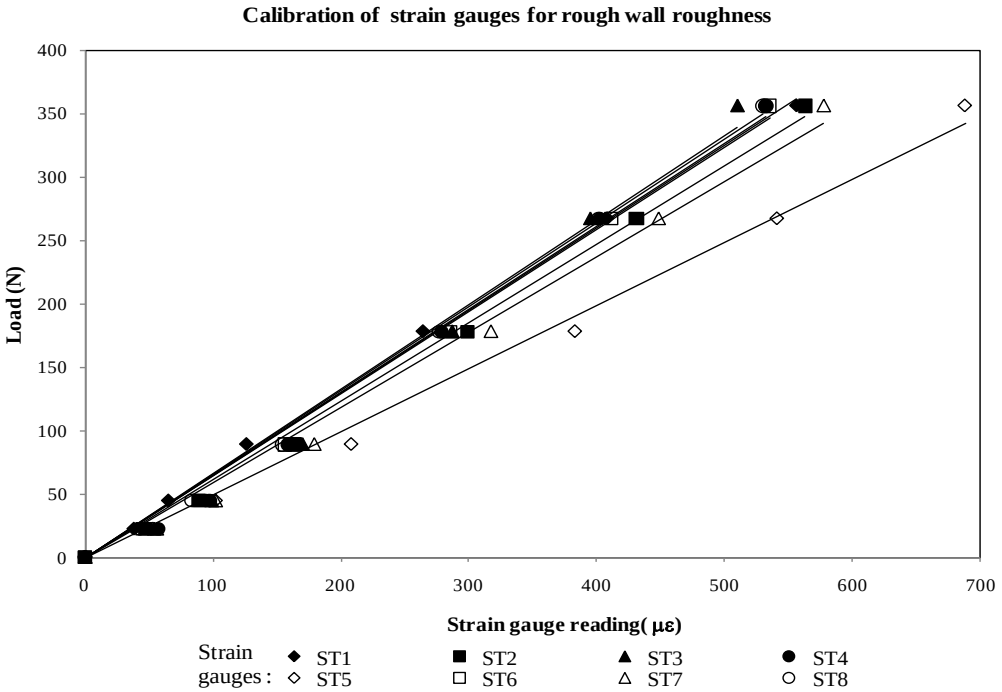

Figure B2. 2. Calibration results of strain gauges for stope with inclination 80^{o} and high wall roughness

Appendix B3

Results of laboratory model at 30% relative density

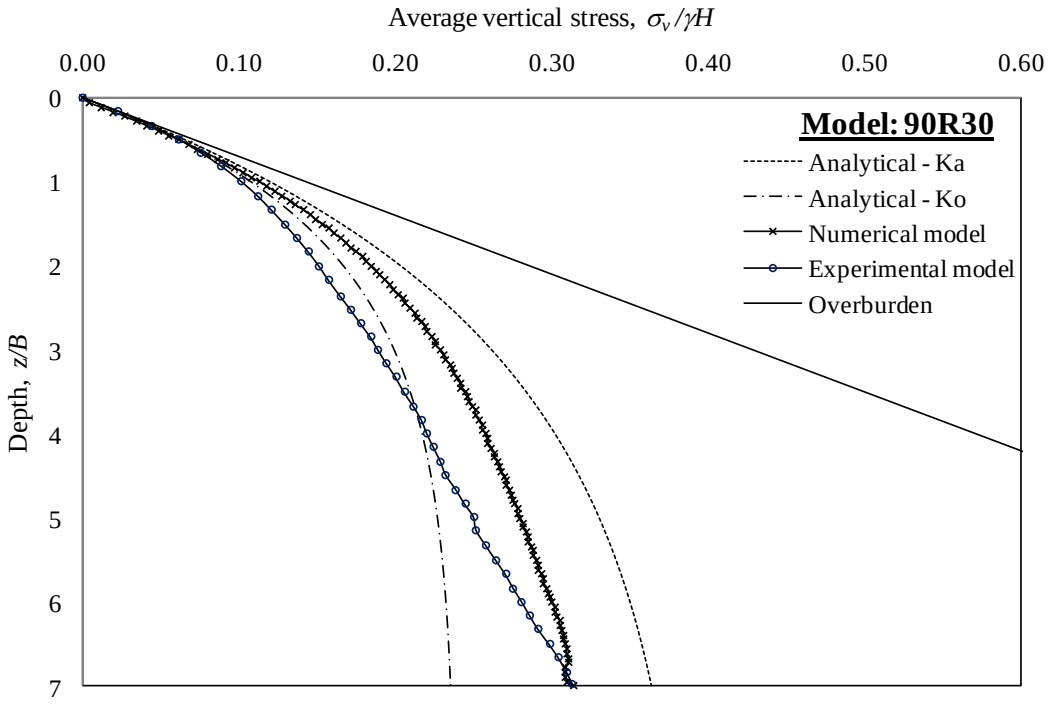

(a)

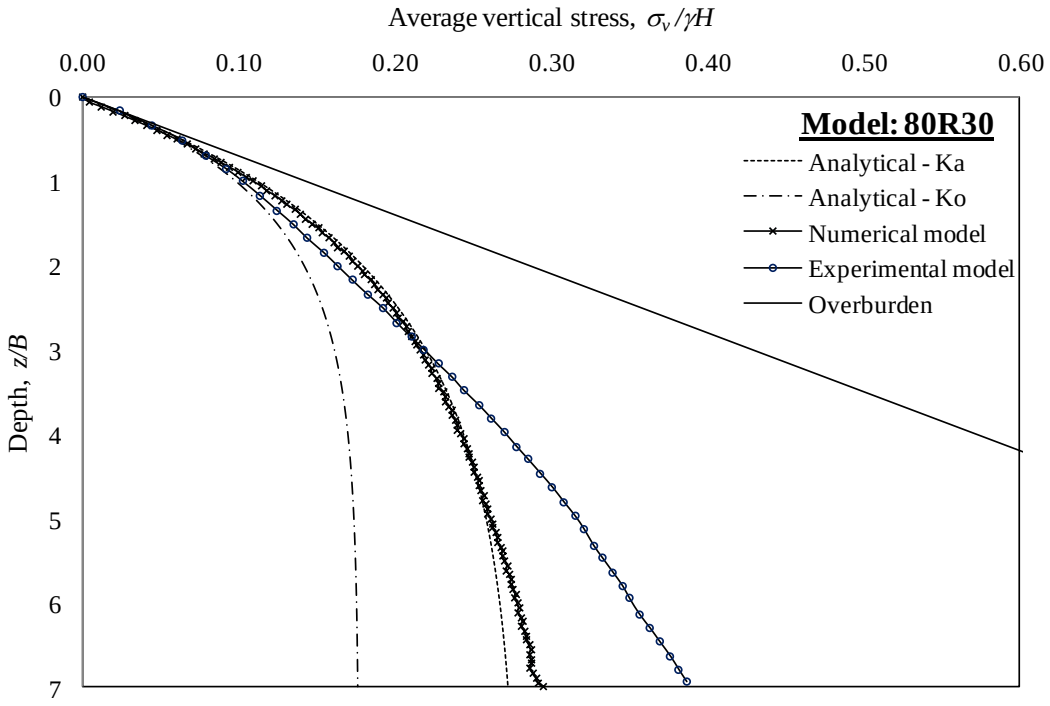

(b)

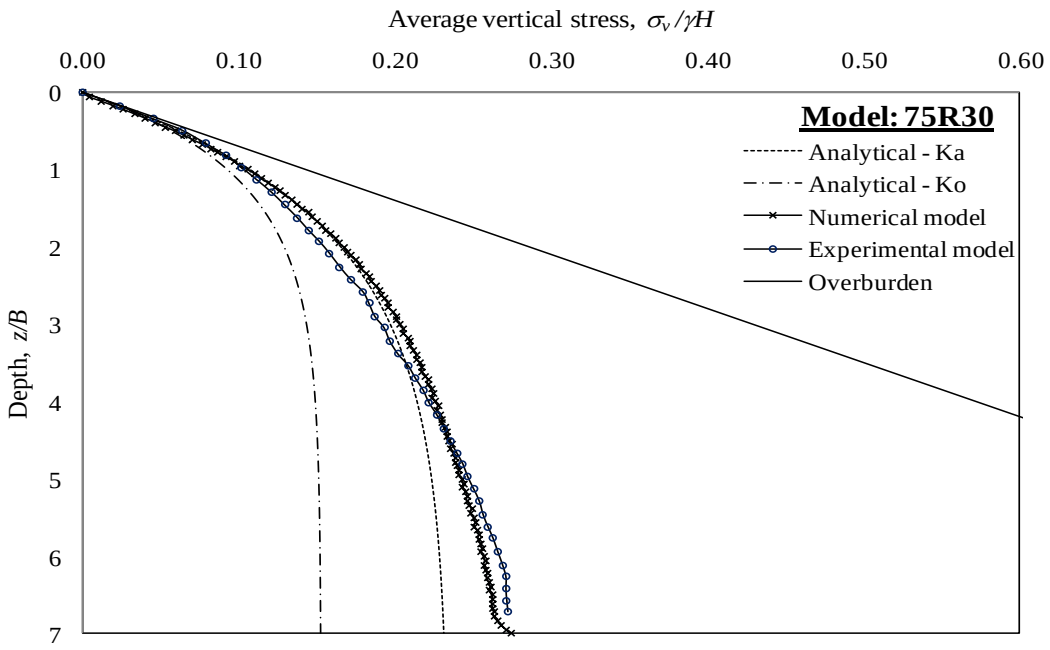

(c)

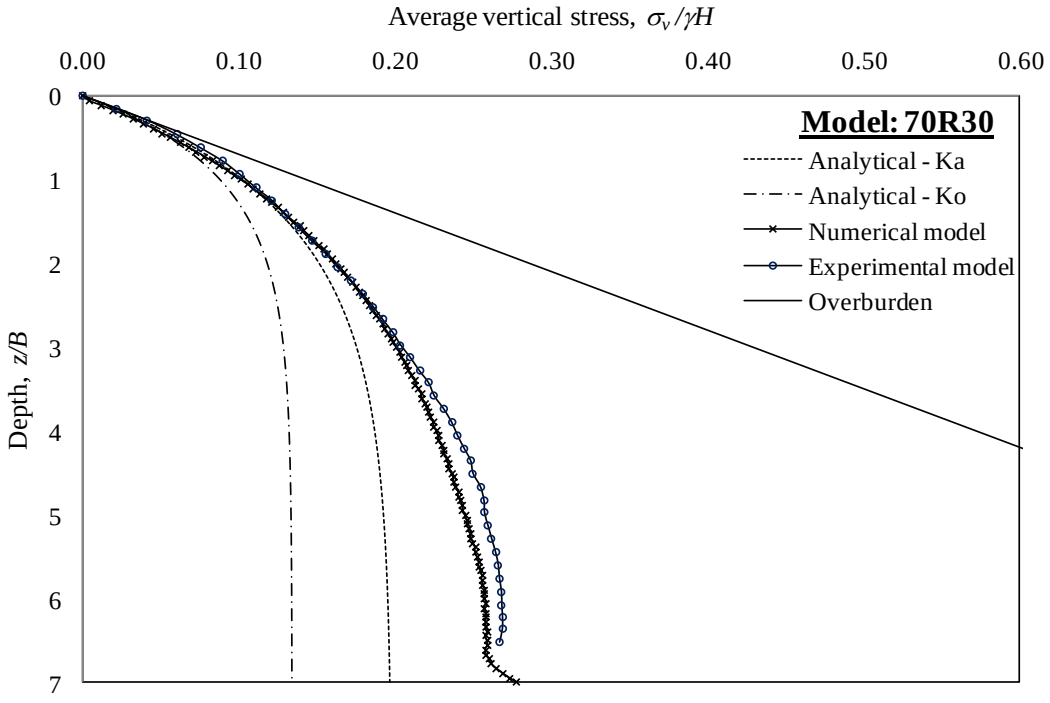

(d)

Figure B3.1. Comparison between the solutions of experimental, numerical and analytical modeling for different slope angle with high wall roughness at 30% relative fill density (a) model 90R30 (b) model 80R30 (c) model 75R30 (d) model 70R30

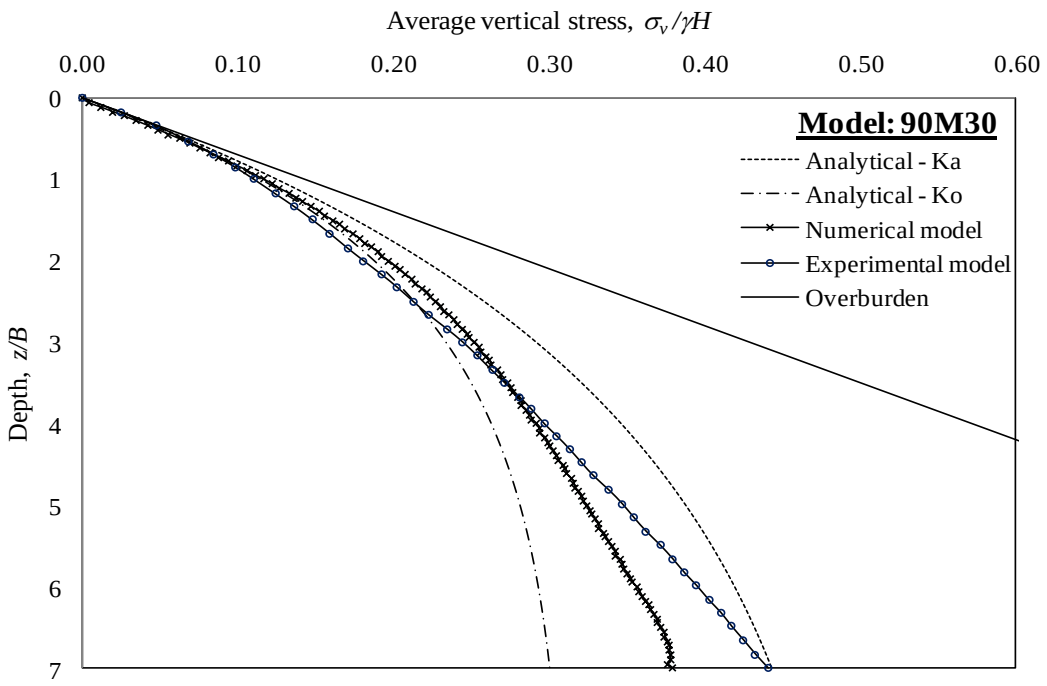
Average vertical stress, $\sigma_v/\gamma H$
0.00
0.10
0.20
0.30
0.40
0.50
0.60
Depth, z/B
0
1
2
3
4
5
6
7
Model: 90M30
Analytical - Ka
Analytical - Ko
Numerical model
Experimental model
Overburden

(a)

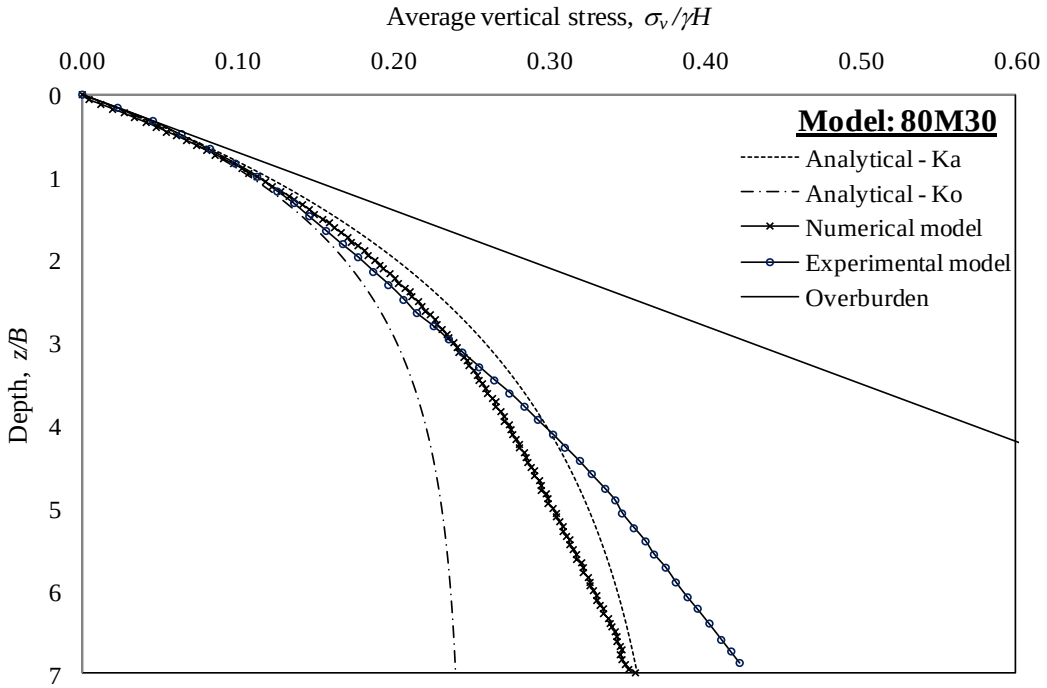
Average vertical stress, $\sigma_v/\gamma H$
0.00
0.10
0.20
0.30
0.40
0.50
0.60
Depth, z/B
0
1
2
3
4
5
6
7
Model: 80M30
Analytical - Ka
Analytical - Ko
Numerical model
Experimental model
Overburden

(b)

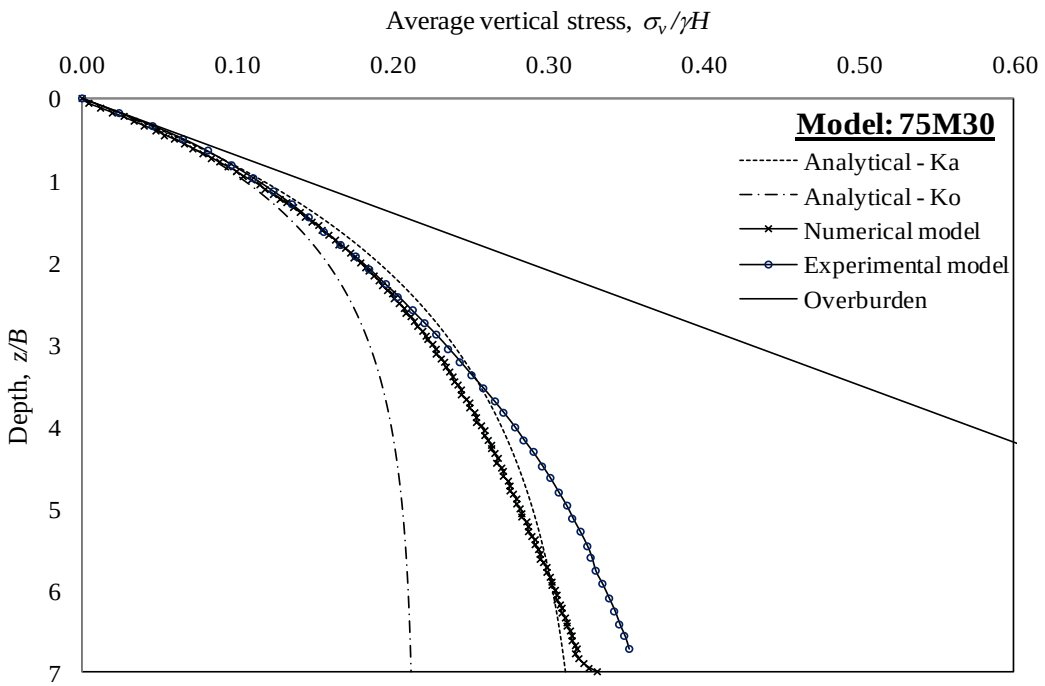

(c)

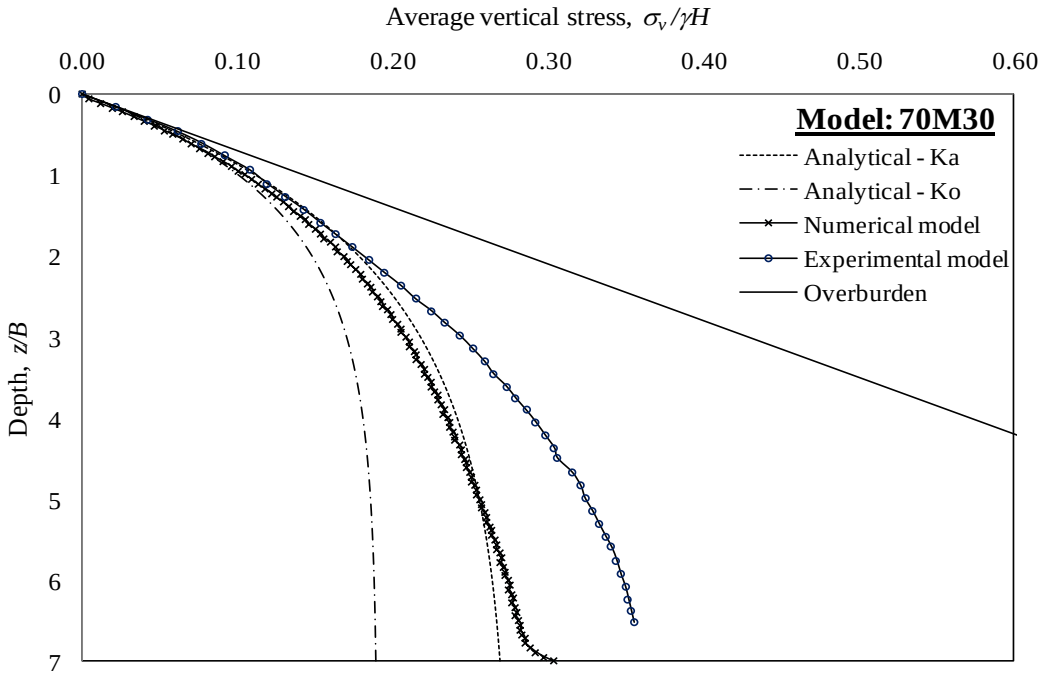

(d)

Figure B3.2. Comparison between the solutions of experimental, numerical and analytical modeling for different slope angle with medium wall roughness at 30% relative fill density (a) model 90M30 (b) model 80M30 (c) model 75M30 (d) model 70M30

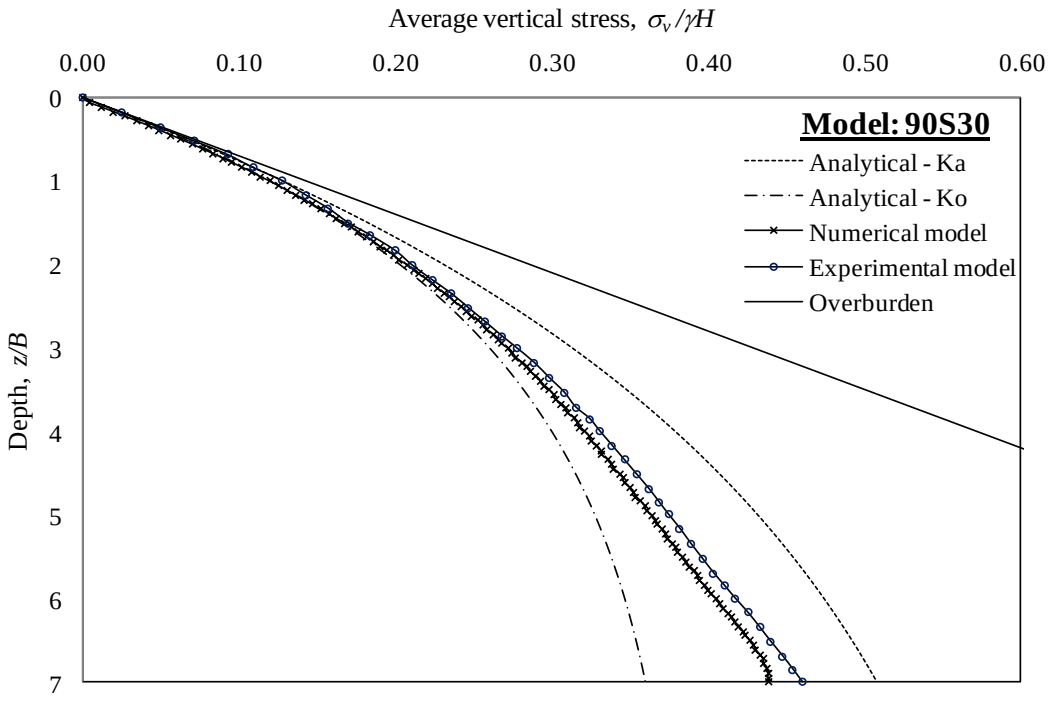
Average vertical stress, $\sigma_v/\gamma H$
0.00
0.10
0.20
0.30
0.40
0.50
0.60
Depth, z/B
0
1
2
3
4
5
6
7
Model: 90S30
Analytical - Ka
Analytical - Ko
Numerical model
Experimental model
Overburden

(a)

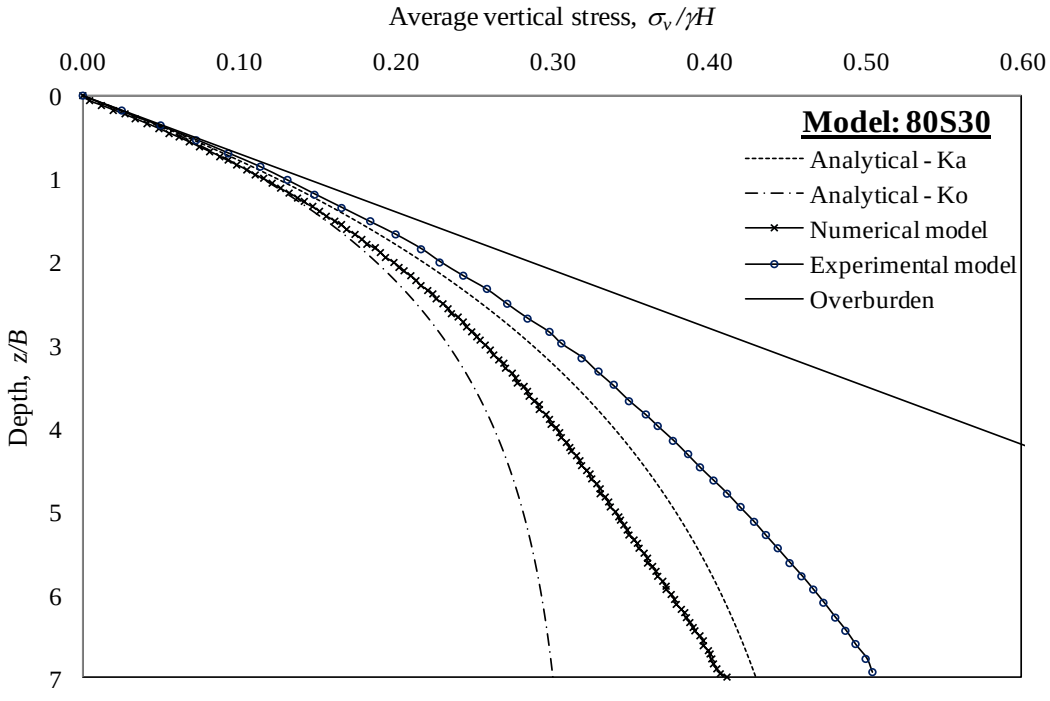
Average vertical stress, $\sigma_v/\gamma H$
0.00
0.10
0.20
0.30
0.40
0.50
0.60
Depth, z/B
0
1
2
3
4
5
6
7
Model: 80S30
Analytical - Ka
Analytical - Ko
Numerical model
Experimental model
Overburden

(b)

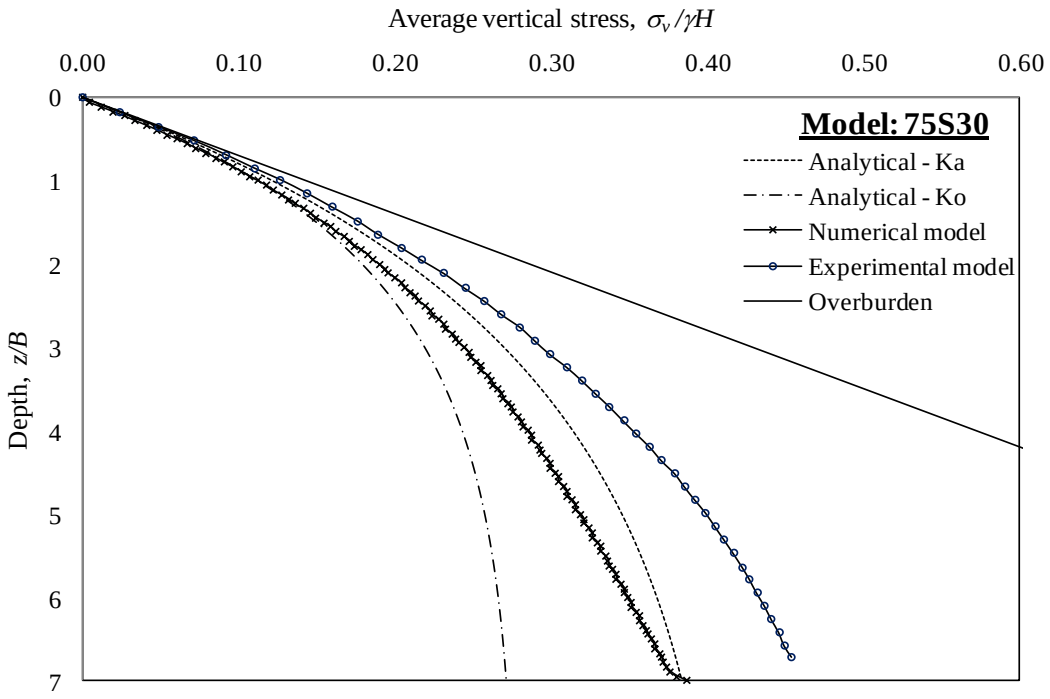

(c)

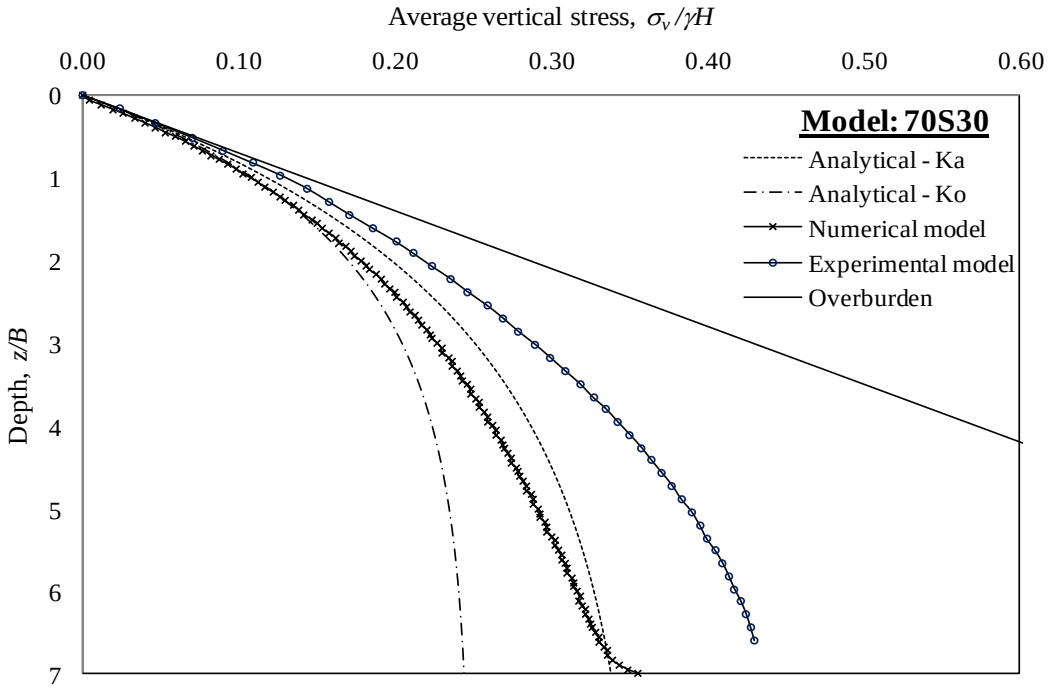

(d)

Figure B3.3. Comparison between the solutions of experimental, numerical and analytical modeling for different slope angle with low wall roughness at 30% relative fill density (a) model 90S30 (b) model 80S30 (c) model 75S30 (d) model 70S30

Average vertical stress at the base of stope with inclination 90º to the horizontal for high wall roughness and 30% fill relative density)

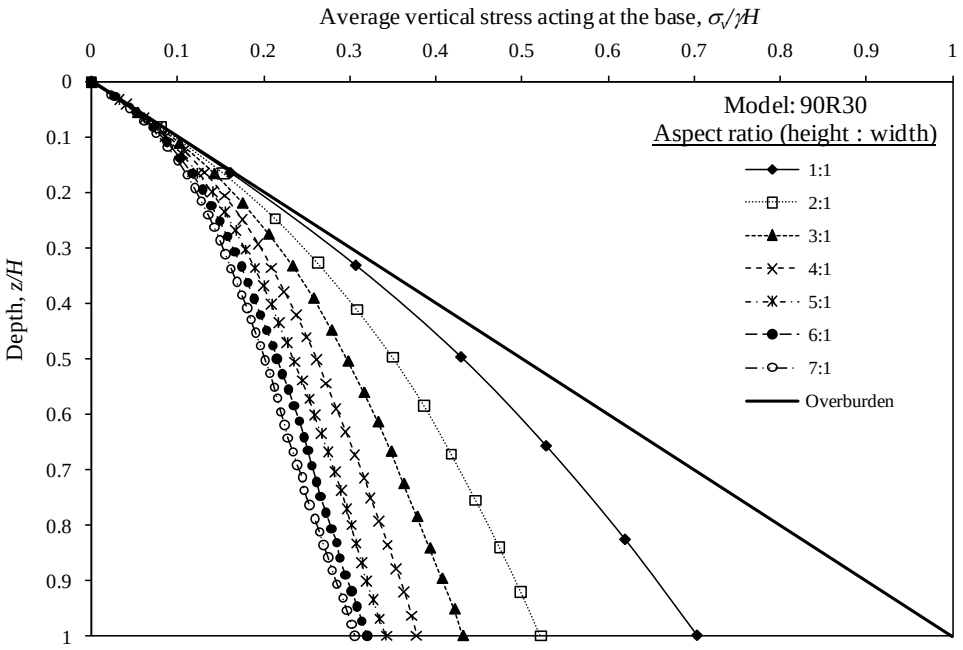

(a)

Average vertical stress at the base of stope with inclination 90º to the horizontal for medium wall roughness and 30% fill relative density

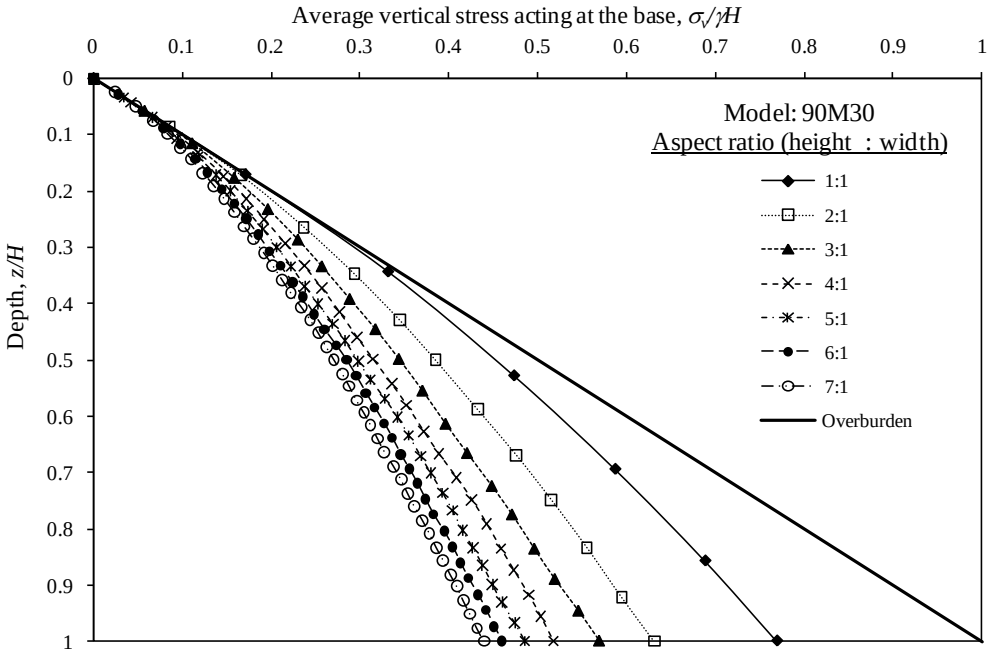

(b)

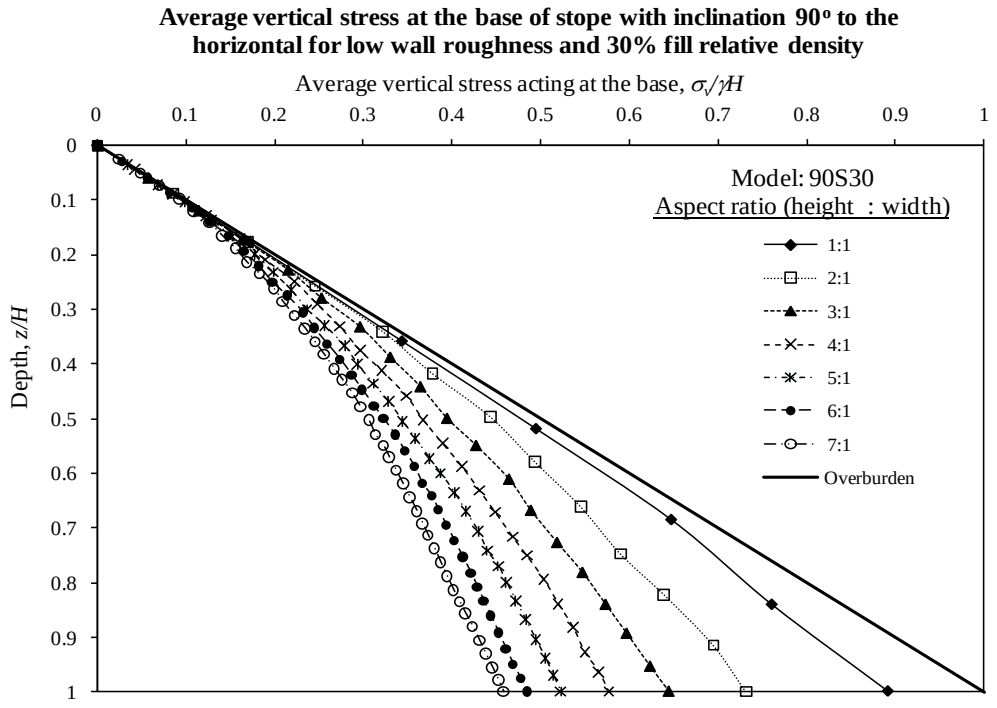

(c)

Figure B3.4. Average vertical stress at the base of stope with inclination 90° to the horizontal at 30% relative density for different aspect ratio (a) high wall roughness (b) medium wall roughness (c) low wall roughness

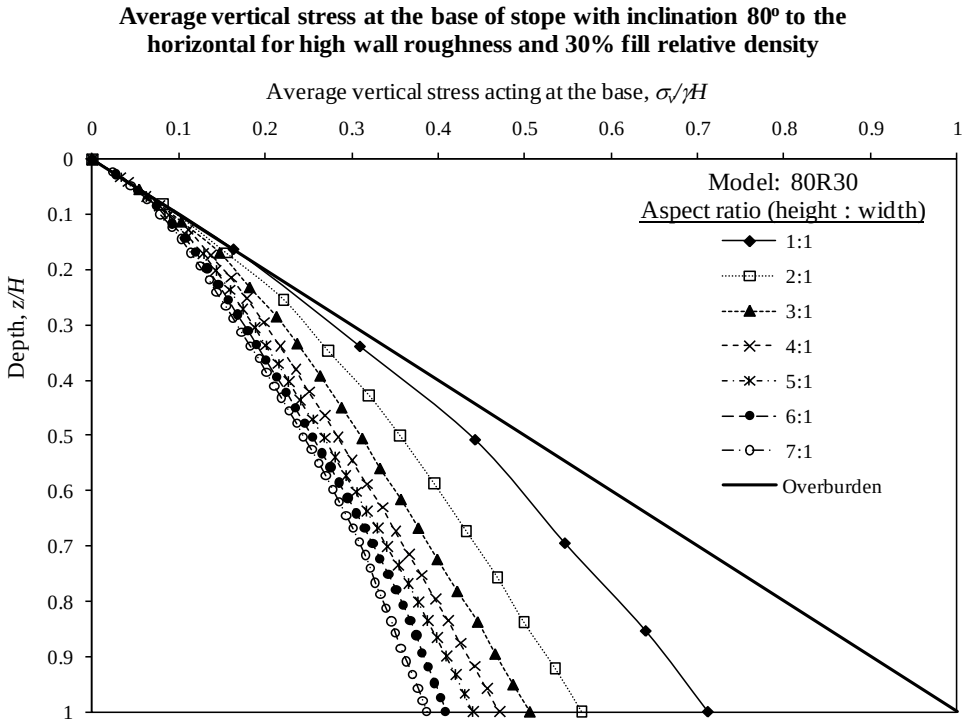

(a)

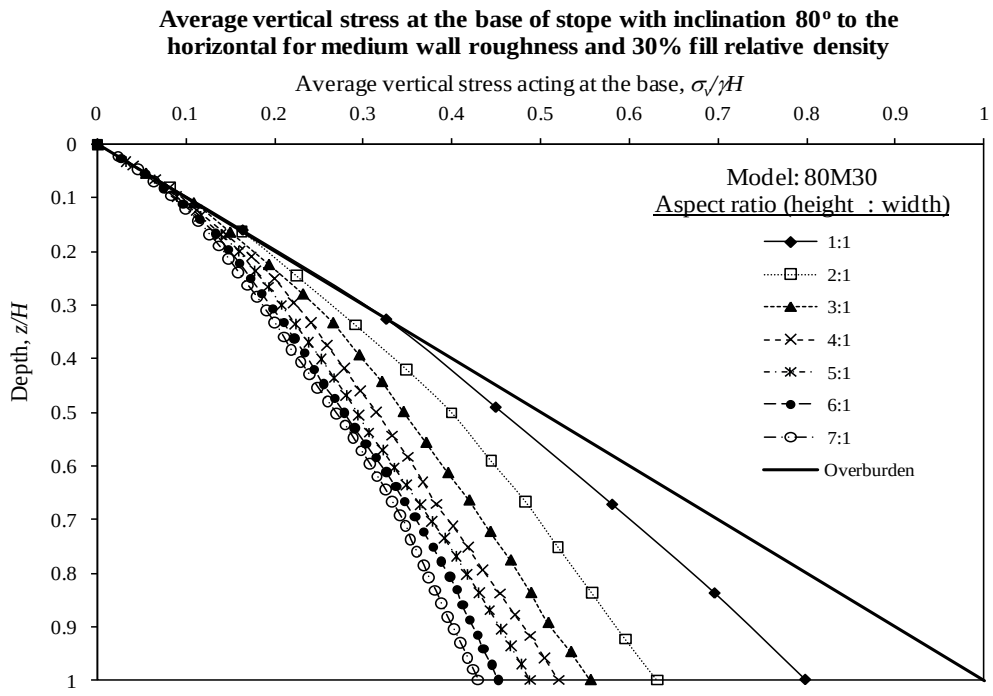

(b)

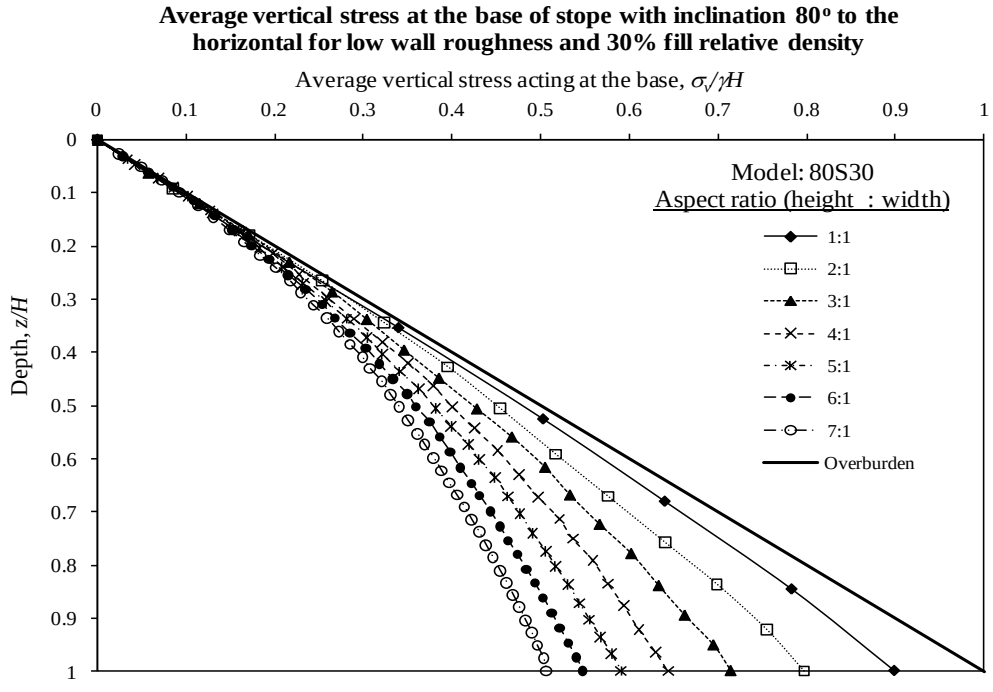

(c)

Figure B3.5. Average vertical stress at the base of stope with inclination 80^o to the horizontal at 30% relative density for different aspect ratio (a) high wall roughness (b) medium wall roughness (c) low wall roughness

Average vertical stress at the base of stope with inclination 70º to the horizontal for high wall roughness and 30% fill relative density

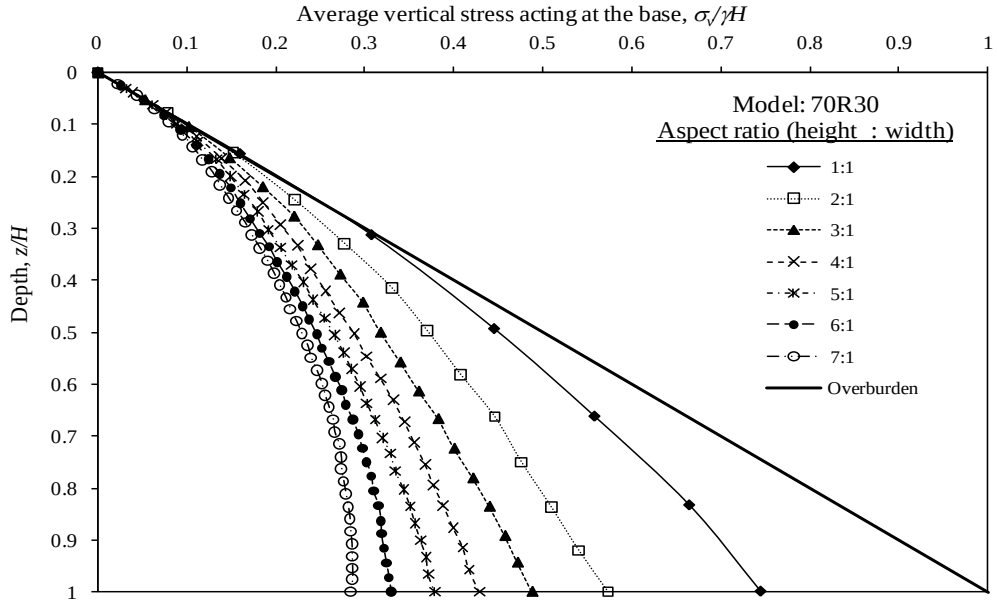

(a)

Average vertical stress at the base of stope with inclination 70º to the horizontal for medium wall roughness and 30% fill relative density

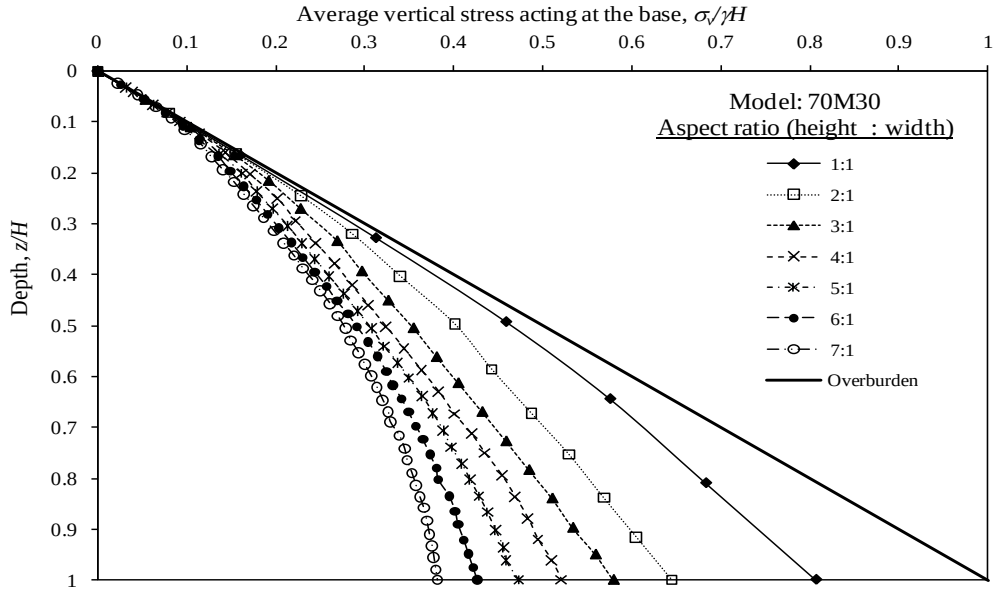

(b)

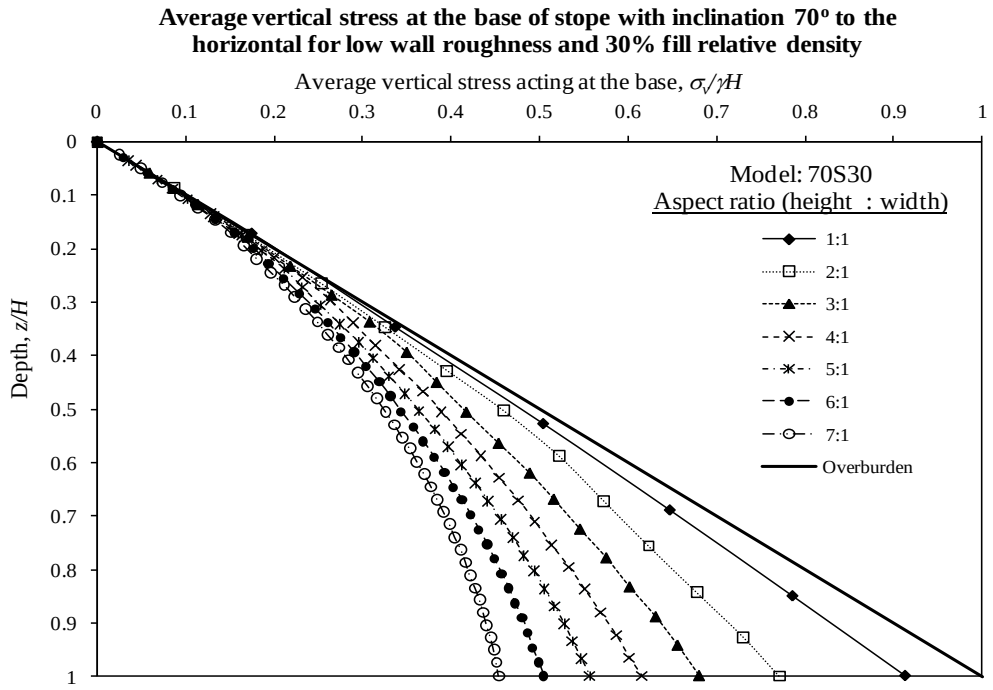

(c)

Figure B3.6. Average vertical stress at the base of stope with inclination 70^{o} to the horizontal at 30% relative density for different aspect ratio (a) high wall roughness (b) medium wall roughness (c) low wall roughness

Appendix B4

Effect of aspect ratio for stope with inclination 90^o and 80^o to the horizontal

Average vertical stress at the base of stope with inclination 90^o to the horizontal for high wall roughness and 60% fill relative density

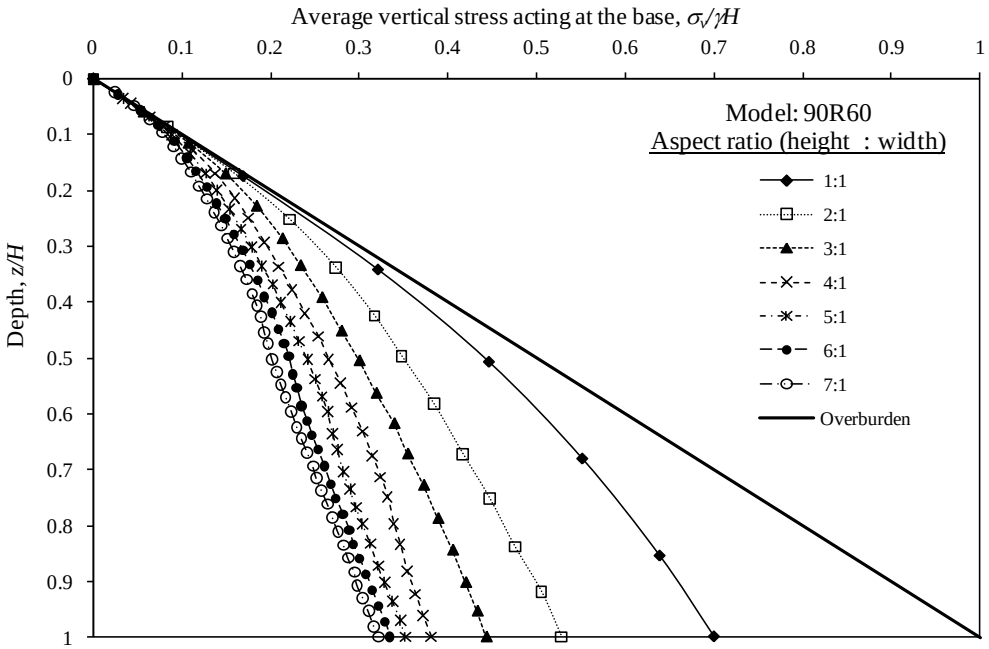

(a)

Average vertical stress at the base of stope with inclination 90^o to the horizontal for medium wall roughness and 60% fill relative density

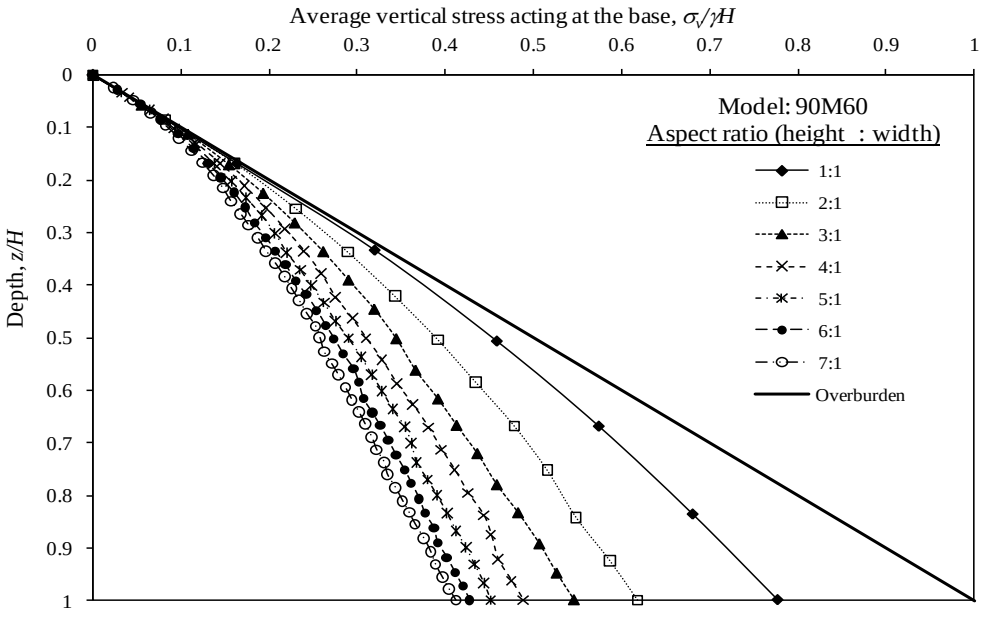

(b)

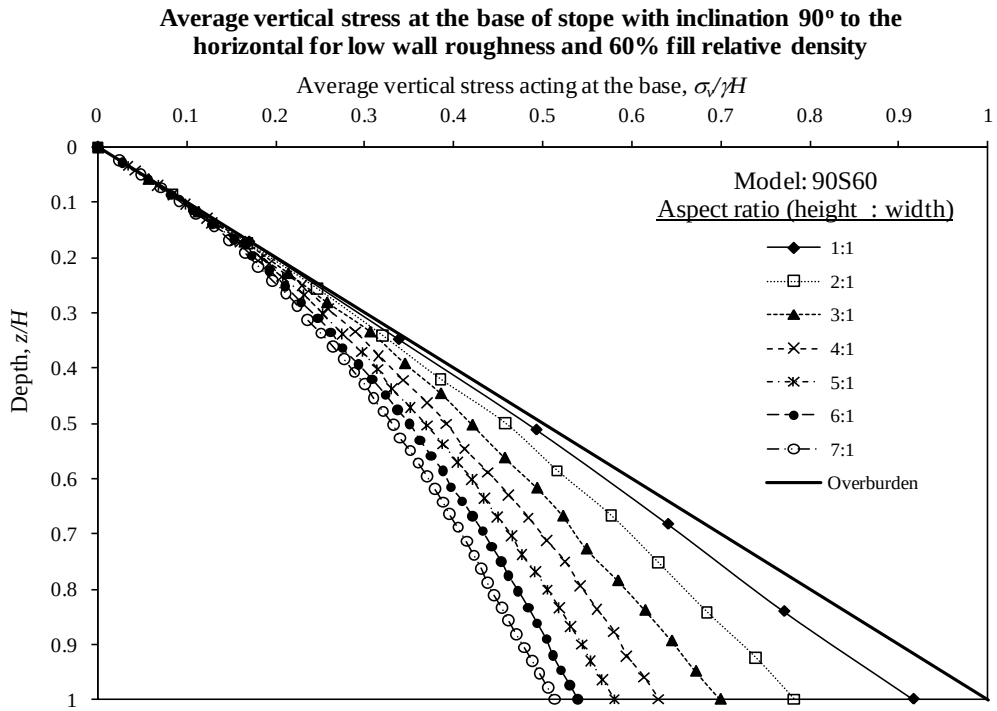

(c)

Figure B4. 1. Average vertical stress at the base of stope with inclination 90° to the horizontal at 60% relative density for different aspect ratio (a) high wall roughness (b) medium wall roughness (c) low wall roughness

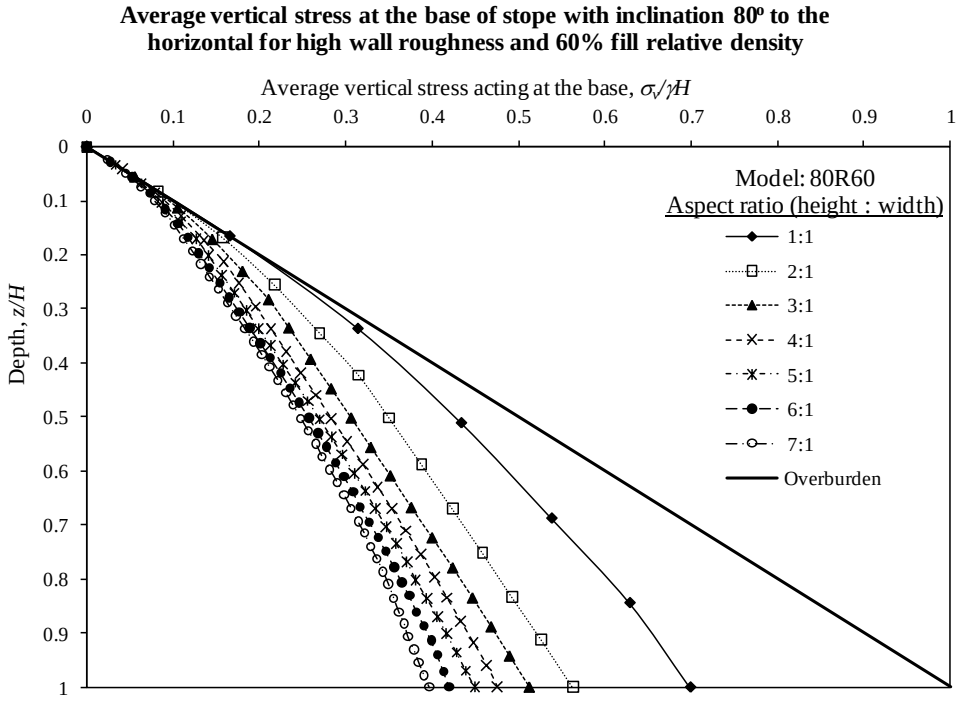

(a)

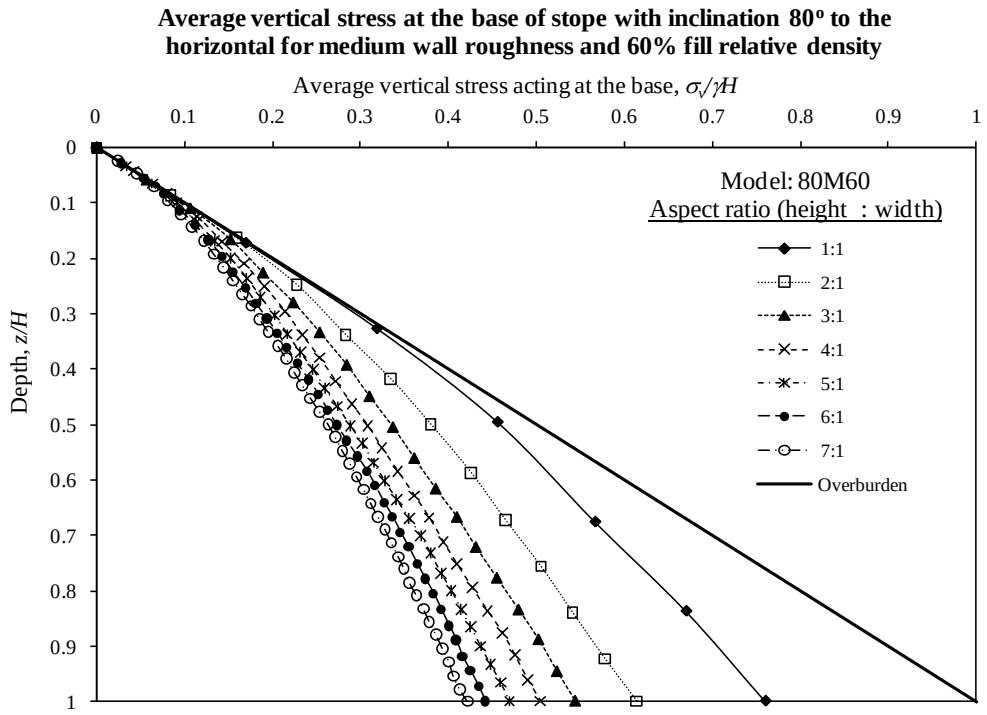

(b)

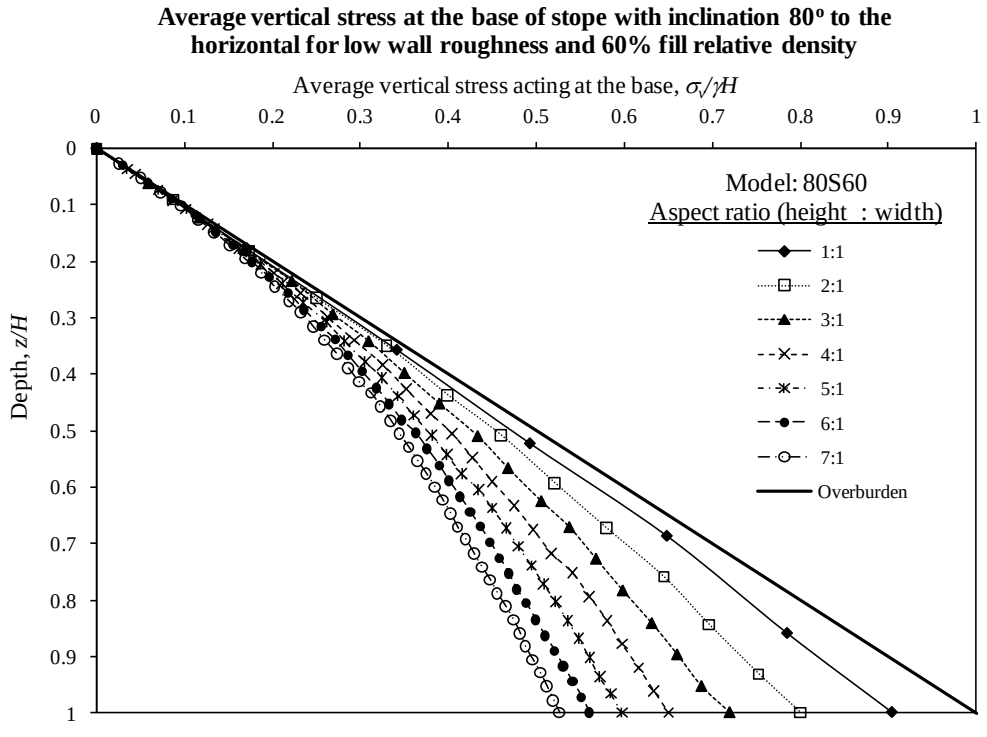

(c)

Figure B4. 2. Average vertical stress at the base of stope with inclination 80^o to the horizontal at 60% relative density for different aspect ratio (a) high wall roughness (b) medium wall roughness (c) low wall roughness

Appendix C1

FLAC code for laboratory model 100 mm x 700 mm

```
;=========================================
; Laboratory stope 100 x 700 mm
; High wall roughness
; Inclination: 70^o
; Filling: 42 Lift
;=========================================
new
define moduli
; Wall : s1-shear modulus, b1-bulk modulus, y1-Young modulus, pr1-Poisson's ratio
;Fill : s2-shear modulus, b2-bulk modulus, y2-Young modulus, pr2-Poisson's ratio
        s1=y1/(2*(1+pr1))
        b1=y1/(3*(1-2*pr1))
        s2=y2/(2*(1+pr2))
        b2=y2/(3*(1-2*pr2))
end

def const
        ; Wall properties: y1-Young modulus, pr1-Poisson's ratio, d1-density
         y1=3.2e9
         pr1=0.3
         d1 = 1190
        ; fill properties
        ;  y2-Young modulus, pr2-Poisson's ratio, d2-density, phi2-friction angle, c2-cohesion
         ; de2-interfacial angle, dil2-dilation, ks2 & kn2 -interface properties
         y2=420e3
         pr2=0.2
         d2=1568
         phi2=41.1
         c2=0
         del2=40
         dil2=3.7
         ks2=1e8
         kn2=1e8
```

```
end
const
moduli

;generate grid
      grid 26,126
      mod elas
      prop den = d1 bulk = b1 shear = s1
      gen      0,0  0.2548,0.7  0.2648,0.7   0.01,0    i = 1,3     j = 1,127
      gen 0.01,0   0.2648,0.7  0.3648,0.7   0.11,0    i = 4,24   j = 1,127
      gen 0.11,0   0.3648,0.7  0.3748,0.7   0.12,0    i = 25,27  j=1,127
      mod null i = 3,24

;boundary condition
     fix x y i = 1
     fix x y i = 27
     fix y j = 1

;initial conditions
     ini xdis = 0 ydis = 0
     ini syy = 0 sxx = 0 szz = 0 sxy = 0
     set grav = 9.81
     set large
     step 2000
     solve
      ini xd 0 yd 0

; ----------------------filling process----------------------------------------
  ;fill first layer
     model mohr i = 4,23 j = 1,3
     prop bulk = b2 shear = s2 den = d2 fric = phi2 coh = c2
     int 1 as from  3,1 to  3,4   bs from  4,1 to  4,4
     int 2 as from 24,1 to 24,4  bs from 25,1 to 25,4
     int 1 ks = ks2 kn = kn2 fric = del2 dil = dil2
     int 2 ks = ks2 kn = kn2 fric = del2 dil = dil2
     step 100
```

```
    set gravity = 9.81
    set large
    solve
; Tiered filling
def fill
    loop k(1,41)
      k1 = k*3+1
      k2 = k1+2
      k3 = k*3+2
      k4 = k3+2
      k5 = k*2+1
      k6 = k5+1
      command
        model mohr i = 4,23 j = k1,k2
        prop bulk = b2 shear = s2 den = d2 fric = phi2 coh = c2
        int k5 aside from  3,1  to 3,k4     bside from 4,k3 to 4,k4
        int k6 aside from 24,k3 to 24,k4 bside from 25,1 to 25,k4
        int k5 ks = ks2 kn = kn2 fric = del2 dil = dil2
        int k6 ks = ks2 kn = kn2 fric = del2 dil = dil2
        step
       set large
       set gravity=9.81
       solve
     end_command
  end_loop
end
fill
```

Appendix C2

FLAC code for full scale model 6 m x 45 m

```
;==========================================
;Full scale model 6 x 45 m
; δ = ϕ
; Grid: 94x131
; Filling: 10 Lift
; Inclination: 70^o
; ==========================================
new
def const
  ; rock properties
  ; y1-Young modulus, pr1-Poisson's ratio, d1-density, ks1 & kn1 – interface properties
    y1=30e9
    pr1=0.3
    d1 = 2700
    ks1=1e13
    kn1=1e13
  ; fill properties
  ;  y2-Young modulus, pr2-Poisson's ratio, d2-density, phi2-friction angle, c2-cohesion
  ; de2l-interfacial angle, dil2-dilation, ks2 & kn2 -interface properties
    y2=300e6
    pr2=0.2
    d2=1800
    phi2=30
    c2=0
    del2=30
    dil2=0
    ks2=1e10
    kn2=1e10
end

define moduli
  ; rock: s1-shear modulus, b1-bulk modulus
  ; backfill: s2-shear modulus, b2-bulk modulus
```

```
    s1=y1/(2*(1+pr1))
    b1=y1/(3*(1-2*pr1))
    s2=y2/(2*(1+pr2))
    b2=y2/(3*(1-2*pr2))
end
const
moduli

; generate grid
    grid 94, 131
    mod elas
    prop den=d1 bulk=b1 shear=s1
    gen   0,0            0,65.5   43.84005,65.5   20,0          i = 1,41    j = 1,132
    gen 20,0  43.84005,65.5   49.84005,65.5   26,0          i = 42,54  j = 1,132
    gen 26,0  49.84005,65.5   69.84005,65.5   69.84005,0    i = 55,95  j = 1,132
    mod null i = 41
    mod null i = 54
    int 1 as from 41,1  to 41,132   bs from 42,1  to 42,132
    int 2 as from 54,1  to 54,132   bs from 55,1  to 55,132
    int 1 glue ks = ks1 kn = kn1
    int 2 glue ks = ks1 kn = kn1

; boundary condition
    fix x i = 1
    fix x i = 95
    fix y j = 1

 ; initial conditions
    ini syy = -6.7674285e6   var 0,1.7348985e6 j =1,132
    ini sxx = -1.3534857e7   var 0,3.469797e6   j = 1,132
    ini szz = -1.3534857e7   var 0,3.469797e6   j = 1,132
    apply syy = -6.7674285e6  i =  1,41   j=1
    apply syy = -6.7674285e6  i = 42,54  j=1
    apply syy = -6.7674825e6  i = 55,95  j=1
    apply syy = -5.03253e6  i = 1,41    j = 132
    apply syy = -5.03253e6  i = 42,54  j = 132
```

```
    apply syy = -5.03253e6  i = 55,95  j = 132
    apply sxx = -1.3534857e7  var 0,3.469797e6  i = 1     j = 1,132
    apply sxx = -1.3534857e7  var 0,3.469797e6  i = 95   j = 1,132
    ini xdis = 0 ydis= 0
    set grav=9.81
    set large
    step 500
    solve

  ; excavate the stope
    model null i = 42,53  j = 21,112
    set grav = 9.81
    set large
    solve
    ini xd 0 yd 0

; ---------- filling process----------------------------------------
  ; first layer filling
    model mohr i = 42,53  j = 41,49
    prop bulk = b2 shear = s2 den = d2 fric = phi2 coh = c2
    int 7 as from 41,21  to 41,50  bs from 42,21  to 42,50
    int 8 as from 54,21  to 54,50  bs from 55,21  to 55,50
    int 7 ks = ks2 kn = kn2 fric = del2 dil = dil2
    int 8 ks = ks2 kn = kn2 fric = del2 dil = dil2
    step 2000
    set gravity=9.81
    set large
    solve
  ; tiered filling
   def fill
     loop k(1,9)
       k1 = k*9+21
       k2 = k1+8
       k3 = k*9+21
       k4 = k3+9
       k5 = k*2+7
```

```
        k6 = k5+1
       command
         model mohr i = 42,53  j = k1,k2
         prop bulk = b2 shear = s2 den = d2 fric = phi2 coh = c2
         int k5 aside from 41,21  to 41,k4  bside from 42,k3 to 42,k4
         int k6 aside from 54,k3  to 54,k4  bside from 55,21 to 55,k4
         int k5 ks = ks2 kn = kn2 fric = del2 dil = dil2
         int k6 ks = ks2 kn = kn2 fric = del2 dil = dil2
         step 2000
        set large
        set gravity=9.81
        solve
      end_command
  end_loop
end
fill
```